Characterisation of the Scs system that confers copper tolerance in *Salmonella enterica* serovar Typhimurium

Buke Yucel

Thesis for the degree of PhD in Microbiology

School of Biosciences

Faculty of Sciences

University of Kent

2019

Declaration

I confirm that no part of this thesis has been submitted in support of an application for any degree or qualification at either the University of Kent, any other university or higher education learning institution.

Buke Yucel

18th July 2019

Abstract

Gram-negative bacteria have a variety of systems that catalyse the formation of disulphide bonds, which are essential for the folding, activity, and stability of many periplasmic and secreted proteins. The *scsABCD* (suppressor of copper sensitivity) locus of *Salmonella enterica* encodes four proteins with thioredoxin-like catalytic motifs. Previous work has shown that *Salmonella* encounters toxic levels of copper during infection and the *scs* system provides protection against copper-mediated toxicity. Given that Cu^{2+} ions are known to promote disulphide oxidation, it was hypothesised that the StScs proteins and copper both influence the thiol redox status of periplasmic proteins *in vivo*. The current work reports that expression of the soluble periplasmic protein StScsC is copper-specific, and copper was found to oxidise StScsC *in vivo*. Using a combination of genetic and proteomics approaches, the abundance of various cysteine-containing periplasmic/secreted proteins were found to be elevated by StScsC and copper in the *Salmonella* periplasm. Co-purification and mass spectrometry approaches provide additional evidence that the arginine-sensing periplasmic protein ArtI interacts with StScsC. Intramacrophage survival data demonstrates that loss of StScsC results in a significant decrease in survival. The current work reports a new role for the thioredoxin-like StScsC protein in disulphide folding of ArtI, a periplasmic L-arginine sensing protein. Given the known impact of arginine sensing/uptake upon c-di-GMP signalling and the production of nitric oxide (NO) by host cells, the current work demonstrates a role for the Scs system in facilitating intramacrophage survival through alleviating copper-stress, and implicates StScsC in a broader role in immune evasion.

In addition, the presence of StScs proteins and copper was shown to increase the yield of Herceptin Fab fragments (used to treat breast cancer) in the *E. coli* periplasm. Hence, the StScs proteins have the potential to facilitate the formation of disulphides in protein therapeutics that can be used in biotechnological platforms.

This work provides novel insights into the *in vivo* role for the Scs system in *Salmonella*, and highlights the importance of disulphide stress responses and copper tolerance during infection.

Acknowledgement

Firstly, I would like to express my deepest gratitude to my supervisor Dr Mark Shepherd who has given me the opportunity to do this PhD. With his supervision, motivation and endless support it has been a great journey.

I would also like to thank Dr Gary Robinson and my co-supervisor Professor Colin Robinson for their advice throughout my project and to the past and present ShepBlomSon lab members especially to Claudia and Taylor. I am so grateful for Sarah's friendship and support right from the start. Things would have been too difficult without her. Many thanks to Kevin Howland who has helped me with mass spectrometry and the Gourlay lab for helping me out with the macrophage infection studies and fluorescence microscopy. I would also like to thank to the Biochemical Society for funding me to attend to I3S conference in St Malo.

I am thankful for my friends and family; my grandparents (especially my granddad Vedat) for their love and faith and my brother for his patience to stay in the UK for weeks to spend time with me.

Last but not least, I would like to thank my parents, for making me who I am today and for their endless encouragement and support in every possible way. Without you two, this would not have been possible.

Table of Contents

Declaration…….....i

Abstract…….....ii

Acknowledgement…….. iii

Table of Contents…….iv

List of Abbreviations…….....viii

List of Figures…….....….....xi

List of Tables……...…...…xiv

Health and Safety……xv

Poster presentations……xvi

Chapter 1 1

Introduction..... 1

1.1- *Salmonella* taxonomy, serovars and diseases 2

1.2- *Salmonella* host invasion and survival 2

1.3- Host response and bacterial defence mechanisms 4

1.3.1- Reactive oxygen species (ROS)..... 5

1.3.2- Nitric oxide 7

1.3.3- Copper 9

1.4- Mechanisms of periplasmic disulphide bond formation in bacteria 12

1.5- The Scs system 16

1.5.1- The ScsC proteins of other Gram-negative bacteria 17

1.5.2-The Scs proteins of *S.* Typhimurium 18

1.5.2.1- Biochemical and structural characterisation of StScsC 19

1.5.2.2- Genetic approaches to investigate functional roles for the StScs proteins ... 22

1.6- Applications for disulphide folding machinery in biotechnology 23

1.7- Project aims 24

Chapter 2 25

Materials and Methods..... 25

2.1- Bacterial strains and plasmids 26

2.2- Bacterial growth media, sterilisation, and cell harvesting 27

2.3- Preparation of competent cells and transformations of plasmids 30

2.4- DNA isolation and analysis 32

2.5- Protein purification 38

2.6- Determination of the redox status of proteins 41
2.7- Sodium dodecyl sulphate-polyacrylamide gel electrophoresis (SDS-PAGE) 43
2.8- Electrophoretic transfer to PVDF membrane 44
2.9- Western Blotting 44
2.10- Identification of protein bands via mass spectrometry 45
2.11- Quantification of protein abundances by electrospray mass spectrometry 46
2.12- Metal binding assay 48
2.13- Macrophage survival assay 49
2.14- Quantification of GFP fluorescence 51
2.15- Fluorescence microscopy 51
Chapter 3 52
Expression analysis and identification of *in vivo* targets for the ScsC protein of *Salmonella* 52
3.1- Introduction 54
3.2- Results 55
3.2.1- StScsC is part of a sub-group of monomeric ScsC proteins that lack an N-terminal dimerization domain 55
3.2.2- StScsC expression is induced specifically by copper 58
3.2.2.1- Mass spectrometry analysis of StScsC expression in the presence of Cu^{2+}. 58
3.2.2.2- Western blot analysis demonstrates that StScsC expression is specifically elevated by copper 59
3.2.2.3- Western blot analysis of StScsC expression in the presence of oxidative/ nitrosative stresses 59
3.2.2.4- Activation of the *scsA* promoter is copper specific 60
3.2.3- StScsC exists in the oxidised state *in vivo* 66
3.2.4 - Copper and StScsC promote the assembly of disulphide-containing proteins involved in peptide uptake 67
3.2.4.1 - StScsC and copper alter the abundance of disulphide/cysteine-containing periplasmic/secreted proteins in *S.* Typhimurium 68
3.2.5 - StScsC elevates the abundance of oxidised BcsC peptide fragment 74
3.2.6 - *Salmonella* survival in murine macrophages is significantly impaired by loss of StScsC 77
3.3- Discussion 78
Chapter 4 81
Biochemical analysis of the StScsC protein and potential redox partners 81
4.1- Introduction 83
4.2-Results 84
4.2.1-Purification of his_6-tagged StScsC 84

4.2.2- Purification of TEV protease 85
4.2.3-Cleavage of his_6-tag from purified StScsC 86
4.2.4- Cu^{+} affinity of StScsC 87
4.2.5- Engineering a $StScsC_{CXXC}$ variant and trapping interaction partners 89
4.2.5.1- Model for trapping the target proteins binding to StScsC 89
4.2.5.2- Cloning of a $scsC_{CXXA}$ construct to pSU2718 vector plasmid 90
4.2.5.3- Purification of $StScsC_{CXXA}$ 91
4.2.5.4- Reduction of putative $ScsC_{CXXC}$-target substrates with DTT 92
4.2.5.5- StScsC binds to ArtI in the *E. coli* periplasm 93
4.2.6- Cloning and purification of *Salmonella* arginine-binding periplasmic protein I 95
4.2.6.1- Cloning of *artI* gene 95
4.2.6.2- Purification of ArtI 97
4.2.7-*In vitro* protein experiments with ArtI and StScsC 98
4.2.7.1- Reduced $StScsC_{CXXA}$ binds to ArtI 98
4.2.7.2- Cu^{2+} promotes dimerization of reduced $StScsC_{CXXA}$ 99
4.2.7.3- Copper ions oxidise wild-type StScsC *in vitro* 102
4.2.7.4- Oxidised StScsC is reduced by *S.* Typhimurium ArtI 103
4.2.8-Structual analysis of ArtI and StScsC 106
4.2.9 - Impact of StScsC upon growth of *Salmonella* on L-arginine 107
4.3- Discussion 109
Chapter 5 112
Investigating the ability of StScsABCD to facilitate disulphide folding of therapeutic proteins 112
5.1 - Introduction 114
5.1.1 - Herceptin 115
5.1.2 - Human growth hormone (hGH) 117
5.2 - Results 119
5.2.1 – Investigating the impact of StScsABCD and copper upon Herceptin assembly 119
5.2.1.1 - Engineering a Herceptin expression vector 119
5.2.1.2 – Engineering a ScsABCD expression plasmid 120
5.2.1.3 - Development of a Western Blotting technique to detect Herceptin 120
5.2.1.4 - Copper elevates periplasmic protein levels in *E. coli* cells 122
5.2.1.5 - Herceptin yield is elevated by both expression of StScs proteins and copper 123
5.2.2 - Investigating the impact of StScsABCD and copper upon Human Growth Hormone assembly 125

5.2.2.1 - Attempts to demonstrate the formation of a StScsC-hGH heterodisulphide 125
5.3 - Discussion 128
Chapter 6 131
Final discussion 131
References 139
Appendix 152

List of Abbreviations

Amp: Ampicillin

AMS: 4-acetamido-4′-maleimidylstilbene-2,2′-disulfonic acid

APS: Ammonium Persulfate

BCIP/NBT: 5-bromo-4-chloro-3-indolyl phosphate/nitro blue tetrazolium

BCS: Bathocuproinedisulfonic acid disodium salt

c-di-GMP: Cyclic diguanylate

CIP: Calf Intestinal Alkaline Phosphatase

Cm: Chloramphenicol

CyDisCo: Cytoplasmic disulphide bond formation in *E. coli*

DMEM: Dulbecco's Modified Eagle Medium

Dsb: Disulphide bond

DTNB: 5,5′-Dithiobis(2-nitrobenzoic acid)

DTT: Dithiothreitol

EDTA: Ethylenediaminetetraacetic acid

Erv1p: Yeast mitochondrial thiol oxidase

ESI: Electrospray ionization

FAD: Flavin adenine dinucleotide

GFP: Green fluorescent protein

GSH: Glutathione

GSNO: S-Nitrosoglutathione

GSSG: Glutathione disulfide

hGH: human Growth Hormone

His: Histidine

IFN-γ: Interferon-gamma

IgG: Immunoglobulin G

iNOS: Inducible nitric oxide synthase

IPTG: Isopropyl-β-D-thiogalactoside

Kan: Kanamycin

LB: Luria Bertani broth

LIC: Ligation independent cloning

LMT: low molecular weight thiol

LPS: Lipopolysaccharide

M9: Minimal media

mAb: Monoclonal antibody

MALDI: Matrix-assisted laser desorption/ionization

MOI: Multiplicity of Infection

NADPH: Nicotinamide adenine dinucleotide phosphate

NLR: NOD-like receptor

NO: Nitric oxide

OD: Optical density

PAGE: Polyacrylamide gel electrophoresis

PAMP: Pathogen-associated molecular patterns

PBS: Phosphate-buffered saline

PDB: Protein Data Bank

PDI: Protein Disulphide Isomerase

PMSF: Phenylmethylsulfonyl fluoride

PRR: Pattern recognition receptor

PVDF: Polyvinylidene difluoride

RBS: Ribosome binding site

RNS: Reactive nitrogen species

ROS: Reactive oxygen species

Scs: Suppressor of copper sensitivity

SCV: *Salmonella* containing vacuole

SDS: Sodium dodecylsulphate

Sec: General secretory pathway

SEM: Standard error of mean

SOC: Super Optimal broth with Catabolite repression

SOD: Superoxide dismutase

SPI: *Salmonella* pathogenicity islands

SRP: Signal Recognition Particle

Strep: Streptomycin

T3SS: Type 3 secretion system

Tat: Twin-arginine translocase

TEMED: Tetramethylethylenediamine

TEV: Tobacco Etch Virus

TFA: Trifluoroacetic acid

TLR: Toll-like receptor

TOF: Time of flight

TRX: Thioredoxin

UPLC: Ultra Performance Liquid Chromatography

WT: Wild-type strain

List of Figures

Figure 1.1- *Salmonella* invasion and replication.

Figure 1.2- Generation of ROS.

Figure 1.3- Production of RNS.

Figure 1.4- Copper detoxification of *Salmonella.*

Figure 1.5- Disulphide bond formation.

Figure 1.6- The archetypal DsbAB system of *E. coli.*

Figure 1.7- Dsb like proteins encoded by *S.* Typhimurium.

Figure 1.8- The *scs* locus of *S.* Typhimurium.

Figure 1.9- Subcellular localisation of StScs proteins of *Salmonella typhimurium.*

Figure 1.10- Structural orthologs of StScsC.

Figure 2.1- The structure of AMS and the formation of an intra-protein disulphide.

Figure 2.2- Model for macrophage infection studies.

Figure 3.1- Sequence alignment of ScsC proteins.

Figure 3.2- The abundance of StScsC in the *Salmonella* periplasm.

Figure 3.3- Western blot detection of StScsC in cells exposed to divalent metals.

Figure 3.4- Western blot detection of StScsC in cells exposed to a variety of stresses.

Figure 3.5- Cloning of a *scsA*-GFP transcriptional fusion plasmid.

Figure 3.6- Impact of copper upon growth and *scsA* promoter activity in *S.* Typhimurium.

Figure 3.7- P*scsA* activity with increasing concentrations of Cu^{2+}.

Figure 3.8- GFP expression of *S.* Typhimurium harbouring the pET23b-P*scsA*-GFP fusion plasmid.

Figure 3.9- Western blot analysis of purified his_6-tagged GFP from *S.* Typhimurium harbouring pET23-P*scsA*-GFP.

Figure 3.10- Excitation and emission spectra of GFP from copper induced cells harbouring pET23-P*scsA*-GFP plasmid.

Figure 3.11- Determination of the *in vivo* redox state of StScsC by Western blotting.

Figure 3.12- Proteomic quantitation of disulphide-containing periplasmic/secreted proteins that have altered abundance in response to copper and StScsC.

Figure 3.13- Fold-changes elicited by copper and StScsC for disulphide-containing periplasmic/secreted proteins.

Figure 3.14- Function of disulphide/cysteine-containing proteins that have altered abundance in response to copper and StScsC.

Figure 3.15- Crystal structure of *Salmonella* BcsC.

Figure 3.16- Amino acid sequence of BcsC.

Figure 3.17- Normalised abundance of reduced and oxidised peptide fragments of BcsC in the *S.* Typhimurium periplasm.

Figure 3.18- StScsC promotes *S.*Typhimurium survival within macrophages during copper stress.

Figure 4.1- SDS-PAGE analysis of purified StScsC.

Figure 4.2- SDS-PAGE analysis of purified TEV protease.

Figure 4.3- SDS-PAGE analysis of cleavage of his_6-tag from purified StScsC.

Figure 4.4- Absorbance spectra of BCS and StScsC with Cu^+.

Figure 4.5- Binding curve of BCS and StScsC to Cu^+ at $A_{483\text{-}550.}$

Figure 4.6- Model for trapping StScsC substrates.

Figure 4.7- Plasmid map for $scsC_{CXXA}$ cloned into pSU2718 vector plasmid.

Figure 4.8- Analysis of DNA fragments for cloning of pSU2718$scsC_{CXXC}$His.

Figure 4.9- SDS-PAGE analysis of purified $StScsC_{CXXA}$ protein.

Figure 4.10- Detection of purified StScsC and the substrate.

Figure 4.11- StScsC forms a disulphide bond with ArtI *in vivo*.

Figure 4.12- Sequence alignment of ArtI from *E. coli* and *S.* Typhimurium.

Figure 4.13- Amplified *artI* and pTrcHis vector.

Figure 4.14- Desired plasmid map of *artI* cloned to pTrcHis vector plasmid.

Figure 4.15- Confirmation of *artI* cloned into pTrcHis vector.

Figure 4.16- SDS-PAGE gel of purified ArtI.

Figure 4.17- ArtI binding to StScsC.

Figure 4.18- Addition of copper dimerizes $StScsC_{CXXA.}$

Figure 4.19- Wild-type StScsC does not dimerise in the presence of copper.

Figure 4.20- StScsC oxidises in the presence of copper.

Figure 4.21- SDS-PAGE analysis of thiol redox status of ArtI and StScsC.

Figure 4.22- ArtI alters the redox status of oxidised StScsC.

Figure 4.23- Crystal structure of *Salmonella* ScsC and structural model of ArtI.

Figure 4.24- Protein docking of ArtI and StScsC.

Figure 4.25- Loss of *scsC* abolishes L-arginine-mediated stimulation of growth.

Figure 5.1- Schematic structure of IgG1.

Figure 5.2- Herceptin inter- and intra-molecular disulphides.

Figure 5.3- Crystal structure of Herceptin Fab fragment.

Figure 5.4- The structure of hGH.

Figure 5.5- Fab pMK-RQ plasmid map.

Figure 5.6- pWSK29*scsABCD* plasmid map.

Figure 5.7- Expression and detection of Herceptin in *E. coli*.

Figure 5.8- Periplasmic protein concentration of *E. coli* is elevated by Cu^{2+}.

Figure 5.9- Copper ions elevate the yield of Herceptin in *E. coli* when StScsABCD proteins are expressed.

Figure 5.10- Densitometry analysis for expression of Herceptin light chain.

Figure 5.11- pKWK2 plasmid map expressing hGH.

Figure 5.12- A $StScsC_{CXXA}$:hGH_{C189S} disulphide bonded complex cannot be detected via Western blotting.

Figure 5.13- Model for Herceptin StScsC-catalysed disulphide folding.

Figure 6.1- Model for copper and StScsC in arginine sensing during intramacrophage survival.

List of Tables

Table 2.1- List of bacterial strains used in this study.

Table 2.2- List of plasmids used in this study.

Table 2.3- Amino acids required for preparation of 10X amino acid stock solution.

Table 2.4- Settings for the electroporator for Gram-negative bacteria.

Table 2.5- Oligonucleotides used in this study.

Table 2.6- Components required for 50 μL PCR reaction with Q5 DNA polymerase of DNA fragments.

Table 2.7- Settings used for PCR with Q5 DNA polymerase on Biometra T3000 Thermocycler.

Table 2.8- Components required for 25 μL PCR reaction with Taq DNA polymerase.

Table 2.9- Settings of Biometra T3000 Thermocycler for colony PCR.

Table 2.10- Components needed for dephosphorylation of DNA.

Table 2.11- Components required for preparation of buffers for protein purification.

Table 2.12- Components required for preparation of buffers for TEV protease buffer exchange.

Table 2.13- Components required for preparation of the reagents for Markwell assay.

Table 2.14- Recipes for stacking and resolving gels for SDS-PAGE.

Table 2.15- The list of antibodies used in this study.

Table 2.16- Components of buffers used in metal binding assay.

Table 3.1- A list of proteins orthologous to StScsC.

Table 3.2- Copper and StScsC influence protein abundance in the *S.* Typhimuruim periplasm.

Health and Safety

The work herein was undertaken following an appropriate Genetically Modified Organisms (GMO) risk assessment.

The host lab has approval from the Health and Safety Executive (HSE) to genetically manipulate Class II bacterial pathogens.

Poster presentations

Buke Yucel; Mark Shepherd. The Scs proteins of *Salmonella*: Applications and *in vivo* roles for a new disulphide-folding system. Metals in Biology BBSRC NIBB Community Meeting, Durham, December 2016.

Buke Yucel; Mark Shepherd. The Scs proteins of *Salmonella*: insights into the *in vivo* role of a novel thioredoxin-like protein. Protein disulphide bonds-biochemistry, biotechnology and biomedical impact, Kent, September 2018.

Buke Yucel. The Scs proteins of *Salmonella*: insights into the *in vivo* role of a novel thioredoxin-like protein. International Symposium *Salmonella* and Salmonellosis (I3S). Saint Malo, September 2018.

Chapter 1

Introduction

1.1- *Salmonella* taxonomy, serovars and diseases

Salmonella are rod-shaped, Gram-negative motile bacteria belonging to the family Enterobacteriaceae (Andino and Hanning, 2015). The *Salmonella* genus is subdivided into two species; *Salmonella enterica* and *Salmonella bongori* (Lan *et al.,* 2009; review). By using the Kauffman-White scheme, more than 2500 serotypes of *Salmonella* have been identified (Eng *et al.,* 2015; review; Ryan *et al.,* 2017; review).

The main niche of *Salmonella* serovars is the intestinal tract of humans and farm animals which is one of the major causes of foodborne disease. It mostly associates with contaminated pig, poultry and bovine meat and due to poor standards of hygiene (contaminated food and water), *Salmonella* is a continuing risk of infection (Broz *et al.,* 2012; review; Andino and Hanning, 2015).

S. enterica serovar Typhi and *S. enterica* serovar Paratyphi A leads to typhiod fever in humans and higher primates (Eng *et al.,* 2015; review). However, the non-typhoidal *Salmonella* strain *S. enterica* serovar Typhimurium has a wider range of hosts including humans, rodents, and cattle (Garai *et al.,* 2012; review), and can lead to gastroenteritis in humans with symptoms including diahorrea, fever, stomach pain and nausea, and can lead to a systemic infection similar to typhoid fever in susceptible mice (Miki *et al.,* 2004).

1.2- *Salmonella* host invasion and survival

Almost all strains of *Salmonella* are pathogenic as they have the ability to invade, replicate and survive in host cells, resulting in potentially fatal disease. The ability of *Salmonella* strains to persist in the host cell is crucial for pathogenesis, as strains lacking this ability are non-virulent (Eng *et al.,* 2015; review). When *Salmonella* enters the digestive tract via contaminated water or food, it tends to penetrate the epithelial cells on the intestinal wall. *Salmonella* can adhere and translocate into eukaryotic epithelia across M cells of Peyer's patches, or membrane of the epithelial cells are modified via the action of *Salmonella* pathogencity islands leading to entry of bacteria. *Salmonella* can also be engulfed by the dendritic cells (Garai *et al.,* 2012; review; Fabrega and Vila, 2013; review). Figure 1.1 shows the mechanism of *Salmonella* invasion of eukaryotic epithelia through M cells where most of the bacterial cells have breached the epithelium. *Salmonella* pathogenicity islands (SPIs)

are gene clusters that encode the most important genetic determinants for *Salmonella* virulence (Hurley *et al.*, 2014; review), and have been acquired during the evolution of *Salmonella* into a successful pathogen from its Enterobacteriaceae ancestor (Hacker and Carniel, 2001; review). The major type 3 secretion systems (T3SS) of *Salmonella* are encoded by two pathogenicity islands, SPI-1 and SPI-2 (Garai *et al.*, 2012; review; Coburn *et al*., 2007; review).

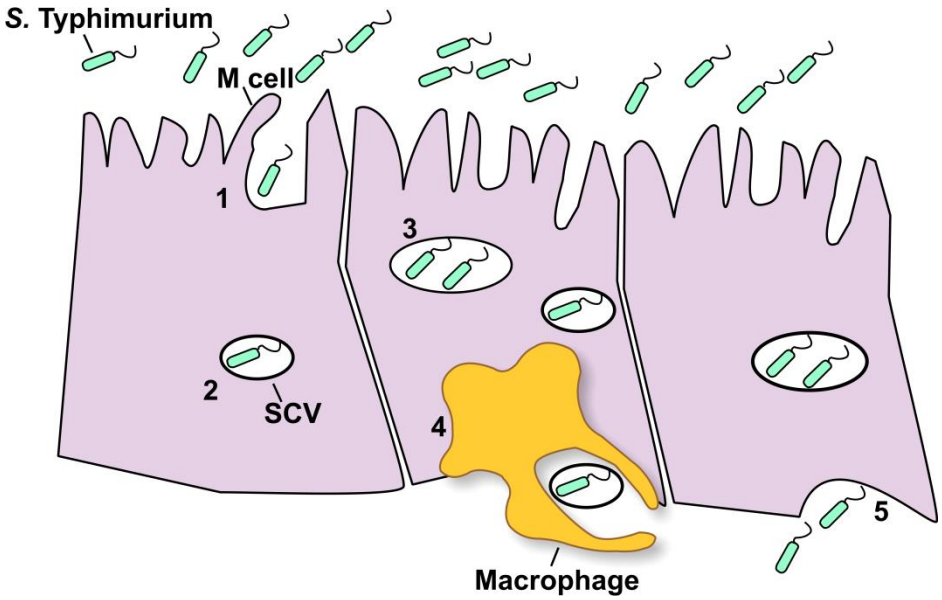


Figure 1.1- *Salmonella* invasion and replication. (1) *Salmonella* is attached to the intestinal epithelium by targeting the M cells. For epithelial invasion and induction of the membrane ruffling, InvJ, InvG, SipB and SipC proteins, encoded by SPI-1, form the needle assembly and modulate the actin cytoskeleton for the injection of bacterial effector proteins. **(2)** *Salmonella* is localised within the *Salmonella* containing vacuole (SCV) inside the eukaryotic cytoplasm. **(3)** *Salmonella* can replicate and survive in the SCV by producing effectors encoded by SPI-2. The SifA effector is secreted for maintenance of the membrane integrity. **(4)** *Salmonella* are internalised by macrophages for killing. **(5)** Internalised *Salmonella* can be released to the submucosa and can be engulfed by the macrophages (Ibarra and Steele-Mortimer, 2009; review; Garai *et al.*, 2012; review; Fabrega and Vila, 2013; review).

The T3SS machinery is regulated by different environmental signals and delivers effector proteins to the host cell membrane and cytosol in Gram-negative bacteria. The T3SS apparatus is a needle-like structure secreting translocons that allow access of secreted effectors to the eukaryotic host cell by forming pores (Waterman and Holden, 2003; review). Expression of SPI-1 T3SS is controlled by two distinct regulatory proteins HilA and InvF (Groisman and Ochman, 1997; review) triggering

invasion of the epithelial cells in *S.* Typhimurium (Srikanth *et al.*, 2011; review). Proteins secreted from the Inv/Spa system are necessary for the formation of cell-surface appendages upon contact with the host epithelial cell and for the assembly of needle-like complexes (Groisman and Ochman, 1997; review). Effector proteins are then translocated into the host cell cytosol in an ATP dependent manner (Green and Mecsas, 2016; review) through the pore formed by SipBCD proteins in the host cell membrane (Fabrega and Vila, 2013; review). Delivery of effectors induces actin cytoskeletal rearrangements resulting in the formation of membrane ruffles that engulf bacteria in large vesicles called *Salmonella*-containing vacuoles (SCVs) (Knodler and Steele-Mortimer, 2003; review), where *Salmonella* can replicate and survive (Garai *et al.*, 2012; review). In addition, *S.* Typhimurium SPI-1 T3SS effectors also trigger the activation of mitogen-activated protein kinase pathways, leading to the production of proinflammatory cytokines inducing acute intestinal inflammation (Srikanth *et al.*, 2011; review). In a mouse model for systemic infection, mutations that affect secretion the SPI-1 effectors have been shown to impair virulence of *S.* Typhimurium (Waterman and Holden, 2003; review).

Upon delivery of the antimicrobial host factors such as free radical generating complexes to the SCV, a series of SPI-2 T3SS virulence factors are synthesised for biogenesis and maintenance of the SCV membrane, impairing the transport of antimicrobials into the SCV and promoting survival and replication of the invading bacteria (Srikanth *et al*., 2011; review; Coburn *et al*., 2007; review). SPI-2 virulence factors remodel the SCV in such way that impairs fusion of the lysosome to the SCV (Eng *et al.,* 2015; review). NADPH oxidase-dependent killing and localisation of the iNOS to the SCV (described in detail on further sections) by macrophages are also avoided (Vazquez-Torres *et al.*, 2000; Chakravortty *et al.*, 2002).

1.3- Host response and bacterial defence mechanisms

Innate and adaptive immune responses are mediated by macrophages that play an essential role in defence against pathogens. Once the pathogen can start to replicate and survive in the SCV, recognition of *Salmonella* by the host immune system is crucial for mounting an immune response (Gogoi *et al*., 2018; review) such as creating anti-microbial milieu with an acidified pH, the generation ROS/ RNS

(reactive oxygen species/ reactive nitrogen species), elevation of protease levels, and the mobilization of iron (Festa and Thiele, 2012; review). Macrophages sense the presence of conserved pathogen-associated molecular patterns (PAMPs) of bacteria via pattern recognition receptors (PRRs) like Toll-like receptors (TLRs) and NOD-like receptors (NLRs) (Kawasaki and Kawai, 2014; review). TLR induces the expression of interferon gamma (IFN-γ) which in turn promotes the activation of macrophages which enhance oxidative (Foster *et al*., 2003) and nitrosative (Vazquez-Torres *et al.,* 2000) killing of pathogens. Antimicrobial peptides are released from macrophages which are positively charged basic amino acids and hydrophobic amino acids that can interact with the Lipopolysaccharide (LPS) on the bacterial membrane resulting in pore formation (Gogoi *et al.,* 2018; review). The pH of the phagosome is lowered and proteases are also released for bacterial killing in the SCV (Hirayama *et al.,* 2018; review; Flannagan *et al*., 2009; review). Coordinated delivery of toxic substances following phagocytosis starts of by production of reactive oxygen species (ROS), and once the ROS production diminishes then iNOS-mediated nitrosative stress is induced. In addition, bacterial replication can be controlled by limitation of the metal ion availability (Gogoi *et al.,* 2018; review).

Salmonella is a very successful enteric pathogen because it produces virulence factors that inhibit the delivery of antimicrobials and promote survival and replication in the phagosome when engulfed by macrophages (Fabrega and Vila, 2013; review). Selected host antimicrobial responses and *Salmonella* defence mechanisms are described in the following sections.

1.3.1- Reactive oxygen species (ROS)

The phagocytic oxidative burst is a primary effector of innate immunity that protects against bacterial infection (Vazquez-Torres *et al.,* 2000). Superoxide ($O_2^{\cdot -}$) is synthesised by the multi-subunit enzyme nicotinamide adenine dinucleotide phosphate (NADPH) oxidase, which is expressed at the site of phagocytosis and incorporated into the phagosome membrane (Linehan and Holden, 2003; review). Superoxide is also produced endogenously in the bacteria by the transfer of an electron to O_2 from flavoproteins such that NADH dehydrogenase II generates superoxide and hydrogen peroxide by autoxidation of its reduced cofactor FAD (which receives electrons from NADH) (Messner and Imlay, 1999). Superoxide can

readily interact with a pathogen or can react with other antimicrobial molecules such as nitric oxide to form the strong oxidant peroxynitrite (Liochev and Fridovich, 1999; review). The flux of superoxide to the bacterial cytoplasm is allowed when the superoxide is protonated in the acidified phagosome (Craig and Slauch, 2009). Cytoplasmic superoxide can directly oxidise and inactivates iron–sulphur clusters in proteins resulting in cluster degradation and release of iron. Dismutation of superoxide by superoxide dismutase enzymes (SOD) leads to the production of hydrogen peroxide (H_2O_2), which is capable of producing toxic hydroxyl radicals ($^{\bullet}OH$) when reduced with free iron (Figure 1.2) released during the oxidation of iron-sulphur clusters (Liochev and Fridovich, 1999; review). Reactive oxygen species are toxic to intracellular pathogens causing DNA damage, lipid peroxidation and protein carbonylation (Craig and Slauch, 2009; Fang, 2004; review; Wang *et al.*, 2018; review).

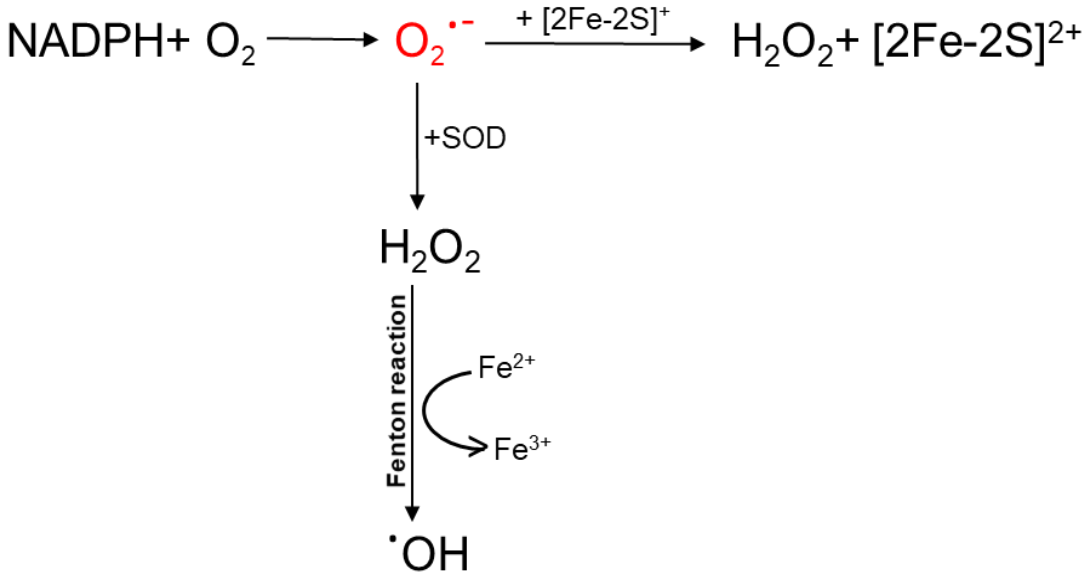


Figure 1.2- Generation of ROS. Superoxide ($O2^{\bullet-}$) is generated by the reduced NADPH. Superoxide can then directly oxidise the Fe-S cluster, converting the $[4Fe\text{-}4S]^{2+}$ form to an unstable $[4Fe\text{-}4S]^{3+}$ state, releasing hydrogen peroxide (H_2O_2). Superoxide also rapidly dismutes, either enzymatically or spontaneously, to form H_2O_2, which is reduced by the free iron that is released from iron-sulphur cluster degradation, to form hydroxyl radical ($^{\bullet}OH$) via the Fenton reaction.

Cellular damage may also result from the oxidation of cysteine residues by oxidative stress. Free thiol groups (-SH) are oxidised by ROS forming sulfenic (-SOH), sulfinic ($-SO_2H$) and sulfonic acids (SO_3H), generating conformational change in protein structure and affecting protein activity (Lo Conte and Caroll, 2013; review).

Protection mechanisms against ROS are crucial for bacterial survival (Cho *et al.,* 2012). *Salmonella* can directly prevent reactive oxygen species damage by inhibiting the localisation of NADPH-oxidase containing vesicles to the SCV by SPI-2 virulence factors (Vazquez-Torres, 2012; review).

One of the most important classes of enzymes that catalyse the detoxification of ROS by conversion of superoxide to hydrogen peroxide is superoxide dismutases (SOD) (Wang *et al.,* 2018; review). SOD enzymes control the levels of a variety of reactive oxygen species and reactive nitrogen species (Craig and Slauch, 2009). Two cytoplasmic (SodA and SodB) and two periplasmic (SodCI and SodCII) superoxide dismutases are encoded by *S.* Typhimurium for decreasing the effect of the oxidative burst of phagocytes (Wang *et al.,* 2018; review; Fenlon and Slauch, 2017; Kim *et al.,* 2010). Loss of SOD activity has also been shown to increase the levels of oxidative damage in *Salmonella* (Wang *et al.,* 2018; review).

1.3.2- Nitric oxide

Reactive nitrogen species contain unpaired electrons with high reactivity. They can donate or obtain electrons initiating chemical reactions and damaging living cells (Phaniendra *et al.,* 2015; review). In the mammalian immune system, nitric oxide (NO) is synthesized by an inducible nitric oxide synthase (iNOS) enzyme, which catalyses the production of nitric oxide from L-arginine and oxygen in activated macrophages (Linehan and Holden, 2003; review) (Figure 1.3) to inhibit bacterial growth in phagocytes. In response to bacterial lipolysaccharide (LPS), IFNγ-dependent signalling cascades upregulate the expression of iNOS (Henard and Vázquez-Torres, 2011; review; Fang, 1997; review). iNOS-deficient mice have been shown to be more susceptible to *S.* Typhimurium (Alam *et al*., 2002). Nitric oxide reacts with many intracellular molecules causing production of reactive nitrogen intermediates. It can exert its toxicity by destruction of iron-sulphur clusters, leading to release of Fe^{2+} which can in turn promote formation of hydroxyl radicals by

reacting with H_2O_2 (Kröncke *et al.*, 1997; review). NO can also reacts with proteins containing reduced cysteine residues and yields S-nitrosothiols (Kröncke *et al.*, 1997; review; Singh *et al.*, 1996). When NO reacts with superoxide, a reactive nitrogen species (RNS) known as peroxynitrite ($ONOO^-$) is produced. $ONOO^-$ is both a strong oxidant and a nitrating agent towards a wide range of macromolecules (Henard and Vázquez-Torres, 2011; review). Decomposition of $ONOO^-$ also results in the formation of reactive species such as $^{\bullet}OH$ and $^{\bullet}NO_2$ (Fang, 2004; review). NO has also been shown to inhibit the transcription of SPI-2 virulence genes within *S.* Typhimurium, which contributes to the killing of intracellular *Salmonella* by IFNγ-primed macrophages (McCollister *et al.*, 2005).

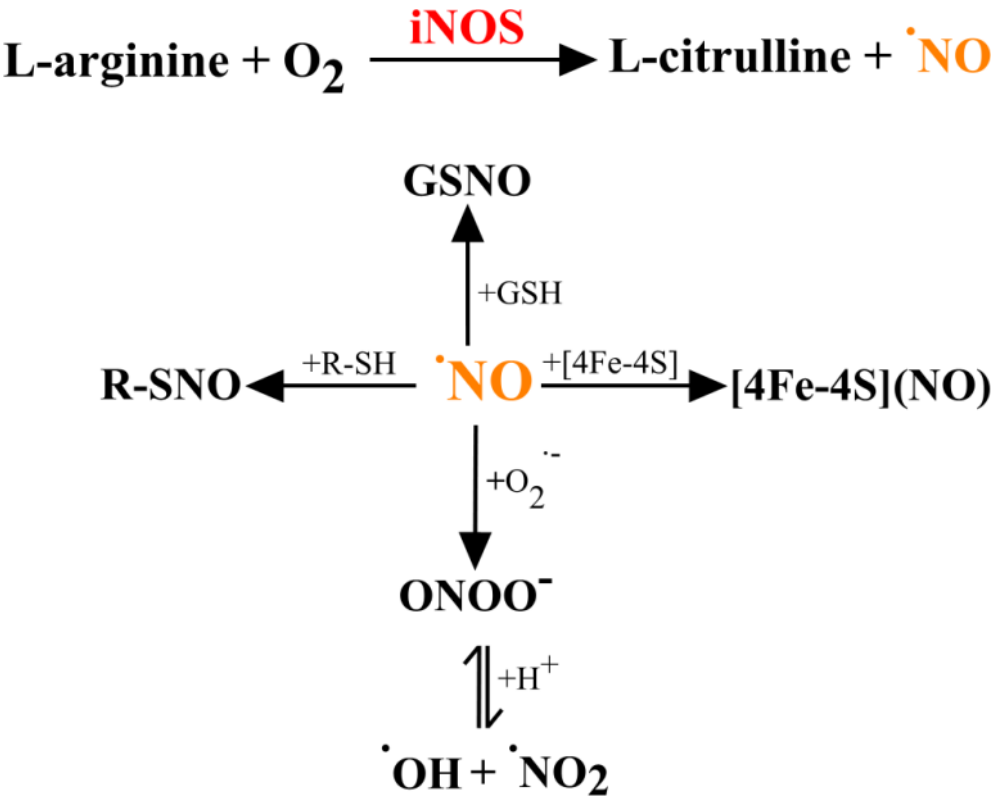


Figure 1.3- Production of RNS. iNOS provides sustained bacteriostatic effect contributing to macrophage antibacterial activity against *Salmonella* by catalysing the formation of nitric oxide ($^{\bullet}NO$) from L-arginine and oxygen. $^{\bullet}NO$ can then react with glutathione (GSH) to form S-nitrosoglutathione (GSNO), an *S*-nitrosating agent. It can destroy [4Fe-4S] clusters leading to the formation of iron-nitrosyls. $^{\bullet}NO$ can react with superoxide to produce peroxynitrite ($ONOO^-$) and lastly, it can bind to reduced thiols groups producing S-nitrosythiols. All these reactive nitrogen species lead to protein and DNA damage as well as lipid peroxidation and promote bacterial killing.

Salmonella has many mechanisms by which it conteracts the RNS employed by the host. As an intracellular pathogen, *Salmonella* possesses several strategies that avoid contact with iNOS-containing vesicles, detoxify NO, or repair lesions incurred by RNS exposure. Mechanisms by which *Salmonella* promotes survival in the presence of RNS can be established by limiting the substrate for iNOS (L-arginine) which will block the formation of NO (Weiss and Schaible, 2015; review). Cationic amino acid transporters mCAT1 and mCAT2B are utilized by *Salmonella* to acquire host arginine towards its own intracellular growth (Das *et al.,* 2010). The effects of peroxynitrite that causes both oxidative and nitrosative stress (through generation of $^{\bullet}OH$ and $^{\bullet}NO_2$) can be reduced by the alkyl hydroperoxidase (AhpC) which can catalyse the reduction of peroxides and peroxynitrites (Vatansever *et al.,* 2013; review) or indirectly by SOD that detoxifies ROS thus preventing $ONOO^-$ formation (Osman *et al.,* 2013). Effectors secreted by the type III secretion system encoded within SPI-2 prevent contact with vesicles containing iNOS (Chakravortty *et al.,* 2002). Lastly, enzymatic detoxification of RNS by Hmp (upregulated in response to NO) limits the accumulation of low-molecular weight nitrosothiols in *Salmonella*-infected macrophages (Henard and Vázquez-Torres, 2011).

1.3.3- Copper

Copper is a transition metal which is an essential micronutrient for all kingdoms of life as a biochemical cofactor and signalling molecule. It is required for fundamental metabolic processes, but can be toxic when accumulated in excess beyond cellular needs due to its redox properties (Besold *et al*., 2016; review). During systemic infection copper is required to attack invading pathogens and maintain immune function in macrophages (Fu *et al.,* 2014; review; Besold *et al*., 2016; review; Li *et al.,* 2019; review). The import of copper into the phagosome is elevated after bacterial internalisation (Fenlon and Slauch, 2017), where toxic levels can cause antimicrobial effects. In the absence of copper, the ability of phagocytes to kill engulfed *S.* Typhimurium has been shown to be diminished (White *et al.,* 2009). The ability of macrophages delivering copper ions to the phagosome and the copper detoxification mechanisms employed by *S.* Typhimurium are described below (Figure 1.4).

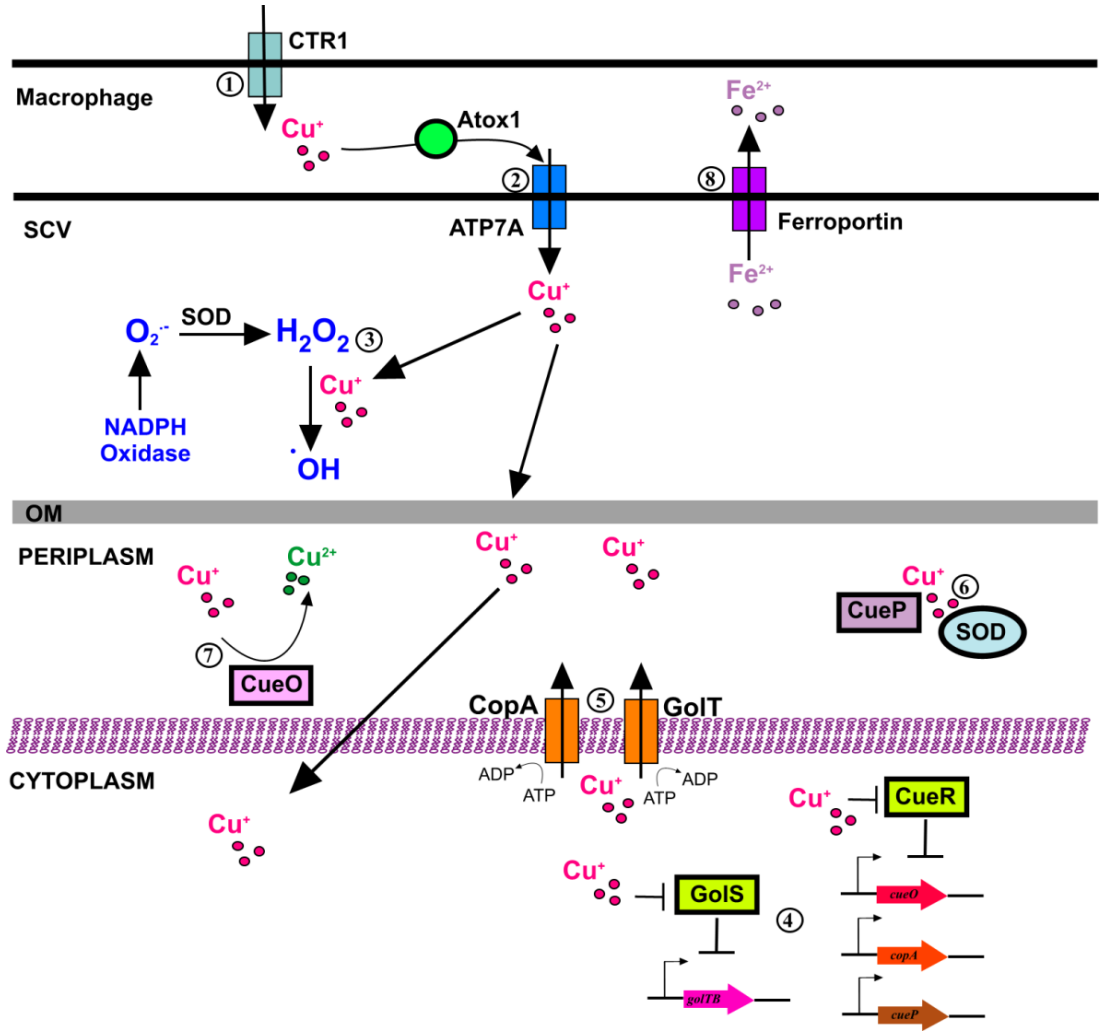


Figure 1.4- Copper detoxification of *Salmonella.* During infection, **(1)** copper is imported to the macrophages via CTRI copper transporter. **(2)** Copper is then binds to Atox1 chaperone and transferred into the SCV by Cu^{+}-transporting P_{1B}-type ATPase ATP7A. **(3)** Copper can react with host-generated hydrogen peroxide to generate free radicals, which damage biological molecules. Copper is transported into *Salmonella* by unknown mechanisms. **(4)** Elevated concentrations of copper binds to GolS and CueR and activate the expression of *copA*, *golT* and *cueO*. **(5)** Copper toxicity in the *Salmonella* cytoplasm is avoided by CopA and GolT copper efflux pumps that pump copper to the periplasm. **(6)** Cu^{+} in the periplasm is delivered to the SOD proteins to be used in ROS detoxification. Also, **(7)** Cu^{+} is converted to the less toxic from Cu^{2+} by CueO. **(8)** Iron efflux by Ferroportin inhibits bacterial replication (Argüello *et al.*, 2013; review; Fu *et al.*, 2014; review).

Delivery of copper from the macrophage to the pathogen is mediated by upregulation of the copper importer CTR1 leading to copper (Cu^{+}) import into activated macrophages (Stafford *et al.*, 2013; review; Festa and Thiele, 2012; review). With the increased expression of copper-specific transporter ATP7A, Cu^{+} is then recruited into the phagosome. Silencing of ATP7A has been shown to impair bactericidal activity, suggesting that ATP7A is required for bacterial killing (White *et al.*, 2009).

The influx of copper into the phagosome promotes bacterial killing in many different ways. Copper is highly reactive and is capable of binding to numerous ligands within a cell. For example, Cu^{+} binding to thiol groups of cysteines and methionines, and Cu^{2+} binding to oxygen and imidazole groups of aspartic/glutamic acids or histidine, can impact upon protein function resulting in toxic effects (Inesi, 2017; review). Furthermore, copper is redox active and can switch between Cu^{+} (reduced) and Cu^{2+} (oxidised) states (Ma *et al.,* 2009), and can promote the formation of non-native disulphide bonds in bacteria leading to protein misfolding and inactivation (Hiniker *et al.,* 2005).

Copper accumulation in the phagosome of macrophages can catalyse Fenton chemistry in the presence of hydrogen peroxide, leading to oxidative damage (White *et al.,* 2009). Excess copper can also disrupt iron-sulphur clusters, displacing and releasing iron, thus, further exacerbating radical production via Fenton chemistry (Porcheron *et al*., 2013; review). Proteins containing iron-sulphur clusters have been identified as targets for copper poisoning (Djoko *et al.,* 2017). Oxidative stress induced by copper and iron results in the formation of reactive hydroxyl radicals which are potent oxidants of DNA causing DNA and lipid membrane damage and can eventually lead to cell death (Macomber and Imlay, 2009). Conversely, excess iron has been shown to increase intracellular survival of *Salmonella*, although macrophages infected with *S.* Typhimurium restrict iron access to the pathogen and inhibit bacterial replication by upregulation of the iron export protein ferroportin1 to elevate iron efflux (Brown *et al.,* 2015).

To counteract the toxic effects of copper, many copper sensing systems and export mechanisms are employed by *S.* Typhimurium that provide tolerance to the host-derived copper that is encountered during infection (Fu *et al.,* 2014; review). Copper export is performed by the *cus* system in *E. coli* (Argüello *et al.,* 2013; review). However, the *cus* system is absent in *S.* Typhimurium, instead it encodes the *cue* and *gol* systems to respond to host-derived copper (Osman *et al.,* 2010). Once the copper ions are in the cytoplasm of *S.* Typimurium, copper-responsive MerR-family transcriptional regulator CueR detects elevated copper levels in macrophages and mediates the copper-induced expression of *cueO* and *copA* genes as well as *cueP* gene (Espariz *et al.,* 2007; Osman *et al.,* 2013). CopA is a cytosolic copper exporter involved in Cu^{+} export from the cytoplasm to the periplasm (Argüello *et al.,* 2013;

review). GolT is a second P1B-type ATPase metal transporter promoting copper efflux to the periplasm which is induced by copper and gold responsive transcription factor GolS (Ladomersky and Petris, 2016; review). Upon efflux of copper to the periplasm, copper binds to the copper chaperone CueP which delivers copper ions for metalloenzymes such as periplasmic copper zinc superoxide dismutases (SodCI and SodCII), and protects against extracellular superoxide stress and phagosomal killing (Fenlon and Slauch, 2017). Copper-sensitive mutants of *S.* Typhimurium, lacking *copA* and *golT*, were more sensitive to macrophage-mediated killing than wild-type cells (Osman *et al.*, 2010).

In the periplasm, the multicopper oxidase CueO neutralizes the toxicity of highly reactive Cu^{+} by oxidising it into less toxic Cu^{2+} form (Fenlon and Slauch, 2017; Hodgkinson and Petris, 2012; review), and possibly slows the entry of copper into the cytoplasm (Macomber and Imlay, 2009).

1.4- Mechanisms of periplasmic disulphide bond formation in bacteria

The formation of disulphide bonds in extracytoplasmic proteins containing more than one cysteine residue takes place in the oxidising periplasm in Gram-negative bacteria (Kadokura *et al.*, 2003; review). The formation of inter- and intra-molecular disulphide bonds between two cysteine residues are essential for protein stability, activity and overall structure (Bardwell *et al.*, 1993). Disulphide bonds are covalent cross-links that are formed by modification of the thiol groups of cysteine residues by thiol oxidoreductases belonging to the thioredoxin protein superfamily (Kadokura *et al.*, 2003; review) (Figure 1.5).

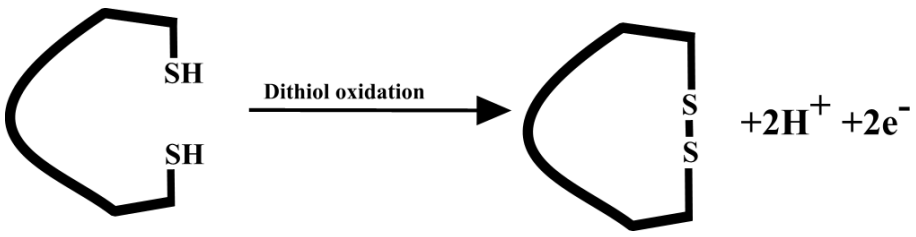


Figure 1.5- Disulphide bond formation. The formation of disulphide bonds involves a redox reaction whereby a covalent link between thiol groups (-SH) of cysteine residues is formed.

Thioredoxins are small antioxidant proteins that has been characterised from a variety of prokaryotes and eukaryotes playing a role in many cellular processes such as redox signalling and oxidative stress responses (Holmgren, 1995; review; Arts *et al*., 2016). The thioredoxin superfamily consists of enzymes that catalyse the reduction, formation, and isomerization of disulphide bonds thus maintaining the global redox environment in cells. They exert their activity through a redox active disulphide in a Cys-X-X-Cys motif and each member of thioredoxin like (TRX-like) enzymes have different redox midpoint potentials for their disulphide couples (Mössner *et al*., 1999; Bechtel and Weerapana, 2017; review).

In Gram–negative bacteria, extracytoplasmic proteins are expressed in the cytoplasm and then targeted to the periplasm or outer membrane via the Sec and TAT pathways with a cleavable N-terminal signal peptide (Tsirigotaki *et al.,* 2017; review). Once in the periplasm the signal peptide is cleaved, and disulphide bonds can then be introduced (Miot and Betton, 2004; review). While disulphide formation is facilitated by a number of protein chaperones, the redox poise is influenced by a variety of low molecular weight thiols (LMTs), which can have a profound effect upon disulphide formation. Glutathione (GSH) is the most abundant LMT that is found in many organisms. The ratio of oxidised/reduced forms of glutathione (GSSG/GSH) in the cell control the formation and reduction of protein disulphides through thiol-disulphide exchange reactions (Smirnova *et al.,* 2012; Bechtel and Weerapana, 2017; review). In *Salmonella typhimurium* strain ATCC 14028, GSH/GSSG ratio is 45 (GSH per cell is 0.72 mM and GSSG per cell is 0.017 mM) (Henard *et al.,* 2010).

Disulphide bond formation is of particular importance in the periplasm of pathogenic bacteria, where motility, type III secretion, and the assembly of a variety of secreted enzymes and toxins all rely upon disulphide folding machinery (Heras *et al.,* 2009; review). Many virulence factors are secreted proteins that are post-translationally modified via disulphide bond formation (Lasica and Jagusztyn-Krynicka, 2007; review). Inactivation of genes involved in the disulphide bond system leads to reduced virulence in many pathogens (Verbrugghe *et al*., 2016). The correct formation of disulphides in γ-proteobacteria proceeds via two routes: (i) disulphide oxidation and (ii) disulphide isomerisation. The archetypal DsbAB system in *E. coli* catalyses thiol oxidation via the periplasmic DsbA protein, and the electrons are then shuttled to the respiratory chain via the membrane protein DsbB (Bader *et al*., 1999). Non-native disulphides are then corrected by the periplasmic disulphide isomerase

DsbC, a process that is driven by electrons from the membrane protein DsbD (previously reviewed Depuydt *et al*., 2011; review) (Figure 1.6).

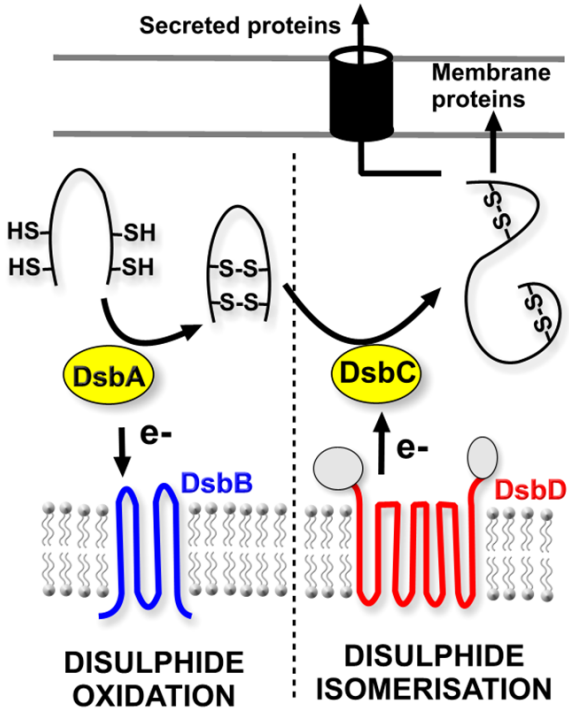


Figure 1.6- The archetypal DsbAB system of *E. coli.* Disulphide bonds are introduced into target proteins by disulphide exchange with the soluble periplasmic protein DsbA. The inner membrane protein DsbB reoxidizes DsbA. Misfolded proteins are reduced and corrected by DsbC. DsbD shuttles electrons from thioredoxins from the cytoplasm to maintain the active reduced state of DsbC.

The thioredoxin superfamily proteins contribute to the virulence of *S.* Typhimurium. Loss of *dsbA* in *Salmonella* blocks the secretion and translocation of SPI-1 and SPI-2 T3SS effectors into the host cells. DsbA is required for the formation of the T3SS apparatus as well as playing a role on disulphide formation of SpiA, an outer membrane protein of SPI-2 TTSS (Miki *et al.*, 2004). *S.* Typhimurium Δ*dsbA* mutants have decreased virulence by approximately 2,000-fold (Ellermeier and Slauch, 2004).

In addition to the DsbAB system, *S.* Typhimurium encodes plasmid-encoded SrgA which is an oxidoreductase that is similar to DsbA. The activity of SrgA is dependent upon the presence of DsbB. SrgA is responsible for the production of plasmid-encoded fimbriae by oxidation of the major fimbrial subunit, PefA (Bouwman *et al.*,

2003). SrgA has also been shown to form the disulphide bond of SpiA in Δ*dsbA E. coli* (Miki *et al.*, 2004). Furthermore, both loss of *srgA* and *dsbA* abolished the ability of *Salmonella* to infect mice, and both proteins have been suggested to be functionally important for the activity of SPI-1 T3SS (Miki *et al.*, 2004).

Thioredoxin 1 (Trx1) is the first member of the thioredoxin family discovered in *E. coli* (Buchner and Moroder, 2009). It is expressed in the cytoplasm, and reduces disulphides of the inner membrane protein DsbD (Rietsch *et al*., 1997), acts as a hydrogen donor for ribonucleotide reductase which provides deoxyribonucleotides for DNA replication (Holmgren, 1989; review) and catalyses the reduction of methionine sulfoxide residues which reduces methionine sulfoxide to methionine (Brot *et al*., 1981). The catalytic redox activity of Trx1 associated with *S.* Typhimurium virulence by diminishing intracellular survival in mouse infection models when absent (Bjur *et al.*, 2006).

In addition to the DsbAB system, *Salmonella enterica* serovar Typhimurium (*S.* Typhimurium) encodes a DsbLI oxidoreductase system that is similar to that found in uropathogenic *E. coli* (Totsika *et al.*, 2009). DsbL efficiently contributes to disulphide bond formation in the presence of DsbI, suggesting that these proteins function best together as a redox pair in *Salmonella* facilitating the folding of arylsulfate sulfotransferase (Grimshaw *et al.*, 2008; Lin *et al.*, 2009; Totsika *et al*., 2009) which catalyses the transfer of a sulfate group from phenolic sulfate esters (Kim *et al.*, 1992). Figure 1.7 demonstrates the subcellular locations and the roles of the Dsb like protein found in *S.* Typhimurium.

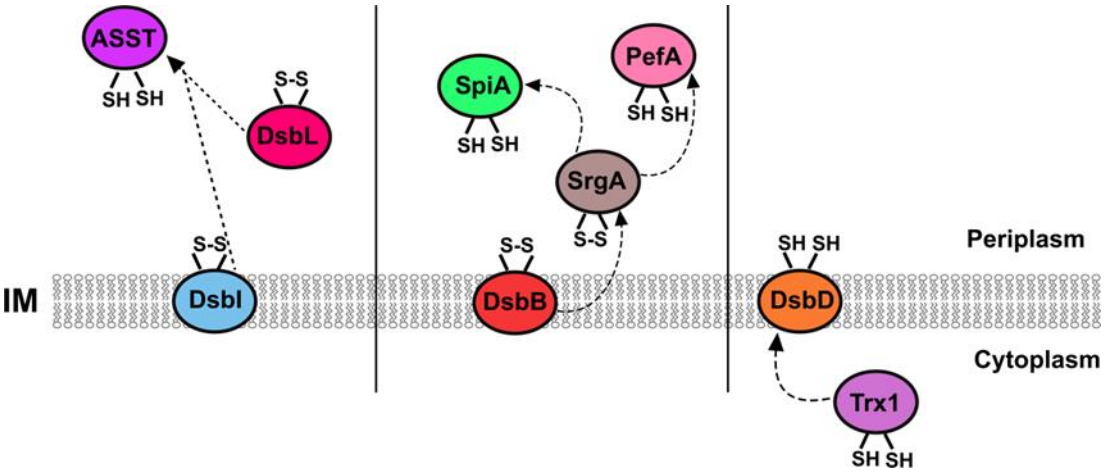


Figure 1.7- Dsb like proteins encoded by *S*. Typhimurium. DsbI is the inner membrane protein which works together with its redox partner DsbL to oxidatively fold ASST (arylsulfate sulfotransferase). DsbB is required for the oxidation of the periplasmic SrgA which promotes disulphide formation of PefA and SpiA. Cytoplasmic protein Trx1 is also required for the reduction of the disulphides of the inner membrane protein DsbD (Arts *et al*., 2016). IM- inner membrane.

In addition to these TRX-like proteins, *S.* Typhimurium encodes four TRX-like proteins at the *scs* locus (**s**uppressor of **c**opper **s**ensitivity), named after the first functional role to be assigned: the expression of the entire *scsABCD* operon was shown to restore tolerance to copper in copper-sensitive mutants of *E. coli* (Gupta *et al*., 1997), which is introduced in more detail below.

1.5- The Scs system

Investigation of genetic determinants involved in copper tolerance has led to the identification and characterisation of the *scs* locus (**s**uppressor of **c**opper **s**ensitivity) of *S.* Typhimurium. This locus encodes four proteins (ScsABCD) that alleviate copper sensitivity in *cut* mutants of *E. coli* (Gupta *et al.*, 1997). When genetic maps of the *E. coli* and *S.* Typhimurium were compared, the *scs* operon was found to be absent in *E.coli*. In *S.* Typhimurium, the *scs* locus is located between the *cbpA* and *agp* genes at the 4.36-kb DNA fragment of *S.* Typhimurium genome (Gupta *et al*., 1997) (Figure 1.8). The *scsA* gene encodes for a protein of 120 amino acids, and the *scsB* gene encodes a 627 amino acid protein 48 bp downstream of *scsA*. The *scsC* gene encodes for a 207 amino acid protein, and *scsD* encodes a protein of 168 amino acids (Gupta *et al.*, 1997).

It has been suggested that the *scs* locus had two promoter regions that regulate two transcripts encoding ScsA and ScsBCD (Gupta *et al.*, 1997). Until recently, the transcriptional regulation at this locus remained understudied. A recent study showed that deletion of the *scsA* gene results in the upregulation of the *scsBCD* operon, and that the *scsA* gene has a role in the proliferation of *S.* Typhimurium in cortisol-stressed macrophages where, firstly, cortisol induce cytoskeletal rearrangements of macrophage to facilitate increased SCV production and *scsA* contributing to alteration of bacterial virulence gene expression resulting in intracellular replication and maintenance (Verbrugghe *et al.*, 2016). Subsequent work has identified a CpxR-binding site upstream of the *scsA* gene in a number of enterobacteriaceae, and transcription of the *scs* operon was confirmed to be stimulated by the CpxR/A regulatory system (Lopez *et al.*, 2018), a well-known copper-responsive two-component system previously characterised in *E. coli* (Yamamato and Ishihama, 2005).

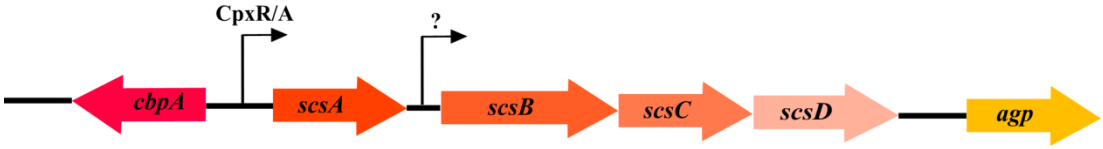


Figure 1.8- The *scs* locus of *S.* Typhimurium. The *scs* genes (*scsA, scsB, scsC* and *scsD*) are positioned at the region between the *cbpA* and *agp* genes with four complete open reading frames. Transcription of the *scs* operon is stimulated by copper responsive CpxR/A regulatory system found upstream of the *scsA* (Lopez *et al.*, 2018).

1.5.1- The ScsC proteins of other Gram-negative bacteria

Scs proteins are expressed in many other Gram-negative bacteria, including *Proteus mirabilis* (Furlong *et al.*, 2017), *Caulobacter crescentus* (Cho *et al.*, 2012), and species of *Citrobacter*, *Klebsiella* and *Yersinia* (Lopez *et al.*, 2018). Differences in the structures of ScsC among different species lead to variation in the function of the protein in different bacteria. The ScsB protein of *C. crescentus* (CcScsB) has been shown to maintain the ScsC protein (CcScsC) in a reduced state, which subsequently delivers electrons for peroxide reduction via redox interactions with peroxiredoxins (Cho *et al.*, 2012). Similarly, the ScsC protein of *P. mirabilis* (PmScsC) was found to be in the reduced state in the presence of copper (Furlong *et al.*, 2017), and the ScsB

protein (PmScsB) was found to provide reducing power for PmScsC-mediated disulphide isomerase activity (Furlong *et al.*, 2018). The PmScsC protein was found to be important for swarming activity in the presence of copper, although unlike StScsC it did not affect growth in the presence of copper in rich media (Furlong *et al.*, 2017). Furthermore, CcScsC and PmScsC are dimeric (Cho *et al*., 2012) and trimeric (Furlong *et al*., 2017), respectively, and this oligomerization is mediated via N-terminal extensions that are not present in the monomeric ScsC from *S.* Typhimurium (StScsC) (Shepherd *et al*., 2013; Furlong *et al*., 2017; Furlong *et al*., 2018). The presence and absence of the N-terminal extension of the ScsC orthologues from different species is illustrated by protein sequence alignment (Figure. 3.1). Given that the well-known disulphide isomerase of *E. coli* DsbC is also a dimer, this suggested that oligomerization of PmScsC was necessary for isomerase activity: indeed, deletion of the N-terminal oligomerization domain converted this protein into a monomeric dithiol oxidase (Furlong *et al*., 2017). These studies are consistent with two functionally distinct classes of ScsC protein.

1.5.2-The Scs proteins of *S.* Typhimurium

ScsA protein of *S.* Typhimurium (StScsA) is predicted to be a copper binding protein. ScsB (StScsB) is a DsbD-like membrane spanning protein (Gupta *et al.*, 1997). The ScsC (StScsC) is a soluble periplasmic monomer and ScsD (StScsD) is a membrane anchored protein (Shepherd *et al*., 2013). The subcellular localization of the StScs proteins are shown on Figure 1.9. Each StScs protein has a single CXXC motif with hydrophobic residues between the cysteine residues, which resembles the catalytic sites of the thioredoxin/glutaredoxin family of oxidoreductases (Anwar *et al.*, 2013).

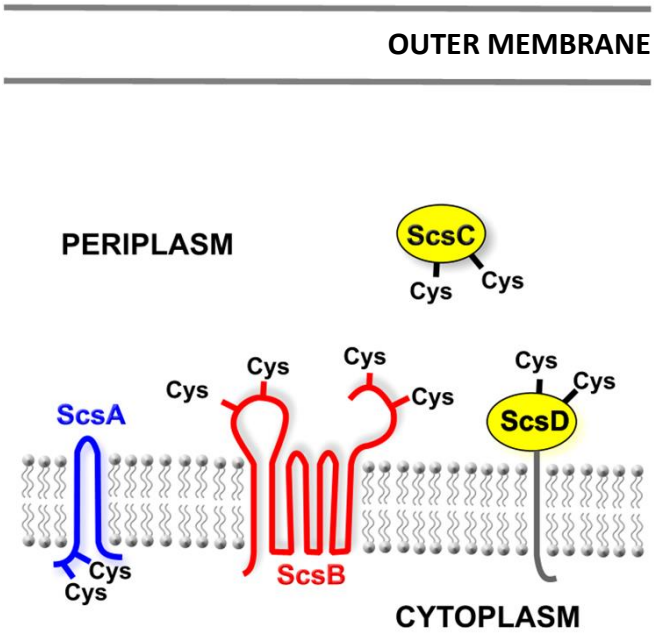


Figure 1.9- Subcellular localisation of StScs proteins of *Salmonella typhimurium*. All StScs proteins are encoded from the *scs* locus and are thioredoxin like proteins with CXXC catalytic motifs. The cysteine residues are shown. Amongst the StScs proteins, only StScsC is a fully soluble periplasmic protein.

1.5.2.1- Biochemical and structural characterisation of StScsC

StScsC has been crystallised and the structure of the soluble periplasmic protein has been characterised (Shepherd *et al.*, 2013). StScsC consists of a TRX domain and a long helical insertion like *Salmonella* DsbA (StDsbA) thus sharing overall structural similarity. However, there are differences on the TRX domains of the two proteins such that the TRX domain of the StDsbA consists 5 alpha helices whereas the alpha 5 helix is lost in the StScsC and is substituted by a short loop (Figure 1.10). In addition, StDsbA has a hydrophobic peptide-binding groove where DsbB binds. However, in StScsC, this groove adjacent to the catalytic active site is altered (Shepherd *et al*., 2013). Gram-positive *Bacillus subtilis* contain DsbA ortholog BdbD (BsBdbD) protein. The presence of a metal site of BsBdbD occupied by Ca^{2+} is the major difference between the two proteins, which leads to boost the oxidising power of the protein (Crow *et al*., 2009). Later on, BsBdbD has been shown to be the closest structural ortholog of StScsC however they only share 24% sequence identity (Shepherd *et al*., 2013). They share similar topology, having acidic patches in the groove between the TRX and the helical domain but BsBdbD has a more acidic surface around the catalytic active site (Shepherd *et al*., 2013). The electrostatic

surface of StScsC has also been shown to resemble that of StDsbA with a hydrophobic patch found adjacent to the catalytic site (Shepherd *et al*., 2013). A positively charged ridge next to the hydrophobic patch of StScsC is likely to stabilise the thiolate form of the active site cysteine. Presence of the positively charged ridge above the active site of the *E. coli* thiol reductase DsbG (EcDsbG) provides evidence that the catalytic active site of StScsC resembles that of EcDsbG.

The alternation between the oxidised and reduced states of the cysteine residues of the CXXC motif can be defined as the reduction potential ($E^{o\prime}$). The higher the reduction potential of the active site, the more oxidising the protein gets. The redox potentials of StScsC and structural orthologues are shown on Figure 1.10. pK_a value of the active cysteine residue of StScsC has been measured as 3.4 which is similar to that of oxidase *E. coli* DsbA (Shepherd *et al.,* 2013).

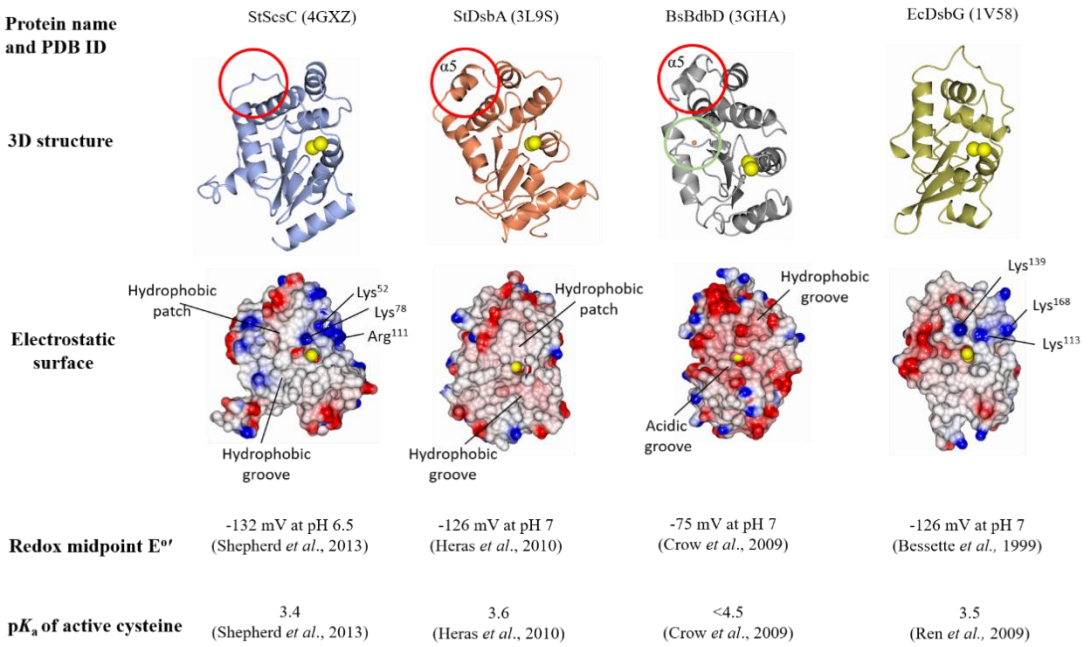


Figure 1.10- Structural orthologs of StScsC. 3D ribbon structure and the electrostatic surface of StScsC and the orthologous proteins are shown. Active cysteine residues were shown in yellow spheres. The absence of the usual α5 helix in StScsC is depicted by the red circle which is present in BsBdbD and StDsbA. Presence of Ca^{2+} was shown by the green circle on BsBdbD. Hydrophobic patches and the hydrophobic/ acidic grooves were shown on the electrostatic surfaces. Presence of positively charged residues around the catalytic active site of the StScsC and EcDsbG are shown. Reduction potentials of the catalytic active site and the pK_a values of the active cysteines are also shown. Reference couple for measuring the redox midpoint is normal hydrogen electrode (NHE).

1.5.2.2- Genetic approaches to investigate functional roles for the StScs proteins

As mentioned above, the *scsABCD* operon (supressor of copper sensitivity) of *Salmonella* restores copper tolerance of selected copper sensitive mutants of *E. coli* (Gupta *et al.*, 1997). Subsequent work confirmed this phenotype whereby an *scsC* mutant is sensitive to copper using disk diffusion assays (Shepherd *et al*., 2013). Indeed, there is a precedent for the involvement of thioredoxin-like proteins in copper tolerance, as the membrane-spanning DsbD (or DipZ) protein has previously been shown to confer tolerance to copper exposure (Fong *et al*., 1995). A subsequent study demonstrated that the conserved cysteine residues Cys^{163} and Cys^{285} of the ScsB homologue DsbD were required for copper tolerance in *E. coli* (Gordon *et al*., 2000). The observation that redox-active Cu^{2+}can directly promote the oxidation of disulphide bonds (Hiniker *et al*., 2005) is consistent with these numerous reports that link copper exposure to disulphide folding. Furthermore, given the potential impact of redox stress upon correct disulphide formation, it is unsurprising that the StScs system has also been reported to protect proteins from carbonylation resulting from hydrogen peroxide exposure (Lopez *et al.*, 2018; Anwar *et al.*, 2013). Growth curve experiments have confirmed that all Scs proteins are required for H_2O_2 tolerance in *S.* Typhimurium (Lopez *et al.*, 2018). In the presence of hydrogen peroxide, carbonylated proteins are accumulated in *S.* Typhimurium when *scsABCD* genes were absent. Thus, the Scs proteins are involved in balancing periplasmic oxidative stress in *S.* Typhimurium (Anwar *et al.*, 2013).

To address whether *scsABCD* genes affected SPI-1 activity, the expression and the secretion of the SPI-1 effector fusion protein SipB has been tested. In the absence of *scs* genes defective secretion of the SipB fusion protein has been demonstrated (Anwar *et al.*, 2013).

1.6- Applications for disulphide folding machinery in biotechnology

Aside from the importance of the disulphide bond formation of virulence factors in bacteria, disulphide folding machineries of prokaryotic cells are also important for the production of functional recombinant proteins that can be used as biotherapeutics. High value pharmaceutical proteins like antibodies and hormones are being produced in engineered *E. coli* strains (Kamionka, 2011; review). Disulphide bond formation usually takes place in the oxidising periplasm because of the lack of active oxidases in the cytoplasm (Hatahet *et al.,* 2014; review). Indeed, in the bacterial cytoplasm the presence of glutathione reductase and the thioredoxin pathways renders disulphide bond formation slow and inefficient due to formation of inactive and aggregated products (Guglielmi and Martineau, 2009). However, researchers have recognised the potential for engineering bacterial cells that can catalyse disulphide formation in the cytoplasm. *E.coli trxB* and *gor* mutants have been engineered which lack the reductive power of the the glutathione and thioredoxin pathways (Ritz and Beckwith, 2001; review) and Shuffle cells® (New England Biolabs) are engineered to express a chromosomal copy of the disulphide bond isomerase DsbC to promote disulphide bond formation in the cytoplasm.

Another strain named the CyDisCo (Cytoplasmic Disulphide bond formation in *E. coli*) has been engineered that expresses the yeast mitochondrial thiol oxidase Erv1p and the human protein disulphide isomerase (PDI) in the cytoplasm. This CyDisCO system efficiently introduces disulphide bonds in the cytoplasm, and the protein of interest can then be exported to the periplasm by the Tat pathway that can provide a quality control step for correct protein folding (Matos *et al.,* 2014). Disulphide bond formation in the periplasm can also be supported by the disulphide oxidoreductase DsbA. Production of proinsulin (used to treat diabetes) in the periplasm is facilitated by expression of a fusion of DsbA to the N-terminus of proinsulin, which elevated the solubility and oxidative folding (Winter *et al.,* 2000). Furthermore, co-secretion of DsbA with leptin (regulates the body weight and metabolism) also elevated the abundance of this protein (Jeong and Lee, 2000). These findings highlight the potential applications for a range of disulphide folding systems, with different target protein specificities, for the assembly of proteins of biotechnological interest.

1.7- Project aims

The demonstration that the *scs* operon was involved in copper tolerance was published over 20 years ago, although functional insights into this system have progressed at a modest rate since then. At the start of this PhD project, the transcriptional regulation of the *scs* operon was poorly understood, and no insights were available for potential redox partners for this system. Furthermore, the potential value of the StScs system to facilitate protein folding of proteins of biotechnological importance had been totally overlooked. Hence, to advance our understanding in these areas, this PhD project aimed to address the following questions:

- How is the *scs* operon regulated by copper?
- Does copper and *scsABCD* promote periplasmic protein assembly?
- Does the *scs* operon promote survival within activated macrophages?
- Can we identify potential redox partners for the StScs system?
- Is it possible to isolate disulphide bonded StScsC and target proteins for biochemical studies?
- Does expression of StScsABCD and/or exposure to copper facilitate the assembly of disulphide-containing therapeutic proteins in the *E. coli* periplasm?

Chapter 2

Materials and Methods

2.1- Bacterial strains and plasmids

The bacterial strains and plasmids that were using in this study are detailed in Table 2.1 and 2.2 below.

Table 2.1- List of bacterial strains used in this study.

Strain	Genotype	Reference
E. coli BL21 DE3	*E. coli* B strain derivative. *fhuA2* [*lon*] *ompT* *gal* (λ *DE3*) [*dcm*] Δ*hsdS*. ***λ DE3***(λ *sBamHIo* Δ*EcoRI-B*) *int::*(*lacI::PlacUV5::T7 geneI*) i21 Δ*nin5*	New England Biolabs
E. coli JM109	*end*A1, *rec*A1, *gyr*A96, *thi*, *hsd*R17 (r_k^-, m_k^+), *rel*A1, *sup*E44, Δ(*lac-pro*AB), [F′ *tra*D36, *pro*AB, *laq*I^qZΔM15]	New England Biolabs
E. coli DH5α	F^- Φ80*lac*ZΔM15 Δ(*lac*ZYA-*arg*F) U169 *rec*A1 *end*A1 *hsd*R17(r_k^-, m_k^+) *pho*A *sup*E44 *thi*-1 *gyr*A96 *rel*A1 λ^-	New England Biolabs
E. coli TOP10 (MS4)	F- *mcrA* Δ(*mrr-hsd*RMS-*mcr*BC) Φ80*lac*ZΔM15 Δ *lac*X74 *rec*A1 *ara*D139 Δ(*araleu*)7697 *gal*U *gal*K *rps*L (StrR) *end*A1 *nup*G	Dr Mark Shepherd, University of Kent
S. Typhimurium SL1344 (MS98)	Wild-type $Strep^R$	Shepherd *et al.*, 2013
S. Typhimurium SL1344 Δ*scsC* (MS99)	Δ*scsC* Kan^R	Shepherd *et al.*, 2013

Table 2.2- List of plasmids used in this study.

Plasmid	Usage	Reference
pWSK29scsABCD	Amp^R vector for overexpression of ScsABCD	Shepherd *et al.*, 2013
pET23b_P*scsA*_GFP	Amp^R vector for overexpression of GFP with *scsA* promoter	This work
pMK-RQ Fab Herceptin	Kan^R vector for overexpression of Herceptin Fab fragment	This work
pET21a_*scsC*_LIC, pLysS	Amp^R , Cm^R for overexpression of ScsC	Shepherd *et al.*, 2013
pTrcHis_*artI*	Amp^R vector for overexpression of ArtI	This work
pSU2718*scsC*$_{CXXA}$His	Cm^R vector for overexpression of $ScsC_{CXXA}$	This work
pKWK2	Amp^R vector for overexpression of hGH (C189S)	Alanen *et al.*, 2015
pRK793	Amp^R vector for overexpression of TEV protease	Kapust *et al*., 2001

2.2- Bacterial growth media, sterilisation, and cell harvesting

Nutrient agar, yeast extract and tryptone were purchased from Oxoid. Distilled-deionised water was used throughout this work. Milli-Q water was used when a greater level of purity was necessary (Thermo scientific, Easy pure II). Growth media and selected solutions greater than 50 mL were sterilized by autoclaving (Prestige) at 121^{o}C at 15 psi (pound-force per square inch) for 15 min, and volumes smaller than 50 mL were sterilized using Millipore filters with a pore size of 0.22 μm. An Eppendorf e5414R centrifuge was used for <2 mL samples, and a Sigma 2K15 centrifuge was used for sample volumes between 15- 50 mL unless otherwise stated. A Beckman Coulter Avanti J-25 was used for 500 mL samples with JA-10 rotor. A Beckman Coulter Avanti J-30I was used for 1 L samples with a JLA 9.1000 rotor. A Beckman Coulter Avanti J-25 was used for 25 mL samples for high speed centrifugation with a JA 25.50 rotor (i.e. to remove cell debris following sonication).

2.2.1- Solid media

Solid media was prepared by dissolving 20 g/L tryptone, 20 g/L NaCl, 5 g/L yeast extract and 15 g/L agar in dH_2O.

2.2.2- Liquid media

Liquid media was prepared by dissolving 20 g/L tryptone, 20 g/L NaCl, and 5 g/L yeast extract in dH_2O. Media containing Cu^{2+} ions was prepared by addition of filter sterilised 1 or 2 mM $CuSO_4.5H_2O$ (Sigma). Filter-sterilised solutions of 1 mM H_2O_2 (Sigma), 1 mM GSNO (prepared as previously described (Hart, 1985)), 1 mM $FeSO_4$, and 1 mM $ZnSO_4$ were added to the growth medium when required.

2.2.3- M9 minimal media

1 litre of 5x stock of M9 salts contained; 80.24 g $Na_2HPO_4.2H_2O$, 15 g KH_2PO_4, 2.5 g NaCl and 5 g NH_4Cl. 1X M9 media was prepared by the addition of final concentrations of 2 mM $MgSO_4$, 1 M $CaCl_2$, 0.2% glucose, 1 mM $CuSO_4.5H_2O$ and 1X amino acid solution (with or without L-arginine (Section 2.2.5.2)) to M9 salts and the solution was topped up with sterile water.

2.2.4- SOC media

20 g tryptone, 5 g yeast extract, 0.584 g NaCl and 0.186 g KCl was dissolved in 970 mL dH_2O. After sterilisation by autoclaving, 10 mL of filter-sterilised 2M Mg^{2+} stock (20.33 g $MgCl_2$ and 24.65 g $MgSO_4$ dissolved in 100 mL dH_2O) and 20 mL of filter-sterilised 1 M glucose stock was added.

2.2.5- Media supplements

2.2.5.1- Antibiotics

Antibiotic stocks were dissolved in dH_2O (*chloramphenicol was dissolved in 100% ethanol) then filter-sterilized and stored in -20 °C. All chemicals were purchased from Sigma. Growth media was supplemented with a final concentration of 100 μg/mL of ampicillin, 25 μg/mL of chloramphenicol, 40 μg/mL of streptomycin and 50 μg/mL of kanamycin where appropriate.

2.2.5.2- Amino acid stock solution

Amino acid stock solutions were prepared as described in Table 2.3.

Table 2.3- Amino acids required for preparation of 10x amino acid stock solution. *In some cases, amino acid stock solutions were prepared without arginine. 500 mL of dH_2O was added to the amino acids, filter sterilized and stored at 4 °C.

Amino acid	Concentration	Final concentration g/ L of mQH_2O for 10x stock
Alanine	8 mM	0.712
Arginine*	5 mM	0.844
Aspargine	4 mM	0.602
Aspartic acid	4 mM	0.684 plus 670 µL 10 M KOH
Glutamic acid	6 mM	1.12 plus 860 µL 10 M KOH
Glutamine	6 mM	0. 878
Glycine	8 mM	0. 6
Histidine	2 mM	0.42
Isoleucine	4 mM	0.524
Leucine	8 mM	1.05
Lysine	4 mM	0.732
Phenylalanine	4 mM	0.66
Proline	4 mM	0.46
Serine	100 mM	10.5
Therionine	4 mM	0.476
Tryptophan	1 mM	0.204
Tyrosine	2 mM	0.362
Valine	6 mM	0.564

2.2.6- Bacterial glycerol stocks and starter cultures

Bacterial cultures were stored at –80 °C in 25% glycerol. Bacterial strains were streaked from frozen onto agar plates. Colonies from the agar plate were used to inoculate 10 mL of LB media (with appropriate antibiotics) in 50 mL conical flasks at 37 °C and 180 rpm for 16 h.

2.2.7- Protein overexpression

10 mL of overnight culture was used to inoculate 1 L sterile LB medium in a 2 L baffled flask with appropriate antibiotic, which was then incubated at 37 °C and 180 rpm. When the OD_{600} reached 0.5, a final concentration 1 mM IPTG was added to the culture medium (where expression was controlled by the *lac* promoter). The cultures were then grown for further 4 h. Optical densities of the cultures were measured by using Cary 60 UV-Vis Spectrophotometer (Agilent Technologies). Cells were harvested by centrifugation at 9,000 rpm for 30 min at 4 °C and the pellets were stored at -80 °C.

2.2.8- Growth curves for *Salmonella* in M9 medium

Overnight cultures grown in LB media were centrifuged for 5 min at 3,000 rcf and cells were resuspended in 10 mL of M9 medium (this was repeated twice). Resuspended cells were then diluted in M9 medium 1 in 10. Diluted cells were then diluted 1 in 10 again in M9 medium in flat bottom 96-well plates. Growth rates were measured using a plate reader (BMG Labtech) at 37 °C and 180 rpm.

2.3- Preparation of competent cells and transformations of plasmids

2.3.1- $CaCl_2$ competent cells

1 mL of overnight starter culture was used to inoculate 100 mL sterile LB medium. Cells were grown at 37 °C and 180 rpm and when the OD_{600} reached to 0.6, the culture was incubated on ice for 10 min. Then cells were centrifuged at 3,000 rcf at 4 °C for 8 min, and the pellets were resuspended in 25 mL chilled 100 mM $CaCl_2$. Resuspended cells were incubated on ice for 10 min, centrifuged as before, and cell

pellets were resuspended in 2 mL of 100 mM $CaCl_2$ and 30% (v/v) glycerol. The resultant chemically competent cells were then aliquoted (100 μL) into chilled 1.5 mL Eppendorf tubes and transformed immediately with plasmid DNA.

2.3.2- Transformation by heat shock

Chemically competent cells and plasmid DNA were thawed on ice. 2 μL plasmid DNA was added to 100 μL of chemically competent cells and then incubated on ice for 30 min. The cells were then placed on a heating block at 42 °C for 90 s and then transferred immediately to ice for 2 min. 900 μL of SOC medium was added to the cells and mixed gently by pipetting up and down. Then the cells were incubated at 37 °C for 45 min. A 10-fold dilution was performed with SOC media then 100 μL from each dilution was spread on agar plates containing appropriate antibiotics.

2.3.3-Electrocompetent cell preparation and electroporation

1 mL of overnight culture was used to inoculate 50 mL sterile LB medium in 500 mL flasks with appropriate antibiotic, which was then incubated at 37 °C at 180 rpm until the OD_{600} reaches to 0.6. The culture was then transferred into pre-chilled falcon tube and centrifuged at 3,000 rcf for 10 min. The pellet was resuspended in 10% ice-cold glycerol (this was repeated twice). After the round of 3rd centrifugation, pellets were resuspended in 100 μL 10% ice-cold glycerol and stored on ice until use.

9 μL of purified DNA was applied to cold electro-cuvette then 40 μL of electrocompetent cells were added on top. Electric shock was applied to the cells to allow DNA to enter the electrocompetent cells. The electroporation conditions are described in Table 2.4. After electroporation, 1 mL of SOC medium was added to the cuvette and cells were incubated for 1 h at 37 °C and 180 rpm. 100 μL of the transformation mix was spread onto an agar plate with appropriate antibiotics and incubated overnight at 37 °C.

Table 2.4- Settings for the electroporator for Gram-negative bacteria.

Electroporation conditions	Settings
Voltage (V)	2450
Capacitance (μF)	25
Resistance (Ω)	200
Cuvette (mm)	2

2.4- DNA isolation and analysis

2.4.1- Isolation of plasmid DNA

Bacterial strains harbouring the plasmid of interest were grown overnight in 10 mL LB at 37 °C and 180 rpm. The plasmids were isolated using a QIAprep Spin Miniprep Kit (QIAGEN) according to manufacturer's protocol.

2.4.2- Isolation of genomic DNA

Bacterial strains were grown overnight in LB at 37 °C and 180 rpm and a GenElute Bacterial Genomic DNA Kit (Sigma-Aldrich) was used for isolation of genomic DNA from according to the manufacturer's protocol.

2.4.3- Restriction endonuclease digestion

Isolated DNA was cleaved using restriction enzymes to generate compatible ends for ligation reactions or for screening purposes. Cleavage was performed by following the supplier's instructions (NEB or Promega). Reactions were incubated for 2 h at 37 °C or overnight at room temperature. For gel-purification of digested DNA, a QIAquick Gel Extraction kit (QIAGEN) was used according to manufacturer's protocol.

2.4.4- Polymerase Chain Reaction

PCR was used to amplify DNA fragments for cloning. Q5 DNA polymerase was mainly used for amplification of fragments and Taq polymerase was also used for

colony PCR screening after transformations. Sequences of the oligonucleotides used in this study are shown in Table 2.5.

Table 2.5- Oligonucleotides used in this study. All oligonucleotides were synthesised by Eurofins MWG. Primers were dissolved in sterile water and kept at -20 °C.

Name	**5' - 3' Sequence**	**Use**
scsC$_{CXXA}$His_F	CCCGGATCCATGAAAGGAAGACCATATGA AAAAGACAGCTATCGCAATTGCAGTGGCC	For amplification of *scsC*$_{CXXA}$*His*
scsC$_{CXXA}$His_R	CCCTGCGCATTAATGATGATGATGATGAT GCCCG	For amplification of *scsC*$_{CXXA}$*His*
pSU2718_seq_F	AAAAGCACCGCCGGACATCA	For screening of *scsC*$_{CXXA}$*His*
pSU2718_seq_R	CGAATTCGAGCTCGGTACCC	For screening of *scsC*$_{CXXA}$*His*
*artI*TEV_F	CATCATGGTATGGCTAGCGAGAATTTATA CTTCCAAGGTTCTAACGCCGCCCAGACCA TTCGT	For amplification of *artI*
*artI*TEV_R	AATCTTCTCTCATCCGCCAAAACAGCCAA GCTTTTACTTCTGGAACCATTTGTTATAGA T	For amplification of *artI*
pTrcHis_F	AAGCTTGGCTGTTTTGGCGGATGAGAGAA GATTTTCAGCCTGATACAGAT	For amplification of pTrcHis
pTrcHis_R	GCTAGCCATACCATGATGATGATGATGAT GAGAACCCCCCATGGTTTATT	For amplification of pTrcHis
pTrcHis_seq_F	GTGGGCACTCGACCGGAATT	For screening of *artI*
pTrcHis_seq_R	TCAGGTGGGACCACCGCGCT	For screening of *artI*
P*scsA*_F	ATAGGGAGACCACAACGGTTTCCCTCTAG AGCACTTCCCATGCTTCAGCAACCTC	For amplification of *scsA* promoter
P*scsA*_R	TCCAGTGAAAAGTTCTTCTCCTTTGCTCAT	For

	GAGCTCTGCGCCCTCACTGTTTAACGCGAGT	amplification of *scsA* promoter
PET23b-GFP_F	GAGCTCATGAGCAAAGGAGAAGAACTTTTCACTGGA	For amplification of PET23b-GFP
PET23b-GFP_R	TCTAGAGGGAAACCGTTGTGGTCTCCCTAT	For amplification of PET23b-GFP
PET23b_seq_F	TAACCAGTAAGGCAACCCCGC	For screening of P*scsA*
PET23b_seq_R	GTGTTGGCCATGGAACAGGTAGTTTTC	For screening of P*scsA*

2.4.4.1- PCR using Q5 proofreading DNA polymerase

For amplification of genes for cloning purposes, the high-fidelity Q5 DNA polymerase was used. PCR components and reaction conditions are shown in Tables 2.6 and 2.7, respectively.

Table 2.6- Components required for 50 μL PCR reaction with Q5 DNA polymerase of DNA fragments.

Component	50 μL reaction
Q5 High-Fidelity 2X Master Mix (NEB)	25 μL
10 μM Forward primer	2.5 μL
10 μM Reverse primer	2.5 μL
Template DNA	5 μg
Sterile water	19 μL

Table 2.7- Settings used for PCR with Q5 DNA polymerase on Biometra T3000 Thermocycler. *Annealing temperature was arranged according to the melting temperatures of the primers (5 °C below the lowest melting temperature) and DNA elongation is set as 30 s per kilo-basepair (kb).

Step	Temperature (°C)	Time
Initial denaturation	98	30 s
DNA denaturation	98	10 s x 35 cycles
Primer annealing	72*	15 s x 35 cycles
DNA elongation	72	30 s* x 35 cycles
Final elongation	72	2 min
Hold	4	-

2.4.4.2- Colony PCR with Taq polymerase

Taq DNA polymerase was used to confirm presence of the correct plasmid from colonies on agar plates. PCR components and reaction conditions are shown in Tables 2.8 and 2.9, respectively.

Table 2.8- Components required for 25 µL PCR reaction with Taq DNA polymerase. (PCRBiosystems). *Cell suspension corresponds to colonies resuspended in 50 µL of mQH_2O.

Component	25 µL reaction
2x Taq Mix Red	12.5 µL
10 µM Forward primer	0.5 µL
10 µM Reverse primer	0.5 µL
Cell suspension*	2 µL
Sterile water	9.5 µL

Table 2.9- Settings of Biometra T3000 Thermocycler for colony PCR. *Annealing temperature was arranged according to the melting temperatures of the primers (5 °C below the lowest melting temperature) and DNA elongation is set as 30 s per kilo-basepair (kb).

Step	Temperature (°C)	Time
Initial denaturation	95	4 min
DNA denaturation	95	15 s x 35 cycles
Primer annealing	57*	45 s x 35 cycles
DNA elongation	72	1 minute* x 35 cycles
Final elongation	72	2 min
Hold	4	-

2.4.5- DNA purification from PCR reactions

A QIAquick PCR purification kit (QIAGEN) was used for purification of DNA fragments after gel extraction as well as for purification of DNA fragments after PCR reactions according to the manufacturer's instructions.

2.4.6- Ligation/ Gibson assembly

The 5' end of insert DNA was dephosphorylated using Calf Intestinal Alkaline Phosphatase (NEB) to prevent self-ligation of vector DNA. Reaction conditions are shown in Table 2.10.

Table 2.10- Components needed for dephosphorylation of DNA.

Component	20 μL reaction (μL)
Insert DNA (40 ng/ μL)	15
CutSmart Buffer (10x)	2
CIP 1 unit	0.59
mQH_2O	2.4

20 µL reaction was incubated at 37 °C for 30 min and dephosphorylated linear DNA was purified using PCR purification clean up Kit. The quantity of DNA was measured by using a NanoPhotometer® N50 (Implen) and ligations were set up using a 3:1 ratio of insert DNA: vector DNA. Ligation of DNA was performed according to the Quick Ligation Protocol (NEB). In brief, 10 µL of 2x Quick Ligation Buffer (NEB) and 1 µL of Quick T4 DNA ligase (NEB) were added to the insert and vector DNA samples. The reaction mixture was centrifuged for 1 min at 4,000 rpm and incubated at room temperature for 5 min. Then the reaction mixture was chilled on ice and then the plasmid was transformed into ultracompetent cells (Promega) following the NEB transformation protocol.

For Gibson assembly, the concentration of amplified insert and vector DNA was quantified using a NanoPhotometer® N50 (Implen). A 3-fold excess of insert DNA was added to vector DNA. 10 µL of Gibson assembly master mix was added and the reaction was topped up to 20 µL with sterile mQH_2O. The reaction mixture was incubated at 50 ℃ for 1 h. Transformation was carried out according to manufacturer's instructions (NEB).

2.4.7- Agarose gel electrophoresis

DNA fragments were separated by size using agarose gel electrophoresis. For analysis of DNA fragment sizes, 1% agarose gels were prepared by dissolving 0.3 g of agarose in 30 mL of TAE buffer (242 g Tris, 57.1 mL acetic acid, 100 mL 0.5 M EDTA was mixed with 1 L of dH_2O, pH 8.0). 5 µL of DNA sample was mixed with 1 µL of 6x loading dye (Promega) and loaded onto wells of the agarose gel. 5 µL of DNA marker (1 kb DNA ladder, Promega) was used. Gels were ran at 150 V, 300 mA for 25 min and stained with 5 µL of Ethidium bromide in 100 mL of dH_2O for 30 min and visualised using a Syngene G: BOX gel dock system.

2.5- Protein purification

2.5.1- Metal Affinity Chromatography

Histidine tagged StScsC, StScsC$_{CXXA}$, ArtI and P*scsA*_GFP were purified using the buffer systems detailed in Table 2.11. Cell pellets from 1 L culture were resuspended in 50 mL of Solubilisation buffer. A final concentration of 1 mM PMSF was added to inhibit protease activity. Pellets were homogenized on ice for 10 min and sonicated 6 times (30 s each) at 10 microns (Soniprep 150) then centrifuged at 15,000 rpm and 4 °C for 30 min. Samples from the supernatant were taken for analysis on SDS-PAGE gel and the rest was applied to a 2 mL Talon Metal Affinity Column (Clontech) that had been pre-equilibrated with Solubilisation buffer. The column was washed with 10 column volumes of Wash buffer for the removal of untagged proteins and then the protein of interest was eluted with Elution buffer. Prior to storing the protein, imidazole was removed via buffer exchange. Protein samples were concentrated using Millipore spin concentrators and then passed through a PD-10 column (GE Healthcare) that had been pre-equilibrated with Equilibration buffer.

Table 2.11- Components required for preparation of buffers for protein purification.

Buffers	Components
Solubilisation buffer (SB)	125 mM Tris pH 7 (pH 8 for ArtI) 50 mM NaCl 0.5% Triton-X-100
Wash buffer	10 mM Imidazole in 25 mL of SB
Elution buffer	300 mM Imidazole in 25 mL of SB
Equilibration buffer	50 mM HEPES pH 7 (pH 8 for ArtI) 150 mM NaCl

2.5.2- TEV protease purification

TEV protease was purified from *E. coli* BL21 harbouring pRK793 plasmid as described above (Section 2.5.1). Buffer exchange was then performed as described below, using the buffer systems described in Table 2.12. Buffer exchange for removal of imidazole was performed using a HiTrap S-sepharose column (GE Healthcare) and a peristaltic pump (Pharmacia Fine Chemicals). The column was equilibrated with 10 mL of mQH_2O, followed by 10 mL of Buffer 2 and finally with 10 mL of Buffer 1. The purified protein sample was diluted 1 in 5 in Buffer 1 and applied to the column. The column was washed with 3 mL of Buffer 1. Protein was eluted with 3 mL of Buffer 3 then 3 mL of Buffer 2 was applied to the column. (Proteins were collected in aliquots and protein-containing fractions were identified using a Bradford assay (2 μL of sample mixed in 50 μL of Bradford reagent). Purified protein was stored at -80 °C. 1 μg of TEV protease was used per 50 μg of protein to be cleaved and the reaction was left at room temperature overnight. To remove uncleaved protein, digests were applied to a Talon metal affinity column equilibrated with Equilibration buffer (Table 2.11) and untagged protein passed straight through.

Table 2.12- Components required for preparation of buffers for TEV protease buffer exchange. All buffers were at pH 8. 10% glycerol (v/v).

Buffers	Components
Buffer 1	50 mM Tris-HCl, 5 mM 2-mercaptoethanol, 10% glycerol
Buffer 2	50 mM Tris-HCl, 1 M NaCl, 5 mM 2-mercaptoethanol, 10% glycerol
Buffer 3	50 mM Tris-HCl, 500 mM NaCl, 5 mM 2-mercaptoethanol, 10% glycerol

2.5.3- Protein quantitation

2.5.3.1- Markwell Assay

This assay was used to determine the protein concentration of the purified samples as previously described (Markwell *et al*., 1978) using the reagents described in Table 2.13.

Table 2.13- Components required for preparation of the reagents for Markwell assay.

Reagent	Chemical	Final concentration g/100 mL of mQH_2O
Reagent A	Na_2CO_3	2
	NaOH	0.4
	Na tartrate	0.16
	SDS	1
Reagent B	$CuSO_4.5H_2O$	4
Reagent C	Reagent A+B	100 parts of Reagent A in 1 parts of Reagent B

In glass test tubes, 1 mL bovine serum albumin (BSA) standards (0-200 µg/mL) and protein sample dilutions in mQH_2O (1:50 and 1:100) were prepared. 3 mL of reagent C was added to 1 mL samples, vortexed and incubated at room temperature for 60 min. Then 0.3 mL of Folin & Ciocalteu's phenol reagent (Sigma) (1:1 in dH_2O) was added to the samples, vortexed and incubated at room temperature for 45 min. The spectrophotometer (Cary 60 UV-Vis Spectrophotometer (Agilent Technologies)) was blanked with mQH_2O and readings were taken at 660 nm. The absorbance of the BSA standards was plotted and the unknown samples were converted into µg/mL concentrations by comparing to the linear regression fit for the standards (Appendix 1) and corrected for dilution. Sample analysis was performed in triplicate and the concentrations were averaged to give the final concentration for the stock protein sample.

2.5.3.2- Calculated extinction coefficients

In order to calculate the concentration of purified protein samples, absorbance of samples were taken at 280 nm (Cary 60 UV-Vis Spectrophotometer (Agilent Technologies) in a quartz cuvette (Sigma). Protein concentrations were then estimated using the calculated molar extinction coefficients for the protein

(http://biotools.nubic.northwestern.edu/proteincalc.html). Since these extinction coefficients are designed to work with denatured proteins, their accuracy was compared to Markwell assay data before this approach was used routinely.

2.6- Determination of the redox status of proteins

Purified protein samples were oxidised with 20 mM GSSG and reduced with 5 mM DTT (final concentrations) or left untreated for 1 h at room temperature. Reduction/ oxidation reagents were removed via buffer exchange on a PD-10 desalting column (GE Healthcare).

2.6.1- DTNB assay

The thiol redox status of purified proteins was assessed using a DTNB assay. DTNB (5,5′-Dithiobis(2-nitrobenzoic acid)) (Sigma) interacts with free thiol groups of protein of interest to produce 2-nitro-5-thiobenzoate anion (TNB^{2-}) and one mixed disulfide ($R\text{-}S\text{-}TNB^{-}$) with the protein of interest. The extinction coefficient of DTNB is 13,600 $M^{-1}cm^{-1}$ at 412 nm (Sigma).

10 mM DTNB stock solution was prepared in 0.1 M sodium phosphate/1 mM EDTA buffer, pH 8. Purified protein was diluted to 3μM in 1 mL of a 1 mM DTNB solution. After 15 min of incubation at room temperature the absorbance was measured at 412 nm. Free thiols in the protein sample were then calculated using the extinction coefficient for DTNB (13,600 $M^{-1}cm^{-1}$).

2.6.2- Thiol alkylation with AMS

The oxidation state of proteins was investigated by using 4-Acetamido-4'-Maleimidylstilbene-2,2'-Disulfonic Acid (AMS) thiol modification reagent (A485, Invitrogen) that reacts with reduced protein thiols as shown in Figure 2.1.

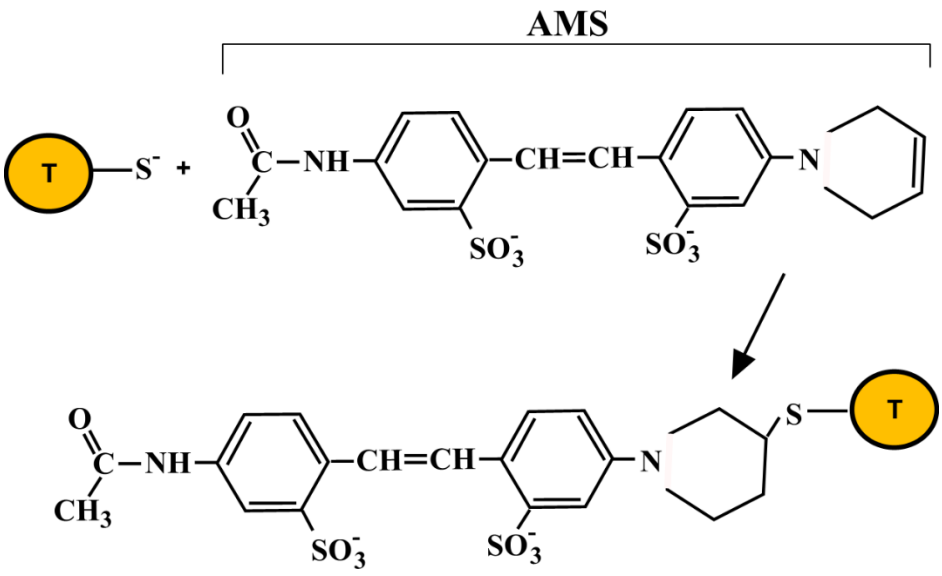


Figure 2.1- The structure of AMS and the formation of an intra-protein disulphide. AMS reacts with reduced protein thiol (shown in orange) resulting in the formation of an intra-protein disulphide. An increase on the mass of the protein (by ~0.5 kDa) leads to a band shift on an SDS-PAGE gel that can then be detected.

For determination of the *in vivo* redox status of ScsC in *S.* Typhimurium, 150 μg of periplasmic fractions (grown in 1 mM Cu^{2+}) were incubated with or without 5 mM DTT for 1 h and protein was acetone precipitated as described in sections 2.11.1 and 2.11.2. For determination of the *in vivo* redox status of StScsC in the presence of copper/ oxidative and nitrastive stresses in *S.* Typhimurium, 150 μg of periplasmic fractions (grown in the presence of 1 mM Cu^{+} / Cu^{2+}), 1 mM GSNO and 1 mM H_2O_2 (or in combination)) were acetone precipitated. Cu^{+} stocks were prepared as described in section 2.12. For determination of the *in vitro* redox status of purified StScsC and ArtI, 3 μM of purified protein samples (that had been previously oxidised/reduced with 20 mM GSSG or 5 mM DTT, respectively) were incubated in the presence and absence of 1 mM Cu^{2+} for 1 h at room temperature. Protein samples were then acetone precipitated. Precipitated protein samples were then resuspended in 8 μL of 20 mM AMS in 50 mM Tris/ HCl, 1% SDS buffer (Inaba and Ito, 2002) and incubated at room temperature for 10 min. SDS loading buffer (without reducing agent) (1:1) was then added and protein samples were resolved via SDS-PAGE.

2.7- Sodium dodecyl sulphate-polyacrylamide gel electrophoresis (SDS-PAGE)

SDS-PAGE was used to separate and visualise proteins samples. Gels were prepared on the day before use using a Mini-Protean Electrophoresis System (BIORAD Laboratories, USA). A 4% stacking gel and 12% resolving gel (Table 2.14) were used unless otherwise stated. The composition of resolving buffer and stacking buffer were 1.5 M Tris/HCl pH 8.8 and 0.5 M Tris/HCl pH 6.8, respectively.

Table 2.14- Recipes for stacking and resolving gels for SDS-PAGE.

Chemical	Stacking gel (4%)	Resolving gel (12%)
Distilled H_2O	6.425 mL	4.35 mL
Stacking buffer	2.5 mL	-
Resolving buffer	-	2.5 mL
10% SDS	100 µL	100 µL
40% Acrylamide/ Bis	0.975 mL	3 mL
10% APS	50 µL	50 µL
TEMED	10 µL	5 µL

When the gels were set completely, they were transferred to the gel tank and submerged in running buffer (250 mM glycine, 25 mM Tris, 0.1% SDS, pH 8.3). Protein samples were mixed with a loading dye (50 mM Tris, 2% SDS, 0.5% Bromophenol Blue, 10% Glycerol, 100 mM DTT) (1:1), boiled for 5 min at 95 °C and loaded onto the gel. For resolving whole cell samples, cell pellets were resuspended in 50 µL of loading dye (in the presence and absence of DTT), then boiled at 95 °C for 10 min, centrifuged at 13,200 rpm for 10 min, and 8 µL of the sample was loaded onto the gel. 3 µL of protein marker was used (Bio-rad dual colour protein standards). The gels were run at 150 V, 300 mA for 1 h. The gel was stained for 1 h with Coomassie stain (1 g/L Coomassie brilliant blue, 20% methanol, 20% acetic acid glacial) and then de-stained (with 20% methanol, 20% acetic acid) until the bands became visible and background became colourless. The gels were stored in dH_2O and visualised using a Syngene G: BOX gel dock system.

2.8- Electrophoretic transfer to PVDF membrane

Proteins from SDS-PAGE gels were transferred to PVDF membrane to be further analysed by Western Blotting. SDS-PAGE gels, filter pads and filter papers were all soaked in western transfer buffer (25 mM Tris and 192 mM glycine was dissolved in 1 L H_2O) prior to transfer. PVDF membrane (0.45 μm, Thermo scientific) was cut and soaked into methanol briefly and then soaked in western transfer buffer. A gel sandwich was made as follows; black side of the gel holder cassette, filter pad, filter paper, gel, PVDF membrane, filter paper, filter pad and red side of the gel holder cassette. The gel holder cassette was put into electrode tank and the tank was filled with western transfer buffer. Transfer was carried out at 10 V, 50 mA for 16 h or at 100 V, 300 mA for 1 h.

2.9- Western Blotting

PVDF membrane was incubated in blotto (5% skimmed milk powder in 1X TBS Buffer) (1X TBS Buffer: 137 mM NaCl and 10 mM Tris was mixed with 900 mL of dH_20 and pH was adjusted to 7.4 and the solution was made up to 1 L) for 1 h with shaking in order to block nonspecific binding. Then the membrane was incubated with a 1:5000 dilution of primary antibody in 10 mL of blotto for 1 h with gentle shaking. The membrane was then washed for 3 x 5 min with TBST (0.1% Tween (Sigma, Tween 20) was mixed with 1X TBS buffer). The secondary antibody (1: 5000) was then added to 10 mL of blotto and applied to the membrane. The liquid was discarded and the membrane was washed 4 times with TBST as described above. One tablet of BCIP/NBT (Sigma Fast) was dissolved in 10 mL of dH_2O and the membrane was developed in the BCIP/NBT solution for 10 min in darkness. The reaction was stopped by washing the membrane with dH_2O. The various antibodies used in this study are listed in Table 2.15.

Table 2.15- The list of antibodies used in this study. *All antibodies were coupled with alkaline phosphatase.

Antibody*	Reference
Anti-Human Kappa Light Chain (Bound and Free)	Sigma- Aldrich
Anti- StScsC	Shepherd *et al*., 2013
Anti-Human IgG (Fab specific)	Sigma- Aldrich
Anti-his$_6$ antibodies	Abcam
Anti-rabbit IgG	Sigma- Aldrich

2.10- Identification of protein bands via mass spectrometry

For identification of peptides resolved on an SDS-PAGE gel, the gel was stained with a Pierce silver staining kit (24600, Thermo scientific) using the manufacturer's protocol. The silver stained gel was washed with ultrapure water twice for 10 min. The bands of interest were excised using a clean scalpel close to the edge of the band and were then transferred to a clean Eppendorf tube. Excised bands were destained using the Pierce silver staining kit following the manufacturer's protocol. The solutions were prepared freshly. The following steps were all carried out in a HEPA filter hood (BSB48 ICN flow). Filter tips were used throughout the protocol (Biosphere filter tips).

Reduction and alkylation of the proteins was performed with DTT and iodoacetamide (Sigma), respectively, as previously described (Shevchenko *et al*., 1996). Tryptic digestion of the proteins was performed as follows: Dried gel pieces were rehydrated in 20 μL of digestion buffer (25 mM NH_4HCO_3 (Fluka, 40867) and 10% acetonitrile (Biosolve)) containing 10 ng/μL of Sequencing Grade Modified Trypsin (Promega) and incubated at 4°C for 30 min. The supernatant was then removed and the gel pieces were incubated overnight at room temperature in 20 μL of the digestion buffer to maintain gel hydration during enzymatic cleavage. Extraction of peptides was performed by the addition of 5 μL of acetonitrile to the gel pieces and sonication in an ultrasound bath (Decon) for 15 min. The gel pieces were centrifuged and the supernatant was collected. 10 μL of 50% acetonitrile with

5% formic acid was added to gel pieces and sonication was carried out for 15 min. Then the gel pieces were centrifuged and the supernatant was collected. Supernatants were pooled together in an Eppendorf tube and stored at -20°C. 0.5 μL of extracted peptides was spotted onto a MTP Anchorchip MALDI-TOF plate (Bruker). Samples were allowed to dry then 1 μL of matrix solution was added on top (0.7 mg/mL alpha-Cyano-4-hydroxycinnamic acid dissolved in solvent mixture containing 85% acetonitrile, 15% water, 0.1% TFA and 1 mM $NH_4H_2PO_4$). The plate was placed into a MALDI-TOF mass spectrometer (Ultraflextreme, Bruker). The instrument was calibrated with commercially available Bruker Peptide Calibration Standard II (Bruker, part number 222570). The spectra from the extracted peptides were collected using the following settings: Polarity, +ve; Laser frequency, 2 kHz; ion sources, 25 kV and 22.35 kV; Lens, 7.5 kV; pulsed ion extraction, 80 nS; range, 700-3500 Da; data sampling rate, 4 Gs/s. For each sample, 3500 shots were summed and saved. The mass spectrometry data files were exported from the Flexicontrol software from Bruker Matrix Science. An automatic search against TrEMBL *E. coli* database (downloaded from Uniprot) was performed using the Mascot search engine.

2.11- Quantification of protein abundances by electrospray mass spectrometry

2.11.1- Extraction of periplasmic fractions

5 mL of overnight bacterial cultures were used to inoculate 500 mL of LB in 2 L baffled flasks (with appropriate antibiotic) in the presence and absence of sub-inhibitory concentrations of copper (2 mM), and cultures were grown at 37 °C at 180 rpm until the OD_{600} was 1.5. 14.25 mL of 1 M NaCl and 14.25 mL of 1 M Tris/HCl pH 7.3 was mixed with the culture and centrifuged at 3,000 rcf for 20 min at 20 °C. The supernatant was then collected and the pellet was resuspended in 3.5 mL of supernatant and 3.5 mL of TSE buffer (40% sucrose, 33 mM Tris/HCl pH 7.3 and 2 mM EDTA) and incubated at room temperature for 20 min then centrifuged at 5,000 rcf for 15 min at 20 °C. The pellet then resuspended in 10 mL of ice cold dH_2O and mixed on ice for 45 s and 10 μL of 1 M $MgCl_2$ was added and chilled on ice for 20 min. The pellet was centrifuged at 5,000 rcf for 15 min at 4 °C, and the supernatant was collected (periplasmic fraction) and stored at -80 °C.

2.11.2- Acetone precipitation

A protein solution containing 10 μg of protein was mixed with excess cold acetone in a 4:1 ratio (v/v). The samples were then kept at -70 °C for 10 min then incubated at -20 °C for 4 h. The samples were centrifuged at 5,000 rcf for 15 min at 4 °C. Supernatants were removed and the tubes were dried using a vacuum centrifuge (ThermoSavant, SPD111V) for 15 min to eliminate any acetone residue.

2.11.3- Tryptic digestion of proteins

10 μg protein pellets (from section 2.11.2) were resuspended in 20 μL of solubilisation buffer (8 M urea, 100 mM ammonium carbonate, 20 mM DTT, and 0.2% octyl-beta glucoside (Fluka)) and incubated for 1 h at room temperature. Then 10 μL of 10 mM iodoacetamide (alkylating reagent that binds covalently with the thiol group of cysteines so the protein cannot form a disulphide bond) was added to the samples and incubated at room temperature for 15 min. 65 μL of mQH_2O was then added to dilute the urea in the samples, and 2.5 μL of 0.2 mg/mL Sequencing Grade Modified Trypsin (Promega) was added and the mixture was incubated for 18 h at room temperature. The trypsin activity was stopped via the addition of 10% TFA (trifluoroacetic acid) and the samples were stored at -20 °C.

2.11.4- UPLC and ESI-MS analysis

10 μL of trypsin-digested protein samples were mixed with 5 μL of 50 fmol/μL BSA standard which was used as an internal standard to allow label-free quantitation. Protein samples were placed into the ACQUITY UPLC M-Class System (Waters) for sample separation. 4 μL of each sample was injected to the column. Peptides were trapped on a 180 μm X 20 mm Acquity Symmetry C18 (5 μM) column for 3 min and then separated on a 75 μm X 150 mm Acquity UPLC HSS T3 column with 1.8 μm particles (Waters). All peptides were separated with a 40 min gradient and data collected for 60 min. Trapping flow rate was 15 μL/ min with 97% A and 3% B (A: water with 0.1% formic acid, B: acetonitrile with 0.1% formic acid). For the 40 min gradient, the flow rate was changed to 0.3 μL/ min with 3% A and 40% B. Peptides were analysed using a Synapt G2-Si Mass spectrometer (Waters) fitted with a Zspray nanospray source. The fragment ion data was collect using HDMSe technique. During the run, the system was in positive ESI-mode. The source temperature was 60

°C. The capillary voltage was 3.5 kV and the cone voltage was 30 V. The m/z range was 50-2000 with scan time of 1 s. Peptides were then analysed by Progenesis QI software against TrEMBL *Salmonella* database. All reagents used were LC-MS grade.

2.12- Metal binding assay

The affinity of the StScsC protein for Cu^+ was investigated using a competition assay with Bathocuproine disulphonate (BCS) (Sigma). BCS binds to Cu^+ and forms a $BCS_2Cu(I)$ complex that absorbs at 483 nm which is used to probe the Cu^+ affinities for proteins (Xiao *et al*., 2011). The buffers used in this assay (Table 2.16) were treated with Chelex resin (Sigma) to remove transition metal ions and N_2-purged for 10 min for the removal of oxygen (Nitrogen was supplied from BOC).

Table 2.16- Components of buffers used in metal binding assay.

Buffer	Components
Buffer A	100 mM HEPES pH 6, 400 mM KCl, 100 mM NaCl, 5 mM EDTA,5 mM DTT
Buffer B	100 mM HEPES pH 6, 400 mM KCl, 100 mM NaCl,
Buffer C	100 mM HEPES pH 7.8, 400 mM KCl
Buffer D	100 mM HEPES pH 7.8, 400 mM KCl, 100 mM NaCl
Buffer E	100 mM HEPES pH 7.8, 400 mM KCl, 1 mM NaCl
Buffer F	0.1 M HCl, 1M NaCl

Since Cu^+ reacts with oxygen and can generate Cu^{2+}, the entire experiment was conducted under anaerobic conditions ($InvivO_2$ Hypoxia workstation). Quartz cuvettes were soaked in 4% nitric acid overnight and washed with distilled water for removal of metals. Absorbance spectra were collected between 200 and 800 nm with USB2000+UV-VIS, Ocean Optics spectrometer.

Cu^+ stock solution was prepared by mixing 1 g of CuCl in 14 mL of Buffer F to produce a solution of 72 mM Cu^+. 72 mM Cu^+ was then diluted 1 in 10 with Buffer C then further 1 in 2.3 dilution with Buffer D resulted in 3.125 mM Cu^+ stock solution which was used during titrations.

2 μM of purified and untagged StScsC was incubated in Buffer A for 2 h at room temperature for reduction of disulphide bonds and the removal of metals from the

protein. Then DTT and EDTA were removed from the sample by using Heparin column (GE Healthcare) that was pre-equilibrated with Buffer B. Reduced and metal-free StScsC was eluted with the high salt Buffer E.

To produce a BCS standard curve, Cu^{+} was titrated to 10 μM BCS solution (prepared in Buffer D). For BCS- StScsC competition assay, Cu^{+} was titrated to 10 μM BCS +2 μM StScsC solution (prepared in Buffer D). Absorbance spectra were recorded every minute after titration of copper with constant mixing until the reaction reached equilibrium.

2.13- Macrophage survival assay

RAW-Blue macrophage stocks (derived from the murine RAW 264.7 macrophages) in aliquots of ~1.5 mL were defrosted and suspended in 10 mL of culture medium containing 10% (v/v) heat inactivated FBS (Sigma) and 200 U/mL of Penicillin-Streptomycin (Sigma) in DMEM (Gibco). Suspended macrophages were centrifuged at 500 rcf for 5 min and the pellet was resuspended in fresh 2.5 mL DMEM media. 2 mL of resuspended macrophages were diluted in 8 mL of fresh DMEM media in T25 flasks and cells were incubated at 37 °C with 5% CO_2 for 48 h. After 48 h, spent media was removed. Confluent monolayers of macrophages were then resuspended in 5 mL of fresh DMEM media and the cells were scraped from the bottom of the flask. The suspensions were centrifuged for 5 min at 500 rcf. The supernatants were removed and the pellets were resuspended in 3 mL of fresh media and mixed with 20 mL of fresh DMEM media in T75 cell culture flasks.

1.5x 10^5 macrophages were counted using a haemocytometer and were plated in a flat bottom 96-well plates. 1ng/ mL of INF-γ Recombinant Human Protein (Gibco) and 10 ng/ mL LPS (Sigma) was added and the total volume of the suspensions was made to 100 μL by the addition of DMEM media without Penicillin-Streptomycin. Cultures were incubated for 18 h at 37 °C with 5% CO_2 in order to prime and activate the macrophages and maintain cell adherence to the bottom of the plate. Single colonies from wild-type and *ΔscsC S.* Typhimurium strains were used to inoculate 10 mL of LB overnight. Bacterial cultures were centrifuged for 5 min at 5,000 rcf and the pellet was washed in 1x PBS then centrifuged for 5 min at 5, 000 rcf. Bacterial pellets were resuspended in DMEM media and bacterial counts were obtained by measuring the optical density of the cultures at 600 nm.

Pre-primed Raw-Blue macrophages were infected with *Salmonella typhimurium* at a multiplicity of infection (MOI) of 10 (10 bacteria: 1 macrophage). Infections were performed in the presence and absence of 100 µM $CuSO_4$.

After 20 min of infection, media was removed and 100 µL of gentamicin-containing media (200 µg/mL) was added to the wells for elimination of the extracellular bacteria. After 10 min of incubation, spent media was removed and macrophages were washed three times with 100 µL PBS then lysed with 100 µL of 0.01% Triton X-100 in PBS to measure of bacterial uptake. In addition, 35 µg/mL gentamicin was added to parallel wells for longer infections. Macrophages were then washed with PBS and lysed with 0.01% Triton X-100 in PBS at 3 or 24 h post infection. Lysates were plated on agar plates with antibiotics. Plates were incubated at 37 °C for 16 h then intracellular bacterial counts were determined by counting the colonies. This work was performed in an Aura-2000 Bioair biosafety cabinet. A diagrammatic representation of these experiments is shown in Figure 2.2.

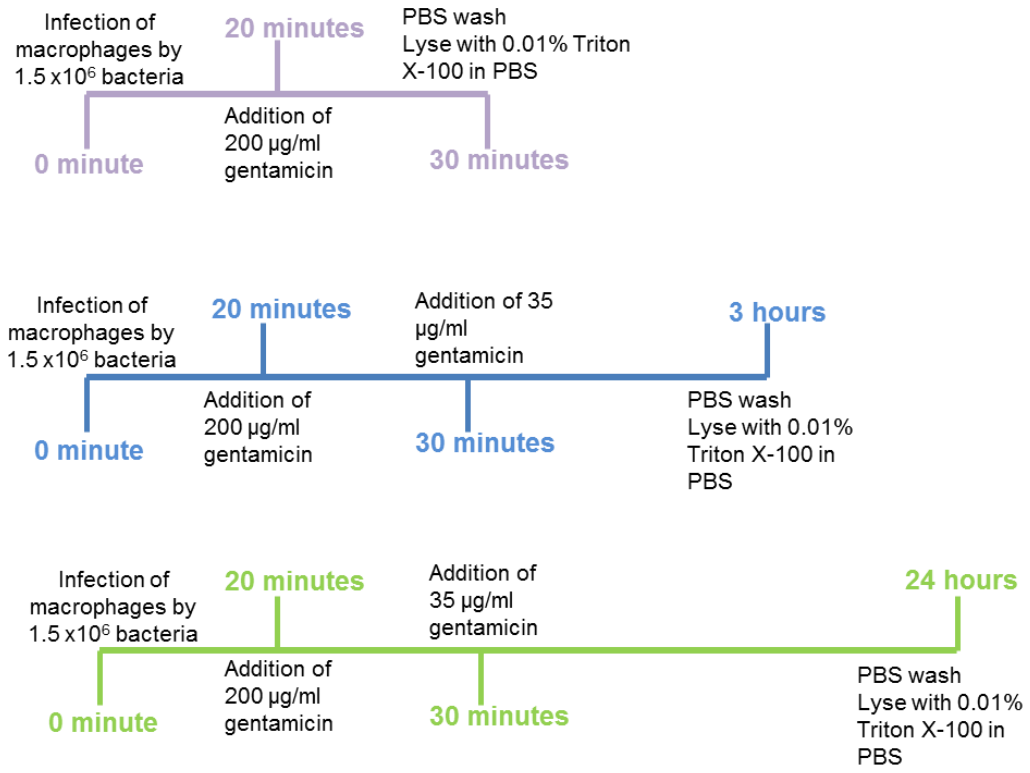


Figure 2.2- Model for macrophage infection studies. The timelines illustrate the stages and conditions of macrophage infection with *S.* Typhimurium. Gentamicin was used to kill extracellular bacteria and Triton X-100 was used for the lysis of macrophages.

2.14- Quantification of GFP fluorescence

Salmonella strains harbouring the pET23b_P*scsA*_GFP plasmid were grown in LB media overnight then the culture is diluted 1 in 10 in LB media. Diluted cells were then diluted 1 in 10 again in LB medium in flat bottom 96-well plates in the presence and absence of 1 mM $CuSO_4$ and the GFP fluorescence was measured by using plate reader (BMG Labtech). GFP fluorescence emission spectra of purified proteins were recorded using a Perkin Elmer LS 50 B Luminescence Spectrometer. Excitation and emission wavelengths were set as 470 and 512 nm, respectively.

2.15- Fluorescence microscopy

GFP that was expressed in *S.* Typhimurium was visualised using an Olympus IX 81 inverted microscope. 3 μL of cultures grown for 8 h were applied to agarose pads on microscope slides. After 5 min, cultures were dried and cover slides were applied before GFP fluorescence was visualised.

Chapter 3

Expression analysis and identification of *in vivo* targets for the ScsC protein of *Salmonella*

Abstract

In this chapter, *in vivo* assays were done in order to demonstrate firstly the expression of StScsC and then to characterise the protein targets of the periplasmic ScsC in *S*. Typhimurium. Bioinformatics search was done to identify other species of bacteria encoding orthologous ScsC proteins. Next, translational ScsC expression studies were accomplished where the abundance of StScsC was found to be significantly upregulated in the presence of copper by mass spectrometry analysis. In addition, by transcriptional assays it was confirmed that the promoter region of *scs* locus (400 bp upstream of *scsA*) is activated by copper. Later, divalent metals other than copper and oxidative and nitrosative stress agents were supplemented to the growth media of *Salmonella typhimurium* and the results showed that the StScsC expression is copper specific.

The thiol redox status of StScsC was studied in the presence of copper, peroxide and nitrosative stress agent GSNO. Herein, we have demonstrated for the first time that StScsC is only expressed in the presence of copper and it is found in the oxidised state *in vivo*. To characterise the role of StScsC, the abundances of periplasmic/ secreted proteins that are expressed in *Salmonella* were analysed via mass spectrometry in the presence and absence of copper and StScsC. In the presence of both, the assembly of disulphide-containing proteins involved in peptide uptake was improved. These proteins are all possible StScsC targets. Presence of StScsC was also shown to alter the redox state of another disulphide-containing protein BcsC in *Salmonella* periplasm.

Finally, addition of exogenous copper ions to murine macrophages infected with wild-type *Salmonella typhimurium* led to an increased survival confirming the role of StScsC in copper tolerance.

3.1- Introduction

S. Typhimurium is one of the most common causes of food-borne disease (CDC, 2015) and over 8,000 cases of *Salmonella* infections are reported each year in England and Wales (PHE, 2018) understanding the mechanisms by which *Salmonella* promotes survival is crucial for targeting pathogens and diminishing the number of infections occurring. Once the bacterium is engulfed by macrophages, these immune cells target the bacteria via the production of toxic reactive oxygen species (ROS), reactive nitrogen species (RNS) and copper ions (Slauch, 2011; review; Achard *et al*., 2010). *Salmonella* responds via the upregulation of a range of virulence factors that promote proliferation and survival in the host cell (Ibarra and Steele-Mortimer, 2009; review) including the Scs locus that is the focus of this thesis. The Scs proteins of *S.* Typhimurium restore copper tolerance in copper-sensitive mutants of *E. coli* (Gupta *et al*., 1997), and this early work suggested a role for these thioredoxin-like proteins in disulphide folding. Later work reported that the *scs* locus plays a role in responding to oxidative stress: the absence of this locus lead to protein carbonylation (Anwar *et al*., 2013).

The soluble periplasmic StScsC protein was later characterised and loss of StScsC was shown to elicit copper sensitivity in *Salmonella* (Shepherd *et al*., 2013). With these studies in mind, the experimental approaches in this chapter were designed to investigate the transcriptional and translational regulation of StScsC, and to measure the impact of stresses encountered during infection upon the redox status of the StScsC *in vivo*. It was also hypothesised that the expression and redox status of StScsC would impact upon the abundance of periplasmic proteins, which could be investigated using mass spectrometry techniques. Finally, it was anticipated that StScsC expression and copper may impact upon the ability of *Salmonella* to survive during infection, so this was investigated using macrophage survival assays.

3.2- Results

3.2.1- StScsC is part of a sub-group of monomeric ScsC proteins that lack an N-terminal dimerization domain

Bioinformatics analysis was undertaken in order to identify orthologs of *Salmonella* ScsC in other bacterial species. The *S.* Typhimurium (SL1344) ScsC (StScsC) protein sequence, lacking the targeting peptide, was submitted to the PSI-Search tool from EMBL-EBI, and the Uniprot Knowledgebase database was used to provide functional annotation. The default value of $1.0e^{-3}$ was used for the expectation value threshold for automatic selection of matched sequences, and BLOSUM62 was used as a comparison matrix. 250 orthologous sequences were detected and ordered according to their E-values (Appendix 2). Table 3.1 shows the proteins from different species with their percentage identities (relative to StScsC). The sequences for proteins listed in Table 3.1 were aligned using the CLUSTAL Omega tool, along with sequences from characterised ScsC proteins from *Yersinia frederiksenii* (Lopez *et al*., 2018), *Caulobacter crescentus* (Cho *et al*., 2012) and *Proteus mirabilis* (Furlong *et al*., 2017) (Figure 3.1). Notably, the presence and absence of an N-terminal extension (which mediates oligomerization, Furlong *et al*., 2017) is evident from the sequence alignment.

Table 3.1- A list of proteins orthologous to StScsC. One representative of each species from the first 250 hit from the bioinfomatics search was selected. The percentage identity of each matched sequence to the query sequence (StScsC) calculated by using BLOSUM62 and the Uniprot accession number of each species as well as a functional annotation was shown.

Organism name	Protein name	Accession number	% identity	Functional annotation
Citrobacter youngae ATCC 29220	DsbA-like protein	D4BBN6	85.1	Protein disulphide oxidoreductase activity
Klebsiella pneumoniae	Suppressor for copper-sensitivity ScsC (bdbD)	A0A377VNR4	84.5	Cell redox homeostasis
Enterobacter sp. GN02600	DsbA oxidoreductase	A0A0J0HNW7	84.0	Protein disulphide oxidoreductase activity
Vibrio parahaemolyticus	DsbA oxidoreductase	A0A0M3ECI2	83.0	Cell redox homeostasis
Shigella flexneri 1235-66	DsbA-like thioredoxin domain protein	I6HBI8	84.3	Cell redox homeostasis
Cedecea sp. NFIX57	Protein-disulfide isomerase	A0A1X7JC62	79.8	Protein disulphide oxidoreductase activity
Buttiauxella brennerae ATCC 51605	ScsC family secreted protein	A0A1B7IP59	65.7	Cell redox homeostasis
Serratia rubidaea	Thiol-disulfide oxidoreductase D (bdbD)	A0A2X5B2S0	54.1	Cell redox homeostasis

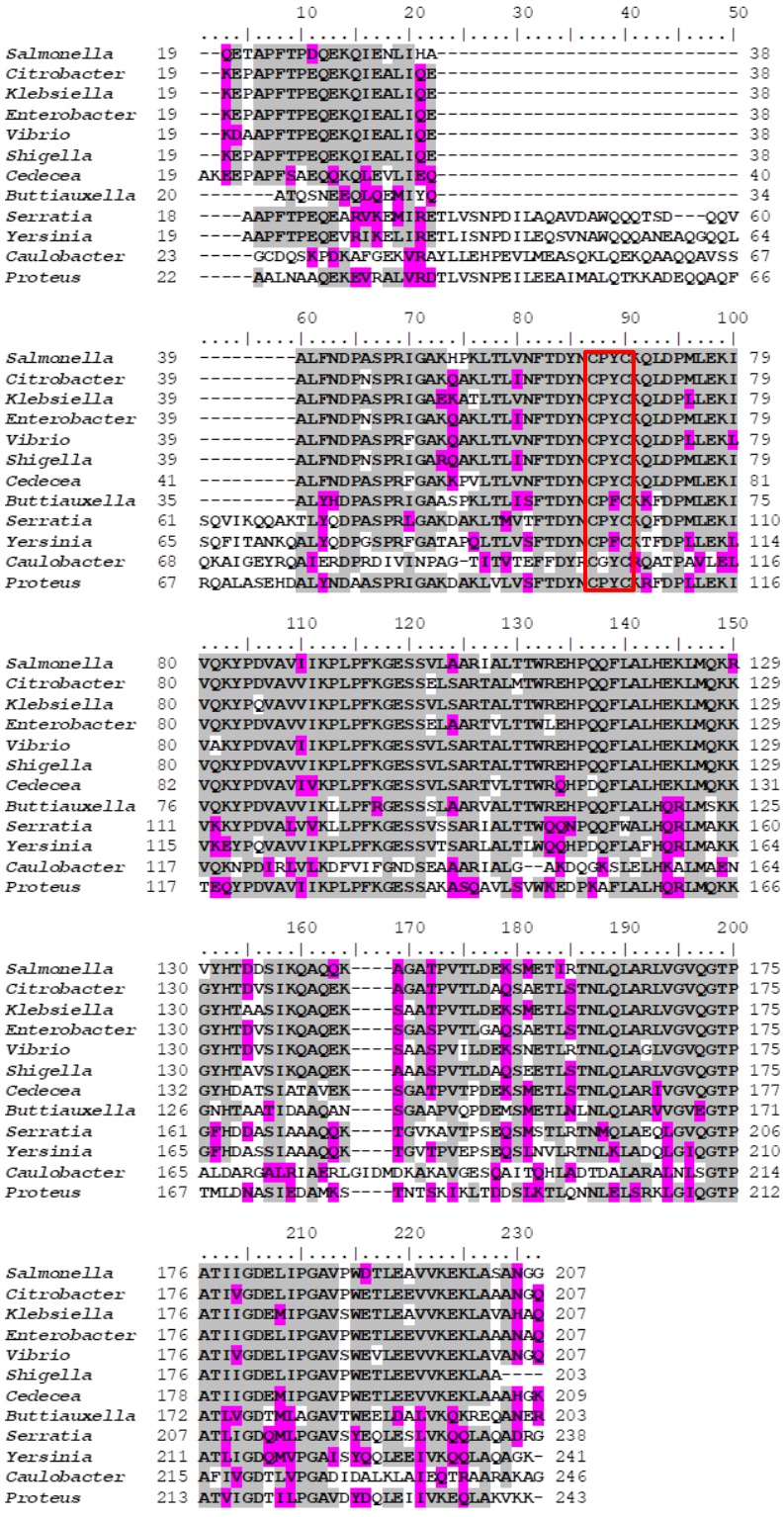


Figure 3.1- Sequence alignment of ScsC proteins. The amino acid sequences of StScsC from *Salmonella typhimurium SL1344* and the orthologous ScsC proteins identified via bioinformatics search as well as *Yersinia frederiksenii* (Uniprot accession number: A0A380PSJ7), *Caulobacter crescentus* (Uniprot accession number: Q9A747) and *Proteus mirabilis* (Uniprot accession number: A0A1Z1SYD5). Fully conserved residues are shaded in grey and residues showing 50% conservation are shaded in pink. The CXXC motif is highlighted by the red box. All sequences except the last four are shown to lack the N-terminal oligomerisation domain.

3.2.2- StScsC expression is induced specifically by copper

Given that the all four *scsABCD* mRNA transcripts had previously been shown to be regulated by copper (Lopez *et al.*, 2018), it was of interest to extend this expression analysis to other stresses and to confirm that the protein abundance was also elevated by copper.

3.2.2.1- Mass spectrometry analysis of StScsC expression in the presence of Cu^{2+}

Native StScsC was quantified in the *Salmonella* periplasm via Synapt G2-Si Mass spectrometer (Waters). Wild-type *Salmonella Typhimurium* SL1344 was grown in the LB media with or without supplementation with 2 mM Cu^{2+}, and periplasmic fractions were isolated. Proteins were digested with Trypsin and peptides were separated by liquid chromatography (UPLC) and analysed by Electrospray ionisation mass spectrometry (ESI-MS). When the growth medium was supplemented with 2 mM Cu^{2+}, the abundance of StScsC was found to be approximately 10-fold higher (Figure 3.2).

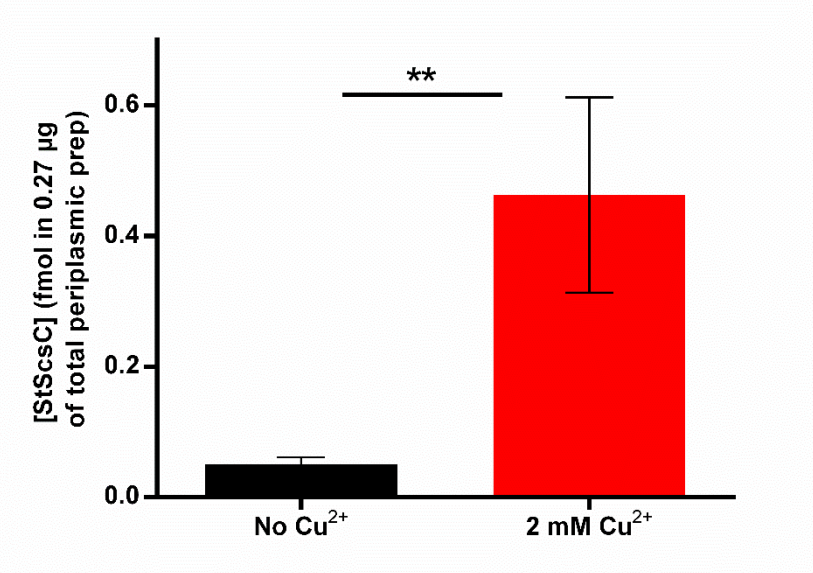


Figure 3.2- The abundance of StScsC in the *Salmonella* periplasm. The abundance of StScsC in the *Salmonella* periplasm was measured using electrospray ionisation mass spectrometry (ESI-MS). In the presence of 2 mM copper, the abundance of StScsC was found to be elevated by 10-fold (red bar). Error bars showing SEM of 4 repeats. P-value < 0.05 for unpaired *t*-test is indicated by asterisks.

3.2.2.2- Western blot analysis demonstrates that StScsC expression is specifically elevated by copper

To invesitage if the expression of StScsC was modulated by other divalent metals, the culture medium was supplemented with $ZnSO_4$, $FeSO_4$, and $CuSO_4$. Whole cell samples were analysed via SDS-PAGE (Appendix 3) and the expression of StScsC was measured via Western blotting with anti-StScsC antibodies. Only the presence of $CuSO_4$ was shown to promote the expression of the StScsC protein (Figure 3.3).

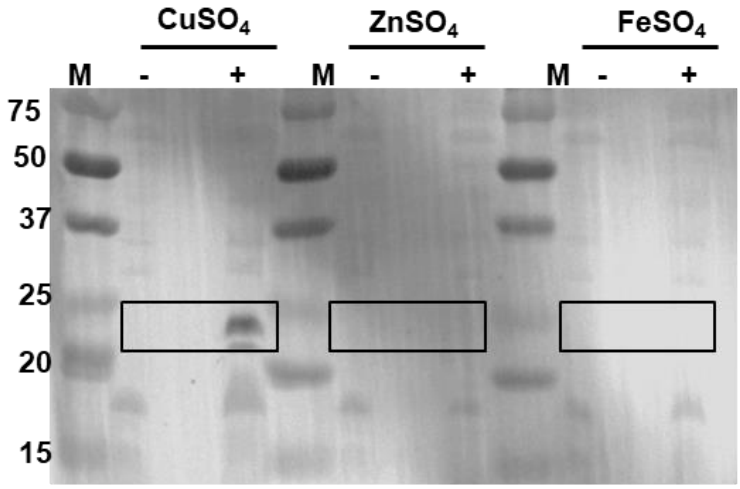


Figure 3.3- Western blot detection of StScsC in cells exposed to divalent metals. Wild-type *Salmonella* was grown in the presence of 2 mM $ZnSO_4$, $FeSO_4$ and $CuSO_4$, and StScsC expression was detected via Western blotting with anti-StScsC antibodies. The black box highlights that the 23 kDa StScsC is only expressed in the presence of copper and not in the presence of zinc or iron sulphate. Marker lanes show the 15, 20, 25, 37, 50 and 75 kDa bands of protein standards (Dual Colour, Bio-Rad). Equal amount of protein was loaded for each whole cell samples.

3.2.2.3- Western blot analysis of StScsC expression in the presence of oxidative/ nitrosative stresses

Since StScs components have previously been implicated in the response to oxidative stress (Lopez *et al*., 2018), it was of interest to measure the expression of StScsC under conditions that promote radical formation via Fenton chemistry. Wild-type *S.* Typhimurium was grown in the presence of various combinations of $CuSO_4$, $FeSO_4$, and peroxide, and expression of StScsC was detected via Western blotting. In addition, the nitric oxide-releaser GSNO was also included in the study. Only copper was found to induce the expression of StScsC (Figure 3.4).

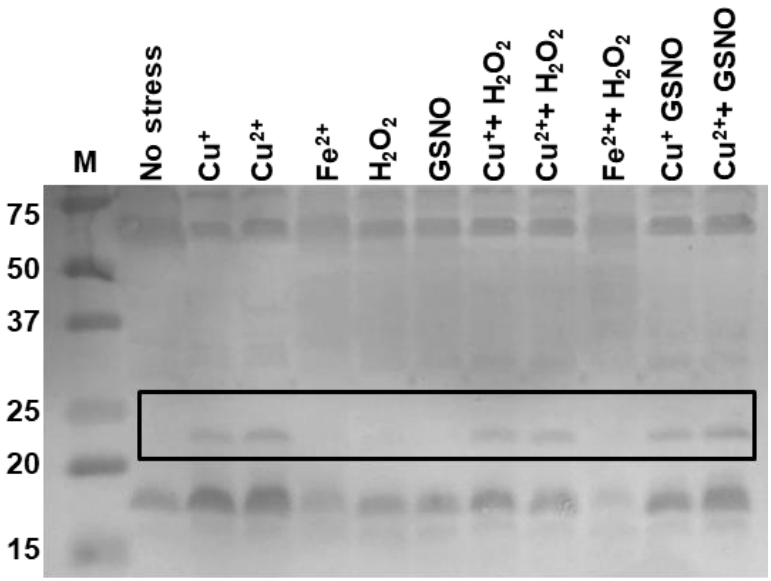


Figure 3.4- Western blot detection of StScsC in cells exposed to a variety of stresses. Wild-type *S.* Typhimurium was grown in the presence of stresses shown on the figure and the periplasmic fractions were isolated. The black box highlights the presence of StScsC only in the presence of copper with anti-StScsC antibodies. Marker lanes show the 15, 20, 25, 37, 50 and 75 kDa bands of protein standards (Dual Colour, Bio-Rad). The SDS-PAGE loading control has been demonstrated (Appendix 4). 18 kDa unidentified band is potentially broken down product of StScsC.

3.2.2.4- Activation of the *scsA* promoter is copper specific

Since production of StScsC is under the control of the *scsA* promoter (Lopez *et al*., 2018) it was of interest to directly investigate the copper-mediated activation of this regulatory region. 400 bp upstream of the *scsA* start codon was cloned (via Gibson assembly) upstream of the *gfp* gene to produce plasmid pET23b_P*scsA*_GFP (Figure 3.5), and the desired sequence was confirmed via sequencing (Appendix 5). Wild-type *S.* Typhimurium harbouring pET23b_P*scsA*_GFP was grown in the presence and absence of 1 mM $CuSO_4$ for 8 h, and the growth curves demonstrate that growth rate is not affected by this concentration of Cu^{2+} (Figure 3.6A). However, copper was confirmed to dramatically elevate the activity of the *scsA* promoter measured by the GFP fluorescence intensity (Figure 3.6B).

A

CTGGCCTTCGTGTTGCTGGAACTGGCGATTAAATTGTGGATCGTTACGGTGTTGCCATAA
CTGGTCATACTCGGCGCGCCGTTGCTCATCACTCAGCACTTCCCATGCTTCAGCAACCTC
TTTGAAACGGGCTTCGGCATCGGGTTCTTTGCTGACATCTGGATGGTACTTGCGGGCCAG
TCGGCGATAGGCGGTCTTAATCGTCTTGAGATCGTCCGTCGGTTTCACGCCCATAATGGC
GTAATAATCCTTAAGTTCCATAGCATCATCTCGCTAAATCAATACATACAGAAGGGACCC
CAAAAGGTTTCTCCACTAAGTGTAGGGTAAACCTGAAAAGTGCGTATGAAAACACCAGTT
ATATCATTAGTAAGAATAAATTACGTTGTTCGACTATCAGAAGGTTGCGCAGCGCGCCGA
CATAACTTTACAGGGGAAAGGTTGCCAAAACCGCGCCAGTGGCTAAGATAACTCGCGTTA
AACAGTGAGGGCGCAATGGCGAAACAACAACGGATGGGCTGGTGGTTTCTTTGCCTTGCA
TGTGTCGTGGTAATGGTTTGTACCGCGCAACGCATGGCGGGCCTGCACGCCTTGCAGATG
CAGGCGACGGCCTCTGCTGCGGTGGTCAGCGCTCCCTCCTCGACAGATGACGGCTCGCCG
GTCACCCCCTGCGAATTAAGCGCCAAGTCGCTGCTGGCGGCGCCTCCGGTACTCTTTGAA
GGCGCTATCCTTGCGCTTTGTCTACTGCTTTCCTTACTGGCGCCTGTCCGGGTCATGCGC
CTGCCGTTTTCGCCTCCACGGGCTATTTCGCCGCCCACATTACGGGTACATCTACGATTT
TGTGTCTTCCGTGAATGA

B

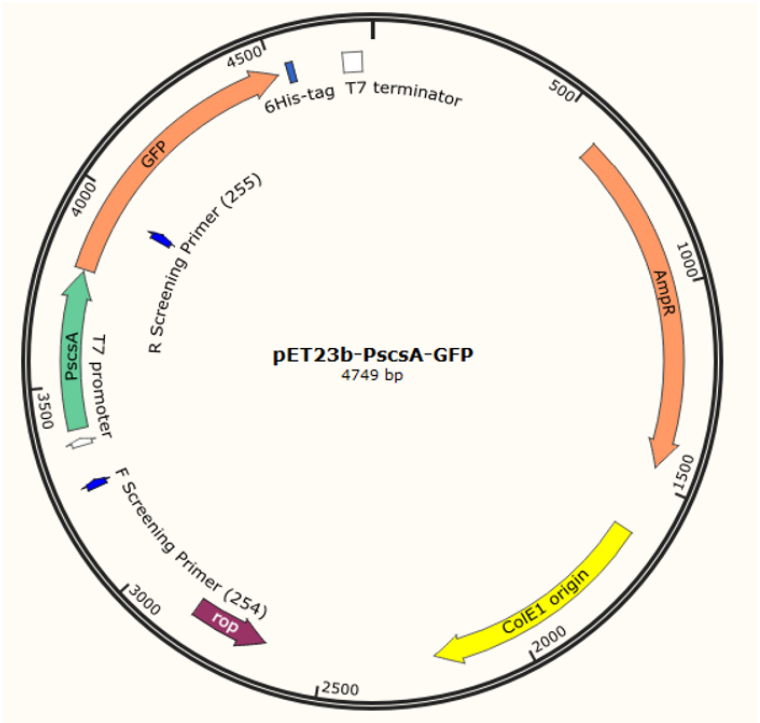


Figure 3.5- Cloning of a *scsA*-GFP transcriptional fusion plasmid. (A) The nucleotide sequence of *scsA* from *S*. Typhimurium SL1344 is shown in red and the promoter region 400 bp upstream of the *scsA* gene is shown in black. -10 and -35 promoter regions are underlined in black. The putative ribosome binding site (RBS) is underlined in green (Gupta *et al*., 1997). Putative CpxR-binding sequences are underlined in red (Lopez *et al*., 2018). The stop codon is indicated in green**. (B)** Plasmid map of pET23b_P*scsA*_GFP. 400 bp upstream of *scsA* (*PscsA*) was cloned upstream of *gfp* in a pET based plasmid. For alternative detection and purification, hexa-histidine tag is also incorporated.

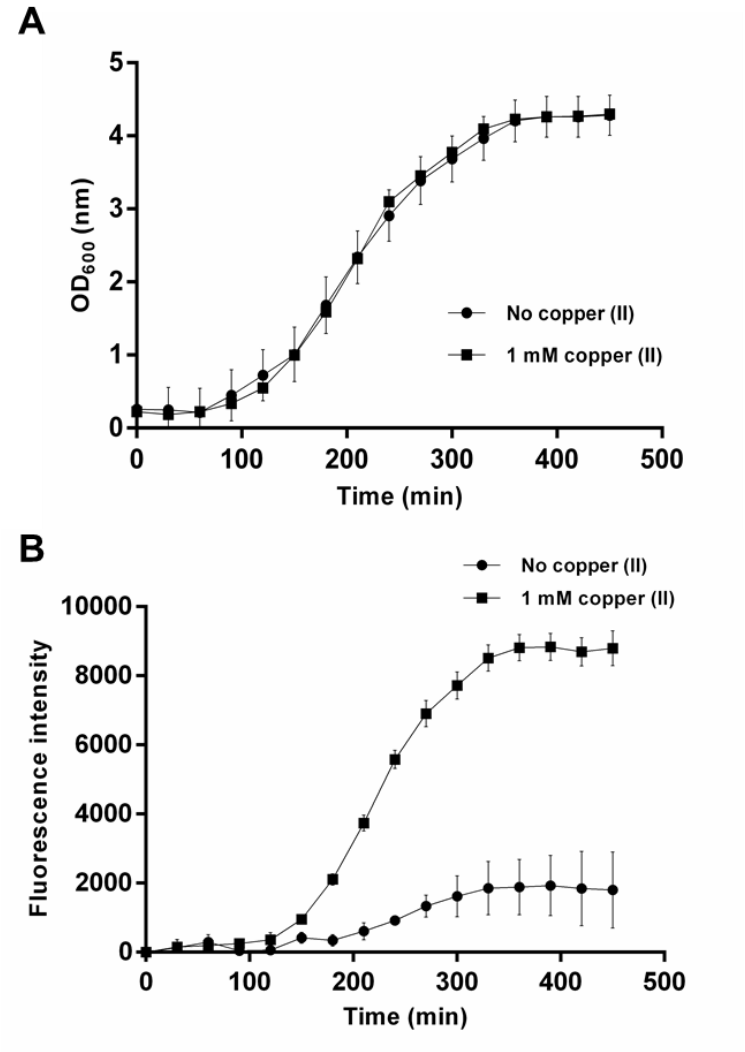


Figure 3.6- Impact of copper upon growth and *scsA* promoter activity in *S.* Typhimurium. Wild-type *S.* Typhimurium harbouring the transcriptional fusion plasmid pET23b_P*scsA*_GFP was grown in the presence (■) and absence (●) of 1 mM Cu^{2+} for 8 h. **(A)** The optical density at 600 nm (Data represents the average of 6 independent repeats and the error bars showing SEM) and **(B)** the GFP fluorescence was recorded (Data represents the average of 6 independent repeats and the error bars show 95% confidence intervals).

To confirm that this copper-mediated elevation in transcriptional activity was concentration dependent, $CuSO_4$ was varied from 0-2 mM and GFP fluorescence was measured after 8 h. Increasing concentration of copper resulted in elevated levels of GFP production in a dose-dependent fashion (Figure 3.7). This copper-mediated activation of the *scsA* promoter was also confirmed using fluorescence microscopy, where *Salmonella* harbouring the pET23b_P*scsA*_GFP emitted GFP fluorescence only in the presence of copper (Figure 3.8).

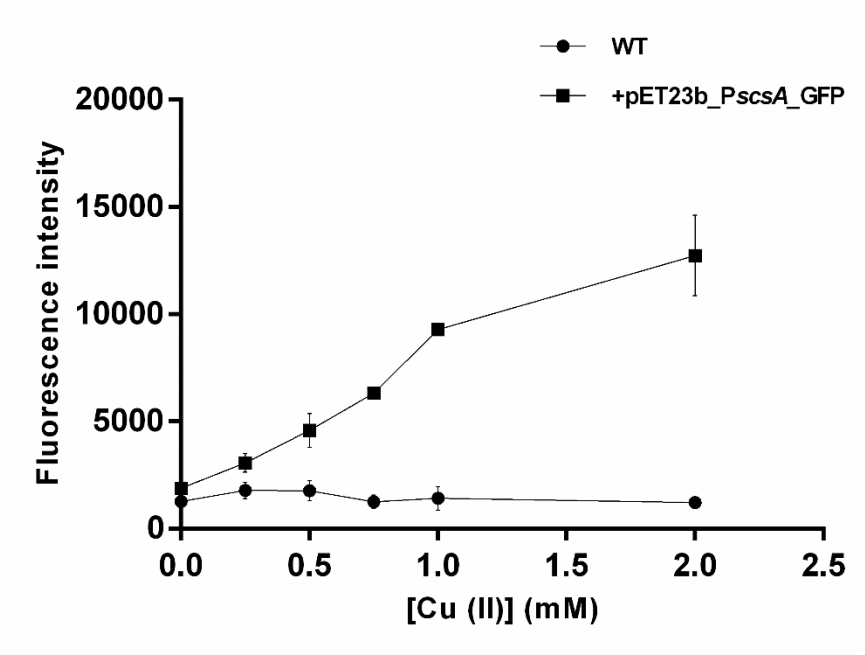


Figure 3.7- P*scsA* activity with increasing concentrations of Cu^{2+}. Wild-type *S.* Typhimurium harbouring the pET23b-P*scsA*-GFP plasmid was grown in the presence of increasing concentrations of Cu^{2+} (0-2 mM) and GFP fluorescence was measured after 8 h. This dose response experiment reveals a concomitant increase in P*scsA* activity with increasing Cu^{2+}. Wild-type control is indicated as (●). Data were collected in triplicate and error bars show 95% confidence intervals.

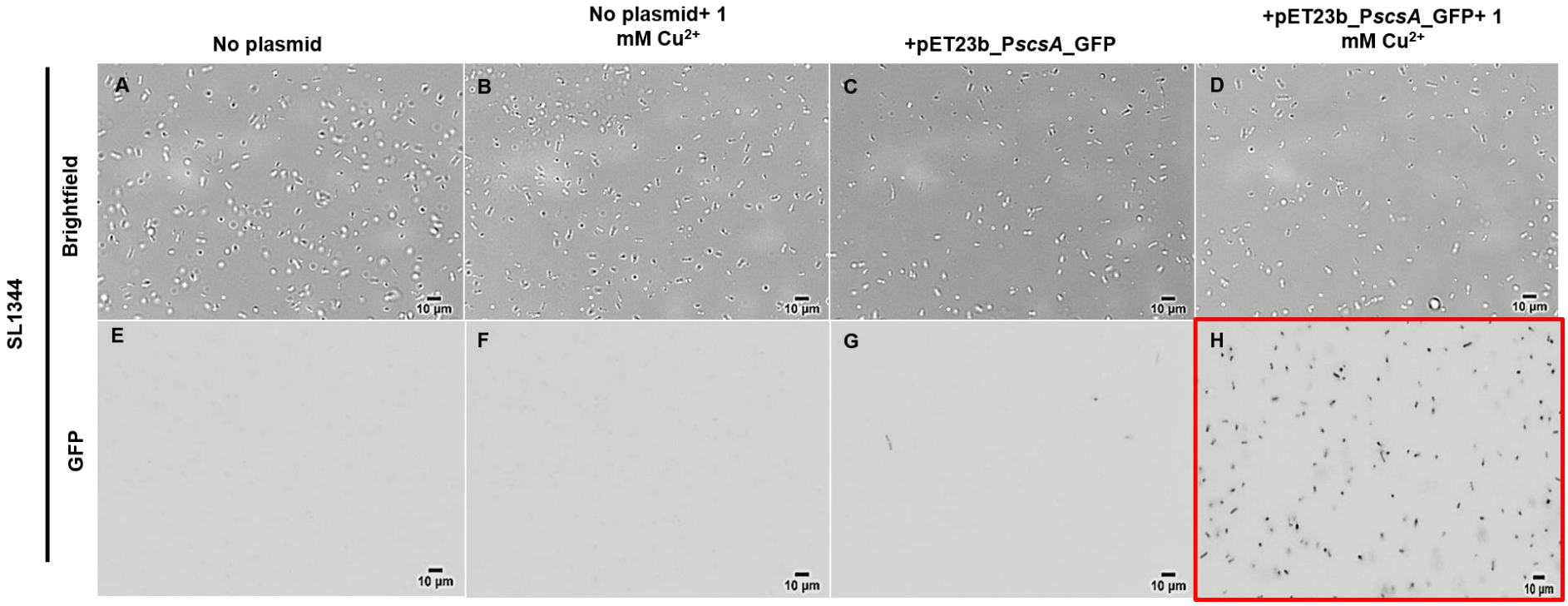


Figure 3.8- GFP expression of *S*. Typhimurium harbouring the pET23b-P*scsA*-GFP fusion plasmid. Fluorescence microscopy images of wild-type *S.* Typhimurium and an isogenic strain expressing GFP under the control of the *scsA* promoter in the presence and absence of 1 mM Cu^{2+}. 3 µL of cell culture was taken after 8 h of growth and was visualised using an Olympus IX 81 inverted microscope**.** Panels A to D shows the brightfield images of the strains and panels E to H represent the fluorescence microscopy images. GFP was only detected in the presence of Cu^{2+} as shown in image H, highlighted by the red box. Scale bar, 10 µM.

Finally, to provide confirmation that the fluorescent signal elicited by copper is indeed that of GFP, his_6-tagged GFP was purified from *Salmonella* harbouring pET23b_P*scsA*_GFP by affinity chromatography. Purified protein was resolved via SDS-PAGE and detected via Western blotting with anti-his_6 antibodies (Figure 3.9). This purified protein was then confirmed to be GFP using fluorescence spectroscopy, where a characteristic emission peak at 512 nm and excitation peak at 470 nm (Remington, 2011; review) were detected (Figure 3.10).

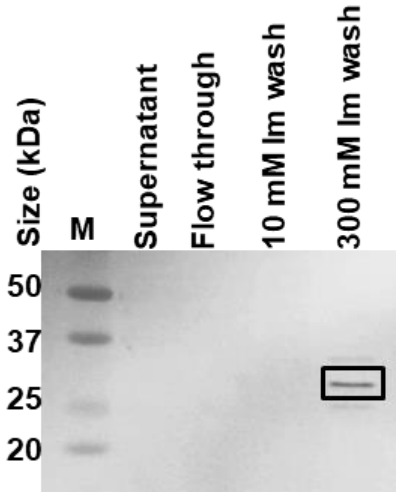


Figure 3.9- Western blot analysis of purified his_6-tagged GFP from *S.* Typhimurium harbouring pET23-P*scsA*-GFP. Affinity chromatography was performed on cell lysate from a strain harbouring the fusion plasmid when grown in the presence of 1 mM Cu^{2+}. Anti-his_6 antibodies fused to alkaline phosphatase were used, and blot was developed with BCIP/NBT solution. A 27 kDa GFP protein (shown by the black box) was detected in the fraction that was eluted with 300 mM imidazole elution. Marker lanes show the 20, 25, 37 and 50 kDa bands of protein standards (Dual Colour, Bio-Rad).

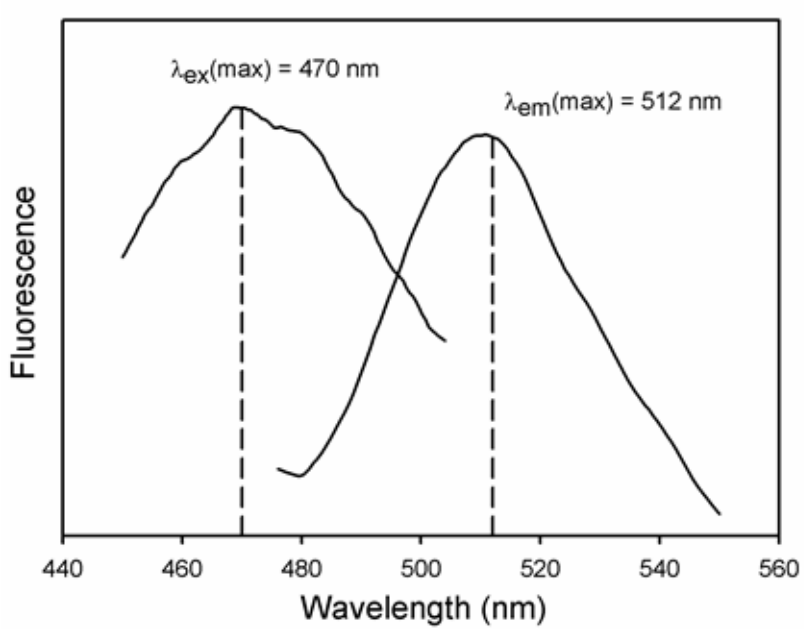


Figure 3.10- Excitation and emission spectra of GFP from copper induced cells harbouring pET23-P*scsA*-GFP plasmid. The 27 kDa protein purified from cells harbouring pET23-P*scsA*-GFP that were exposed to copper (Figure 3.9) was subjected to fluorimetric analysis. Excitation and emission peaks were recorded as 470 nm and 512 nm, respectively.

3.2.3- StScsC exists in the oxidised state *in vivo*

Low levels of StScsC exist in the reduced state *in vivo* in the absence of copper (Shepherd *et al*., 2013), but since copper causes a significant elevation in StScsC levels it was of interest to investigate if copper can also modulate the *in vivo* redox state of StScsC. The redox status of StScsC was monitored in the periplasm of *S.* Typhimurium using the thiol modification reagent 4-Acetamido-4'-Maleimidylstilbene-2,2'-Disulfonic Acid (AMS), as previously described (Rudyk and Eaton, 2014; review). Periplasmic preparations of *S.* Typhimurium grown in the presence of 1 mM copper were reduced with DTT or left untreated and cysteines were alkylated with AMS. Each AMS adduct adds 0.5 kDa and therefore elicits a 1kDa shift in molecular weight for the fully-oxidised and fully-reduced CPYC motif of StScsC (Shepherd *et al.*, 2013). After performing the necessary positive controls with reduced and oxidised StScsC (Figure 3.11A), the thiol redox state was monitored in the presence of copper, peroxide and the NO-releasing agent GSNO (Figure 3.11B). Since expression of StScsC could not be detected in the absence of

copper via Western blotting (Figure 3.3), this condition was not included. StScsC was found to be in the oxidised state under all conditions tested.

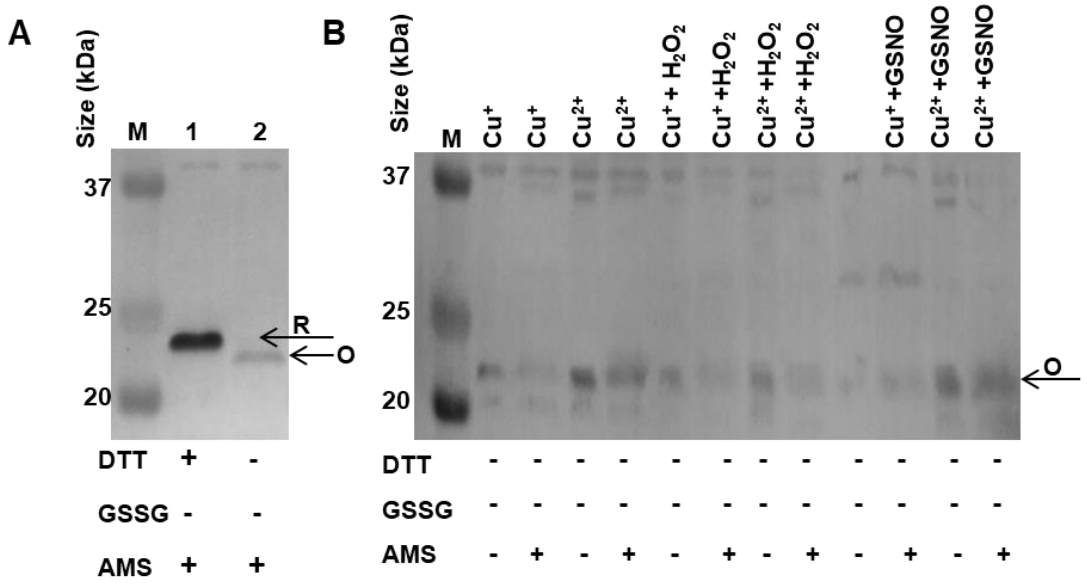


Figure 3.11- Determination of the *in vivo* redox state of StScsC by Western blotting. StScsC was detected using anti-StScsC antibodies. Marker lane corresponds to the 20, 25 and 37 kDa bands of protein standards (Dual Colour, Bio-Rad). **(A)** Periplasmic fractions of *S.* Typhimurium isolated from cultures grown in the presence of 1 mM $CuSO_4$ were incubated with 5 mM DTT or left untreated. After the precipitation of proteins, samples were incubated with 20 mM AMS. The higher-molecular weight band shown in lane 1 indicates reduced StScsC (R) and the lower-molecular weight band in lane 2 shows oxidised StScsC (O). **(B)** Western blot detection of StScsC disulphide redox status in the presence of oxidative (hydrogen peroxide) and nitrosative (GSNO) stresses in combination with copper ions. Periplasmic fractions of *Salmonella* were isolated and samples were either left untreated or subjected to thiol modification with 20 mM AMS.

3.2.4 - Copper and StScsC promote the assembly of disulphide-containing proteins involved in peptide uptake

Given the likely role of copper and StScsC in disulphide chemistry in the periplasm of *S.* Typhimurium, it was of interest to investigate the impact of both upon the abundance of cysteine- and disulphide-containing secreted and periplasmic proteins. It was assumed that improved disulphide folding would result in an increase in abundance of protein. Wild-type and Δ*scsC S.* Typhimurium strains were grown in the presence and absence of 2 mM Cu^{2+}, periplasmic fractions were extracted and the protein concentrations were determined by Markwell assay as described in section 2.5.3.1.

3.2.4.1 - StScsC and copper alter the abundance of disulphide/cysteine-containing periplasmic/secreted proteins in *S*. Typhimurium

Since StScsC has a likely role in disulphide folding, and incorrectly folded proteins are anticipated to be degraded in the periplasm, it was hypothesised that StScsC expression and copper would influence the concentrations of a variety of periplasmic proteins and in doing so provide a list of candidate target proteins for StScsC. Hence, periplasmic fractions were prepared from wild-type and Δ*scsC S.* Typhimurium grown in the presence and absence of 2 mM copper, and protein concentrations were determined using a Markwell assay. 10 μg of periplasmic protein was then acetone precipitated as described in section 2.11.2 and peptides were digested using trypsin. Protein samples were mixed with a known concentration of BSA standard to allow label free quantitation. Peptides were separated with UPLC for subsequent mass spectrometry analysis. Peptides were then analysed using Progenesis QI software against the TrEMBL *Salmonella* database. Table 3.2 shows the intial dataset of periplasmic/secreted proteins that was detected by mass spectrometry. To further narrow down potential interaction partners for StScsC, cysteine- and disulphide-containing proteins were identified from the initial dataset and those that displayed elevated abundance in response to Cu^{2+} and StScsC were selected for further analysis (Figure 3.12).

Table 3.2- Copper and StScsC influence protein abundance in the *S.* Typhimuruim periplasm. Wild-type and *ΔscsC S.* Typhimurium strains were grown in the presence and absence of 2 mM $CuSO_4$, and periplasmic preparations were isolated. Peptide abundances were measured using a Synapt G2-Si Mass spectrometer (Waters) and proteins were identified based on abundance of a range of peptide fragments. Periplasmic and secreted proteins were identified based on their functional annotation (from TrEMBL *Salmonella* database), and other proteins were removed from the list. Protein abundance (black numbers) is expressed as an average of 6 repeats (including three biological repeats). Unpaired *t*-tests were performed to assess if fold-changes for ([*ΔscsC*] *vs.* [WT]) and ([WT+ Cu^{2+}] *vs.* [WT]) were significant. Fold-changes were also calculated for ([*ΔscsC*+ Cu^{2+}] *vs.* [WT+Cu^{2+}]), and unpaired *t*-tests were performed. Fold-changes and *P*-values are shown in red and blue, respectively.

			Protein abundance (fmoles)			
Protein name	**Uniprot accession**	**Function**	**WT**	***ΔscsC***	**WT+ Cu^{2+}**	***ΔscsC*+ Cu^{2+}**
				Fold-change *P*-value	**Fold-change** *P*-value	**Fold-change** *P*-value
ArgT	A0A0H3NP23	Amino acid binding	2.81	3.71 1.32 0.24	5.68 2.02 0.00	3.31 -1.72 0.01
ArtI	A0A0H3NEU6	Amino acid binding	0.01	0.04 4.47 0.14	0.16 19.88 0.05	0.06 -2.53 0.24
ArtJ	A0A0H3NJH7	Amino acid transporter	0.83	1.26 1.51 0.11	4.21 5.04 0.03	2.60 -1.62 0.24
CpxP	A0A0H3NI70	Repressor of *cpx* regulon	0.12	0.21 1.74 0.21	1.11 9.31 0.04	2.39 2.15 0.32
DsbA	A0A0H3NUM9	Thiol:disulfide interchange	4.73	9.93 2.10 0.10	31.18 6.59 0.01	23.04 -1.35 0.30
DsbC	A0A0H3NRG8	Thiol:disulfide interchange	1.42	2.64 1.86 0.09	2.58 1.82 0.15	3.08 1.19 0.65
DsbG	A0A0H3N8T4	Thiol:disulfide interchange	0.30	0.54 1.79 0.00	0.27 -1.11 0.76	0.19 -1.40 0.48
DsbL	A0A0H3NG38	Thiol:disulfide interchange	0.02	0.05 2.53 0.22	0.06 2.99 0.08	0.04 -1.28 0.66
GltI	A0A0H3N9H9	Amino acid transporter	5.28	7.83 1.48 0.08	10.22 1.94 0.01	5.43 -1.88 0.02
HisJ	A0A0H3NDX8	Amino acid binding	13.51	24.59 1.82 0.02	63.87 4.73 0.00	40.84 -1.56 0.06
MalE	A0A0H3NIS1	Carbohydrate import	0.42	1.16 2.75 0.04	2.63 6.25 0.03	0.98 -2.67 0.08
MalM	A0A0H3NIF0	Carbohydrate transport	1.73	3.21 1.86 0.05	0.90 -1.92 0.07	1.83 2.03 0.04

MppA	A0A0H3NC08	Peptide binding protein	0.44	0.78 1.77 0.05	0.94 2.12 0.26	0.68 -1.37 0.56
OmpA	A0A0H3N9Z8	Outer membrane protein	3.90	3.53 -1.11 0.75	8.82 2.26 0.04	8.05 -1.09 0.78
OsmY	A0A0H3NLC0	Transmembrane transport	16.27	32.06 1.97 0.03	60.41 3.71 0.01	34.62 -1.74 0.07
PotD	A0A0H3NC70	Putrescine transport	0.11	0.13 1.28 0.15	0.75 7.19 0.00	0.18 -4.28 0.00
ProX	A0A0H3NF33	Glycine betaine-binding	7.02	13.16 1.87 0.07	17.28 2.46 0.03	17.47 1.01 0.98
SlrP	A0A0H3N9B0	Ubiquitin-protein transferase activity	0.10	0.15 1.60 0.02	0.11 1.14 0.62	0.13 1.20 0.60
SodC	A0A0H3NF91	Superoxide dismutase activity	0.24	0.31 1.29 0.48	0.42 1.76 0.37	0.06 -6.99 0.10
SodCII	A0A0H3NB27	Superoxide dismutase activity	0.27	0.92 3.40 0.00	1.97 7.28 0.00	1.35 -1.46 0.06
SopA	A0A0H3NIK3	Bacterial invasion of the host	0.27	0.45 1.69 0.00	0.59 2.22 0.09	0.49 -1.22 0.63
SopD	A0A0H3NH64	Bacterial invasion of the host	0.05	0.09 1.97 0.34	0.15 3.22 0.15	0.07 -2.21 0.26
SopE	A0A0H3NGI8	Promote bacterial entry into host cell	0.50	0.43 -1.18 0.12	0.16 -3.18 0.00	0.24 1.52 0.48
TreA	A0A0H3NHH6	Utilisation of trehalose	0.78	1.33 1.71 0.14	0.69 -1.13 0.71	1.16 1.68 0.36
UgpB	A0A0H3NH34	Transmembrane transport	2.12	4.57 2.15 0.01	4.98 2.35 0.06	4.05 -1.23 0.54
YhjJ	A0A0H3NH75	Zinc protease	2.41	5.31 2.20 0.00	8.17 3.39 0.10	5.80 -1.41 0.49
YliB	A0A0H3N9X5	Transmembrane transport	0.21	0.19 -1.09 0.86	0.12 -1.67 0.42	0.16 1.25 0.66
ZnuA	A0A0H3NCN2	Metal ion binding	1.11	1.76 1.58 0.20	3.53 3.17 0.02	2.78 -1.27 0.49

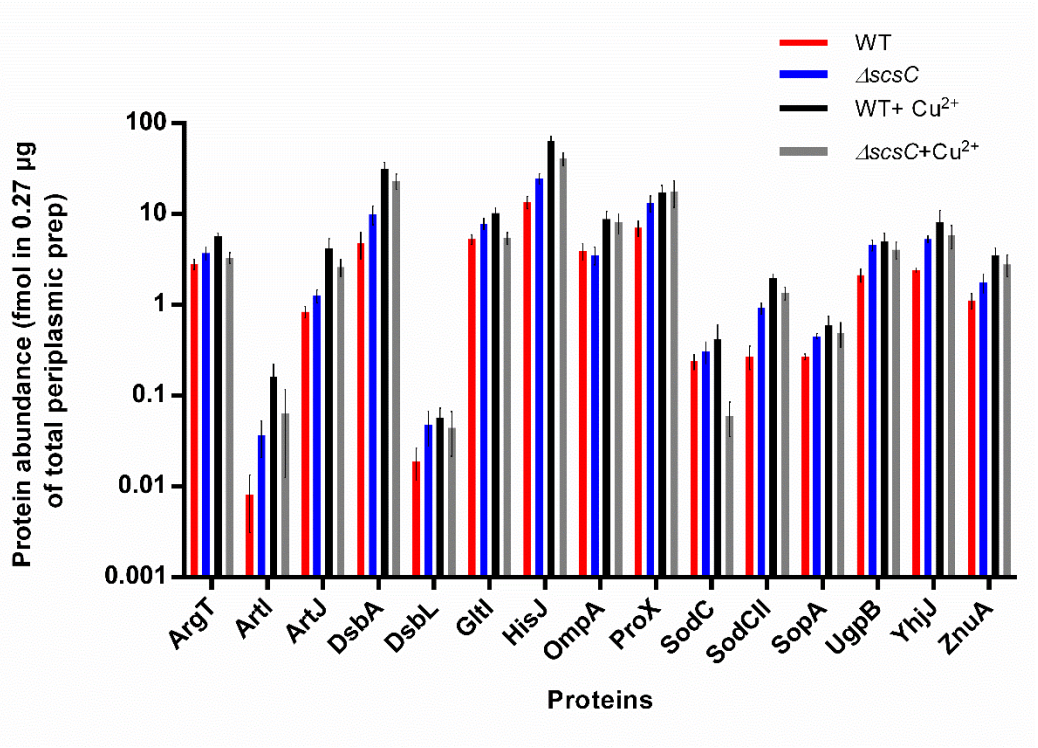


Figure 3.12 - Proteomic quantitation of disulphide-containing periplasmic/secreted proteins that have altered abundance in response to copper and StScsC. The protein abundance (fmol) in 0.27 µg of total periplasmic protein of wild-type and *ΔscsC S.* Typhimurium strains grown in the presence and absence of 2 mM Cu^{2+}. Data points are averages of 6 repeats and error bars show SEM.

Given the low level of StScsC expression in the absence of copper (Figure 3.2, 3.3), it was hypothesised that a ([*ΔscsC*] *vs.* [WT]) comparison would reveal only minimal decreases in protein abundance. Indeed, no significant loss of protein abundance was observed in the *ΔscsC* strain in the absence of copper (fold-changes and *P*-values are shown in Table 3.2). In the presence of copper, however, it was hypothesised that loss of StScsC would diminish the abundance of potential target proteins, resulting in negative fold-changes for the ([*ΔscsC*+ Cu^{2+}] *vs.* [WT+Cu^{2+}]) comparison. Furthermore, we hypothesised that exposure of the wild-type strain to copper might elevate the abundance of StScsC target proteins, resulting in positive fold-changes for the ([WT + Cu^{2+}] *vs.* [WT]) comparison. The data in Figure 3.13 shows fold-changes for these comparisons, and proteins fitting the hypothesised abundance changes for a StScsC target were highlighted in red. All proteins from Figure 3.13 were mapped onto a diagram to illustrate *in vivo* functions for these candidate target proteins (Figure 3.14), and those fitting the hypothesised abundance changes for a StScsC target were again highlighted in red. Notably, proteins involved in amino

acid and peptide uptake displayed greater abundance when copper and StScsC were present ([WT + Cu^{2+}] *vs.* [WT]), and diminished abundance when StScsC was lost ([*ΔscsC*+ Cu^{2+}] *vs.* [WT+Cu^{2+}]), suggesting that assembly of these disulphide-containing periplasmic proteins may be facilitated by StScsC.

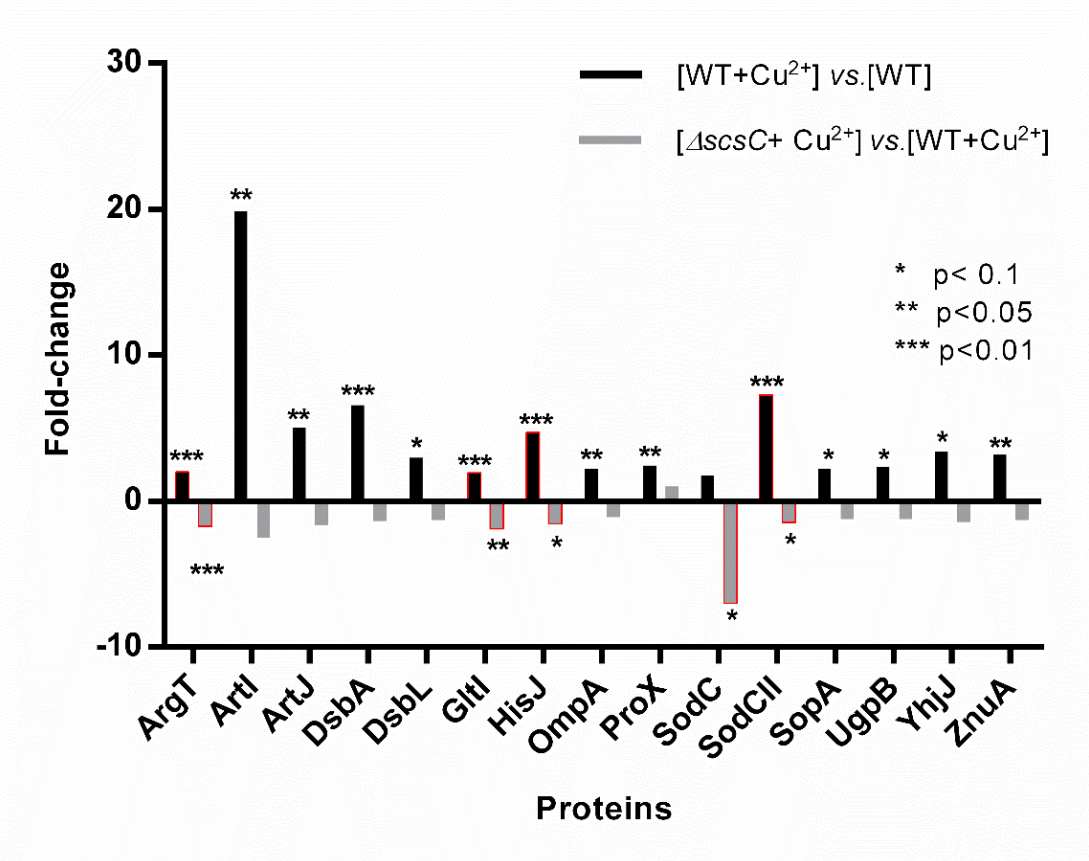


Figure 3.13 - Fold-changes elicited by copper and StScsC for disulphide-containing periplasmic/secreted proteins. Fold-changes that are elicited by copper alone ([WT + Cu^{2+}] *vs.* [WT]) are shown in black, and fold-changes elicited by loss of StScsC in the presence of copper ([Δ*scsC* + Cu^{2+}] vs. [WT + Cu^{2+}]) are shown in grey. Data highlighted in red are predicted StScsC targets where protein abundance is elevated by copper and diminished by loss of StScsC. *P*-values for unpaired *t*-tests are indicated on the figure.

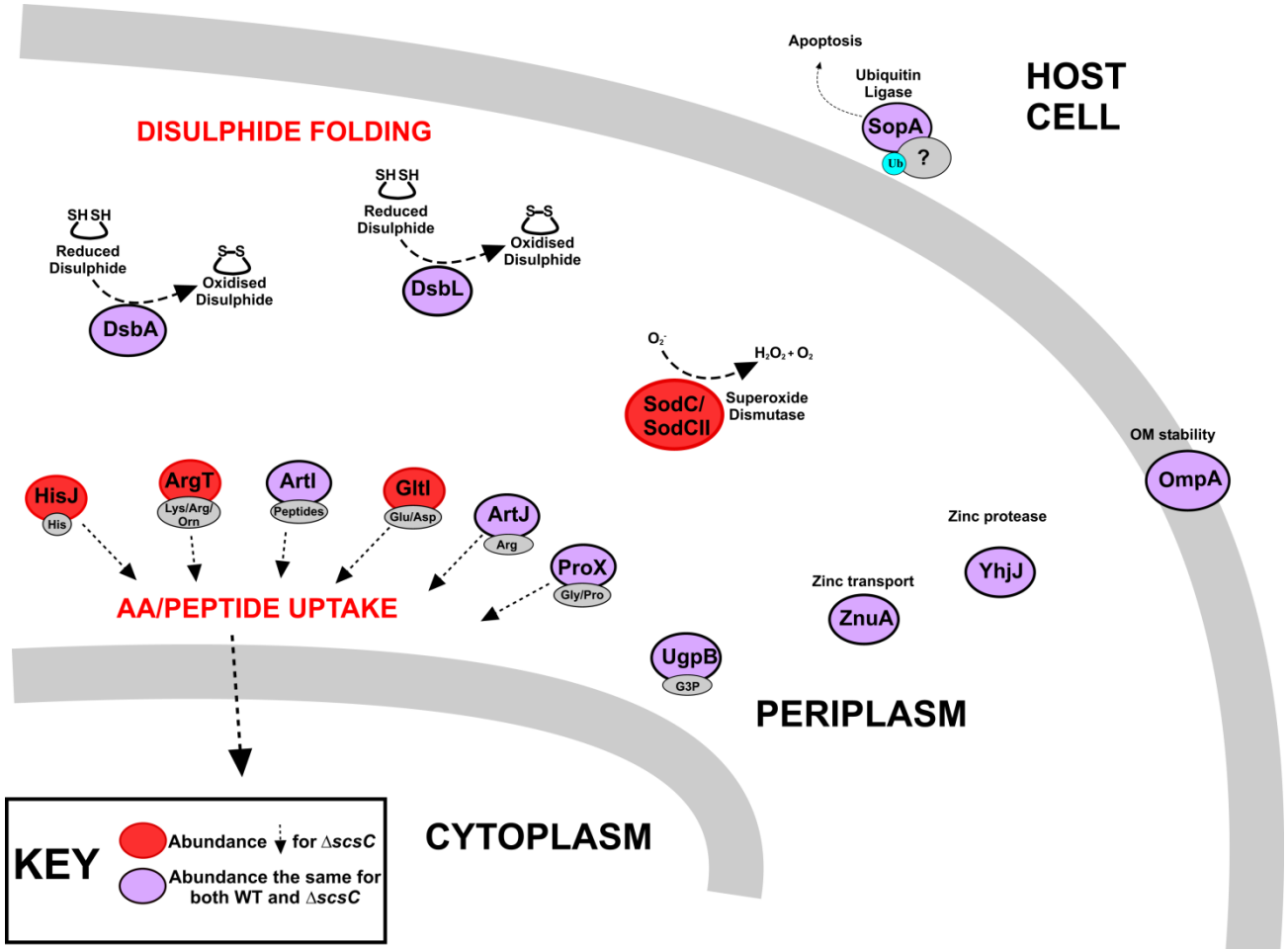


Figure 3.14 - Function of disulphide/cysteine-containing proteins that have altered abundance in response to copper and StScsC.

3.2.5 - StScsC elevates the abundance of oxidised BcsC peptide fragment

While it is useful to measure changes in protein abundance in response to StScsC and copper, it would be especially informative if one could detect changes in thiol redox state of periplasmic proteins in response to changing levels of copper and StScsC. In order to measure the abundance of reduced and oxidised disulphides from periplasmic preparation, a similar mass spectrometry approach as above was undertaken. Wild-type and Δ*scsC Salmonella* strains were grown in the presence and absence of copper ions, periplasmic fractions were isolated, and 10 µg protein samples were trypsin digested in the absence of a reducing agent (DTT) in order to detect peptide fragments in their native form (either oxidised or reduced). Peptides were then analysed by Progenesis QI software against Swissprot *Salmonella* database. The raw mass dataset from the analysis was used where the masses of all peptides present in the sample was shown. At this stage, reduced peptide fragments could be assigned for a protein, whereas oxidised peptide fragments had not yet been identified. From the 'reduced fragment' dataset, periplasmic/secreted cysteine-containing proteins were identified. Protein sequences were subjected to *in silico* trypsin digestion and the raw mass data was mined for both reduced and oxidised peptide fragment of a protein. Fragment sizes for disulphide-containing fragments were individually calculated for each protein using online peptide mass calculator tool (http://www.peptidesynthetics.co.uk/tools/).

Cellulose synthase operon protein C (BcsC) was the only protein for which a reduced peptide and a disulphide-containing peptide could be identified. A reduced peptide fragment (YDNNWGTCTLEK) was detected as well as a 1980.825 Da peptide that is the exact mass of a disulphide-containing peptide fragment of BcsC (YDNNWGTCTLEK-CSGHR). This could have been detected due to an incomplete trypsin digestion or due to an incomplete reaction with iodoacetamide however, two cysteine residues have been highlighted on the crystal structure of the BcsC from the best template from the PDB (Figure 3.15) to show that the cysteine residues are in relatively close proximity to form a disulphide. However; this remains elusive before any structural/ biochemical analysis. A section of the amino acid sequence of BcsC where the cysteine residues are found is shown in Figure 3.16.

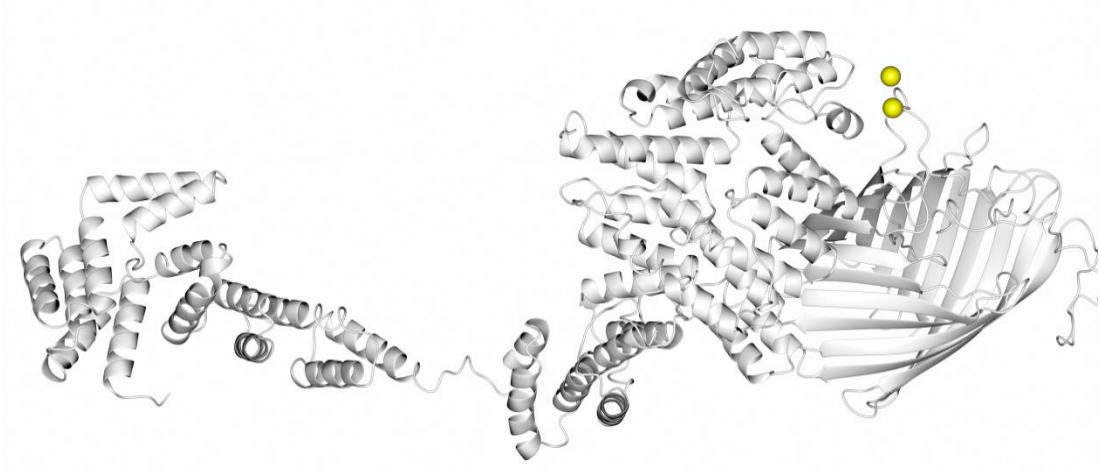


Figure 3.15 – Crystal structure of *Salmonella* BcsC. Ribbon structure of BcsC (from best template using RaptorX server (Källberg et al., 2012)). Yellow spheres indicating sulphur atoms of cysteine residues at positions Cys829 and Cys834.

781 DLKAHTTMLQVDAPWSDGRAFFRTDMVNMDVGRFSTDADGKYDNNWGTCTLEKCSGHRSQ 840

Figure 3.16 - Amino acid sequence of BcsC. The 1135 amino acid sequence of BcsC, lacking the targeting peptide, was *in silico* digested with trypsin (ExPASy peptide cutter). Residues positioned from 781 to 840 are shown. Two cysteine residues at positions Cys_{829} and Cys_{834} are underlined. Red lines on top of the residues indicate the Trypsin cleavage sites. The reduced peptide fragment of BcsC identified via mass spectrometry is shown in blue (YDNNWGTCTLEK) and the oxidised disulphide-containing peptide fragment is the combination of the blue and green residues (YDNNWGTCTLEK-CSGHR). The mass of the reduced peptide fragment is 1442.603 and the mass of the oxidised peptide fragment is 1980.825.

The normalised peptide abundances of reduced and oxidised peptides of BcsC were compared for periplasmic samples isolated from WT and Δ*scsC* strains grown in the presence and absence of Cu^{2+} (Figure 3.17). While the reduced peptide fragment is more abundant in all samples, the abundance of the oxidised peptide is elevated specifically by the presence of both StScsC and Cu^{2+}.

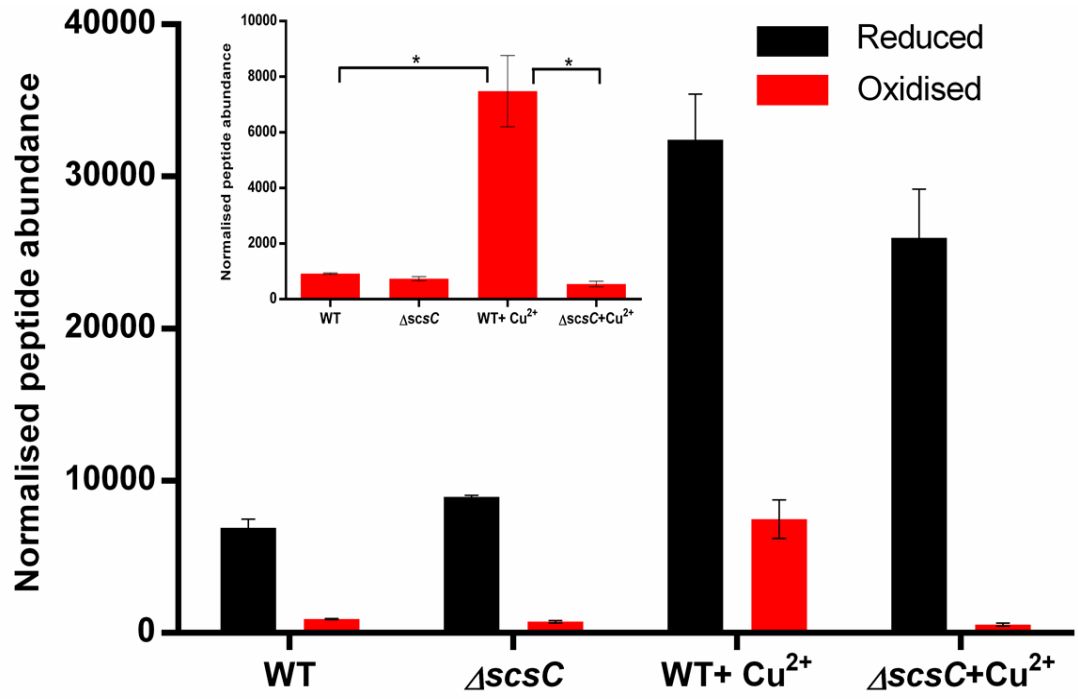


Figure 3.17 - Normalised abundance of reduced and oxidised peptide fragments of BcsC in the *S.* Typhimurium periplasm. Peptide abundance was normalised against a known quantity of BSA. Data for the reduced YDNNWGTCTLEK fragment is shown by black bars; red bars show the oxidized YDNNWGTCTLEK-CSGHR fragment in the presence and absence of copper and StScsC. Error bars show the standard error of 4 repeats. The inset shows the abundance of the oxidized fragment alone. In the presence of StScsC and copper, the abundance of oxidized fragment is significantly elevated. *P*-value < 0.05 for unpaired *t*-test is indicated by an asterisk.

3.2.6 - *Salmonella* survival in murine macrophages is significantly impaired by loss of StScsC

Given that membrane-bound disulphide oxidoreductases are generally quite promiscuous and the unique roles of the *scs* operon are therefore likely to be mediated through the periplasmic chaperones StScsC and StScsD, it was of interest to investigate whether loss of the *scsC* gene affected bacterial loads during infection. Activated macrophages were infected with WT and Δ*scsC* strains in the presence of copper (i.e. to stimulate StScsC expression in the wild-type), and survival after 3 h and 24 h was expressed as a % of bacterial load following uptake (20 min post-infection). At 20 min post-infection, there was no significant difference between bacterial loads of the wild-type and the mutant strains, confirming that loss of *scsC* did not influence uptake into macrophages. At 3 h post-infection, survival of the wild-type strain was 8-fold higher than that of the Δ*scsC* mutant (Figure 3.18). At 24 h post infection, this trend continued with the wild-type strain displaying approximately 5-fold higher survival compared to the Δ*scsC* mutant.

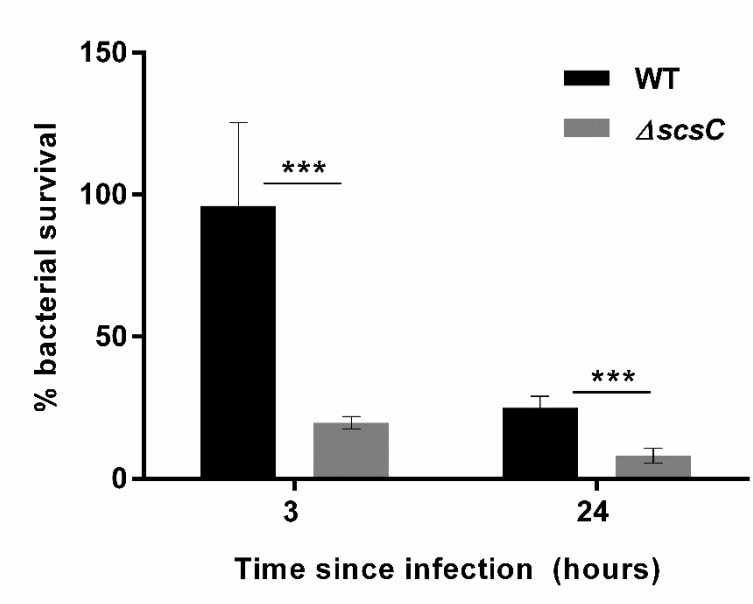


Figure 3.18 - StScsC promotes *S.* Typhimurium survival within macrophages during copper stress. RAW-Blue macrophages were infected with wild-type (black bars) and Δ*scsC* (grey bars) *S.* Typhimurium strains using culture medium supplemented with 100 μM $CuSO_4$. Intracellular bacterial survival is expressed as % survival at 3 h and 24 h post infection compared to 20 min post-infection (i.e. following bacterial uptake). Datapoints represent averages of five repeats including three biological repeats. Asterisks denote $P < 0.01$ for unpaired *t*-tests, and error bars showing standard deviation.

3.3- Discussion

Disulphide mediated folding of proteins is important for their activity and stability. Copper accumulates in the *Salmonella* containing vacuoles of macrophages (Achard *et al.,* 2012), and copper promotes the oxidation of native and non-native disulphide bonds (Hiniker *et al*., 2005). The *scs* operon of *Salmonella* encodes TRX-like proteins that confer tolerance to copper (Gupta *et al.,* 1997) and also controlled by copper at the transcriptional level (Lopez *et al*., 2018).

Bioinformatic searches revealed that orthologues ScsC proteins are found in many other bacterial species and the redox active site (CXXC) is highly conserved in the proteins identified that lack the N-terminal extention, which is consistent with a common functional *in vivo* role. CcScsC and PmScsC are dimeric (Cho *et al.,* 2012) and trimeric (Furlong *et al.,* 2017), respectively, and this oligomerization is mediated via N-terminal extensions that are not present in the monomeric StScsC from *S.* Typhimurium (Shepherd *et al*., 2013; Furlong *et al*., 2017 and Furlong *et al*., 2018).

Given the similarities between ScsC and members of the Dsb family of proteins (Shepherd *et al*., 2013), it was hypothesised that the Scs system and copper play a combined role in disulphide folding in *S.* Typhimurium. Herein, our initial goals were to verify that the *scsA* promoter, which controls transcription of the entire operon (Lopez *et al*., 2018), was indeed copper specific, and to demonstrate that copper could induce the expression of the periplasmic StScsC protein beyond the mRNA level tested in previous studies. Copper was shown to activate the *scsA* promoter in a dose-dependent fashion using a transcriptional GFP fusion (Figure 3.7). Furthermore, expression of the soluble periplasmic StScsC protein was confirmed to be copper-specific using Western blotting. Given the presence of a copper specific CpxR-binding site in the *scsA* promoter region (Lopez *et al*., 2018) it is unsurprising that copper is an activator, although the StScs system has been shown to counteract oxidative stress (Lopez *et al*., 2018; Anwar *et al*., 2013) so it is interesting that other stresses (e.g. peroxide) did not elevate StScsC levels.

It is difficult to predict the function of a TRX-like protein based on structural information alone, although TRX-like proteins that catalyse the reduction of disulphides (e.g. DsbC, DsbG) are usually found to dimerise via an N-terminal extension. Previous work identified structural similarities between the core structures

of StScsC, DsbA, and DsbG, although the monomeric nature and absence of an N-terminal dimerisation domain (Figure 3.1) would suggest that StScsC is more related to DsbA in this respect. While low levels of reduced StScsC have been detected in the *S.* Typhimurium periplasm in the absence of copper (Shepherd *et al*., 2013), the current work reports that in the presence of copper, elevated levels of StScsC are found primarily in the oxidised form. This finding is consistent with StScsC being a disulphide oxidase *in vivo*, although it would be premature to assign such a functional role based on this evidence alone.

A powerful approach to investigate the functional role for TRX-like proteins is to measure the abundance of candidate target proteins under conditions where StScsC is differentially expressed: the hypothesis being that in the absence of the chaperone the target proteins will undergo misfolding and degradation, resulting in lower abundance. To this end, the proteomics study described herein was undertaken to identify protein targets that displayed elevated abundance in the presence of copper (which stimulates StScsC production) and were less abundant when copper-mediated expression of StScsC could not take place (i.e. in the *scsC* mutant). This approach identified a number of potential candidates, including the Zn/Cu superoxide dismutase SodCII and a range of peptide/amino acid transporters. Since loss of the copper export transporters CopA and GolT results in inactive SodCII (Osman *et al.*, 2013), it is perhaps unsurprising that an abundance of copper appears to elevate levels of this enzyme. Perhaps more interesting, however, is that SodCII of *S.* Typhimurium is orthologue of *E. coli* SodC, and both contain a disulphide bond (Mori *et al*., 2008). Furthermore, disulphide formation in SodC has previously been shown to be crucial for enzyme activation and stability (Sakurai *et al.*, 2014), so the current data directly implicate the StScs system in response to oxidative stress, which is consistent with previous reports that StScs proteins confer tolerance to hydrogen peroxide (Lopez *et al*., 2018; Anwar *et al.*, 2013). Given that DsbA is known to be regulated by the copper-responsive Cpx system (Pogliano *et al*., 1997) and that DsbC is involved in the response to copper stress (Hiniker *et al*., 2005), it is unsurprising that the DsbA and DsbL (Grimshaw *et al*., 2008) disulphide oxidoreductases are found in higher abundance when *S.* Typhimurium is exposed to copper. Since the StScs operon is also up-regulated by copper (Lopez *et al*., 2018), and herein we demonstrate elevated StScsC protein levels in response to copper, this elevated

abundance of numerous disulphide-folding catalysts indicates an 'all hands on deck' approach to dealing with copper-mediated disulphide-misfolding. The disulphide reductase TlpA has previously been shown to reduce the disulphide bonds of the TRX-like copper chaperone ScoI in *Bradyrhizobium japonicum* (Mohorko *et al.,* 2012), so it is a little surprising that the TlpA ortholog was not picked up in our mass spectrometry analysis. However, it is also logical that the TlpA/ScoI redox pair might be more important under conditions of copper deficiency, where intracellular copper is exported for insertion into the haem-copper oxidases.

Similar proteomics approaches were employed in an attempt to identify proteins in which disulphide formation was promoted by StScsC and copper. A disulphide-containing peptide from the Cellulose synthase operon protein C (BcsC) was found to have elevated abundance only in the presence of copper and StScsC. This protein has previousy been shown to play a role in cellulose biosynthesis and biofilm formation (Solano *et al*., 2002). Interestingly, *Salmonella* is known to perform BcsA-mediated synthesis of cellulose within macrophages (Pontes *et al.,* 2015), although the exact reason for this is unclear. Nevertheless, the data herein are consistent with copper-mediated expression of StScsC facilitating disulphide folding in BcsC *in vivo*, which may modulate cellulose production during infection.

To further investigate the role of StScsC during infection, macrophage survival assays were carried out for wild-type and Δ*scsC* strains in the presence of exogenous copper (i.e. to ensure that StScsC was expressed in the wild-type). These experiments gave a clear result that showed a significant decrease in survival when StScsC was lost, indicating an important role for StScsC targets within the macrophage. This observation is consistent with previous work that demonstrated that loss of the *scsA* gene gave a similar result (Verbrugghe *et al*., 2016), especially given that subsequent studies have demonstrated that the entire operon is under the control of the *scsA* promoter (Lopez *et al.,* 2018) and that polar effects of the *scsA* mutation might be expected to diminish the expression of StScsC.

Chapter 4

Biochemical analysis of the StScsC protein and potential redox partners

Abstract

In this chapter, *in vitro* protein assays were performed with purified StScsC protein in order to gain further functional insights. Copper binding was investigated via competition assays with Bathocuproine disulphonate (BCS), a copper-binding probe, although the presence of even low concentrations of StScsC appeared to abolish the binding of copper to BCS which precluded the measurement of copper binding affinities for StScsC. Aside from metal affinities, it was also of interest to identify thiol interaction partners for StScsC. In order to trap native protein targets for StScsC, a $StScsC_{CXXA}$ mutant variant was engineered. By resolving the purified $StScsC_{CXXA}$ on an SDS-PAGE gel in reducing and non-reducing conditions, it was possible to demonstrate that StScsC can form a disulphide link with another protein, later identified as the ArtI arginine binding protein via mass spectrometry approaches. The *artI* gene was cloned and the ArtI protein was purified to investigate if disulphide exchange could be demonstrated between the two proteins *in vitro*. It was shown that StScsC changed from the oxidised to the reduced state in a dose-dependent manner when 'as purified' ArtI was titrated in, confirming that disulphide exchange can occur. Since the two proteins clearly interact, it was of interest to investigate the structural basis for this interaction. While a crystal structure exists for StScsC, a structural model had to be generated for ArtI. Subsequent molecular docking approaches predicted several models for interactions, although none of them produced a disulphide bonded complex whereby cysteine residues were in close enough proximity for disulphide exchange. Finally, since arginine can be used as a carbon source and ArtI was likely to be involved in arginine uptake, it was hypothesised that the loss of StScsC would lead to impaired growth when grown on arginine. The data herein showed no specific difference between the growth of the wild-type and *ΔscsC Salmonella,* perhaps suggesting alternative routes for arginine uptake (for use as a carbon source) and an alternative role for ArtI (e.g. in arginine sensing) *in vivo*.

4.1- Introduction

The transition metal copper can bind to a variety of proteins with high affinity and influence their structure and function (Inesi, 2017; review). Many extra-cytoplasmic copper-binding proteins contain the H-X-X-M-X-X-M motif however, none of the gene products of the *scs* locus of *S.* Typhimurium were shown to contain this copper binding motif (Gupta *et al*., 1997). However, the role for StScs proteins in resistance to copper was confirmed (Shepherd *et al.,* 2013, Anwar *et al*., 2013; Lopez *et al.,* 2018). Although many other copper binding motifs are present in wide range of proteins and the H-X-X-M-X-X-M is not the only one as reviewed in Koch *et al*., (1997; review) using competition assays as described previously by Dainty *et al*., (2010) and Foster *et al.,* 2014, we sought to investigate the binding of copper to StScsC.

Five potential substrates for StScsC have been identified in the previous chapter. The oxidizing/reducing power of StScsC has been quantified previously by measuring the equilibrium constant for the disulphide exchange reaction with glutathione (Shepherd *et al.,* 2013). In addition, the ability of StScsC to catalyse Dsb isomerisation and its *in vitro* oxidoreductase activity has been investigated using the scrambled RNaseA refolding assay and insulin reduction assay, respectively to gain further insight to StScsC function (Shepherd *et al*., 2013). To provide alternative approaches to identify StScsC targets and validate these as *bona fide* interaction partners, biochemical techniques were employed to trap redox partners with a $StScsC_{CXXA}$ mutant. There is a precedent for this approach, as a similar variant of *E. coli* DsbG was engineered and was trapped in a complex with the YbiS protein (Depuydt *et al.,* 2009). It was anticipated that this approach could be used to isolate StScsC disulphide bonded with target proteins, and use mass spectrometry approaches to identify these redox partners for subsequent *in vitro* biochemical assays.

4.2-Results

4.2.1-Purification of his_6-tagged StScsC

S. Typhimurium ScsC protein was overexpressed in *E. coli BL21* (DE3) cells using pET21a_*scsC*_LIC vector plasmid (Shepherd *et al.*, 2013) and the purification was performed by affinity chromatography as described in section 2.5.1. SDS-PAGE analysis below (Figure 4.1) shows the purified his_6-tagged StScsC eluted with 300 mM imidazole migrating at a rate corresponding to a 23 kDa protein. The eluted protein was buffer exchanged using a PD-10 desalting column equilibrated in purification buffer for removal of imidazole for long term storage. The protein concentration was estimated by using the extinction coefficient of the protein (16620 $M^{-1}cm^{-1}$), molecular weight of the protein (23749 g/mol) and the absorbance at 280 nm with the formula: [Protein concentration (mg/mL)]= (A_{280} x molecular weight)/ extinction coefficient. A TEV protease site had been engineered for cleavage of the affinity-tag, so next step was to isolate TEV protease.

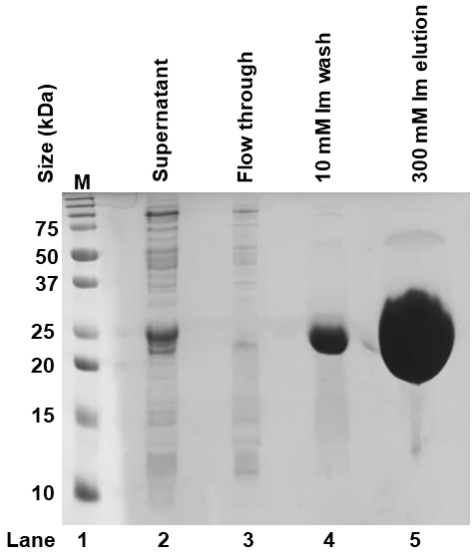


Figure 4.1- SDS-PAGE analysis of purified StScsC. Lane 2 showing the cell supernatant that has been applied to the column after centrifugation. Lane 3 shows the unbound flowthrough proteins. Lane 4 contains proteins after wash with 10 mM imidazole and lane 5 shows the ~23 kDa his_6-tagged StScsC protein that was eluted with 300 mM imidazole containing purification buffer. Dual Colour protein marker from Bio-Rad was used.

4.2.2- Purification of TEV protease

The nuclear inclusion protease from tobacco etch virus (TEV) is a highly sequence specific protease that has been well-characterized (Dougherty and Parks, 1991). This 27 kDa protein is used to cleave the affinity tags form purified proteins by recognising a specific 7 amino acid cleavage sequence (ENLYFQG) that is inserted between the the target protein and the affinity tag. TEV protease was overexpressed in *E. coli* BL21 (DE3) from pRK793 vector plasmid (Kapust *et al*., 2001) and purified by affinity chromatography. Figure 4.2 shows the SDS-PAGE gel of purified TEV protease at 27 kDa which was eluted with 300 mM Imidazole. Removal of imidazole was done using a HiTrap S-Sepharose column. The concentration of purified protein was then estimated using the extinction coefficient of the protein (34050 $M^{-1}cm^{-1}$), molecular weight of the protein (27526 g/mol) and the absorbance at 280 nm with the formula: [Protein concentration (mg/mL)]= (A_{280} x molecular weight)/ extinction coefficient.

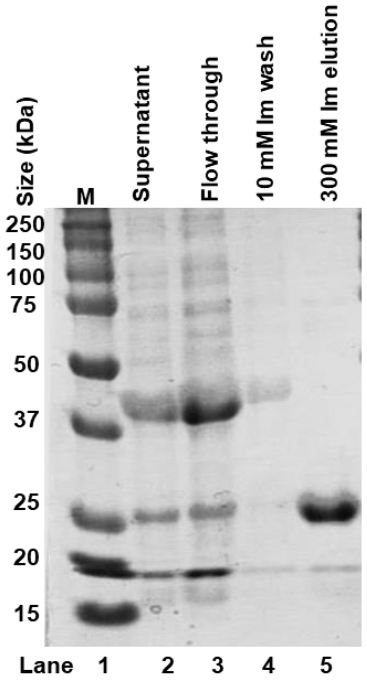


Figure 4.2- SDS-PAGE analysis of purified TEV protease. Lane 2 showing the cell supernatant that has been applied to the column after centrifugation. Lane 3 shows the unbound flowthrough proteins. Lane 4 contains proteins after wash with 10 mM imidazole and lane 5 shows the ~27 kDa TEV protease that was eluted with 300 mM imidazole containing purification buffer. Dual Colour protein marker from Bio-Rad was used.

4.2.3-Cleavage of his_6-tag from purified StScsC

When the StScsC protein was required without the histidine tag, the N-terminal his_6-tag of purified StScsC was cleaved using the purified TEV protease. 1 μg of purified TEV protease was used for the cleavage of the histidine tag to cleave 50 μg of StScsC. Tagged StScsC and TEV protease was incubated overnight at room temperature and the cleaved protein was separated from the tagged protein using affinity chromatography. Protein samples from each step were taken and loaded on an SDS-PAGE gel (Figure 4.3). The concentration of untagged StScsC protein was estimated by using the extinction coefficient of the protein (18020 $M^{-1}cm^{-1}$), molecular weight of the protein (236676 g/mol) and the absorbance at 280 nm with the formula: [Protein concentration (mg/mL)]= (A_{280} x molecular weight)/ extinction coefficient.

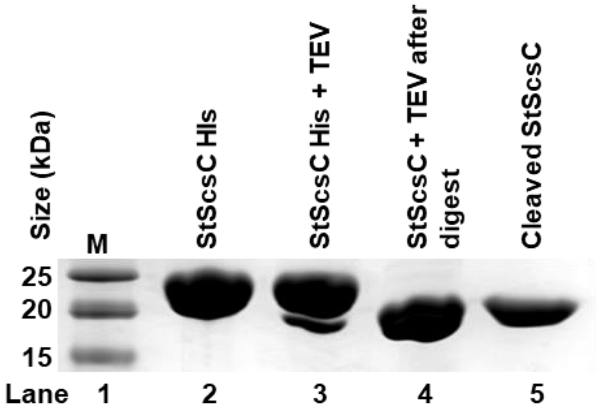


Figure 4.3- SDS-PAGE analysis of cleavage of his_6-tag from purified StScsC. Lane 2 is the purified his_6-tagged StScsC. Lane 3 shows the combination of the his_6-tagged StScsC and TEV protease prior to incubation. Lane 4 shows the combination of TEV protease and the StScsC after digestion and lane 5 shows the his_6-tag cleaved StScsC that was eluted with the equilibration buffer. Dual Colour protein marker from Bio-Rad was used.

4.2.4- Cu^+ affinity of StScsC

The StScsC protein promotes copper tolerance (Shepherd *et al*., 2013), expression is induced in the presence of copper, and copper was found to promote oxidation of the StScsC active site disulphide (Chapter 3). While the oxidation of the active site to form a disulphide is probably a transient association and is unlikely to yield a stable disulphide bonded complex, it was of interest to investigate if StScsC could bind copper at all. In order to gain more insights, Cu^+ affinity of StScsC was studied via a competition experiment with Bathocuproine disulphonate (BCS), which binds Cu^+ specifically forming a $BCS_2Cu(I)$ complex that absorbs at 483 nm (Dainty *et al*., 2010). BCS binds to Cu^+ with a 2:1 stoichiometry (Xiao *et al*., 2011).

The BCS standard curve was produced by titrating Cu^+ into 10 μM BCS solution (Figure 4.4A), where the formation of $BCS_2Cu(I)$ complex was detected by an increase in absorbance at 483 nm. Elevation of absorbance was detected until the addition of 8 μM of Cu^+ and further addition of copper did not change the absorbance suggesting that 8 μM copper was adequate to bind to all BCS molecules present (10 μM).

Binding of Cu^+ to StScsC was initially measured by titrating Cu^+ to 10 μM BCS and 10 μM StScsC, although no change in absorbance could be seen (data not shown). Hence, lower concentrations of StScsC were trialled, such as 2 μM in Figure 4.4B, with titrations of copper going up to 460 μM. No change of absorbance was observed initially suggesting that Cu^+ was binding to StScsC with high affinity and not to BCS. Continued titration with copper yielded no definitive peak at 483 nm, and high concentrations of copper (up to 460 μM) led to the precipitation of StScsC. To account for increasing light scattering at high copper concentrations, the magnitude of the 483 peak was defined as $A_{483\text{-}550}$, and a binding curve was plotted (Figure 4.5).

To investigate if higher concentrations of Cu^+ interfered with the absorbance signal, increasing concentrations of Cu^+ were titrated into the reaction buffer. No absorbance at 483 nm was detected (Appendix 6) suggesting that Cu^+ alone does not interfere with the assay. Hence, we concluded that copper binding to StScsC could not be verified with this experimental setup.

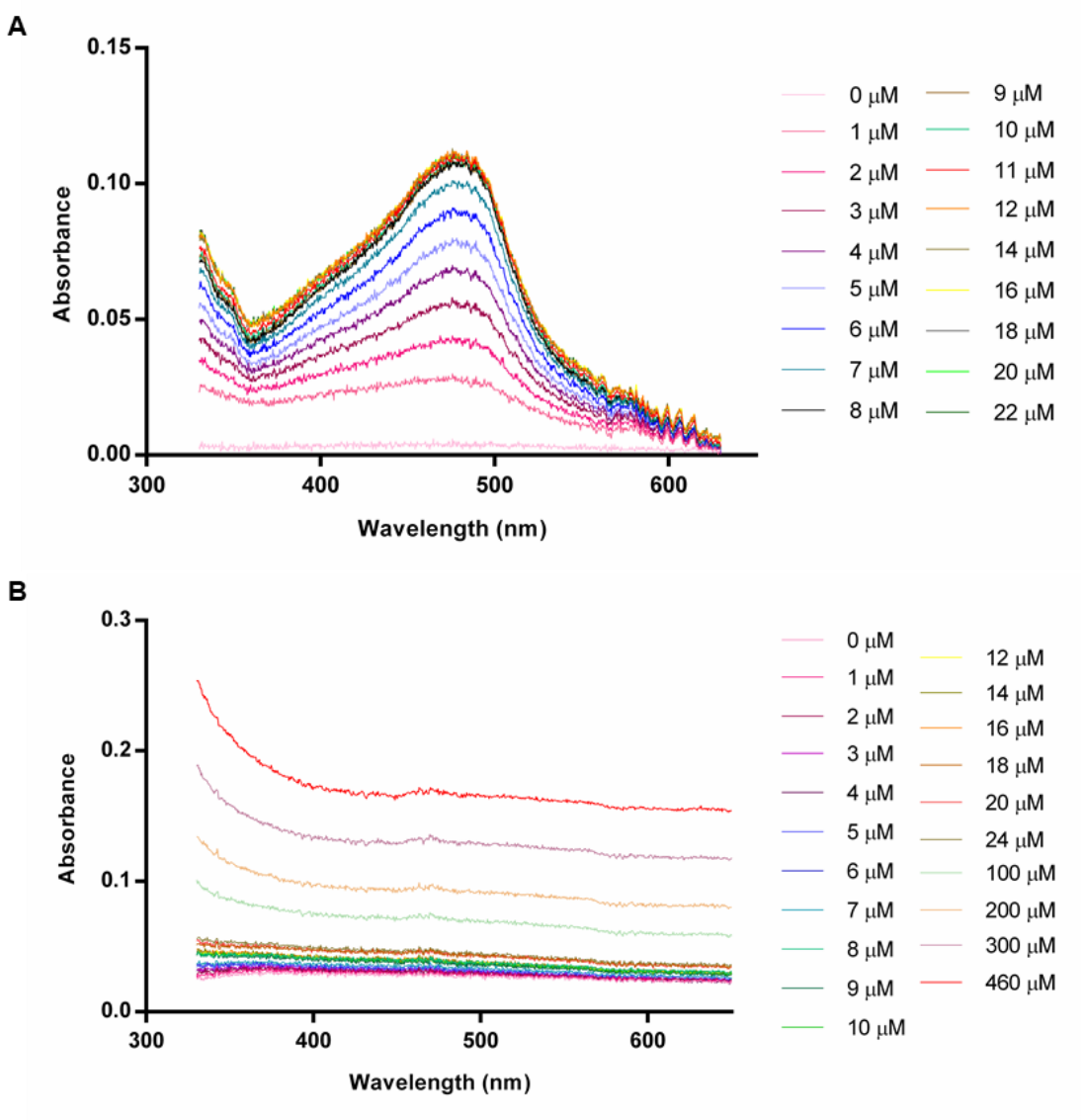


Figure 4.4- Absorbance spectra of BCS and StScsC with Cu^{+}. (A) BCS standard curve showing an increase in absorbance at 483 nm as the BCS forms a complex with Cu^{+}. Reaction reaches to equilibrium at 8 µM copper indicating 8 µM copper is enough to bind to 10 µM BCS. **(B)** Absorbance spectrum of 2 µM StScsC with 10 µM BCS. No definitive absorbance was observed with subsequent additions of Cu^{+} to BCS-StScsC mixture at 483 nm. StScsC was also found to be precipitated with the addition of higher concentrations of Cu^{+} into the solution. Concentrations of copper that has been added to the BCS alone or BCS-StScsC mixture is shown on the right of each spectrum.

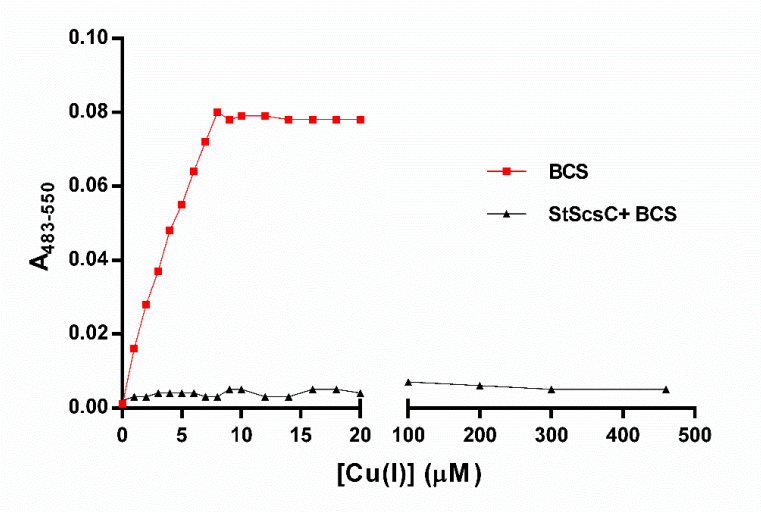


Figure 4.5- Binding curve of BCS and StScsC to Cu^+ at $A_{483-550}$. Curve shown in red represents Cu^+ binding to BCS. 8 μM Cu^+ was adequate for binding to 10 μM BCS. Curve shown in black represents copper binding to BCS-StScsC mixture. No change in absorbance was observed until 20 μM Cu^+ is added to the mixture. Continuous titration of Cu^+ led to an increase in absorbance but not due to the formation of BCS-Cu(I) complex but due to the precipitation of the protein.

4.2.5- Engineering a $StScsC_{CXXC}$ variant and trapping interaction partners

A biochemical technique was employed to trap StScsC bound to redox partners to provide independent evidence for StScsC target proteins.

4.2.5.1- Model for trapping the target proteins binding to StScsC

A $StScsC_{CXXA}$ variant was engineered where the second cysteine of the CXXC catalytic motif was replaced by an alanine, with the aim that this $StScsC_{CXXA}$ would form a disulphide bond *in vivo* with a redox partner (Figure 4.6). The absence of the second thiol group in $StScsC_{CXXA}$ would then limit the ability of $StScsC_{CXXA}$ to dissociate from the redox partner. There is a precedent for using this approach with the TRX-like chaperone DsbG in *E. coli* (Depuydt *et al*., 2009).

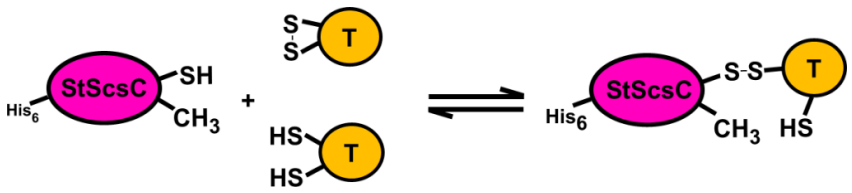


Figure 4.6- Model for trapping StScsC substrates. $StScsC_{CXXA}$ (magneta) forming a disulphide bond with target proteins (orange).

4.2.5.2- Cloning of a *scsC*$_{CXXA}$ construct to pSU2718 vector plasmid

A *scsC*$_{CXXA}$ gene encoding a C-terminal his$_6$-tag was synthesised using the Invitrogen GeneArt Gene synthesis service (Thermo-fisher) and cloned into pSU2718 vector. The desired plasmid is shown in Figure 4.7. Firstly, the parent pSU2718 vector was digested with *Fsp*I and *Bam*HI restriction enzymes. The insert was amplified and digested with the same restriction enzymes (Figure 4.8A). In order to prevent self ligation, phosphate groups were removed by dephosphorylation. The insert and the vector were then ligated together with T4 DNA ligase and transformed into *E. coli K12* JM109 strain. Colonies from the transformations were screened for the presence of 750 base-pair *scsC*$_{CXXA}$ fragment by colony PCR by using primers *scsC*$_{CXXA}$His_F and *scsC*$_{CXXA}$His_R. Only colony 2 had the desired fragment (Figure 4.8B). A sequence analysis of the plasmid was performed and it was confirmed to contain the desired sequence (Appendix 7).

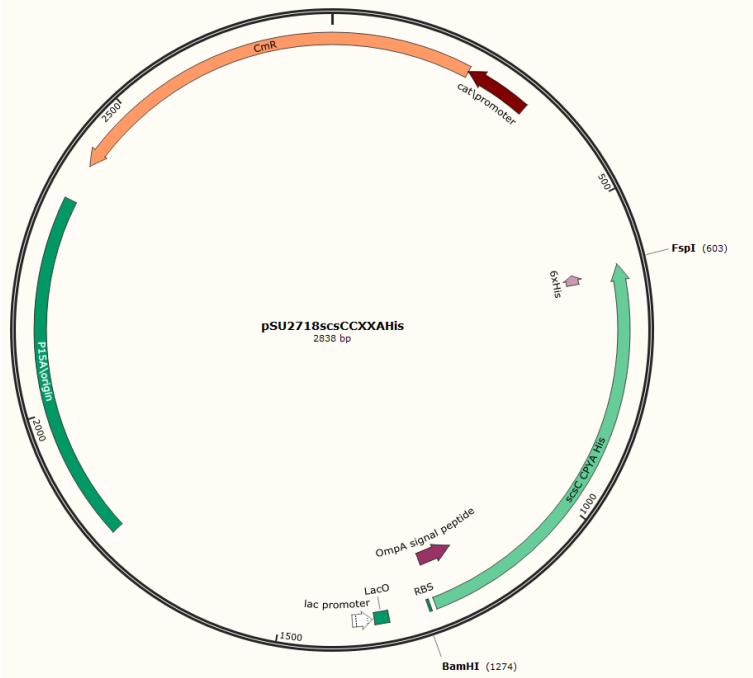


Figure 4.7- Plasmid map for *scsC*$_{CXXA}$ cloned into pSU2718 vector plasmid. The expression of the ScsC$_{CXXA}$ was controlled by the lac promoter. Presence of the OmpA signal peptide will target the protein to the periplasm (Movva *et al.*, 1980).

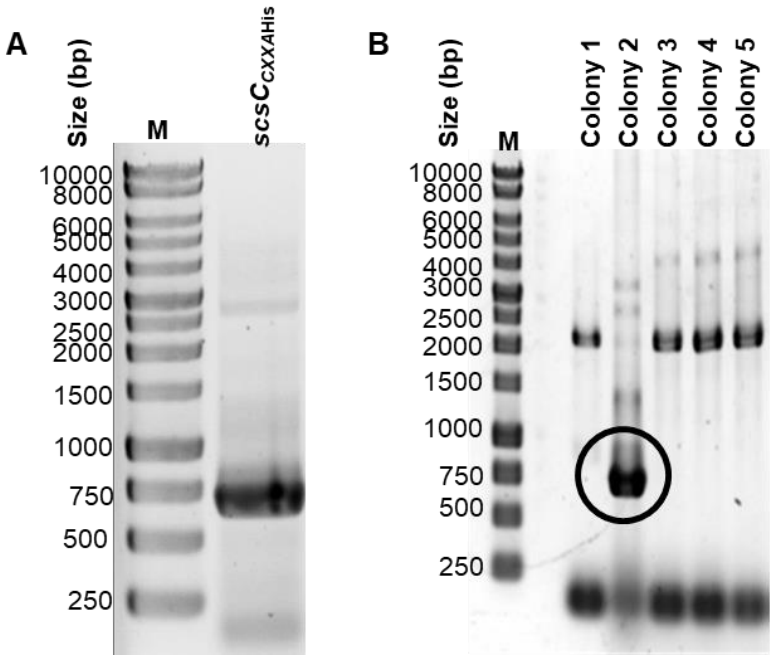


Figure 4.8- Analysis of DNA fragments for cloning of pSU2718*scsC*$_{CXXC}$His. (A) Amplified *scsC*$_{CXXA}$ was resolved on a 1% agarose gel migrating at a rate corresponding to ~700 bp. **(B)** Colony PCR analysis of the colonies from the transformation of the amplified insert into the pSU2718 vector plasmid. Only colony 2 was found to contain the desired plasmid shown by the black circle at around 700 bp. 5 µl of 1 kb DNA ladder from Promega was used.

4.2.5.3- Purification of StScsC$_{CXXA}$

StScsC$_{CXXA}$ was overexpressed in *E. coli* K12 strain with IPTG induction and then the protein was purified by affinity chromatography. Following elution with buffer containing 300 mM imidazole, the ~23 kDa StScsC$_{CXXA}$ was detected with another significant band at approximately 50 kDa in the same lane. At this stage, it was anticipated that this band could either be a StScsC dimer or StScsC bound to a target protein. The 50 kDa band is highlighted by the black box on Figure 4.9.

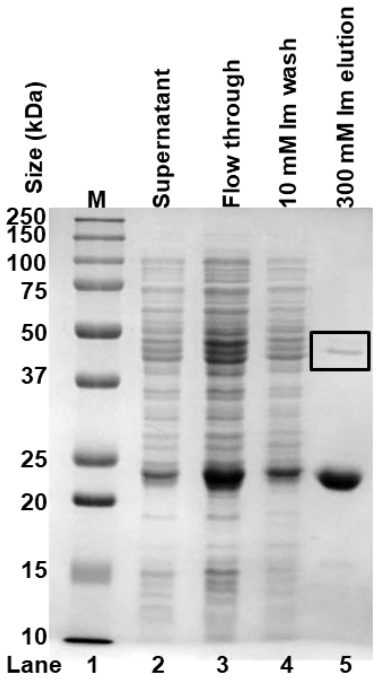


Figure 4.9- SDS-PAGE analysis of purified StScsC$_{CXXA}$ protein. Lane 2 showing the cell supernatant that has been applied to the column after centrifugation. Lane 3 shows the unbound flowthrough proteins. Lane 4 contains proteins after wash with 10 mM imidazole and lane 5 shows the ~23 kDa StScsC$_{CXXA}$ that was eluted with 300 mM imidazole containing purification buffer. Another band at around 50 kDa was also present shown by the black box. Dual Colour protein marker from Bio-Rad was used.

4.2.5.4- Reduction of putative ScsC$_{CXXC}$-target substrates with DTT

The work herein involved expression of his$_6$-tagged StScsC$_{CXXA}$ in the *E.coli* periplasm, followed by affinity chromatography and analysis of disulphide bond formation via SDS-PAGE in the presence and absence of DTT (Figure 4.10A). Copper was omitted from this experiment as it was not required for StScsC expression and could have a profound impact upon the thiol-redox balance in *E. coli*. The 23 kDa band (in both lanes 2 and 3) is the monomeric StScsC protein, and it was hypothesised that the the slower-migrating bands (highlighted by the black box in lane 2) that dissappear in the presence of DTT could be disulphide bonded complexes containing StScsC. Western blotting using anti-his$_6$ antibodies confirmed the presence of StScsC in these higher molecular weight bands, and also confirmed the DTT-mediated dissociation of the putative disulphide-bonded complexes (Figure 4.10B).

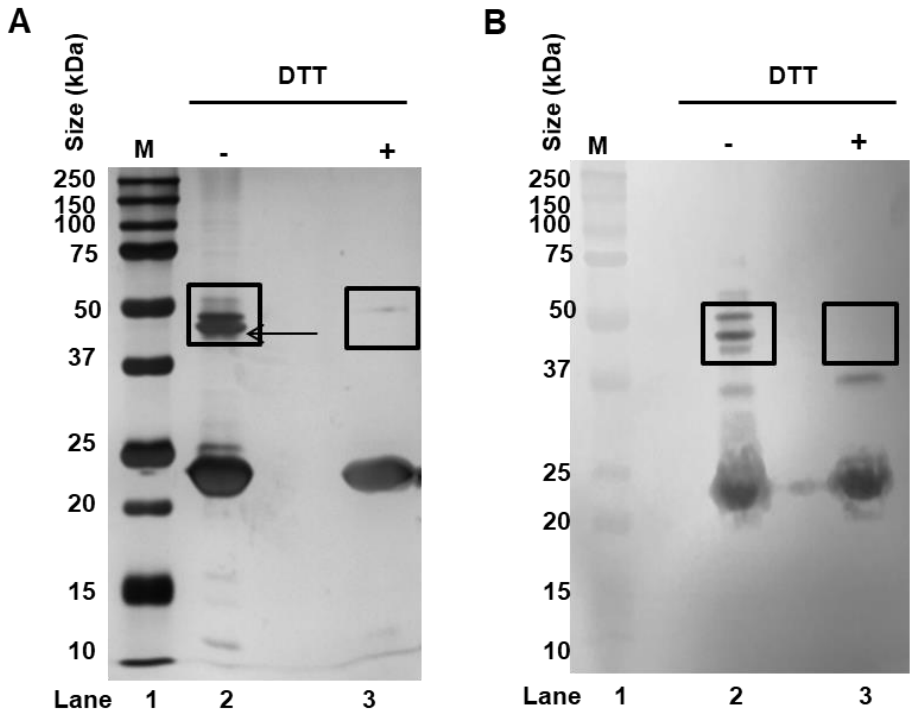


Figure 4.10- Detection of purified StScsC and the substrate. (A) Silver stained SDS-PAGE analysis of purified $StScsC_{CXXA}$ in the absence (lane 2) and the presence of DTT (lane 3). Black boxes indicate a higher molecular weight protein hypothesised to be StScsC disulphide-bonded to a target protein, which dissociates when DTT is present. The protein band indicated by the arrow was analysed using MALDI-TOF mass spectrometry (Section 4.2.5.5). **(B)** Western blot analysis of purified $StScsC_{CXXA}$ in the absence (lane 2) and the presence (lane 3) of DTT with anti-his_6 antibodies. Boxes indicate higher molecular weight proteins that disappear when DTT is added. Dual Colour protein marker from Bio-Rad was used.

4.2.5.5- StScsC binds to ArtI in the *E. coli* periplasm

Protein bands were excised from the silver-stained SDS-PAGE gel (Figure 4.10A), and were analysed via mass spectrometry as described in Section 2.10. Peptide fragments were identified using the Mascot search engine (Perkins *et al.*, 1999) by using the TrEMBL_*Salmonella* database to detect StScsC and then by using the TrEMBL_*E. coli* database as the proteins were overexpressed in *E. coli* strain. The band highlighted by the arrow on Figure 4.10A was identified as StScsC bound to ArtI (Arginine ABC transporter substrate binding protein) (Figure 4.11). Arginine ABC transporter substrate binding protein, has a closely-related orthologue in *S.* Typhimurium (sequence identity = 95.5%) (Figure 4.12). Other bands contained StScsC but no other partner protein could be detected, indicating that $StScsC_{CXXA}$ may also form an intermolecular disulphide with itself.

MASCOT Search Results

Protein View: A0A0L7AJ51_ECOLX

Arginine ABC transporter substrate-binding protein OS=Escherichia coli GN=artI

Database:	TrEMBL_ecoli
Score:	55
Expect:	3.8
Nominal mass (M_r):	27065
Calculated pI:	5.78
Taxonomy:	Escherichia coli

Sequence similarity is available as an NCBI BLAST search of A0A0L7AJ51_ECOLX against nr.

Search parameters

Enzyme:	Trypsin: cuts C-term side of KR unless next residue is P.
Fixed modifications:	Carbamidomethyl (C)
Variable modifications:	Oxidation (M)
Mass values searched:	43
Mass values matched:	6

Protein sequence coverage: 22%

Matched peptides shown in ***bold red***.

```
  1 MKKVLIAALI AGFSLSATAA ETIRFATEAS YPPFESMDAN NQIVGFDVDL
 51 AQALCKEIDA TCTFSNQAFD SLIPSLKFRR VDAVMAGMDI TPEREKQVLF
101 TTPYYDNSAL FVGQQGKYTS VDQLKGKKVG VQNGTTHQKF IMDKHPEITT
151 VPYDSYQNAK LDLQNGRIDG VFGDTAVVTE WLKDNPKLAA VGDKVTDKDY
201 FGTGLGIAVR QGNTELQQKF NTALEKVKKD GTYETIYNKW FQK
```

Figure 4.11- StScsC forms a disulphide bond with ArtI *in vivo*. The band shown by the black arrow on figure 4.10A was assigned to be the Arginine ABC transporter substrate-binding protein (ArtI) by Mascot search by using TrEMBL_*E.coli* database.

```
                        10        20        30        40        50
                ....|....|....|....|....|....|....|....|....|....|
E. coli         20  AETIRFATEASYPPFESMDANNQIVGFDVDLAQALCKEIDATCTFSNQAF 69
S. Typhimurium  20  AQTIRFATEASYPPFESMDANNKIVGFDVDLANALCKEIDASCTFTNQAF 69

                        60        70        80        90        100
                ....|....|....|....|....|....|....|....|....|....|
E. coli         70  DSLIPSLKFRRVDAVMAGMDITPEREKQVLFTTPYYDNSALFVGQQGKYT 119
S. Typhimurium  70  DSLIPSLKFRRFDAVMAGMDITPEREKQVLFTTPYYDNSALFVGQQGKYT 119

                        110       120       130       140       150
                ....|....|....|....|....|....|....|....|....|....|
E. coli         120 SVDQLKGKKVGVQNGTTHQKFIMDKHPEITTVPYDSYQNAKLDLQNGRID 169
S. Typhimurium  120 SVDQLKGKKVGVQNGTTHQKFIMDKYPEITTVPYDSYQNAKLDLQNGRID 169

                        160       170       180       190       200
                ....|....|....|....|....|....|....|....|....|....|
E. coli         170 GVFGDTAVVTEWLKDNPKLAAVGDKVTDKDYFGTGLGIAVRQGNTELQQK 219
S. Typhimurium  170 AVFGDTAVVTEWLKANPKLAPVGDKVTDKDYFGTGLGIAVRQGNTELQQK 219

                        210       220
                ....|....|....|....|....
E. coli         220 FNTALEKVKKDGTYETIYNKWFQK 243
S. Typhimurium  220 FNTALEKVKKDGTYETIYNKWFQK 243
```

Figure 4.12- Sequence alignment of ArtI from *E. coli* and *S.* Typhimurium. Amino acid sequences of *E. coli* ArtI (Uniprot accession number: A0A0L7AJ51) and *S.* Typhimurium ArtI (Uniprot accession number: A0A0H3NEU6). Sequences lacking the targeting peptide are aligned by using Bioedit sotware (Hall, 1999) using ClustalW Multiple alignment. Fully conserved residues are shaded in grey and residues showing 50% conservation are shaded in pink. The percentage identities of the sequences were calculated by using BLOSUM62 ExPASy SIM Alignment tool (Gasteiger *et al.*, 2003). ArtI is 27 kDa periplasmic protein containing 2 cysteine residues which are highlighted in red.

4.2.6- Cloning and purification of *Salmonella* arginine-binding periplasmic protein I

As StScsC was shown to form a disulphide bond with ArtI, *S.* Typhimurium *artI* gene was cloned and ArtI protein purified, and *in vitro* protein assays were performed to investigate the interaction between the two proteins.

4.2.6.1- Cloning of *artI* gene

Genomic DNA from *S.* Typhimurium SL1344 was extracted using a GenElute Bacterial Genomic DNA Kit according to manufacturer's instructions (Sigma). The *artI* gene was amplified (Figure 4.13A) from genomic DNA using primers *artI*TEV_F and *artI*TEV_R (Table 2.5), and the construct was engineered to include a TEV cleavage site to remove the N-teminal his_6-tag. The bacterial expression vector plasmid pTrcHis was also amplified by using primers pTrcHis_F and pTrcHis_R (Table 2.5) (Figure 4.13B) for subsequent cloning steps. Figure 4.14 shows the desired plasmid map after cloning of *artI* into pTrcHis vector plasmid, using a Gibson assembly cloning kit (NEB) according to manufacturer's instructions. Competent cells were transformed with the Gibson assembly reaction mixture, and plasmid DNA was purified and digested with restriction enzymes for confirmation of the presence of the desired construct. Figure 4.15 shows the result of the digestion alongside an identical digestion with the parent pTrcHis plasmid, where differences in band sizes confirmed the presence of *artI*. The plasmid was also sent off for sequencing and was confirmed to contain the correctly inserted *artI* gene (Appendix 8).

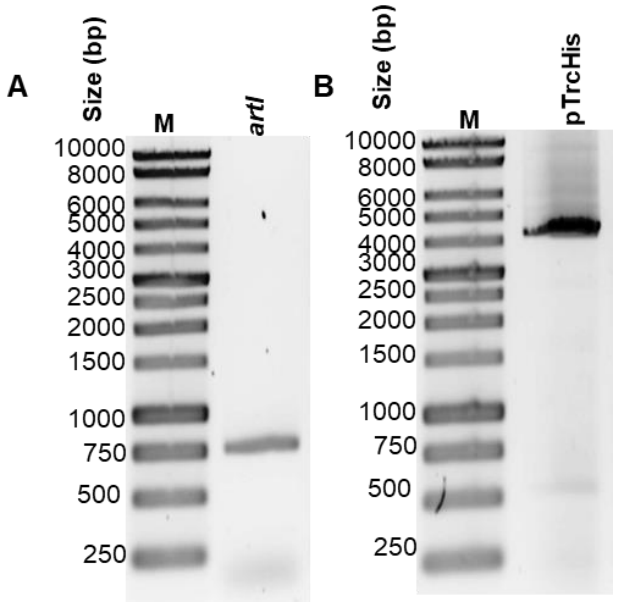


Figure 4.13- Amplified *artI* and pTrcHis vector. (A) Agarose gel of amplified *artI* at ~700 bp. **(B)** Amplified pTrcHis vector plasmid (~4300 bp).

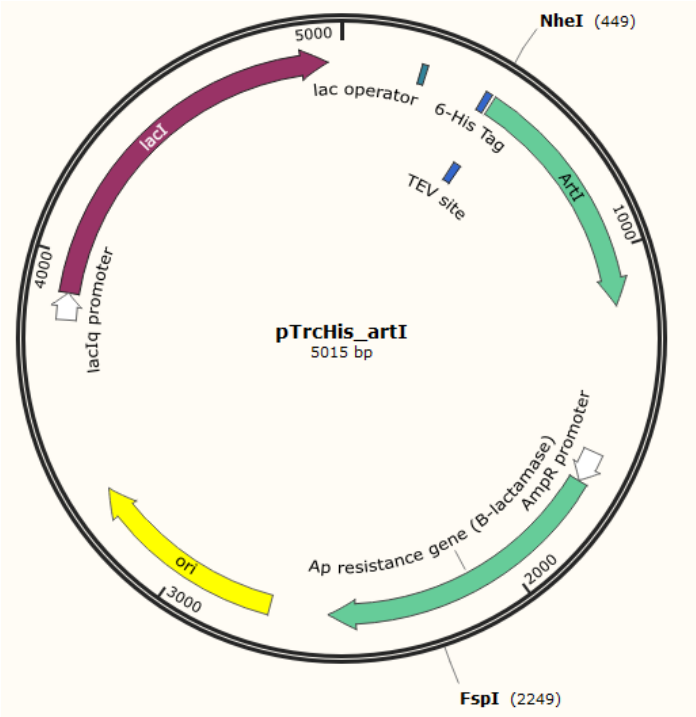


Figure 4.14- Desired plasmid map of *artI* cloned to pTrcHis vector plasmid. TEV site is included for cleavage of the his_6-tag when necessary at the N-teminal of the *artI* that is inserted to the vector plasmid which contains an Ampicillin resistance cassette.

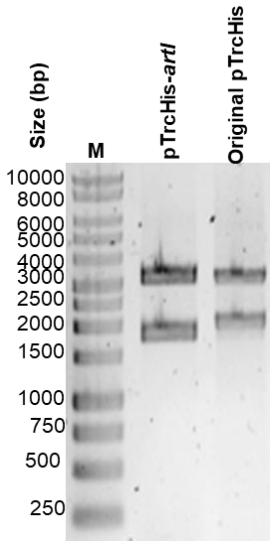


Figure 4.15- Confirmation of *artI* cloned into pTrcHis vector. Agarose gel showing restriction digest of miniprep plasmid DNA of pTrcHis*artI* and the original pTrcHis plasmid. *Nhe*I and *Fsp*I restriction enzymes were used to digest the plasmids. Desired bands for pTrcHis*artI* are ~1800 bp and ~3200 bp and desired band for the original plasmid digest are ~2000 bp and ~3200 bp.

4.2.6.2- Purification of ArtI

ArtI was overexpressed in DH5α competent cells using IPTG induction. By affinity chromatography, ArtI was purified and eluted with buffer containing 300 mM imidazole (Lane 5) (Figure 4.16). Imidazole was then removed by buffer exchange chromatography. By using TEV protease digestion, the his_6-tag was also cleaved off (Lane 9) (Figure 4.16).

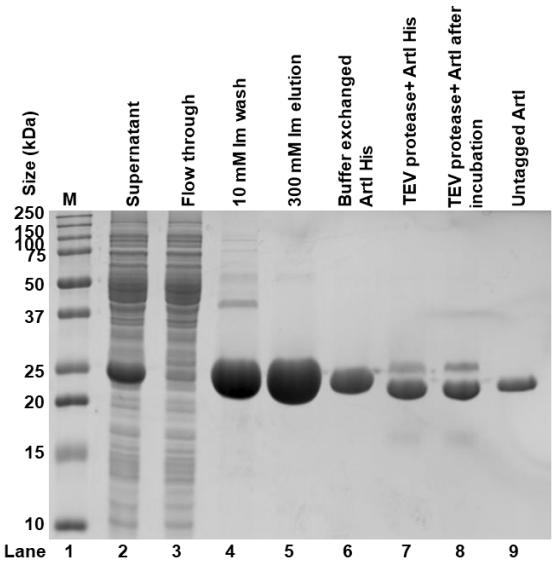


Figure 4.16- SDS-PAGE gel of purified ArtI. The ~27 kDa band shown on lane 5 is the purified his_6-tagged ArtI. Imidazole was removed by buffer exchange chromatography (Lane 6) and the his_6-tag was cleaved off using TEV protease. Purified untagged ArtI is shown in lane 9.

4.2.7-*In vitro* protein experiments with ArtI and StScsC

The main aim of the next phase of the project was to demonstrate the interaction between ArtI and StScsC. Both proteins were reduced and oxidized with 5 mM DTT and 20 mM GSSG, respectively, and exogenous reductant/oxidant was removed using a PD-10 column, and the anticipated redox state of StScsC was confirmed using DTNB assays as previously described (Eyer *et al*., 2003). The addition of DTT or GSSG had no noticeable effect upon the redox state of ArtI, so the interaction of 'as purified' ArtI with oxidised and reduced StScsC was investigated. To note, purified wild-type StScsC runs on SDS-PAGE at 25 kDa.

4.2.7.1- Reduced StScsC$_{CXXA}$ binds to ArtI

In order to detect binding of ArtI to StScsC, his$_6$-tagged StScsC or StScsC$_{CXXA}$ and untagged ArtI was used. Equimolar concentrations of proteins were incubated together for 1 h and protein samples were resolved via SDS-PAGE for detection of a band at around 50 kDa, which is the correct size for ArtI: StScsC disulphide bonded complex (Figure 4.17A). Lane 12 shows reduced StScsC$_{CXXA}$ at 23 kDa, which increases to 50 kDa when ArtI is added (shown by lanes 5 and 9). The same result was confirmed by Western blot analysis with anti-his$_6$ antibodies (Figure 4.17B). Unfortunately, the interaction of ArtI with wild-type StScsC could not be demonstrated, this might be due to the covalent bond not being strong enough between the ArtI and StScsC so ArtI can not be trapped and detected.

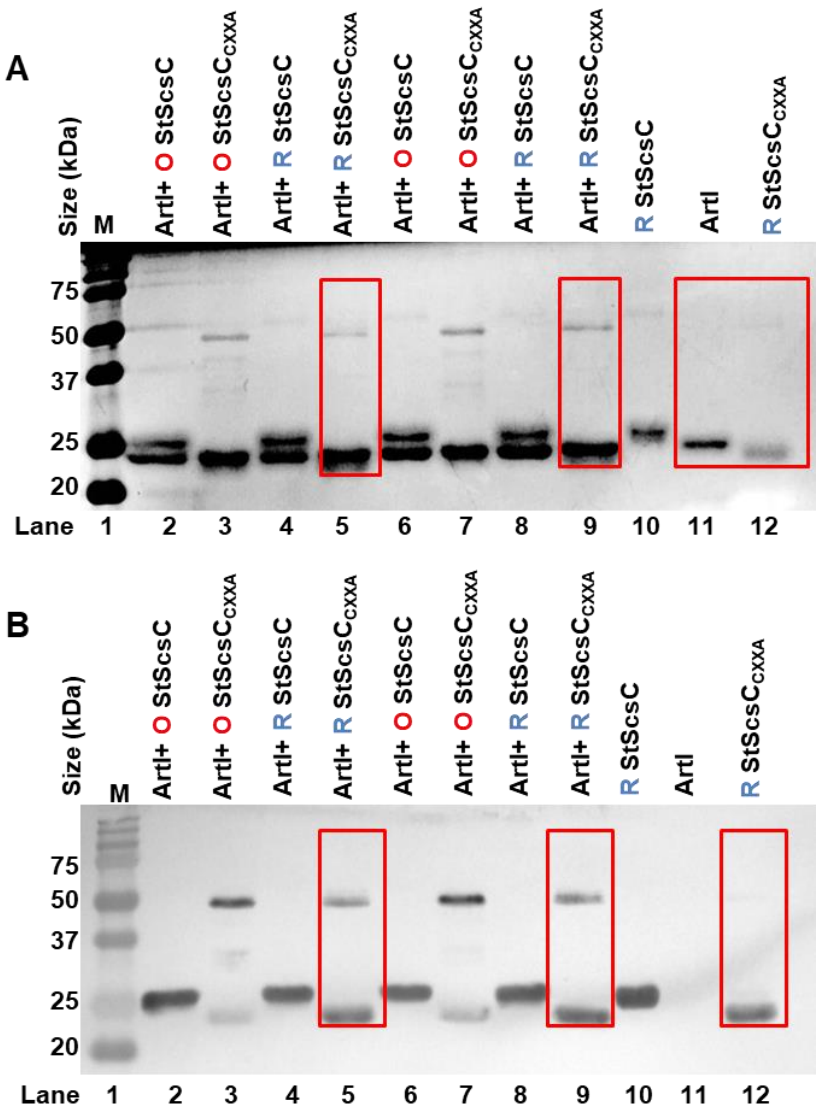


Figure 4.17- ArtI binding to StScsC. (A) SDS-PAGE gel showing protein samples in combination with each other. Presence of 50 kDa band when reduced StScsC$_{CXXA}$ was incubated with ArtI suggested that ArtI binds to StScsC (Lanes 5 and 9) when compared to reduced StScsC$_{CXXA}$ only and ArtI only controls (Lane 11 and 12) (shown by the red boxes). Presence of 50 kDa band on lanes 3 and 7 when oxidised StScsC$_{CXXA}$ was incubated with ArtI cannot be described as ArtI binding to StScsC as no control for oxidised StScsC$_{CXXA}$ was present. **(B)** Western blot analysis of the same samples with anti-his$_6$ antibodies. A 50 kDa protein appeared when ArtI was incubated with reduced StScsC$_{CXXA}$. (O) oxidised, (R) reduced. N.B. Treatment with DTT or GSSG had little effect upon the redox state of ArtI, which remained in the 'as purified' redox state.

4.2.7.2- Cu^{2+} promotes dimerization of reduced StScsC$_{CXXA}$

Detection of an interaction between reduced StScsC$_{CXXA}$ and ArtI lead to investigation into whether copper can influence this disulphide bond formation. Proteins on their own or in combination with each other were incubated with 1 mM

Cu^{2+} and were resolved via SDS-PAGE (Figure 4.18A). In the presence of copper, reduced $StScsC_{CXXA}$ was shown to dimerise, as shown by the red box on lane 5. Western bloting performed using anti-his_6 antibodies confirmed the same result (Figure 4.18B).

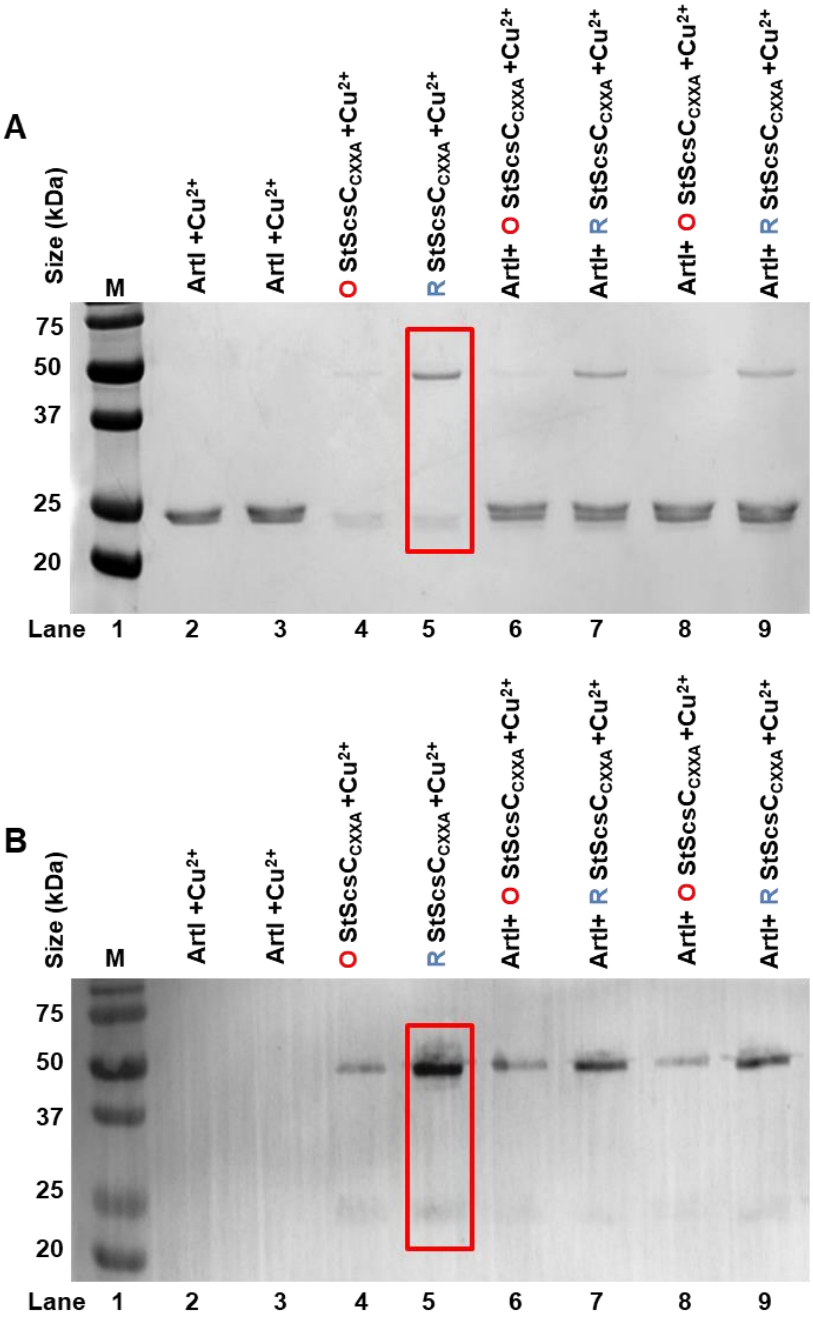


Figure 4.18- Addition of copper dimerizes $StScsC_{CXXA}$. (A) SDS-PAGE showing equimolar concentrations (3 μM) of ArtI and $StScsC_{CXXA}$ alone or in combination in the presence of 1 mM Cu^{2+}. **(B)** Western blot analysis of the same gel with anti-his_6 antibodies. The presence of copper led to dimerisation of reduced $StScsC_{CXXA}$ and ArtI binding could not be detected under these conditions. His_6-tagged $StScsC_{CXXA}$ and untagged ArtI were used. N.B. Treatment with DTT or GSSG had little effect upon the redox state of ArtI, which remained in the 'as purified' redox state.

Since $StScsC_{CXXA}$ dimerization is promoted by copper, it was of interest to investigate if wild-type StScsC also dimerises in the presence of copper ions. Addition of copper ions to reduced or oxidised wild-type StScsC samples did not alter the oligomerisation state of the wild-type protein as it did for the mutant reduced $StScsC_{CXXA}$ (Figure 4.19). Lane 6 shows oxidised $StScsC_{CXXA}$ is already in the dimerised form prior to addition of copper. Figure 4.19B shows Western blot detection of the his_6-tagged StScsC proteins with anti-his_6 antibodies.

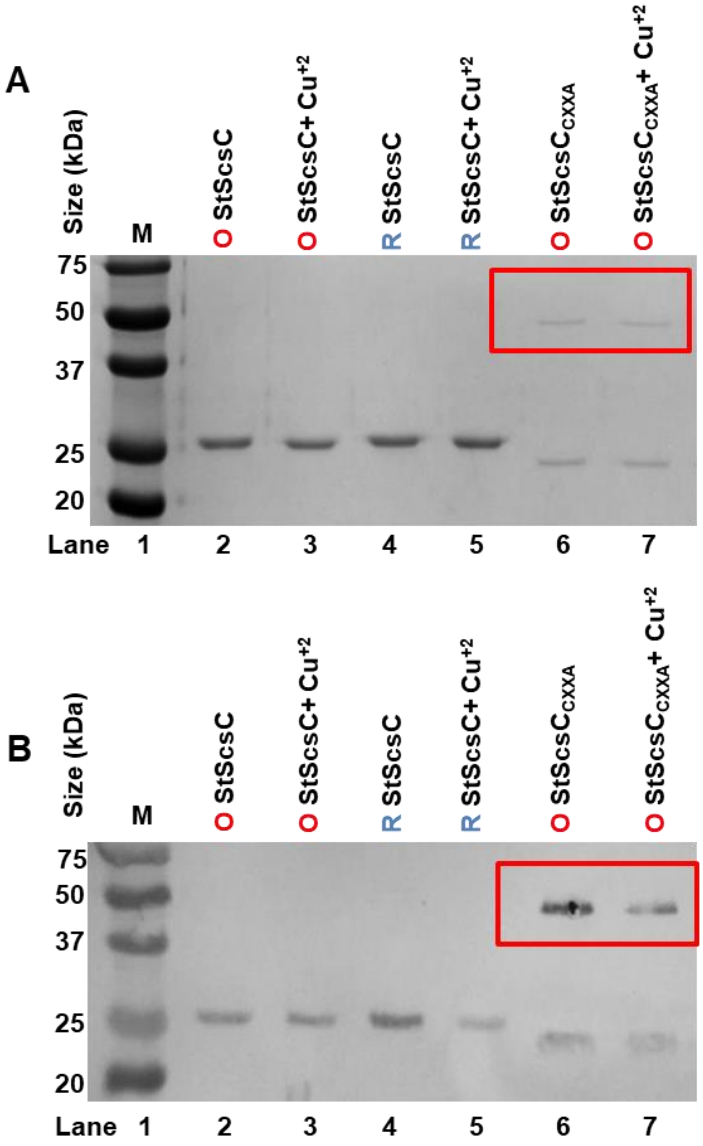


Figure 4.19- Wild-type StScsC does not dimerise in the presence of copper. (A) SDS-PAGE gel showing 3 μM of purified StScsC and $StScsC_{CXXA}$ incubated with or without Cu^{2+}. **(B)** Western blot analysis with anti-his_6 antibodies. Dimerisation of wild-type StScsC was not detected. Red boxes indicate that oxidised $StScsC_{CXXA}$ is already found in a dimeric state.

4.2.7.3- Copper ions oxidise wild-type StScsC *in vitro*

To detect the thiol redox status of wild-type StScsC *in vitro* in the presence and absence of copper ions, the thiol modification reagent AMS was used. After reduction and oxidation of the purified his_6-tagged StScsC, samples were incubated with Cu^{+}/ Cu^{2+} ions and protein was precipitated and resuspended in buffer containing 20 mM AMS. Proteins were resolved via SDS-PAGE (Figure 4.20), and a 1 kDa change in the band size was expected if the protein was reduced and therefore able to bind AMS. The technique was validated by showing a 1 kDa band shift between reduced and oxidised StScsC in lanes 2 and 3. Reduced StScsC was also shown to be oxidised by the addition of both $Cu^{+}$and Cu^{2+} ions shown in lanes 4 and 6, respectively.

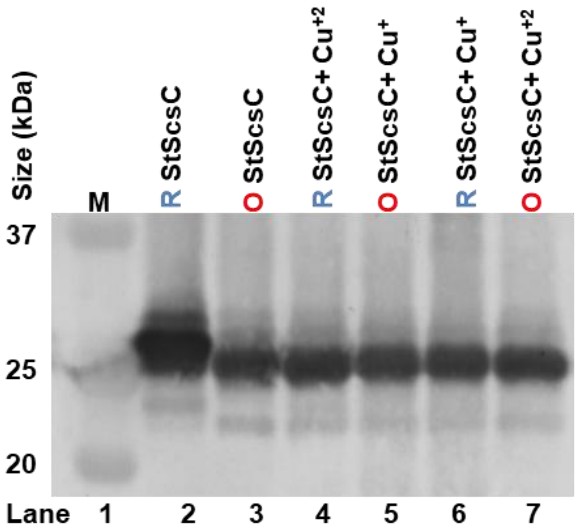


Figure 4.20- StScsC oxidises in the presence of copper. Precipitated protein samples were incubated with copper ions and resuspended in buffer containing 20 mM AMS in order to alkylate reduced thiols. Western blot analysis with anti-StScsC antibodies revealed that reduced StScsC is oxidised in the presence of copper (Lanes 4 and 6). Lanes 2 and 3 are reduced and oxidised StScsC controls, respectively.

4.2.7.4- Oxidised StScsC is reduced by *S.* Typhimurium ArtI

The change in the redox state of StScsC and/or ArtI was studied by using purified proteins with different redox states alone or in combination. The thiol modification reagent AMS was used to detect a band shift due to binding of AMS to reduced cysteines. All samples were incubated with AMS and reduced proteins were expected to migrate slower than the oxidised proteins. Firstly, ArtI was determined to be the same size in both 'oxidised' and 'reduced 'samples in the presence and absence of copper, confirming previous observations with DTNB assays on DTT- and GSSG-treated ArtI that suggest that the redox state of these cysteines are difficult to modify and are likely to be inaccessible (data could also be explained by ArtI being resistant to modification with AMS). In order to double confirm that the disulphide status of ArtI could not be changed by the addition of oxidising and reducing reagents, the intact mass the protein was measured using mass spectrometry approach. Firstly, intact mass of the as purified protein was measured in order to detect posttranslational modifications that might be present. Posttranslational modifications on free thiols of the protein such as sulfenylation (Poole, 2015; review) might have been affected the reduction, alkylation of the protein. However, no specific modification was observed (Appendix 9A). Later, the ArtI protein was reduced with DTT alone and reduced with DTT and alkylated with chloroacetamide to measure the mass difference, although no specific band difference was observed when chloroacetamide was added (Appendix 9B-C). This suggested that the cysteines of the folded protein are inaccessible.

Hence, while ArtI was still treated with reductant and oxidant, the redox state remained 'as purified' for these experiments. When reduced StScsC was incubated with ArtI, StScsC becomes partially oxidised (Figure 4.21) (red box). However, the presence of copper was shown to oxidise reduced StScsC (blue box). The change in the thiol redox status of StScsC was compared to the reduced ScsC alone control sample on the lane at the far right.

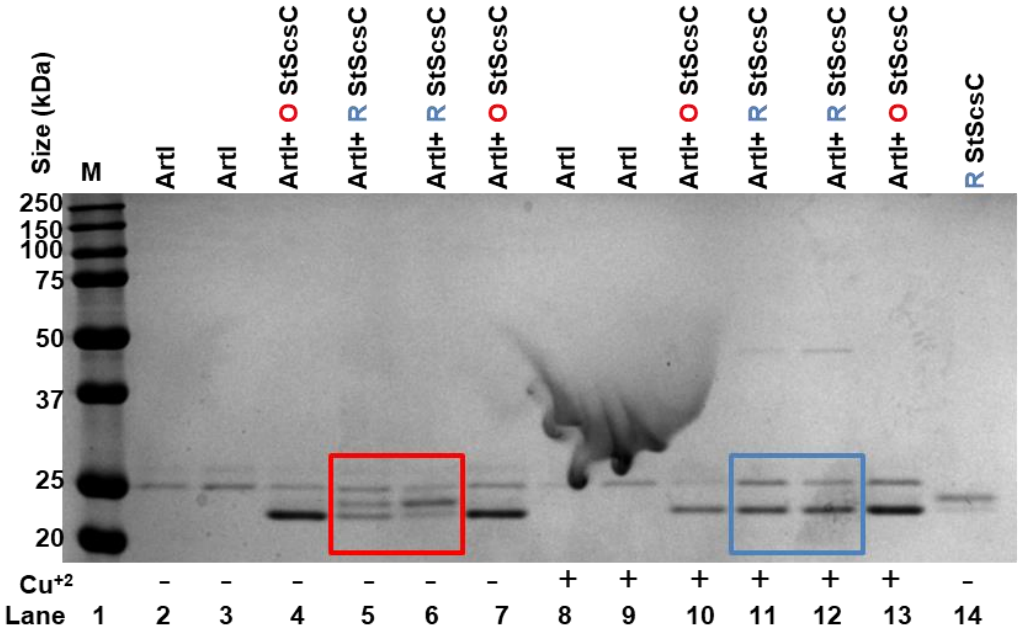


Figure 4.21- SDS-PAGE analysis of thiol redox status of ArtI and StScsC. 3 μM of each protein or combination of the two were incubated 1 h with or without copper at room temperature. Precipitated proteins were resuspended in buffer containing 20 mM AMS thiol modification reagent. Samples were run on SDS-PAGE. Reduced StScsC was found to be partially oxidized when incubated with ArtI as shown in the red box (compare to reduced StScsC on far right). The blue box indicates complete oxidation of StScsC in the presence of Cu^{2+}. The band shift for StScsC was compared to the reduced StScsC control run on the right hand side of the gel.

As the redox status of StScsC was found to be altered in the presence of ArtI, the interaction of increasing concentrations of 'as purified' ArtI with oxidised and reduced StScsC was investigated using AMS (Figure 4.22A). The addition of 'as purified' ArtI to reduced StScsC had no effect (lanes 1-4), whereas incremental addition of 'as purified' ArtI to oxidised StScsC (lanes 5-8) resulted in a corresponding reduction of StScsC (Figure 4.22B). Hence, these data indicate that ArtI is purified at least partially in the reduced state and can undergo disulphide exchange with StScsC.

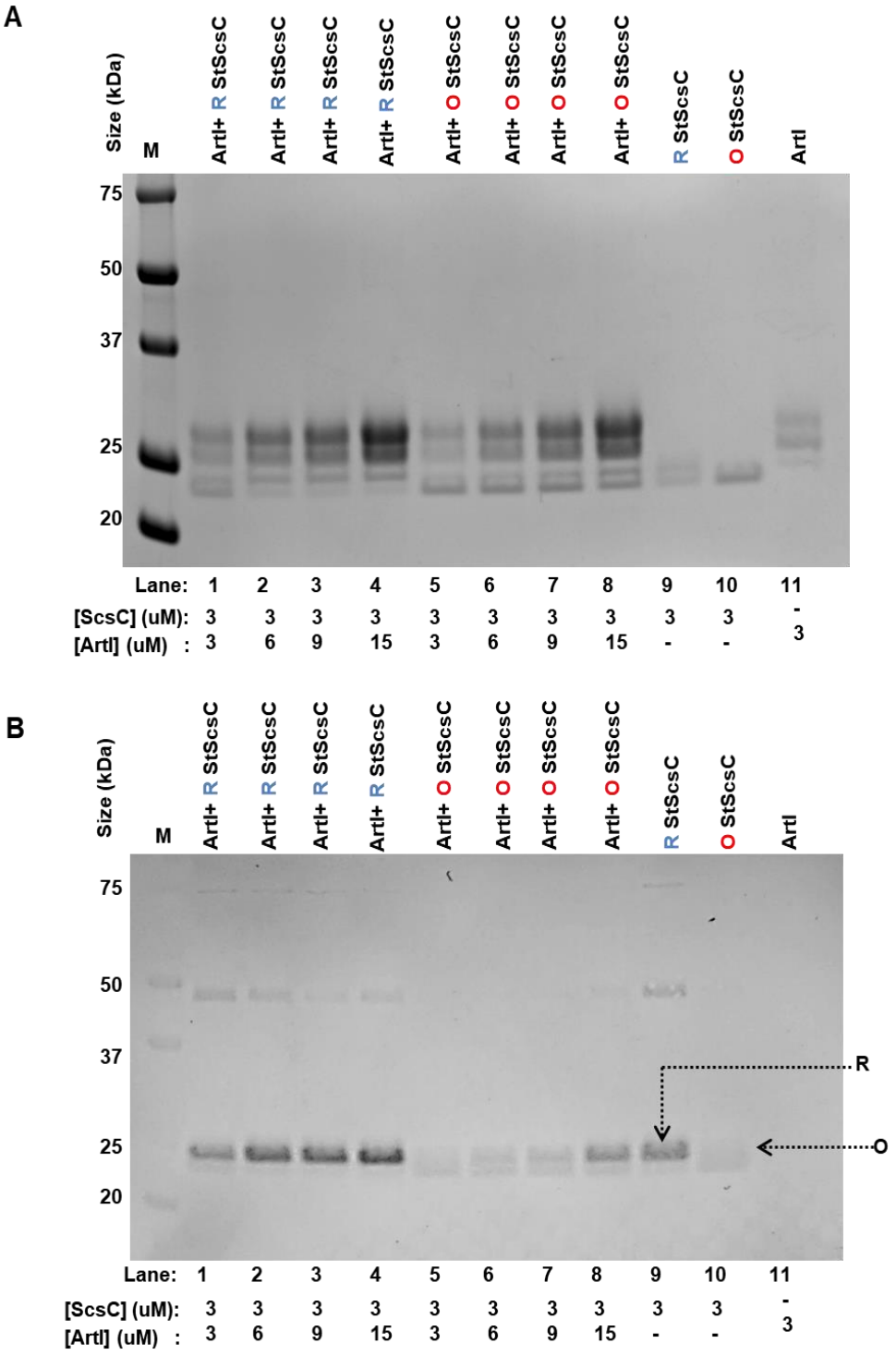


Figure 4.22- ArtI alters the redox status of oxidised StScsC. 'As-purified' ArtI and oxidised/reduced StScsC were incubated together under various conditions **(A)** SDS-PAGE and **(B)** Western blot analysis with anti-StScsC antibodies was used to probe the redox status of StScsC. The decrease in migration rate of oxidized StScsC with increasing concentrations of ArtI, following treatment with AMS, demonstrates that ArtI promotes the reduction of StScsC. ArtI does not have any effect on reduced StScsC. (O) oxidized StScsC control, (R) reduced StScsC control.

4.2.8-Structual analysis of ArtI and StScsC

This study revealed an interesting interaction between StScsC and ArtI using genetic and biochemical approaches. It was therefore of interest to gain a better understanding of the structural basis for this interaction. The predicted structure of ArtI and the crystal structure of StScsC were analysed using computational protein docking approaches to visualise the positions of the cysteine residues and to predict protein: protein interactions. The crystal structure of StScsC was available from the PDB (Shepherd *et al.,* 2013) and the position of the cysteine residues and surface electrostatics are shown in Figure 4.23A-B. A structural model of *Salmonella* ArtI was generated using the RaptorX server (Källberg *et al*., 2012) based on the crystal structure of a periplasmic arginine binding protein (PDBid = 2Y7I). The positions of cysteine residues and surface electrostatics are shown in (Figure 4.23C-D), with the bound arginine from the 2Y7I template superposed onto the model of ArtI in panel C.

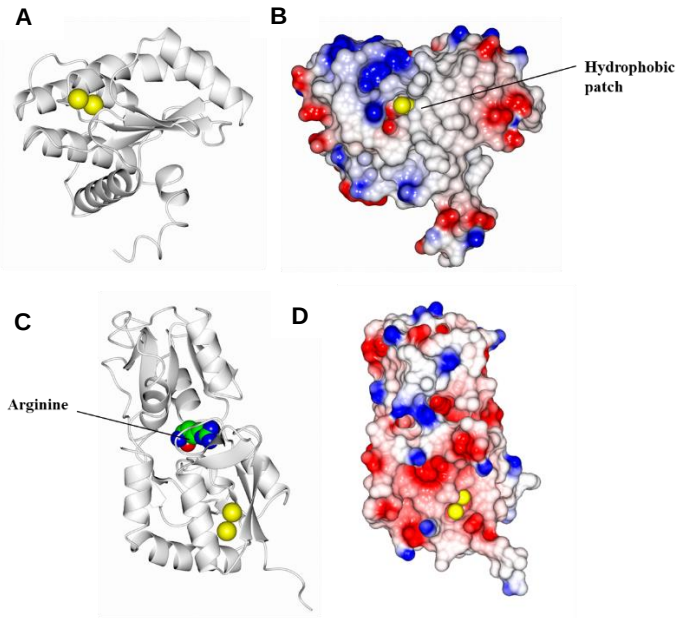


Figure 4.23- Crystal structure of *Salmonella* ScsC and structural model of ArtI. **(A)** Ribbon structure of StScsC. Yellow spheres indicating sulphur atoms of cysteine residues at positions Cys48 and Cys51. **(B)** Electrostatic surface structure of StScsC. Structure was obtained from PDB accession number 4GXZ (Shepherd *et al.,* 2013). Surface is omitted from the exposed active site cysteine residues to show the sulphur atoms (yellow spheres). White surface indicates hydrophobic surface adjacent to the cysteine residues. **(C)** The predicted structure of *S.* Typhimurium SL1344 ArtI was obtained using the RaptorX server based on a homologous template from the PDB (PDBid = 2Y7I). Two sequences were 56% identical that were calculated by using BLOSUM62 ExPASy SIM Alignment tool (Gasteiger *et al*., 2003). Arginine that was bound to the protein is indicated. Sulphur atoms are shown in yellow spheres. **(D)** Electrostatic surface of the protein was shown. Surface is omitted from the exposed active site cysteine residues to show the sulphur atoms (yellow spheres).

To investigate potential interactions between StScsC and ArtI, computational protein docking studies were performed using ClusPro software (Kozakov *et al*., 2017) where 30 structures for ArtI and StScsC interactions were predicted. However, none of the structures indicate a close enough proximity of cysteine residues for confirmation of the interaction between the two proteins by disulphide exchange confirmed in previous sections. The docked structure with the cysteines in closest proximity is shown in Figure 4.24, and the other selected structures are shown in Appendix 10.

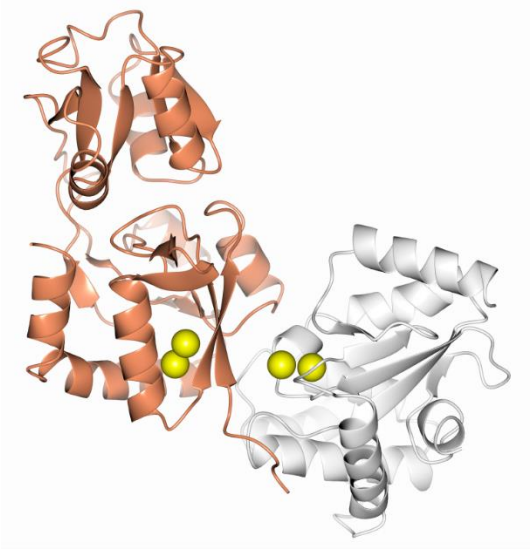


Figure 4.24- Protein docking of ArtI and StScsC. The ribbon structure of StScsC is shown in white and the ribbon structure of the ArtI is shown in coral. The sulphur atoms are shown as yellow spheres. The cysteine residues of the two proteins are located far apart to be able to interact via disulphide formation.

4.2.9 - Impact of StScsC upon growth of *Salmonella* on L-arginine

Since StScsC has been shown to interact with ArtI, a putative periplasmic binding protein with a potential role in arginine uptake, it was of interest to test if loss of StScsC affected growth on L-arginine as a carbon source. Wild-type and Δ*scsC* *Salmonella* strains were grown in M9 media with a low glucose concentration. 0.5 mM L-arginine was also omitted from the media in order to measure the effect of StScsC on the growth of *Salmonella*. Copper (1 mM) was supplemented to the growth medium in order to facilitate the expression of StScsC in wild-type cells. Under these conditions it was hypothesised that the wild-type strain would be stimulated by addition of L-arginine, whereas the Δ*scsC* strain would be impaired in

arginine uptake and addition of this amino acid would not affect growth. The growth curves indicate a subtle increase in growth in the presence of L-arginine for the wild-type strain, whereas there was no difference in growth of the Δ*scsC* strain (Figure 4.25).

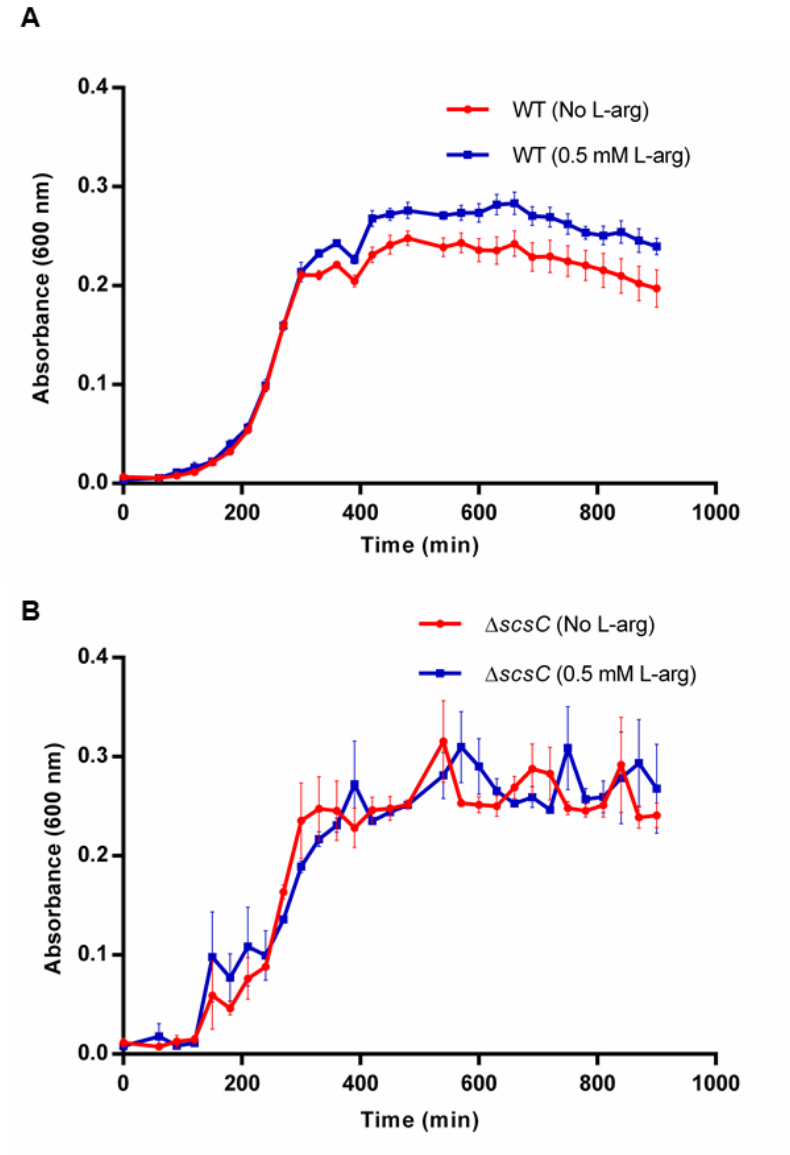


Figure 4.25- Loss of *scsC* abolishes L-arginine-mediated stimulation of growth. (A) Wild-type *S.* Typhimurium was grown in the presence and absence of 0.5 mM L-arginine in the presence of 1 mM copper. After 8 h, growth of cells in the presence of arginine was higher than in the absence of arginine. **(B)** Δ*scsC Salmonella* strains were grown in the presence and absence of 0.5 mM L-arginine.

4.3- Discussion

The characteristic H-X-X-M-X-X-M motif that is present in many predicted copper-binding and transport proteins has previously been reported to be absent in all StScs proteins (Gupta *et al*., 1997). Despite this, all StScs proteins have been shown to be regulated by copper specific transcriptional regulator (Lopez *et al*., 2018). In addition, StScsC has been shown to confer copper tolerance (Shepherd *et al*., 2013). Hence, it was of interest to measure the copper binding affinity of StScsC. A competition assay with BCS was performed (as described previously in Foster *et al*., 2014). Cu^{+} binding to BCS was demonstrated as a control, however, under our conditions, Cu^{+} binding to StScsC could not be demonstrated. No change in absorbance at 483 nm was observed when increasing concentration of Cu^{+} was being titrated in. It was expected that StScsC would become saturated with Cu^{+}, or not bind it at all, and then a BCS-Cu(I) complex would form leading to an increase in absorption at 483 nm (Xiao *et al.*, 2011). The initial interpretation of the data was that there may be multiple copper binding sites on StScsC, although this was discounted because of the very high concentration of copper that was used for some data points. A more likely scenario might be that BCS bound directly to StScsC, which may have prevented binding of copper to BCS precluding the formation of a BCS-Cu(I) complex. In the future, higher concentrations of BCS could be used in order to have a highly chance of observing the formation of the BCS-Cu(I) complex.

To provide biochemical data to confirm predicted interactions with StScsC based on the mass spectrometry experiments (Chapter 3), a his_6-tagged $StScsC_{CXXA}$ mutant protein was expressed in *E. coli* with the aim of trapping StScsC disulphide bonded with a redox partner. This method has been used previously to identify DsbG targets (Depuydt *et al*., 2009). Using a combination of affinity chromatography and mass spectrometry, an arginine binding periplasmic protein (ArtI) was identified to be bound to the $StScsC_{CXXA}$ protein via a disulphide bond. In Chapter 3, copper was shown to increase the abundance of ArtI in the *S.* Typhimurium periplasm by 20-fold (Figure 3.13), and lack of *scsC* in the presence of copper did decrease ArtI abundance, although *t*-tests did not support this as a significant difference (Table 3.2). Given that the relative abundance of ArtI compared to these other chaperones is much lower (Figure 3.12), it is surprising that ArtI is the only protein that was

identified in the $StScsC_{CXXA}$ trapping experiment, although this might reflect a high affinity for ArtI.

Binding of ArtI to reduced $StScsC_{CXXA}$ was also demonstrated using purified protein samples. The influence of copper upon the yield of ArtI: $StScsC_{CXXA}$ disulphide bonded complex formation was also investigated, and surprisingly $StScsC_{CXXA}$ was found to dimerise in the presence of copper. Following this observation, dimerisation of wild-type StScsC was tested in the presence of copper, although no change in the oligomerisation state was detected upon copper addition. It was hypothesised that this discrepancy could be explained by copper promoting the formation of intramolecular disulphide bonds in wild-type StScsC (as shown *in vivo* in Chapter 3), whereas the $StScsC_{CXXA}$ protein is unable to form intramolecular disulphides in the active site so copper will promote the formation of intermolecular disulphides instead.

To investigate the impact of copper upon the redox properties of purified StScsC and ArtI proteins, thiol modification assays were performed with AMS. Consistent with the results from the *in vivo* thiol modification assays (Chapter 3), StScsC was found to be in the oxidised state when copper is present *in vitro*. The redox status of ArtI could not be changed by the addition of oxidising and reducing reagents, suggesting that the cysteines of the ArtI protein are inaccessible and cannot be easily modified by small molecules, although StScsC can clearly form a disulphide bond with ArtI *in vivo*.

To further invesigate the interaction between StScsC and ArtI, 'as purified' ArtI was added to oxidised and reduced StScsC and was shown to reduce the oxidised StScsC in a dose-dependent manner (Figure 4.22). This clearly shows that disulphide exchange takes place between StScsC and ArtI, and supports the idea that the purified heterodisulphide complex (Figure 4.10) is not an artefact of the CXXA mutation described above. Since StScsC has been shown to exist in the oxidised state in the periplasm (in the presence of copper), this observation is consistent with a role for disulphide oxidation of ArtI by StScsC.

To gain structural insights into the StScsC: ArtI interaction, a structural model of ArtI was generated to dock to the crystal structure of StScsC. The best template for

ArtI modelling from the PDB was the periplasmic binding protein STM4351 (PDB accession number 2Y7I). Docking experiments with StScsC and ArtI yielded many different complexes, and while some complexes showed disulphides in relatively close proximity a convincing approximation of the disulphide bonded complex for the StScsC-ArtI heterodisulphide remained elusive. This may be because the disulphide of ArtI is buried too far in the structure, and the docking algorithms do not allow for large conformational rearrangements. In future, it would be interesting to perform structural dynamics simulations to gain better models for the heterodisulphide.

The exact substrate for ArtI has not been experimentally verified, but since ArtI is encoded by the *artIPQM* operon it has previsouly been hypothesized to be involved in arginine transport and metabolism (Weissenbach *et al.,* 1995). Assuming ArtI is indeed involved in L-arginine uptake, it was of interest to investigate whether the absence of StScsC impacted upon growth of *Salmonella* on L-arginine. The data herein demonstrate that L-arginine elicits a subtle increase in growth at late log phase, consistent with a diauxic shift from glucose to L-arginine, whereas this growth stimulation is lost in a Δ*scsC* mutant. This is consistent with StScsC facilitating L-arginine uptake possible via facilitating assembly of ArtI, although there are other amino acid chaperones besides ArtI that may also be involved. Indeed, ArgT has been shown to be important for utilisation of host arginine during macrophage infection, which also lowers the amount of L-arginine available for the production of toxic nitric oxide (Das *et al*., 2010).

Chapter 5

Investigating the ability of StScsABCD to facilitate disulphide folding of therapeutic proteins

Abstract

Many recombinant therapeutic proteins are produced in *E. coli*, including antibodies and certain hormones that require disulphide bonds for their biological activity and stability. Developing new strategies to improve the assembly and yield of the proteins in the *E. coli* periplasm is therefore important. In this chapter, two important protein therapeutics were used to test the ability of StScs proteins to facilitate the formation of disulphide bonds in targets of biotechnological importance. Herceptin (Trastuzumab) is a monoclonal antibody used for the treatment of aggressive breast cancer and Human Growth Hormone (hGH) is used to treat growth hormone deficiencies. Firstly, it was of interest to investigate if expression of the Scs system of *S.* Typhimurium could improve the yield of Herceptin Fab fragment in the *E. coli* periplasm. It was demonstrated by Western blot analyses that the StScs proteins can elevate the yield of Herceptin when copper is present. Secondly, a C189S variant of hGH and a CXXA variant of StScsC were used to investigate whether a heterodisulphide of these two proteins could be demonstrated. However, under the conditions tested, no covalent disulphide bond formation could be observed, although this approach could be used in future to investigate disulphide bond formation between StScs proteins and other potential protein targets.

5.1 - Introduction

In 1986, the first therapeutic monoclonal antibody was commercialised (Ecker *et al*., 2015). Since then, the production of these protein therapeutics has advanced significantly with improvements in manufacturing capacity and cell culture and purification processes (Kelley, 2009; review). A multi-billion pound industry now exists for recombinant monoclonal antibodies (mAb) like rituximab (Rituxan), trastuzumab (Herceptin), and infliximab (Remicade) (Ecker *et al.*, 2015). High-value therapeutic antibody fragments are produced in microbial systems with low-cost, simple purification and downstream processing with high yields (Berkmen, 2011; review). *E. coli* was the first microbial organism to be used for the production of recombinant biopharmaceuticals (Spadiut *et al*., 2014; review), where expression of recombinant monoclonal antibodies takes place in the cytoplasm of *E. coli* and disulphide formation usually takes place in the periplasm: due to the presence of thioredoxin and glutathione, cytoplasm is a reducing environment and disulphide oxidation is ordinarily not possible (Ritz and Beckwith, 2001; review). Hence, proteins that are expressed in the cytoplasm are usually exported to the oxidising periplasm and the correct formation of disulphides proceeds via disulphide oxidation and disulphide isomerisation by the Dsb (**di**s**s**ulphide **b**ond) machinery (as reviewed in Heras *et al*., 2009; review; Berkmen, 2011; review). In *E. coli*, translocation of more than 90% of secreted/periplasmic proteins is achieved by the Sec pathway through the SecYEG pore, where an N-terminal Sec-type signal peptide attached to the protein is recognised by the Sec machinery (Tsirigotaki *et al*., 2017; review). Proteins can also be targeted to the periplasm via the signal recognition particle (SRP)-dependent pathway and also by the Tat-dependent pathway (Georgiou and Segatori, 2005; review). The Tat-dependent pathway exports folded or partially-folded proteins with a signal sequence containing a twin arginie motif as reviewed in Kudva *et al.*, (2013; review) and Berks *et al*., (2000; review).

E. coli does not naturally form disulphide bonds in the cytoplasm, although strains have been engineered to do just that. To enable correct formation of disulphide bonds in the cytoplasm, a CyDisCo (Cytoplasmic Disulphide formation in *E. coli*) strain can be used which expresses Erv1p (yeast mitochondrial thiol oxidase) and PDI (human protein disulphide isomerase) to catalyse cytoplasmic disulphide bond formation and isomerisation (Matos *et al*., 2014; Gaciarz *et al.*, 2016). This can then

be coupled to Tat-dependent export of the protein to the periplasm (Matos *et al.,* 2014). Correct folding of proteins in the cytoplasm can also be achieved by using the SHuffle cells which express a chromosomal copy of the disulphide bond isomerase DsbC (Lobstein *et al*., 2012). In addition, cytoplasmic disulphide bond formation can be achieved by removing two cytoplasmic systems that promote disulphide reduction (*Δgor/ΔtrxB*) from the cytoplasm (Prinz *et al.,* 1997). Hence, this chapter focusses on a novel approach using StScs proteins and copper to facilitate disulphide folding for a Herceptin Fab fragment and human growth hormone in the *E. coli* periplasm that have been exported in their unfolded state by the Sec machinery.

5.1.1 - Herceptin

Cell division and repair in breast cell is controlled by a transmembrane tyrosine kinase Human epidermal growth factor receptor 2 (HER2). Approximately in 20% of the breast carcinomas, overexpression of HER2 leads to uncontrolled growth and division of the breast cell (Wilson *et al*., 2017; review). Therefore, targeting HER2 for the production of therapeutics is an appealing approach. Herceptin (Trastuzumab) is a recombinant humanized IgG1 monoclonal antibody and was the first FDA-approved therapy for breast cancer (Gajria and Chandarparty, 2011; review). It targets and down-regulates HER2 during development and progression of breast cancer (Baselga and Albanell, 2001; review), inhibiting cell signalling involved in cell proliferation and survival (Ross *et al*., 2009; review). Figure 5.1 shows the general structure of an IgG antibody highlighting the Fab and Fc fragments. The light and heavy chains are connected via disulphide bonds, which is crucial for antibody stability and function (Liu *et al.,* 2010). In the anti-HER2 monoclonal antibody (mAb), 12 intra-molecular and 4 inter-molecular disulphides are present (Wang *et al*., 2011). Figure 5.2 shows the positions of these inter- and intra-molecular disulphides. Incomplete formation of disulphide bonds could have the potential to trigger an immune response when administered because of formation of aggregates and unfolded protein (Liu *et al*., 2012; review). Figure 5.3 demonstrates the crystal structure of the heavy and the light chain of the Herceptin Fab fragment which was used in this study. As the *scs* operon of *S.* Typhimurium has a likely role in disulphide folding, the change in the yield of Herceptin Fab fragment in the presence and absence of StScs proteins and Cu^{2+} was measured.

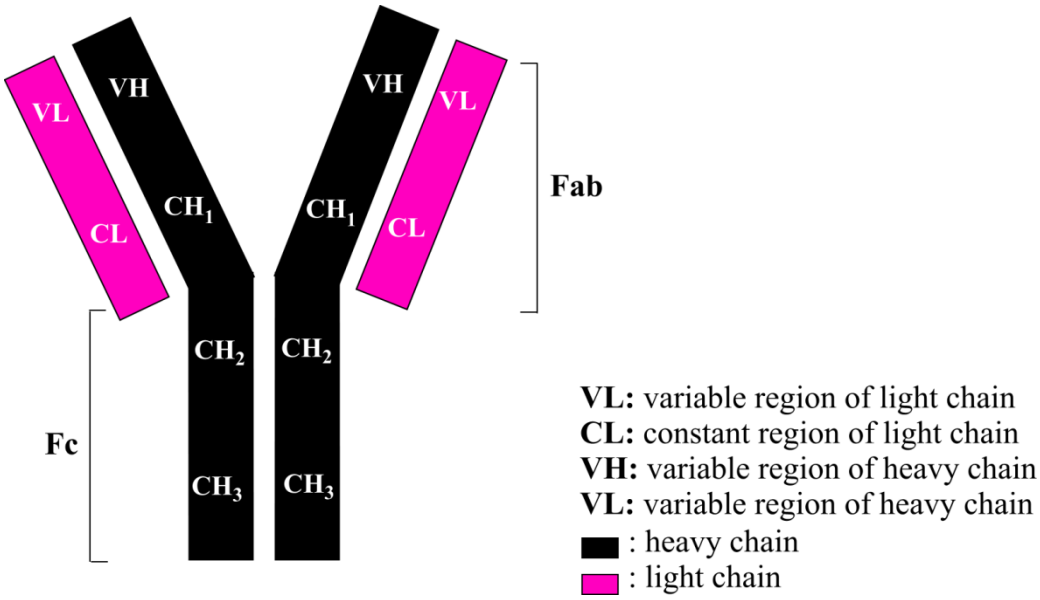


Figure 5.1 - Schematic structure of IgG1. The heavy chains are shown in black and the light chains are shown in pink.

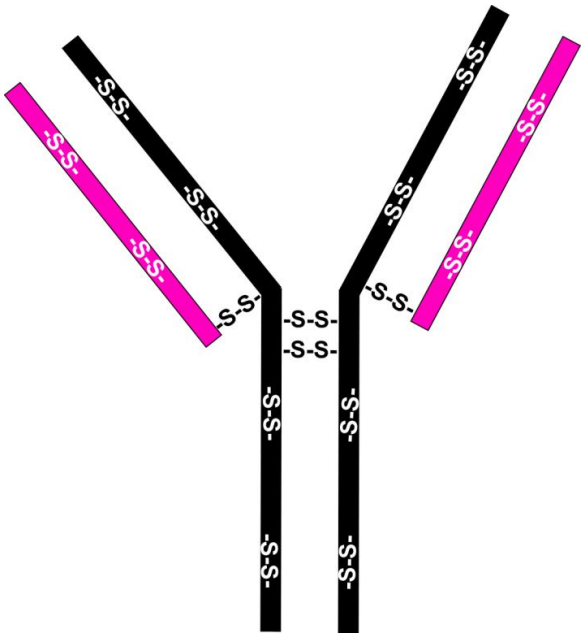


Figure 5.2 - Herceptin inter- and intra-molecular disulphides. Intra-molecular disulphides on the light chain (shown in pink) of Herceptin are formed between Cys23-88 and Cys134-194. Bonds formed between the Cys22-96 and Cys147-203 are the intra-molecular disulphides formed in the heavy chain (shown in black) of the Fab fragment. The inter-molecular disulphide bond formation between the Cys214 found at the C-terminal end of the light chain and the Cys223 of the heavy chain connects the two chains together. Two parallel inter-chain disulphides are formed between the Cys229-232 of the two heavy chains (Adapted from Wang *et al*., 2011).

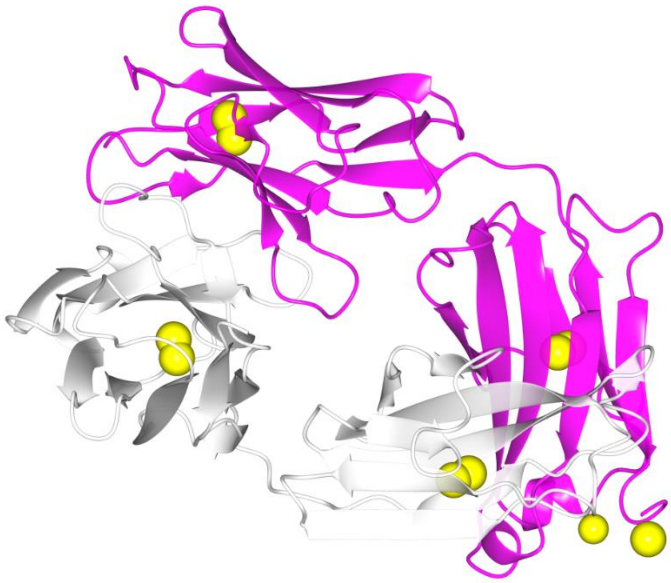


Figure 5.3 - Crystal structure of Herceptin Fab fragment. The Fab fragment light chain is shown in pink and the heavy chain is shown in white. The position of the cysteine residues where intra-molecular disulphides are formed are depicted by yellow spheres and are as follows; Cys23-88 and Cys134-194 on the light chain and the Cys22-96 and Cys147-203 on the heavy chain. An inter-molecular disulphide bond also forms between the Cys214 of the light chain and Cys223 of the heavy chain. Two sulphur atoms for the intra-molecular disulphide is shown at the bottom right corner of the figure. The second intra-molecular disulphide bond cannot be demonstrated as it is formed between two heavy chains. Model from PDB accession number: 1N8Z was used to produce this figure.

5.1.2 - Human growth hormone (hGH)

Human growth hormone (hGH) is a small, single chain, globular protein with 191 amino acid residues. It is synthesised by the pituitary gland. It has a role in growth, development and immune regulation (Rezaei and Zarkesh-Esfahani, 2012). Human growth hormone is used to treat dwarfism and bone fractures due to growth hormone deficiencies in children where it has an effect on stimulation of the bone, muscle and cartilage metabolism (Doessing *et al.*, 2010). It is also used to treat growth impediments in girls with Turners syndrome which is the most common chromosomal disorder in women (Spiliotis, 2008; review). Expression in the *E. coli* periplasm provides safe, abundant and low-cost production of recombinant hGH (Kamionka, 2011; review): pituitary-derived hGH was prohibited due to the risk of human pathogen transfer and association with Creutzfeldt-Jakob disease (Rezaei and Zarkesh-Esfahani, 2012). The 22 kDa hGH protein contains two disulphide bonds. Areas that are structurally remote in the primary structure are connected by the bond between cysteine residues 53 and 165, which is called the large loop, and the second

bond is near the C-terminal end of the protein where a small loop is formed between cysteine 182 and 189 (Youngman *et al*., 1995). The crystal structures and the position of the cysteine residues are shown in Figure 5.4. The large loop disulphide has been shown to be necessary for biological activity of the protein and the second disulphide bond has been shown to be required for the stability of hGH (Junnila and Kopchick, 2013).

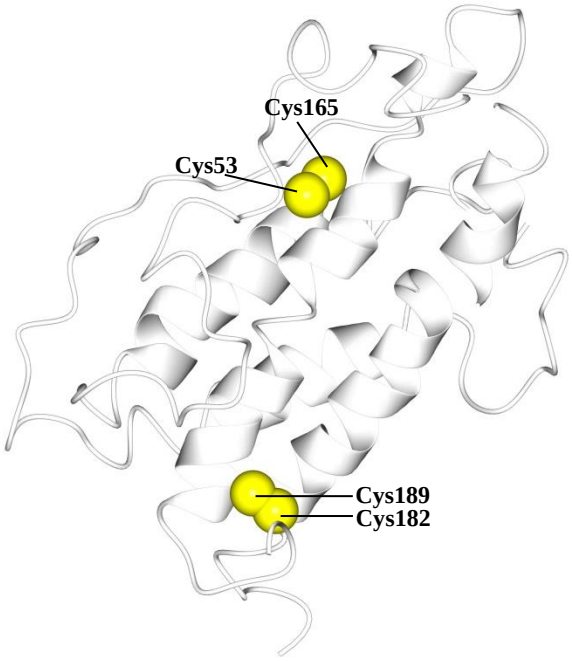


Figure 5.4 - The structure of hGH. This figure was made using the CCP4MG molecular graphics programme (McNicholas *et al.,* 2011) using the structure form the Protein Data Bank (accession number 1HGU, Chantalat *et al*., 1995). The active site sulphur atoms are shown as yellow spheres where 2 inter-molecular disulphide bridges are formed between Cys53-165 and Cys182-189. Cys182- Cys189 forms a small loop disulphide and the Cys53-Cys165 forms a large loop disulphide.

5.2 - Results

5.2.1 – Investigating the impact of StScsABCD and copper upon Herceptin assembly

5.2.1.1 - Engineering a Herceptin expression vector

An operon was designed to utilise the OmpAI signal peptide (Humphreys *et al.*, 2000) to target both the Fab fragment heavy and light chains of Herceptin to the periplasm, downstream of the inducible *lac* promoter. A short intergenic region based on IGS2 (Patent number 7419659, UCB Pharma S.A.) was placed between the two open reading frames to provide efficient translational read-through and to negate the need for a second promoter. This sequence was synthesised and cloned in the standard pMKRQ plasmid vector by Invitrogen GeneArt Gene synthesis service (Thermo-fisher) (Figure 5.5). *E. coli* TOP10 cells were transformed with this vector and protein expression was induced by IPTG.

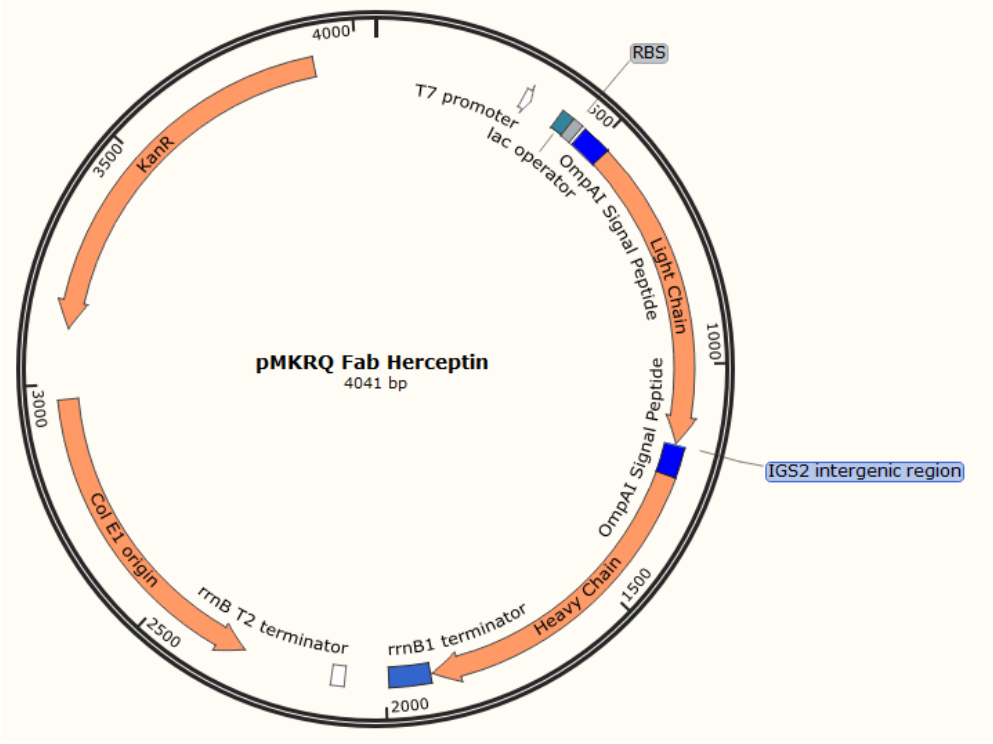


Figure 5.5 - Fab pMK-RQ plasmid map. Expression of the heavy and the light chain of the Herceptin Fab fragment is controlled by the *lac* promoter. Protein chains are targeted to the periplasm by the OmpAI signal peptide. The pMK-RQ plasmid contains a kanamycin resistance cassette with a ColEI replication origin.

5.2.1.2 – Engineering a ScsABCD expression plasmid

The *scsABCD* operon was amplified from the *S.* Typhimurium SL1344 chromosome and was cloned into *Eco*RI-*Xho*I digested pWSK29 plasmid downstream of the *lac* promoter (Shepherd *et al*., 2013). The plasmid map is shown in Figure 5.6. This plasmid backbone was chosen as the pSC101 origin of replication is compatible with the ColE1 origin of the pMK-RQ vector.

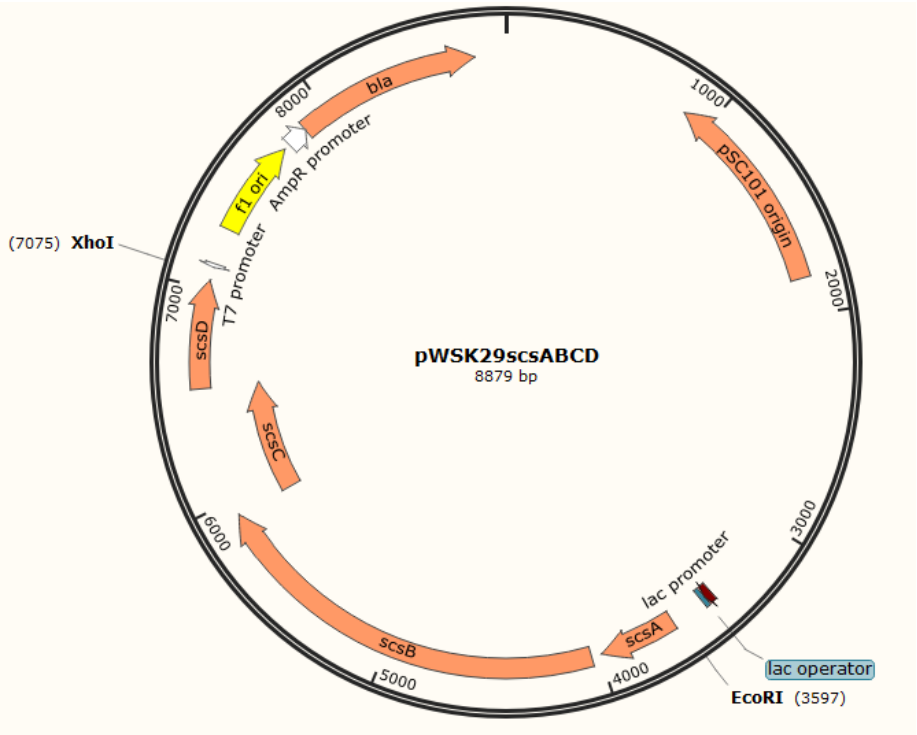


Figure 5.6- pWSK29*scsABCD* plasmid map. Expression of the StScs proteins was controlled by the *lac* promoter.

5.2.1.3 - Development of a Western Blotting technique to detect Herceptin

E. coli TOP10 cells were transformed with the pWSK29*scsABCD* and pMKRQ Fab Herceptin plasmids. Whole cell samples of the strains harbouring one or both plasmids were resolved on an SDS-PAGE gel (Figure 5.7A) and the 50 kDa Fab fragment or the 25 kDa kappa light chain of Herceptin were detected by Western blotting. When the reducing agent DTT was absent, the 50 kDa Herceptin Fab fragment was detected both in the presence and absence of StScs proteins by using an anti-Fab specific antibody (Figure 5.7B). The heavy and light chain was reduced by the addition of reducing agent DTT and the 24 kDa light chain of the Herceptin was detected by using an anti-kappa light chain antibody (Figure 5.7C).

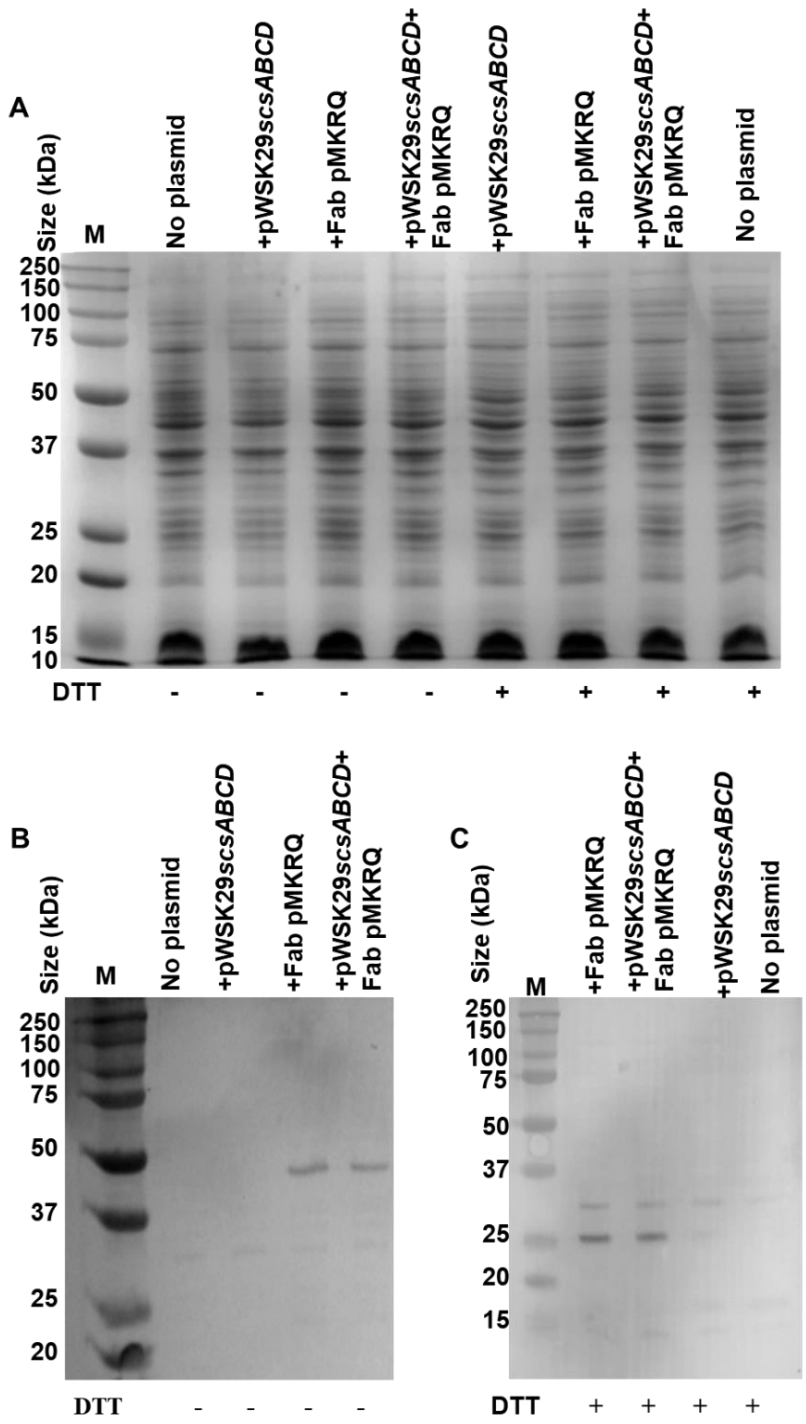


Figure 5.7- Expression and detection of Herceptin in *E. coli*. (A) SDS-PAGE analysis of whole cell samples from *E. coli* TOP10 harbouring the pWSK29*scsABCD* plasmid alone, pMKRQ Fab Herceptin plasmid alone, or harbouring both plasmids. Samples were pre-incubated +/- DTT before proteins were resolved on the gel. *E. coli* TOP10 without any plasmid was also used as a control. **(B)** Western blot detection of Herceptin Fab fragment (~48 kDa) using anti-Fab specific alkaline phosphatase antibody in the absence of DTT. **(C)** DTT was used to reduce and separate the heavy and light chains, and the ~24 kDa Herceptin light chain was detected using an anti-kappa light chain alkaline phosphatase antibody. Dual Colour protein marker from Bio-Rad was used.

5.2.1.4 - Copper elevates periplasmic protein levels in *E. coli* cells

Given that copper is required for expression of native StScsABCD (Chapter 3) and may be important for the activity of StScs proteins, it was of interest to investigate if the presence of copper elevates the yield of periplasmic proteins in the presence of StScs proteins. Strains harbouring pWSK29*scsABCD*, pMKRQ Fab Herceptin, or both plasmids were grown in the presence of Cu^{2+}. The total periplasmic protein concentration of strains grown in the presence and absence of copper was determined by Markwell assay (Section 2.5.3.1). As shown on Figure 5.8, the total protein levels were higher in the presence of copper in cells harbouring just one plasmid. No significant difference in protein concentration was detected for *E. coli* harbouring both plasmids when grown in the presence and absence of copper.

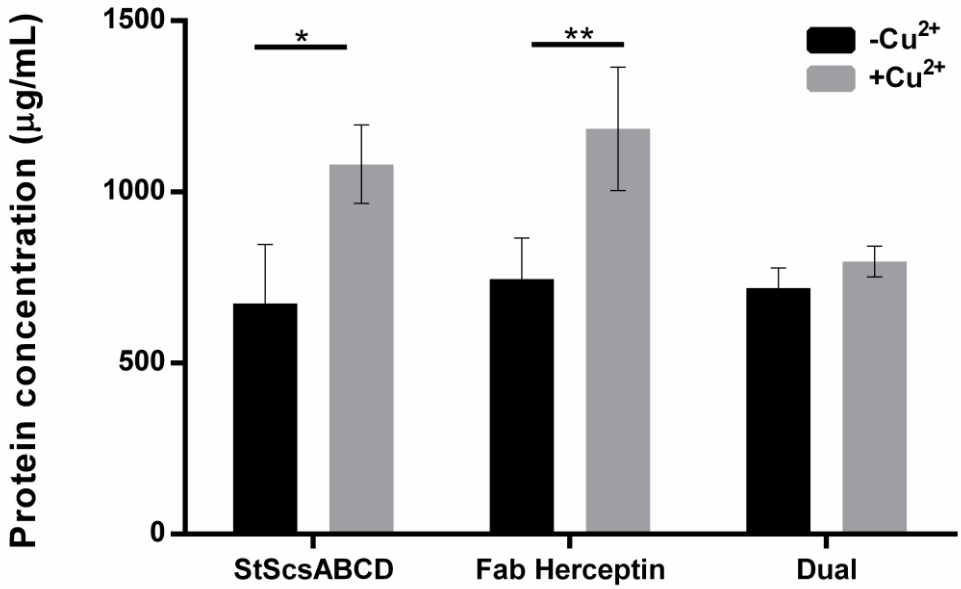


Figure 5.8- Periplasmic protein concentration of *E. coli* is elevated by Cu^{2+}. *E. coli* strains harbouring pKMRQ Fab Herceptin plasmid alone, pWSK29*scsABCD* plasmid alone, and harbouring both plasmids were grown to an OD_{600} of 1.0 and periplasmic fractions were extracted and the protein concentrations were measured. Error bars indicate the SEM of 4 biological repeats. Asterisk denotes $P < 0.1$ (*) and $P < 0.05$ (**) for unpaired *t*-test.

5.2.1.5 - Herceptin yield is elevated by both expression of StScs proteins and copper

To investigate if the yield of Herceptin was influenced by the presence of copper and/or the expression of StScs proteins, Western blot experiments were undertaken. Copper has previously been confirmed to catalyse the oxidation of protein disulphides (Hiniker *et al*., 2005), and copper promotes oxidation of StScsC (Section 4.2.7.3). Herein, the pMKRQ Fab Herceptin plasmid and pWSK29*scsABCD* plasmid were co-induced in *E. coli* with IPTG in the presence and absence of 2 mM Cu^{2+}. Whole cell samples were resolved via SDS-PAGE (Figure 5.9A), and Western blot detection of 25 kDa Herceptin light chains was performed using an anti-kappa light chain antibody as described in Section 2.9. When copper was present, the band intensity was higher (Figure 5.9B, lanes 3-4, 7-8, 11-12). This result suggests that the presence of copper elevates the yield of Herceptin. In order to analyse this data quantitatively, densitometry analyses were performed using Image J software (Schneider *et al*., 2012). The difference in yield (i.e. band intensity) of the Herceptin light chain in the presence and absence of StScs proteins was measured when copper was present. The image was inverted and the pixel intensity of a fixed area around each band was measured (Ctrl+ M). Figure 5.10 shows the mean band intensities from the blot, where all band areas have been subtracted from data obtained for the empty well control.

When Herceptin was expressed on its own, the addition of copper did not make any significant difference on the yield of the protein (Figure 5.10). However, when both plasmids were co-expressed, the addition of copper ions elevated the yield of Herceptin light chain significantly. This suggests that copper plays an indirect role in disulphide folding of Herceptin by facilitating StScs-mediated disulphide folding of Herceptin.

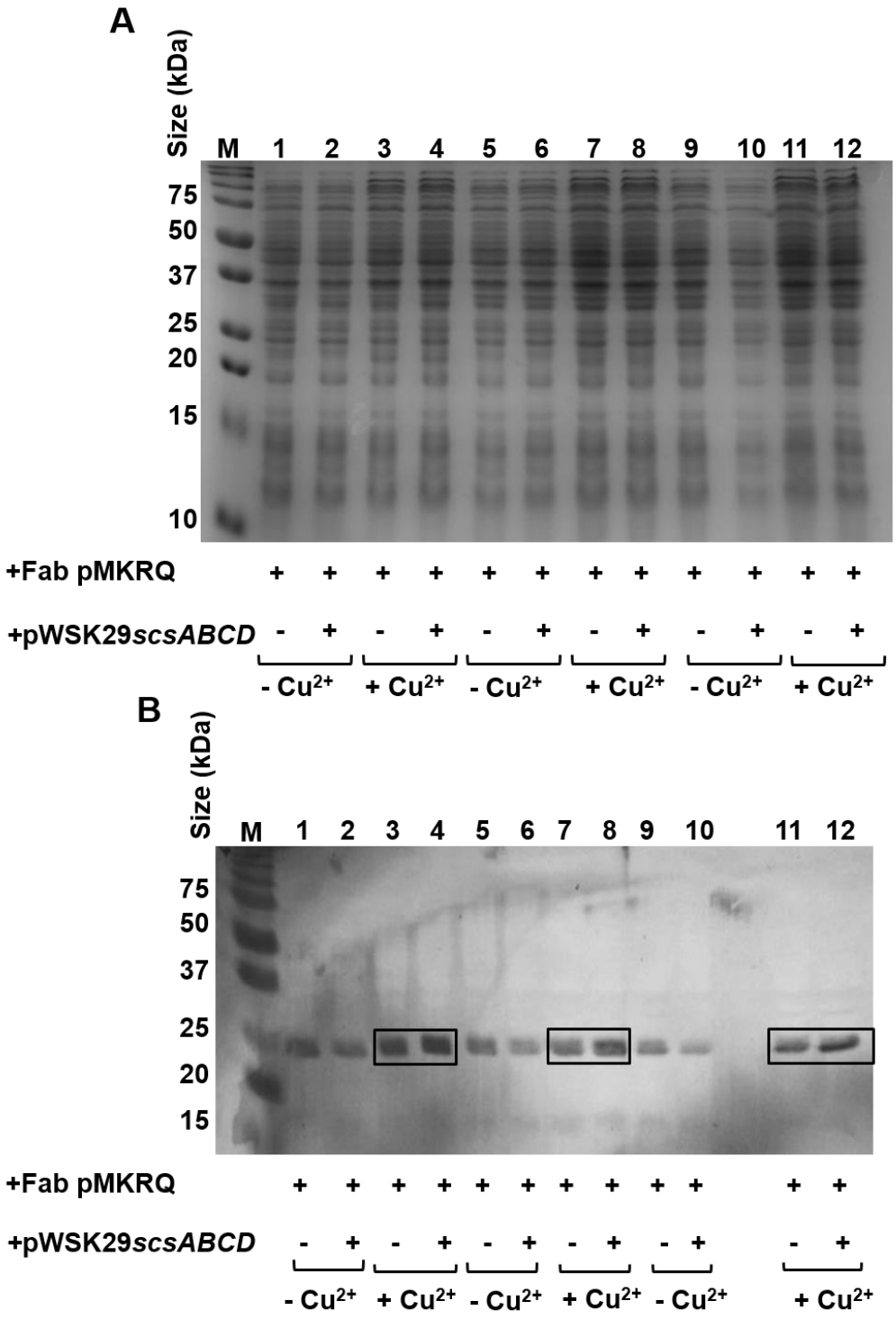


Figure 5.9- Copper ions elevate the yield of Herceptin in *E. coli* when StScsABCD proteins are expressed. (A) SDS-PAGE analysis of whole cell samples of strains expressing Herceptin Fab fragment in the presence and absence of StScsABCD proteins and Cu^{2+}. **(B)** Western blot analysis of Herceptin light chain using anti-kappa light chain alkaline phosphatase antibody under reducing conditions. A ~24 kDa band corresponding to the Herceptin light chain fragment was detected. An increase in band intensity is shown for lanes 3-4, 7-8 and 11-12 where copper ions were present (bands shown in black boxes).

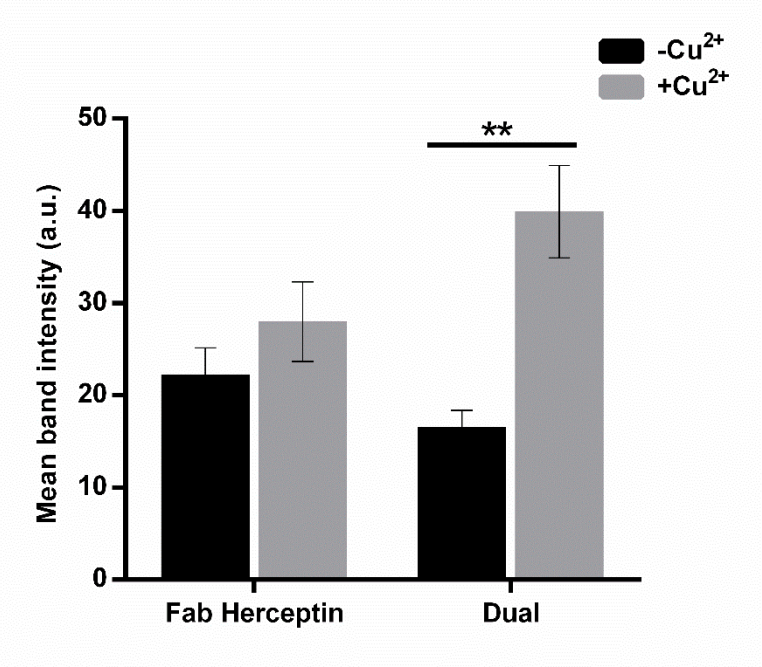


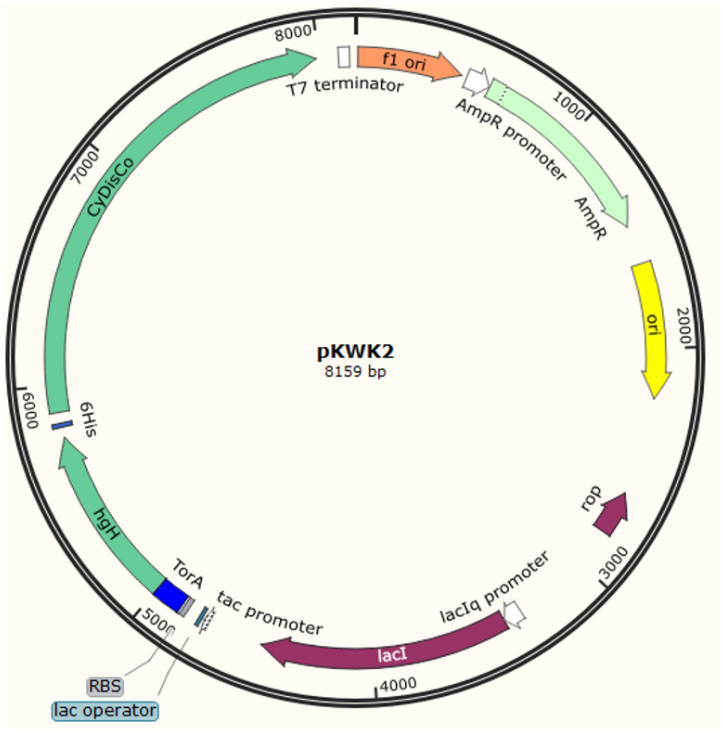
Figure 5.10- Densitometry analysis for expression of Herceptin light chain. Results displayed as mean band intensity as a function of empty well control. The presence of StScs proteins elevate the yield of Herceptin when copper is present. Error bars show standard error (SEM) of three independent repeats. Asterisk denotes P< 0.05 for unpaired *t*-test.

5.2.2 - Investigating the impact of StScsABCD and copper upon Human Growth Hormone assembly

5.2.2.1 - Attempts to demonstrate the formation of a StScsC-hGH heterodisulphide

The ability of $StScsC_{CXXA}$ to form a disulphide bond with target proteins (Section 4.2.5) was exploited to investigate a potential interaction of StScsC with hGH. *E. coli* JM109 was co-transformed with pSU2718*scsC*$_{CXXA}$His (Figure 4.7) and a pET23-based vector expressing mature hGH-His_6 with a C189S mutation and a TorA signal peptide (pKWK2 in Alanen *et al*., 2015) for export via the Tat system. The rationale for using this variant is that mutation of a single cysteine will prevent an inter-molecular disulphide bond forming in hGH, leaving a reduced thiol permanently free to form a heterodisulphide with the single free cysteine of $StScsC_{CXXA}$. The protein sequence of hGH, and the plasmid map for the hGH vector is shown in Figure 5.11. This vector also encodes the CyDisCo system to facilitate disulphide folding in the cytoplasm (Matos *et al.*, 2014).

A



B

FPTIPLSRLFDNAMLRAHRLHQLAFDTYQEFEEA
YIPKEQKYSFLQNPQTSL**C**FSESIPTPSNREETQ
QKSNLELLRISLLLIQSWLEPVQFLRSVFANSLV
YGASDSNVYDLLKDLEEGIQTLMGRLEDGSPRTG
QIFKQTYSKFDTNSHNDDALLKNYGLLY**C**FRKDM
DKVETFLRIVQ**C**RSVEGS**C**GF

Figure 5.11- pKWK2 plasmid map expressing hGH. (A) C189S version of hGH cloned into a pET23-based plasmid with a pTac promoter. Inclusion of the CyDisCo systems enables expression of a codon-optimised Erv1p and mature codon-optimised hPDI. Cytoplasmic disulphide bond formation will take place and the expressed hGH will be exported to the periplasm by Tat-dependent pathway with TorA signal peptide attached to the N-terminus of the protein. **(B)** Protein sequence of hGH. Four cysteine residues located at positions 53, 165, 182 and 189 are highlighted in red. The cysteine residue at position 189 highlighted in red circle has been substituted with a serine residue (sequence from PDB accession number 1HGU).

E.coli K12 JM109 strains harbouring pKWK2 alone or pKWK2 and pSU2718*scsC*$_{CXXA}$His were grown in LB medium (37 °C, 180 rpm) in the presence of 0.1 mM IPTG until an OD_{600} of 1.0. Periplasmic fractions were resolved on an SDS-PAGE gel and Western blot analyses were used for the detection of StScsC-hGH heterodisulphides using an anti-hGH antibody (Alanen *et al.*, 2015). Figure 5.13 shows data for cells expressing the hGH C189S variant alone or when it is co-expressed with StScsC$_{CXXA}$. As the cysteine at position 189 was mutated to a serine,

the small loop intra-molecular disulphide cannot be formed and it was hypothesised that if StScsC could facilitate disulphide folding of hGH, an inter-molecular disulphide might be formed with the single free cysteine of $StScsC_{CXXA}$. If StScsC bound to hGH C189S, a band at approximately 45 kDa would be expected. Both in the presence and absence of mutant StScsC, bands at same molecular weight were observed. The addition of reducing agent DTT caused reduction of the intra-molecular disulphide of hGH, which has previously been shown to result in a band shift (Alanen *et al*., 2015). However, the formation of a heterodisulphide between StScsC and hGH (at approximately 45 kDa) could not be demonstrated using this approach.

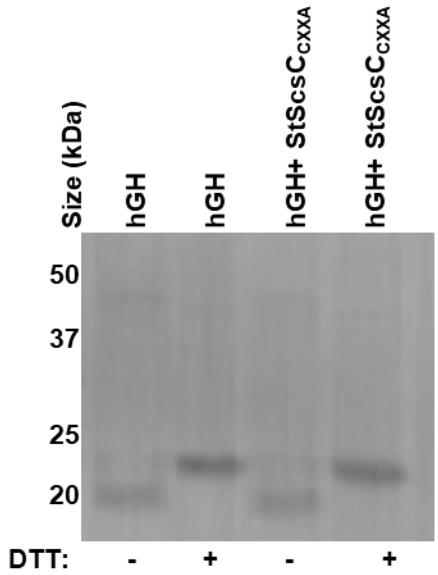


Figure 5.12- A $StScsC_{CXXA}$:hGH_{C189S} disulphide bonded complex cannot be detected via Western blotting. Western blotting with Anti-hGH antibody showing hGH C189S alone and expressed with $StScsC_{CXXA}$ in reducing and non-reducing conditions. The shift in the band size of hGH hormone is due to disulphide bond formation between Cys53 and Cys165. No band was observed at about 45 kDa when hGH was co-expressed with the StScsC.

5.3 - Discussion

To ensure the function, stability, assembly and quality of therapeutic proteins that are produced in microbial systems, the formation of correct disulphides can be crucial (Patil *et al*., 2015; review; Guglielmi and Martineau, 2009; Wang *et al.,* 2011). The production of misfolded proteins may have destabilising effects due to formation of insoluble aggregates and inclusion bodies leading to protein degradation (Guglielmi and Martineau, 2009). Factors associated with disulphide folding should be investigated both in the cytoplasm and periplasm of *E. coli* for enhancing the production of high quality and high yield products. Bacterial expression systems have been engineered for promoting the production of disulphide folded proteins in the cytoplasm (Matos *et al.,* 2014 and Prinz *et al*., 1997). In this chapter, the ability of the Dsb-like Scs proteins of *Salmonella* to improve the assembly of a disulphide-containing therapeutic antibody was investigated (i.e. Herceptin Fab). Redox-active copper was also used in this study, alone or in combination with StScs proteins. One of the reasons for that was to investigate the influence of copper on the yield of Herceptin, as it had been previously shown to promote oxidation of protein thiols (Hiniker *et al.,* 2005) and copper can also alter the thiol-redox status of StScsC (Chapter 3). Using Western blot analysis, it was confirmed that the presence of copper alone or StScs proteins alone does not have any significant effect upon the yield of Herceptin. However, when StScs proteins were expressed in the presence of copper, a significant increase in the band intensity of Herceptin light chain was observed, which suggested an increased in protein abundance. A plausible explanation for this is that the StScsC protein is able to catalyse disulphide formation in Herceptin, and Cu^{2+} ions can catalyse the recycling of reduced StScsC to the oxidised form (Figure 5.13), promoting enhanced disulphide formation in Herceptin and diminishing the degradation of misfolded antibody.

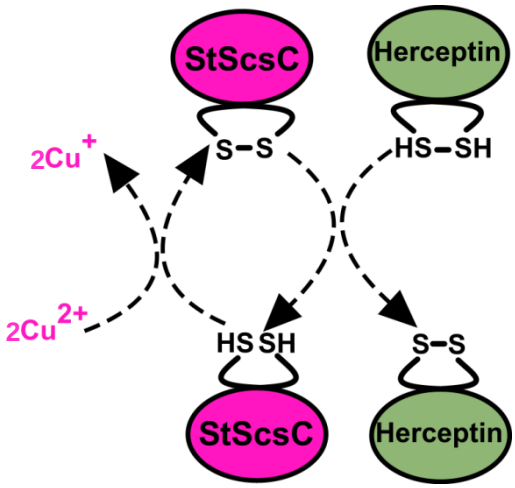


Figure 5.13- Model for Herceptin StScsC-catalysed disulphide folding. Reduced StScsC is oxidised by copper ions. Oxidised StScsC is then able to promote disulphide oxidation of Herceptin.

In future, mass spectrometry approaches could be used to quantify the concentration of Herceptin Fab fragment in the presence of copper alone, StScs proteins alone or in the presence of both. In addition to this, the abundance of disulphide-containing fragments could be measured using differential thiol labelling techniques (McDonagh *et al.*, 2014) to measure the impact of StScs proteins and copper upon Herceptin quality. Furthermore, Herceptin Fab fragment and the StScs proteins could be expressed in *ΔdsbA*/ *ΔdsbC* knockout strains to provide insights into whether StScs proteins can replace the function of Dsb proteins. Notably, DsbA has been shown to be induced by copper during this PhD project (Section 3.2.4) as well as by Pogliano *et al.*, (1997): this could potentially impact upon disulphide folding in the current experiments, so this further highlights the necessity to undertake functional investigations into StScs function in strains that lack Dsb machinery. Preliminary studies indicate that Herceptin assembly is totally abolished in a *ΔdsbB* strain, and cannot be compensated for by StScsABCD expression or exposure to copper (Dr. Alex Jones, personal communication). Given the stimulatory effect of StScs proteins and copper upon Herceptin assembly observed herein, this suggests that the StScsC/StScsD periplasmic chaperones may shuttle electrons to DsbB, potentially via a Cu^{+} intermediate, although further work will be required to confirm this.

A C189S variant of human growth hormone, which lacks the ability to form an intramolecular disulphide, was previously used to confirm the export of partially folded proteins to the *E. coli* periplasm by the Tat export pathway (Alanen *et al.*,

2015). In this chapter, this C189S hGH was co-expressed with $StScsC_{CXXA}$ to investigate the ability of StScsC to form a heterodisulphide with hGH with the aim of demonstrating the formation of covalent disulphide bond between these two proteins. The Western blotting approach undertaken did not demonstrate the formation of a StScsC:hGH heterodisulphide. However, this approach was quite limited in the sense that only one cysteine in a single protein was investigated. It is still possible that StScsC might interact with hGH but the nucleophilic cysteine of StScsC (i.e. the first in the CXXC motif) may preferentially target another cysteine in hGH. Clearly, the interaction of StScsC with a broader range of protein therapeutic targets can be investigated in future. In addition, the presence of the whole *scs* operon might be required for efficient disulphide oxidoreductase activity of StScsC.

Chapter 6

Final discussion

The Scs proteins were first characterised in *S.* Typhimurium 20 over years ago (Gupta *et al.,* 1997), where they have shown to confer copper tolerance in *E. coli* mutant strains that were defective in copper metabolism. The Scs proteins exhibit close sequence homology to proteins of the Dsb (disulphide bond) family of proteins, and have therefore been predicted to play a role in forming disulphide bonds in target proteins in *S.* Typhimurium (Shepherd *et al.,* 2013; Gupta *et al.,* 1997). However, very little was known about the environmental factors that control the *scs* operon, the functional role of the StScs system *in vivo* (e.g. redox partners), how expression of different StScs components influences the levels of other proteins in *S.* Typhimurium, and whether the StScs system could be used to improve the assembly of disulphide-containing proteins of biotechnological importance. These gaps in knowledge were the driving force behind this PhD project.

6.1- Expression and oxidation status analysis of ScsC

Copper had previously been shown to control the transcription of *scsB, scsC* and *scsD* genes through acting on the upstream *scsA* promoter (Lopez *et al.,* 2018), and the data described herein are consistent with this work through demonstrating a dose-dependent response to copper for the *scsA* promoter using GFP fluorescence. In addition, the abundance of ScsC in wild-type *S.* Typhimurium was also detected at higher levels in the presence of copper. Aside from copper exposure, the StScs proteins are known to play a role in oxidative stress (Lopez *et al.,* 2018; Anwar *et al.,* 2013). Hence, expression of the StScsC protein has previously been measured in the presence of various stresses such as hydrogen peroxide, nitric oxide and other divalent metals like iron and zinc. However, western blot analysis has revealed that production of ScsC in the *Salmonella* periplasm is increased by copper only amongst the conditions tested. Given that copper is required to express StScsC, and redox-active copper ions are well-known to influence disulphide formation (Hiniker *et al*., 2005) the redox status of the ScsC was measured in the *Salmonella* periplasm in the presence of copper as well as with other stresses that are found during infection. Copper did indeed promote the oxidation of StScsC, so the range of stresses was again expanded to hydrogen peroxide, nitric oxide and other divalent metals, although only copper was shown to affect the redox state of StScsC.

6.2- Potential targets and predicted roles of ScsC during infection

It was hypothesised that the StScs system and copper play a combined role in disulphide folding of proteins during infection. To characterise the function of the ScsC in *S.* Typhimurium, it was important to identify potential redox partners for StScsC in the periplasm. Mass spectrometry approaches were undertaken to measure the impact of StScsC expression and copper exposure upon the abundance cysteine and disulphide-containing proteins in the *Salmonella* periplasm. It was anticipated that in the absence of StScsC, the target proteins will undergo misfolding and degradation, resulting in lower abundance. This approach identified HisJ, ArgT, and GltI as having significantly lower abundance in a *ΔscsC* strain compared to wild-type, suggesting a potential interaction of these periplasmic amino acid binding chaperones with StScsC. In addition, the data also highlighted the periplasmic superoxide dismutase SodCII (Wang *et al.,* 2018; review) as being significantly upregulated in the presence of StScsC, which is consistent with previous observations that the StScs system has a role in tolerance of oxidative stress (Anwar *et al*., 2013; Lopez *et al*., 2018). The impact of StScsC upon the assembly of a variety of proteins led to the hypothesis that loss of StScsC would impair survival within macrophages. Indeed, infection of activated macrophages with wild-type/*ΔscsC Salmonella* strains in the presence of copper clearly demonstrated an important role for StScsC (and redox partners) during infection.

In an attempt to isolate StScsC bound to a partner protein, a disulphide trapping approach was undertaken using the $StScsC_{CXXA}$ variant, as performed previously with a similar variant of DsbG (Depuydt *et al.,* 2009). Following a combination of affinity chromatography and mass spectrometry approaches, ArtI was demonstrated to form a heterodisulphide with StScsC, suggesting an *in vivo* interaction between the two proteins. Interestingly, ArtI is part of a family of disulphide-containing peptide/amino acid binding proteins, including HisJ, ArgT, GltI, ArtJ, and ProX, all of which were detected in significantly greater abundance in the presence of copper (Chapter 3). The role of StScsC in modulating the thiol redox state of ArtI was investigated and oxidised StScsC was found to be reduced by ArtI, supporting a role for ScsC in disulphide oxidation of ArtI in the *Salmonella* periplasm.

During infection, utilisation of amino acids is important for intracellular proliferation of *S.* Typhimurium (Popp *et al.,* 2015). The *artI* gene is encoded by the *artMQIP* operon in *E. coli* and *Salmonella* (Wissenbach *et al.,* 1995), and is regulated by the ArgR repressor in response to arginine. While *in vitro* amino acid binding experiments with purified ArtI were unsuccessful (Wissenbach *et al.,* 1995), a functional role in L-arginine sensing has been reported where ArtI is required for the L-arginine-mediated modulation of c-di-GMP levels in *S.* Typhimurium: ArtI and the periplasmic diguanylate cyclase STM1987 are required for the L-arginine-mediated elevation in c-di-GMP (Mills *et al.,* 2015). Indeed, there is a precedent for the involvement of disulphide folding machinery in the modulation of c-di-GMP levels, as deletion of *dsbA* or *dsbB* increases biofilm formation, a response that is dependent on the GGDEF-EAL domain of the guanylate cyclase/phosphodiesterase STM3615 (YhjK) (Anwar *et al.,* 2014). Furthermore, L-arginine is a well-known precursor to nitric oxide in host cells (via the action of iNOS), where NO has an established role in biofilm dispersal in other bacterial species through decreasing c-di-GMP levels. Nitric oxide has also been shown to disperse *S.* Typhimurium and *E. coli* biofilms (Marvasi *et al.,* 2014). Taken together, it is straightforward to assemble a simple signalling network involving StScsC, copper, ArtI, L-arginine, nitric oxide, and c-di-GMP (Figure 6.1). The signalling network that is influenced by c-di-GMP is complex and goes beyond biofilm formation, although it is worth noting that elevated c-di-GMP levels in *Salmonella* impact upon host: pathogen interactions and result in: i) inhibition of invasion phenotype (inhibition of secretion of the type three secretion system effector proteins) ii) diminished immunogenicity, and iii) biofilm characteristics (Ahmad *et al.,* 2011). The current model predicts that L-arginine and NO would have antagonistic effects upon the c-di-GMP pool, where the former would elevate c-di-GMP and the latter would diminish the pool of this second messenger. Indeed, it is worth noting that the L-arginine uptake protein ArgT (Wissenbach *et al.,* 1995), a predicted target for StScsC (Chapter 3), has previously been shown to deplete the L-arginine pool in macrophages to use as a carbon source. The current data directly support the role for copper and StScsC in disulphide formation for ArtI, which is likely to elicit an elevation in c-di-GMP in the presence of arginine that would elicit favourable adaptations (Ahmad *et al.,* 2011) for survival in *Salmonella* containing vacuoles (Figure 6.1), where copper accumulates (Achard *et al.,* 2012). Hence, this work provides novel insights into how copper and StScsC

impacts directly upon arginine sensing in *S.* Typhimurium, which has broader implications for survival adaptations within the macrophage. In addition, Pontes *et al.*, (2015) have shown that decreased levels of *bcsA* (encodes catalytic subunit of cellulose synthase complex) and c-di-GMP levels promote bacterial virulence by diminishing cellulose production. The Scs system of *Salmonella* can also play a role in virulence by interacting with BcsC which is another protein required during cellulose production as shown in section 3.2.5.

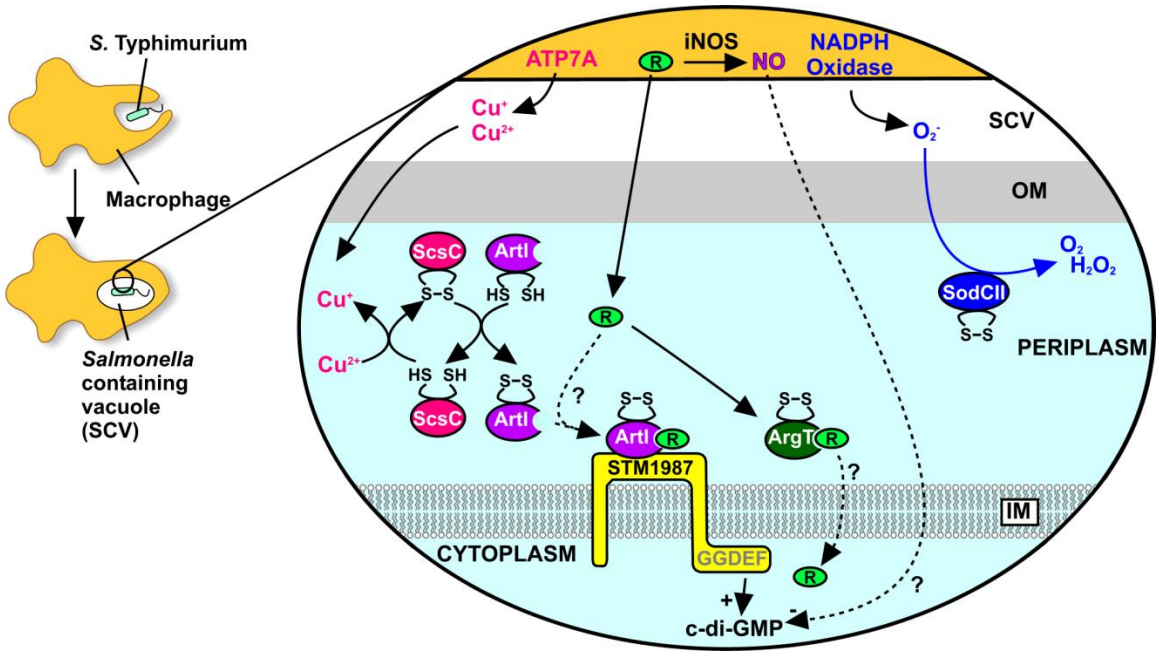


Figure 6.1- Model for copper and StScsC in arginine sensing during intramacrophage survival. During infection, *Salmonella* is engulfed by macrophages and copper ions are targetted to the *Salmonella* containing vacuoles (SCVs) (Achard *et al.*, 2012). **(1)** Copper ions present in the bacterial periplasm can be used to oxidise StScsC which in turn facilitates disulphide folding the ArtI protein (current work). **(2)** ArtI senses L-arginine (R) resulting in elevated c-di-GMP levels (Mills *et al.*, 2015), potentially via binding to the guanylate cyclase STM1987 (Mills *et al.*, 2015), which has dramatic physiological changes for the bacterium including inducing biofilm growth (Ahmad *et al.*, 2011). In addition, ArgT (where assembly is facilitated by copper and StScsC- current work) is involved in L-arginine uptake and is used as a carbon source (Das *et al.*, 2010). **(3)** Inducible Nitric Oxide Synthase (iNOS) generates nitric oxide (NO) from L-arginine, which diffuses into the bacterium and can diminish biofilm formation (Marvasi *et al.*, 2014) via an unknown mechanism (possibly via modulation of c-di-GMP levels). **(4)** The Cu/Zn superoxide dismutase enzyme SodCII (where assembly is facilitated by copper and StScsC- current work), detoxifies superoxide generated by NADPH oxidase and via Fenton chemistry catalysed by redox acive copper ions (Hebrard *et al.*, 2009). In addition, copper is required as a cofactor in SodCII.

6.3- Role of Scs proteins on production of biotherapeutics

E. coli has long been employed to produce disulphide-containing therapeutic applications, and there has is a constant desire to engineer proteins used in cellular machinery to improve protein yield and quality. However, each protein is different and responses to different disulphide folding machineries may vary. As a preliminary study, it was therefore of interest to investigate the ability of the StScsABCD system to improve the yield of some well-known protein therapeutics. In the presence of copper, the expression of the scs operon was confirmed to increase the yield of Herceptin antibody fragment, presumably due to catalysis of disulphide bond formation by StScs proteins. It was also of note that the presence of copper ions had an additive effect in terms of Herceptin yield, which might suggest that copper plays a part in redox cycling of StScs-catalysed disulphide folding. In future it will be interesting to test this system on other protein therapeutics, and also to investigate whether copper alone can impact upon periplasmic protein yield/quality.

Future work

Many potential StScsC targets were identified via mass spectrometry analyses in Chapter 3. As an alternative approach, *in vitro* binding assays with purified protein samples could confirm these as StScsC interaction partners. In addition, oxidised/ reduced peptide fragments of StScsC targets could be assessed via mass spectrometry approaches.

In Chapter 4, attempts to measure affinity of StScsC for Cu^{+} were unsuccesful. It was proposed that StScsC had multiple binding sites, or more likely that BCS bound directly to StScsC thus preventing the binding of copper to BCS and StScsC. Future binding studies could be undertaken using microscale thermophoresis approaches, fluorescence quenching titrations, or via isothermal titration calorimetry (ITC). Alternatively, the interaction and the affinity between metals and the proteins could be estimated by using an alternative metal ion-binding dye as described in Wilkinson-White and Easterbrook-Smith, (2008).

The presence of arginine leads to an increase in c-di-GMP levels (Mills *et al.,* 2015) that regulate biofilm formation and motility in *S.* Typhimurium (Ahmad *et al*., 2011). Host L-arginine has also been shown to be diverted to *S.* Typhimurium for its own metabolic use (Das *et al*., 2010). Hence, arginine sensing/ binding proteins are important for bacterial survival and virulence. It would therefore be interesting to investigate the survival of wild-type and Δ*scsC* strains in murine macrophages exposed to varying levels of copper/arginine. In addition, presence of ArgT which has been found to be a likely StScsC target, was shown to lower the amount of available host L-arginine thus decreasing the amount of toxic NO being produced (Das *et al.,* 2010). It would therefore also be of interest to investigate the impact of StScsC upon macrophage-derived NO production.

In Chapter 5, the interaction between hGH and StScsC could not be demonstrated under the current experimental conditions. In hGH, one of the cysteine residues was mutated to a serine, although hGH does contain several other cysteines involved in disulphide folding. In the future, other cysteine residues could be mutated and the same experiment could be repeated. It should also be noted that the presence of the whole *scs* operon might be required for optimum activity of StScsC.

Perhaps one of the most important issues that pervade the work on Dsb-like is the topic of redundancy. Hence, the capability of the *scs* operon to complement the oxidoreductase activity of the Dsb proteins should be investigated by expression of the *scs* operon strains containing single or multiple mutations in *dsb* genes. A wide variety of molecular tools and techniques have been developed during this PhD project that could be applied to investigate the interaction of StScs proteins with Dsb machinery and Dsb targets. This will help to further elucidate the role of the Scs system *in vivo* and assess the potential for this system for use in industrial biotechnology.

References

Achard, M. E. S., Stafford, S. L., Bokil, N. J., Chartres, J., Bernhardt, P. V., Schembri, M. A., Sweet, M. J., and McEwan, A. G. (2012). Copper redistribution in murine macrophages in response to *Salmonella* infection. *Biochem J* **444**: 51–57.

Achard, M. E. S., Tree, J. J., Holden, J. A., Simpfendorfer, K. R., Wijburg, O. L. C., Strugnell, R. A., Schembri, M. A., Sweet, M. J., Jennings, M. P., and McEwan, A. G. (2010). The multi-copper-ion oxidase CueO of *Salmonella enterica serovar typhimurium* is required for systemic virulence. *Infect Immun* **78**: 2312–2319.

Ahmad, I., Lamprokostopoulou, A., Le Guyon, S., Streck, E., Barthel, M., Peters, V., Hardt, W. D., and Römling, U. (2011). Complex c-di-GMP signaling networks mediate transition between virulence properties and biofilm formation in *Salmonella enterica serovar typhimurium*. *PLoS ONE* **6**: e28351.

Alam, M. S., Akaike, T., Okamoto, S., Kubota, T., Yoshitake, J., Sawa, T., Miyamoto, Y., Tamura, F., and Maeda, H. (2002). Role of nitric oxide in host defense in murine salmonellosis as a function of its antibacterial and antiapoptotic activities. *Infect Immun* **70**: 3130–3142.

Alanen, H. I., Walker, K. L., Lourdes Velez Suberbie, M., Matos, C. F. R. O., Bönisch, S., Freedman, R. B., Keshavarz-Moore, E., Ruddock, L. W., and Robinson, C. (2015). Efficient export of human growth hormone, interferon α2b and antibody fragments to the periplasm by the *Escherichia coli* Tat pathway in the absence of prior disulfide bond formation. *Biochim Biophys Acta* **1853**: 756–763.

Andino, A. and Hanning, I. (2015). *Salmonella enterica*: Survival, colonization, and virulence differences among serovars. *Scientific World Journal* **2015**: 520179.

Anwar, N., Sem, X. H., and Rhen, M. (2013). Oxidoreductases that Act as Conditional Virulence Suppressors in *Salmonella enterica Serovar Typhimurium*. *PLoS ONE*, **8**: e64948.

Anwar, N., Rouf, S. F., Römling, U., and Rhen, M. (2014). Modulation of biofilm-formation in *Salmonella enterica serovar typhimurium* by the periplasmic DsbA/DsbB oxidoreductase system requires the GGDEF-EAL domain protein STM3615. *PLoS ONE*, **9**: e106095.

Argüello, J. M., Raimunda, D., and Padilla-Benavides, T. (2013). Mechanisms of copper homeostasis in bacteria. *Front Cell Infect Microbiol* **3**: 1–14.

Arts, I. S., Vertommen, D., Baldin, F., Laloux, G., and Collet, J.-F. (2016). Comprehensively characterizing the thioredoxin interactome *in vivo* highlights the central role played by this ubiquitous oxidoreductase in redox control. *Mol Cell Proteomics* **15**: 2125–2140.

Bader, M., Muse, W., Ballou, D. P., Gassner, C., and Bardwell, J. C. (1999). Oxidative protein folding is driven by the electron transport system. *Cell* **98**: 217–227.

Bardwell, J. C., Lee, J. O., Jander, G., Martin, N., Belin, D., and Beckwith, J. (1993). A pathway for disulfide bond formation *in vivo*. *Proc Natl Acad Sci USA* **90**: 1038–1042.

Baselga, J., and Albanell, J. (2001). Mechanism of action of anti-HER2 monoclonal antibodies. *Ann Oncol* **12**: 35–41.

Bechtel, T. J., and Weerapana, E. (2017). From structure to redox: the diverse functional roles of disulfides and implications in disease *Proteomics* **7**: 1–34.

Berkmen, M. (2011). Production of disulfide-bonded proteins in *Escherichia coli*. *Protein Expr Purif* **82**: 240-251.

Besold, A. N., Culbertson, E. M., and Culotta, V. C. (2016). The yin and yang of copper during infection. *J Biol Inorg Chem* **21**: 137–144.

Berks, B. C., Sargent, F., and Palmer, T. (2000). The Tat protein export pathway. *Mol Microbiol* **35**: 260–274.

Bessette, P. H., Cotto, J. J., Gilbert, H. F., and Georgiou, G. (1999). *In vivo* and *in vitro* function of the *Escherichia coli* periplasmic cysteine oxidoreductase DsbG. J Biol Chem **274**:7784–7792.

Bjur, E., Eriksson-Ygberg, S., Åslund, F., and Rhen, M. (2006). Thioredoxin 1 promotes intracellular replication and virulence of *Salmonella enterica serovar typhimurium*. *Infect Immun* **74**: 5140–5151.

Bouwman, C. W., Kohli, M., Killoran, A., Touchie, G. A., Kadner, R. J., and Martin, N. L. (2003). Characterization of SrgA, a *Salmonella enterica Serovar Typhimurium* virulence plasmid-encoded paralogue of the disulfide oxidoreductase DsbA, essential for biogenesis of plasmid-encoded fimbriae. *J Bacteriol* **185**: 991–1000.

Brot, N., Weissbach, L., Werth, J., and Weissbach, H. (1981). Enzymatic reduction of protein-bound methionine sulfoxide. *Proc Natl Acad Sci USA* **78**: 2155–2158.

Brown, D. E., Nick, H. J., McCoy, M. W., Moreland, S. M., Stepanek, A. M., Benik, R., O'Connell, K. E., Pilonieta, M. C., Nagy, T. A., and Detweiler, C. S. (2015). Increased ferroportin-1 expression and rapid splenic iron loss occur with anemia caused by *Salmonella enterica serovar typhimurium* infection in mice. *Infect Immun* **83**: 2290–2299.

Broz, P., Ohlson, M. B., and Monack, D. M. (2012). Innate immune response to *Salmonella typhimurium*, a model enteric pathogen, *Gut Microbes* **3**: 62–70.

Buchner, J., and Moroder, L. (2009). *Oxidative folding of peptides and proteins*, RSC publishing, Cambridge.

CDC, (2015, September). *Salmonella* infection. Retrieved from: https://www.cdc.gov/healthypets/diseases/salmonella.html.

Chakravortty, D., Hansen-Wester, I., and Hensel, M. (2002). *Salmonella* pathogenicity island 2 mediates protection of intracellular *Salmonella* from reactive nitrogen intermediates. *J Exp Med* **195**: 1155–1166.

Chantalat, L., Jones, N.D., Korber, F., Navaza, J., and Pavlovsky, A.G. (1995). The crystal structure of wild- type growth hormone at 2.5 angstrom resolution. *Protein Pept Lett* **2**: 333-340.

Cho, S. H., Parsonage, D., Thurston, C., Dutton, R. J., Poole, L. B., Collet, J. F., and Beckwith, J. (2012). A new family of membrane electron transporters and its substrates, including a new cell envelope peroxiredoxin, reveal a broadened reductive capacity of the oxidative bacterial cell envelope. *mBio*, **3**: e00291-11.

Coburn, B., Sekirov, I., and Finlay, B. B. (2007). Type III secretion systems and disease. *Clin Microbiol Rev* **20**: 535–549.

Craig, M., and Slauch, J. M. (2009). Phagocytic superoxide specifically damages an extracytoplasmic target to inhibit or kill *Salmonella*. *PLoS ONE* **4**: 1–9.

Crow, A., Lewin, A., Hecht, O., Carlson Möller, M., Moore, G. R., Hederstedt, L., and Le Brun, N. E. (2009). Crystal structure and biophysical properties of *Bacillus subtili*s BdbD. An oxidizing thiol:disulfide oxidoreductase containing a novel metal site *J Biol Chem* **284**: 23719–23733.

Dainty, S. J., Patterson, C. J., Waldron, K. J., and Robinson, N. J. (2010). Interaction between cyanobacterial copper chaperone Atx1 and zinc homeostasis. *J Biol Inor Chem* **15**: 77–85.

Das, P., Lahiri, A., Lahiri, A., Sen, M., Iyer, N., Kapoor, N., Balaji, K. N., and Chakravortty, D. (2010). Cationic amino acid transporters and *Salmonella Typhimurium* ArgT collectively regulate arginine availability towards intracellular *Salmonella* growth. *PLoS ONE*, **5**: e15466.

Depuydt, M., Leonard, S. E., Vertommen, D., Denoncin, K., Morsomme, P., Wahni, K., Messens, J., Carroll, K. S., and Collet, J.-F. (2009). A periplasmic reducing system protects single cysteine residues from oxidation. *Science* **326**: 1109–1111.

Depuydt, M., Messens, J., and Collet, J.-F. (2011). How proteins form disulfide bonds. *Antioxid Redox Signal* **15**: 49–66.

Djoko, K. Y., Phan, M-D., Peters, K. M., Walker, M. J., Schembri, M. A. and McEwan, A. G. (2017). Interplay between tolerance mechanisms to copper and acid stress in *Escherichia coli*. *Proc Natl Acad Sci* **114**: 818-6823.

Doessing, S., Heinemeier, K. M., Holm, L., Mackey, A. L., Schjerling, P., Rennie, M., Smith, K., Reitelseder, S., Kappelgaard, A. M., Rasmussen, M. H., Flyvbjerg, A., and Kjaer, M. (2010). Growth hormone stimulates the collagen synthesis in human tendon and skeletal muscle without affecting myofibrillar protein synthesis, *J Physiol* **588**: 341–351.

Dougherty, W. G., and Parks, T. D. (1991). Post-translational processing of the tobacco etch virus 49-kDa small nuclear inclusion polyprotein: Identification of an internal cleavage site and delimitation of VPg and proteinase domains. *Virology* **183**: 449–456.

Ecker, D. M., Jones, S. D., and Levine, H. L. (2015). The therapeutic monoclonal antibody market. *mAbs*, **7**: 9–14.

Ellermeier, C. D., and Slauch, J. M. (2004). RtsA coordinately regulates DsbA and the *Salmonella* pathogenicity island 1 type III secretion system. *J Bacteriol* **186**: 68–79.

Eng, S. K., Pusparajah, P., Ab Mutalib, N. S., Ser, H. L., Chan, K. G. and Lee, L. H. (2015). *Salmonella*: A review on pathogenesis, epidemiology and antibiotic resistance, *Front Life Sci* **8**: 284–293.

Espariz, M., Checa, S. K., Audero, M. E. P., Pontel, L. B., and Soncini, F. C. (2007). Dissecting the *Salmonella* response to copper. *Microbiology* **153**: 2989–2997.

Eyer, P., Worek, F., Kiderlen, D., Sinko, G., Stuglin, A., Simeon-Rudolf, V., and Reiner, E. (2003). Molar absorption coefficients for the reduced Ellman reagent : reassessment. *Anal Biochem* **312**: 24–227.

Fàbrega, A., and Vila, J. (2013). *Salmonella enterica serovar Typhimurium* skills to succeed in the host: virulence and regulation. *Clin Microbiol Rev* **26**: 308–341.

Fang, F. C. (1997). Perspectives Series : Host / pathogen interactions. Mechanisms of nitric oxide-related antimicrobial activity. *J Clin Invest* **99**: 2818–2825.

Fang, F. C. (2004). Antimicrobial reactive oxygen and nitrogen species: Concepts and controversies. *Nat Rev Microbiol* **2**: 820–832.

Fenlon, L. A., and Slauch, J. M. (2017). Cytoplasmic copper detoxification in *Salmonella* can contribute to SodC metalation but is dispensable during systemic infection. *J Bacteriol* **199**: e00437-17.

Festa, R. A., and Thiele, D. J. (2012). Copper at the front line of the host-pathogen battle. *PLoS Pathog* **8**: e1002887.

Flannagan, R. S., Cosío, G., and Grinstein, S. (2009). Antimicrobial mechanisms of phagocytes and bacterial evasion strategies. *Nat Rev Microbiol* **7:** 355–366.

Fong, S. T., Camakaris, J., and Lee, B. T. (1995). Molecular genetics of a chromosomal locus involved in copper tolerance in *Escherichia coli* K-12. *Mol Microbiol* **15**: 1127–1137.

Foster, A. W., Pernil, R., Patterson, C. J., and Robinson, N. J. (2014). Metal specificity of cyanobacterial nickel-responsive repressor InrS: Cells maintain zinc and copper below the detection threshold for InrS. *Mol Microbiol* **92**: 797–812.

Foster, N., Hulme, S. D., and Barrow, P. A. (2003). Induction of antimicrobial pathways during early-phase immune response to *Salmonella* spp. in murine macrophages: Gamma interferon (IFN-γ) and upregulation of IFN-γ receptor alpha expression are required for NADPH phagocytic oxidase gp91-stimulated oxidative burst and control of virulent *Salmonella* spp. *Infect Immun* **71**: 4733–4741.

Fu, Y., Chang, F-M, J., and Giedroc, D. P. (2014). Copper transport and trafficking at the host−bacterial pathogen interface. *Acc Chem Res* **47**: 3605−3613.

Furlong, E. J., Choudhury, H. G., Kurth, F., Duff, A. P., Whitten, A. E. and Martin, J. L. (2018). Disulfide isomerase activity of the dynamic, trimeric Proteus mirabilis ScsC protein is primed by the tandem immunoglobulin-fold domain of ScsB. *J Biol*

Chem **293**: 5793–5805.

Furlong, E. J., Lo, A. W., Kurth, F., Premkumar, L., Totsika, M., Achard, M. E. S., Halili, M. A., Heras, B., Whitten, A. E., Choudhury, H. G., Schembri, M. A., and Martin, J. L. (2017). A shape-shifting redox foldase contributes to *Proteus mirabilis* copper resistance. *Nat Commun* **8**: 16065.

Gaciarz, A., Veijola, J., Uchida, Y., Saaranen, M. J., Wang, C., Hörkkö, S., and Ruddock, L. W. (2016). Systematic screening of soluble expression of antibody fragments in the cytoplasm of *E. coli*. *Microb Cell Fact* **15**: 22.

Gajria, D., and Chandarlapaty, S. (2011). HER2-amplified breast cancer: mechanisms of trastuzumab resistance and novel targeted therapies. *Expert Rev Anticancer Ther* **11**: 263–275.

Garai, P., Gnanadhas, D. P., and Chakravortty, D. (2012). *Salmonella enterica serovars Typhimurium* and *Typhi* as model organisms: revealing paradigm of host-pathogen interaction. *Virulence* **3**: 377–388.

Gasteiger, E., Gattiker, A., Hoogland, C., Ivanyi, I., Appel, R. D., Bairoch, A., and Servet, R. M. (2003). ExPASy : the proteomics server for in-depth protein knowledge and analysis. *Nucleic Acids Res* **31**: 3784–3788.

Georgiou, G., and Segatori, L. (2005). Preparative expression of secreted proteins in bacteria: status report and future prospects. *Curr Opin Biotechnol* **16**: 538–545.

Gogoi, M., Shreenivas, M. M., and Chakravortty, D. (2018). Hoodwinking the big-eater to prosper: the *Salmonella*-macrophage paradigm. *J Innate Immun* **11**: 289-299.

Gordon, E. H. J., Page, M. D., Willis, A. C., and Ferguson, S. J. (2000). *Escherichia coli* DipZ: Anatomy of a transmembrane protein disulphide reductase in which three pairs of cysteine residues, one in each of three domains, contribute differentially to function. *Mol Microbiol* **35**: 1360–1374.

Green, E. R. and Mecsas, J. (2016). Bacterial secretion systems: An overview. *Microbiol Spectr* **4**: 1–32.

Grimshaw, J. P. A., Stirnimann, C. U., Brozzo, M. S., Malojcic, G., Grütter, M. G., Capitani, G., and Glockshuber, R. (2008). DsbL and DsbI form a specific dithiol oxidase system for periplasmic arylsulfate sulfotransferase in uropathogenic *Escherichia coli*. *J Mol Biol* **380**: 667–680.

Groisman , E. A., and Ochman, H. (1997). How *Salmonella* became a pathogen. *Trends Microbiol* **5**: 343-349.

Guglielmi, L., and Martineau, P. (2009). Expression of single-chain Fv fragments in *E. coli* cytoplasm. *Methods Mol Biol* **562**: 215–224.

Gupta, S. D., Wu, H. C., and Rick, P. D. (1997). A *Salmonella typhimurium* genetic locus which confers copper tolerance on copper-sensitive mutants of *Escherichia coli*, *J Bacteriol* **179**: 4977–4984.

Hacker, J., and Carniel, E. (2001). Ecological fitness, genomic islands and bacterial pathogenicity: A Darwinian view of the evolution of microbes, *EMBO Rep* **2**: 376–

381.

Hall, T. (1999) BioEdit: a user-friendly biological sequence alignment editor and analysis program for Windows 95/98/NT. *Nucleic Acids Symp Ser* **41**: 95–98.

Hart, T.W. (1985). Some observations concerning the S-nitroso and S-phenylsulphonyl derivatives of L-cysteine and glutathione. *Tetrahedron Lett* **26**: 2013–2016.

Hatahet, F., Boyd, D., and Beckwith, J. (2014). Disulfide bond formation in prokaryotes: History, diversity and design. *Biochim Biophys Acta* **1844**: 1402–1414.

Hebrard, M., Viala, J. P. M., Méresse, S., Barras, F., and Aussel, L. (2009). Redundant hydrogen peroxide scavengers contribute to *Salmonella* virulence and oxidative stress resistance. *J Bacteriol* **191**: 4605–4614.

Henard, C. A., Bourret, T. J., Song, M., and Vázquez-Torres, A. (2010). Control of redox balance by the stringent response regulatory protein promotes antioxidant defenses of *Salmonella*. *J Biol Chem* **285**: 36785–36793.

Henard, C. A., and Vázquez-Torres, A. (2011). Nitric oxide and *Salmonella* pathogenesis. *Front Microbiol* **2**: 1–11.

Heras, B., Shouldice, S. R., Totsika, M., Scanlon, M. J., Schembri, M. A., and Martin, J. L. (2009). DSB proteins and bacterial pathogenicity. *Nat Rev Microbiol* **7**: 215–225.

Heras, B., Totsika, M., Jarrott, R., Shouldice, S. R., Guncar, G., Achard, M. E. S., Wells, T. J., Argente, M. P., McEwan, A. G., and Schembri, M. A. (2010). Structural and functional characterization of three DsbA paralogues from *Salmonella enterica* serovar Typhimurium. *J Biol Chem* **285**:18423–18432.

Hiniker, A., Collet, J. F., and Bardwell, J. C. A. (2005). Copper stress causes an *in vivo* requirement for the *Escherichia coli* disulfide isomerase DsbC. *J Biol Chem* **280**: 33785–33791.

Hirayama, D., Iida, T., and Nakase, H. (2018). The phagocytic function of macrophage-enforcing innate immunity and tissue homeostasis. *Int J Mol Sci* **19**: 1-14.

Hodgkinson, V., and Petris, M. J. (2012). Copper homeostasis at the host-pathogen interface. *J BiolChem* **287**: 13549–13555.

Holmgren, A. (1989). Electron transport to reductive enzymes. *J Biol Chem* **264**: 13963–13966.

Holmgren, A. (1995). Thioredoxin structure and mechanism: conformational changes on oxidation of the active-site sulfhydryls to a disulfide. *Structure* **3**: 239–243.

Humphreys, D. P., Sehdev, M., Chapman, A. P., Ganesh, R., Smith, B. J., King, L. M., Glover, D. J., Reeks, D. G., and Stephens, P. E. (2000). High-level periplasmic expression in Escherichia coli using a eukaryotic signal peptide: importance of codon usage at the 5' end of the coding sequence. *Protein Expr Purif* **20**: 252-64.

Hurley, D., McCusker, M. P., Fanning, S., and Martins, M. (2014). *Salmonella*-host interactions-modulation of the host innate immune system. *Front Immunol* **5**: 1–11.

Ibarra, J. A., and Steele-Mortimer, O. (2009). *Salmonella*- the ultimate insider. *Salmonella* virulence factors that modulate intracellular survival. *Cell Microbiol* **11**: 1579–1586.

Inaba, K., and Ito, K. (2002). Paradoxical redox properties of DsbB and DsbA in the protein disulfide-introducing reaction cascade. *EMBO J* **21**: 2646–2654.

Inesi, G. (2017). Molecular features of copper binding proteins involved in copper homeostasis. *IUBMB Life* **69**: 211–217.

Jeong, K. J., and Lee, S. Y. (2000). Secretory production of human leptin in *Escherichia coli*. *Biotechnol Bioeng* **67**: 398-407.

Junnila, R. K., and Kopchick, J. J. (2013). Significance of the disulphide bonds of human growth hormone. *Endokrynol Pol* **64**: 300-305.

Kadokura, H., Katzen, F., and Beckwith, J. (2003). Protein disulfide bond formation in prokaryotes. *Annu Rev Biochem* **72**: 111–135.

Källberg, M., Wang, H., Wang, S., Peng, J., Wang, Z., Lu, H., and Xu, J. (2012). Template-based protein structure modeling using the RaptorX web server. *Nat Protoc* **7**: 1511-1522.

Kamionka, M. (2011). Engineering of therapeutic proteins production in *Escherichia coli*. *Curr Pharm Biotechnol* **12**: 268–274.

Kapust, R. B., Tozser, J., Fox, J. D., Anderson, D. E., Cherry, S., Copeland, T. D., and Waugh, D. S. (2001). Tobacco etch virus protease : mechanism of autolysis and rational design of stable mutants with wild-type catalytic proficiency. *Protein Eng* **14**: 993–1000.

Kawasaki, T., and Kawai, T. (2014). Toll-like receptor signaling pathways. *Front Immunol* **5**: 1-8.

Kelley, B. (2009). Industrialization of mAb production technology: the bioprocessing industry at a crossroads. *mAbs* **1**: 443-452.

Kim, D-H., Yoon, H-K., Koizumi, M., and Kobashi, K. (1992). Sulfation of phenolic antibiotics by sulfotransferase obtained from a human intestinal bacterium. *Chem Pharm Bull* **40**: 1056-1057.

Kim, B., Richards, S. M., Gunn, J. S., and Slauch, J. M. (2010). Protecting against antimicrobial effectors in the phagosome allows SodCII to contribute to virulence in *Salmonella enterica serovar Typhimurium*. *J Bacteriol* **192**: 2140–2149.

Knodler, L. A., and Steele-Mortimer, O. (2003). Taking possession: Biogenesis of the *Salmonella*-containing vacuole. *Traffic* **4**: 587–599.

Koch, K. A., Marjorette, M., and Thiele, D. J. (1997). Copper-binding and signaling motifs in catalysis , transport , detoxification and signalling. *Chem Biol* **4**: 549–560.

Kozakov, D., Hall, D. R., Xia, B., Porter, K. A., Padhorny, D., Yueh, C., Beglov, D.,

and Vajda, S. (2017). The ClusPro web server for protein-protein docking. *Nat Protoc* **12**: 255-278.

Kröncke, K-D., Fehsel, K., and Kolb-Bachofen, V. (1997). Nitric Oxide : cytotoxicity versus cytoprotection- how , why , when , and where ? *Nitric Oxide* **1**: 107–120.

Kudva, R., Denks, K., Kuhn, P., Vogt, A., Müller, M., and Koch, H-G. (2013). Protein translocation across the inner membrane of Gram-negative bacteria : the Sec and Tat dependent protein transport pathways. *Res Microbiol* **164**: 505-534.

Ladomersky, E., and Petris, M. J. (2016). Copper tolerance and virulence in bacteria. *Metallomics* **7**: 957–964.

Lan, R., Reeves, P. R., and Octavia, S. (2009). Population structure, origins and evolution of major *Salmonella enterica* clones. *Infect Genetand Evol* **9**: 996–1005.

Lasica, A. M., and Jagusztyn-Krynicka, E. K. (2007). The role of Dsb proteins of Gram-negative bacteria in the process of pathogenesis. *FEMS Microbiol Rev* **31**: 626–636.

Li, C., Li, Y., and Ding, C. (2019). The role of copper homeostasis at the host-pathogen axis: from bacteria to fungi. *Int J MolSci* **20**: 1-15.

Lin, D., Kim, B., and Slauch, J. M. (2009). DsbL and DsbI contribute to periplasmic disulfide bond formation in *Salmonella enterica serovar Typhimurium*. *Microbiology* 155: 4014–4024.

Linehan, S. A., and Holden, D. W. (2003). The interplay between *Salmonella typhimurium* and its macrophage host- What can it teach us about innate immunity? *Immunol Lett* **85**: 183–192.

Liochev, S. I., and Fridovich, I. (1999) Superoxide and iron: Partners in crime. *IUBMB Life* **48**: 157–161.

Liu, H., Chumsae, C., Gaza-Bulseco, G., Hurkmans, K., and Radziejewski, C. H. (2010). Ranking the susceptibility of disulfide bonds in human IgG1 antibodies by reduction, differential alkylation, and LC-MS analysis. *Anal Chem* **82**: 5219–5226.

Liu, H., and May, K. (2012). Disulfide bond structures of IgG molecules structural variations, chemical modifications and possible impacts to stability and biological function. *mAbs,* **4**: 17-23.

Lo Conte, M., and Carroll, K. S. (2013). The redox biochemistry of protein sulfenylation and sulfinylation. *J Biol Chem* **288**: 26480–26488.

Lobstein, J., Emrich, C. A., Jeans, C., Faulkner, M., Riggs, P., and Berkmen, M. (2012). SHuffle, a novel *Escherichia coli* protein expression strain capable of correctly folding disulfide bonded proteins in its cytoplasm. *Microb Cell Fact* **11**: 1-16.

López, C., Checa, S. K., and Soncini, F. C. (2018). CpxR/CpxA controls *scsABCD* transcription to counteract copper and oxidative stress in *Salmonella enterica serovar Typhimurium*. *J Bacteriol* **200**: e00126-18.

Ma, Z., Cowart, D. M., Scott, R. A., and Giedroc, D. P. (2009). Molecular insights into the metal selectivity of the Copper(I)-sensing repressor CsoR from *Bacillus subtilis*. *Biochemistry* **48**: 3325–3334.

Macomber, L., and Imlay, J. A. (2009). The iron-sulfur clusters of dehydratases are primary intracellular targets of copper toxicity. *Proc Natl Acad Sci* **106**: 8344–8349.

Markwell, M. A., Haas, S. M., Bieber, L. L., and Tolbert, N. E. (1978). A modification of the Lowry procedure to simplify protein determination in membrane and lipoprotein samples. *Anal Biochem* **87**: 206-210.

Marvasi, M., Chen, C., Carrazana, M., Durie, I. A., and Teplitski, M. (2014). Systematic analysis of the ability of Nitric Oxide donors to dislodge biofilms formed by S*almonella enterica* and *Escherichia coli* O157:H7. *AMB Express*, **4**.

Matos, C. F. R. O., Robinson, C., Alanen, H. I., Prus, P., Uchida, Y., Ruddock, L. W., Freedman, R. B. and Keshavarz-Moore, E. (2014). Efficient export of prefolded, disulfide-bonded recombinant proteins to the periplasm by the Tat pathway in Escherichia coli CyDisCo strains. *Biotechnol Prog* **30**: 281–290.

McCollister, B. D., Bourret, T. J., Gill, R., Jones-Carson, J., and Vázquez-Torres, A. (2005). Repression of SPI2 transcription by nitric oxide-producing, IFNγ-activated macrophages promotes maturation of *Salmonella* phagosomes. *J ExpMed* **202**: 625–635.

McDonagh, B., Sakellariou, G. K., Smith, N. T., Brownridge, P., and Jackson, M. J. (2014). Differential cysteine labeling and global label-free proteomics reveals an altered metabolic state in skeletal muscle aging. *J Proteome Res* **13**: 5008−5021.

McNicholas, S., Potterton, E., Wilson, K. S., and Noble, M. E. M. (2011). Presenting your structures: the CCP4mg molecular-graphics software. *Acta Crystallogr D Biol Crystallogr* **67**: 386–394.

Messner, K. R., and Imlay, J. A. (1999). The identification of primary sites of superoxide and hydrogen peroxide formation in the aerobic respiratory chain. *J Biol Chem* **274**: 10119–28.

Miki, T., Okada, N., and Danbara, H. (2004). Two periplasmic disulfide oxidoreductases, DsbA and SrgA, target outer membrane protein SpiA, a component of the of the *Salmonella* pathogenicity island 2 type III secretion system. *J Biol Chem* **279**: 34631–34642.

Mills, E., Petersen, E., Kulasekara, B. R., and Miller, S. I. (2015). A direct screen for c-di-GMP modulators reveals a *Salmonella Typhimurium* periplasmic L-arginine–sensing pathway. *Sci Signal* **8**: ra57.

Miot, M., and Betton, J-M. (2004). Protein quality control in the bacterial periplasm. *Microb Cell Fact* **3**.

Mohorko, E., Abicht, H. K., Bühler, D., Glockshuber, R., Hennecke, H., and Fischer, H. M. (2012). Thioredoxin-like protein TlpA from *Bradyrhizobium japonicum* is a reductant for the copper metallochaperone ScoI. *FEBS Lett* **586**: 4094–4099.

Mori, M., Jimenez, B., Piccioli, M., Battistoni, A., and Sette, M. (2008). The solution

structure of the monomeric copper, zinc superoxide dismutase from *Salmonella enterica*: Structural insights to understand the evolution toward the dimeric structure. *Biochemistry* **47**: 12954–12963.

Mössner, E., Huber-Wunderlich, M., Rietsch, A., Beckwith, J., Glockshuber, R., and Aslund, F. (1999). Importance of redox potential for the *in vivo* function of the cytoplasmic disulfide reductant thioredoxin from *Escherichia coli*. *J Biol Chem* **274**: 25254–25259.

Movva, N. R., Nakamura, K., and Inouye, M. (1980). Amino acid sequence of the signal peptide of OmpA protein, a major outer membrane protein of *Eschericia coli*. *J Biol Chem* **255**: 27-29.

Osman, D., Patterson, C. J., Bailey, K., Fisher, K., Robinson, N. J., Rigby, S. E. J., and Cavet, J. S. (2013). The copper supply pathway to a *Salmonella* Cu,Zn-superoxide dismutase (SodCII) involves P1B-type ATPase copper efflux and periplasmic CueP. *Mol Microbiol* **87**: 466–477.

Osman, D., Waldron, K. J., Denton, H., Taylor, C. M., Grant, A. J., Mastroeni, P., Robinson, N. J., and Cavet, J. S. (2010). Copper homeostasis in *Salmonella* is atypical and copper-CueP is a major periplasmic metal complex. *J Biol Chem* **285**: 25259–25268.

Patil, N. A., Tailhades, J., Hughes, R. A., Separovic, F., Wade, J. D., and Hossain, M. A. (2015). Cellular disulfide bond formation in bioactive peptides and proteins. *Int J Mol Sci* **16**: 1791–1805.

Perkins, D. N., Pappin, D. J., Creasy, D. M., and Cottrell, J. S.(1999). Probability-based protein identification by searching sequence databases using mass spectrometry data. *Electrophoresis* **20**: 3551-3567.

Phaniendra, A., Jestadi, D. B., and Periyasamy, L. (2015). Free radicals: Properties, sources, targets, and their implication in various diseases. *Indian J Clin Biochem* **30**: 11–26.

PHE, (2018, May). *Salmonella* data 2007 to 2016. Retrieved from: https://assets.publishing.service.gov.uk/government/uploads/system/uploads/attachment_data/file/711972/salmonella_data_2007_to_2016_may_2018.pdf.

Pogliano, J., Lynch, A. S., Belin, D., Lin, E. C. C., and Beckwith, J. (1997). Regulation of *Escherichia coli* cell envelope proteins involved in protein folding and degradation by the Cpx two-component system. *Genes Dev* **11**: 1169-1182.

Pontes, M. H., Lee, E-J., Choi, J., and Groisman, E. A. (2015). *Salmonella* promotes virulence by repressing cellulose production. *Proc Natl Acad Sci* **112**: 5183–5188.

Poole, L. B. (2015). The basics of thiols and cysteines in redox biology and chemistry. *Free Radic Biol Med* **80**: 148-157.

Popp, J., Noster, J., Busch, K., Kehl, A., Hellen, G. Zur, and Hensel, M. (2015). Role of host cell-derived amino acids in nutrition of intracellular *Salmonella enterica*. *Infect Immun* **83**: 4466–4475.

Porcheron, G., Garénaux, A., Proulx, J., Sabri, M., and Dozois, C. M. (2013). Iron,

copper, zinc, and manganese transport and regulation in pathogenic Enterobacteria: correlations between strains, site of infection and the relative importance of the different metal transport systems for virulence. *Front Cell Infect Microbiol* **3**: 90.

Prinz, W. A., Åslund, F., Holmgren, A., and Beckwith, J. (1997). The role of the thioredoxin and glutaredoxin pathways in reducing protein disulfide bonds in the *Escherichia coli* cytoplasm. *J Biol Chem* **272**: 5661–15667.

Remington, S. J. (2011). Green fluorescent protein: A perspective. *Protein Sci* **20**: 1509–1519.

Ren, G., Stephan, D., Xu, Z., Zheng, Y., Tang, D., Harrison, R. S., Kurz, M., Jarrott, R., Shouldice, S. R., Hiniker, A., Martin, J. L., Heras, B., and Bardwell, J. C. A. (2009). Properties of the thioredoxin fold superfamily are modulated by a single amino acid residue. *J Biol Chem* **284**:10150–10159.

Rezaei, M., and Zarkesh-Esfahani, S. H. (2012). Optimization of production of recombinant human growth hormone in *Escherichia coli*. *J Res Med Sci* **17**: 681-685.

Rietsch, A., Bessette, P., Georgiou, G., and Beckwith, J. (1997). Reduction of the periplasmic disulfide bond isomerase, DsbC, occurs by passage of electrons from cytoplasmic thioredoxin. *J Bacteriol* **179**: 6602–6608.

Ritz, D., and Beckwith, J. (2001). Roles of thiol-redox pathways in bacteria. *Ann Rev Microbiol* **55**: 21–48.

Ross, J. S., Slodkowska, E. A., Symmans, W. F., Pusztai, L., Ravdin, P. M., and Hortobagyi, G. N., (2009). The HER-2 receptor and breast cancer: Ten years of targeted Anti-HER-2 therapy and personalized medicine. *Oncologist* **14**: 320–368.

Rudyk, O., and Eaton, P. (2014). Biochemical methods for monitoring protein thiol redox states in biological systems. *Redox Biol* **2**: 803–813.

Ryan, M. P., O'Dwyer, J., and Adley, C. C. (2017). Evaluation of the complex nomenclature of the clinically and veterinary significant pathogen *Salmonella*. *Bio Med Res Int* **2017**: 3782182.

Sakurai, Y., Anzai, I., and Furukawa, Y. (2014). A primary role for disulfide formation in the productive folding of prokaryotic Cu,,Zn-superoxide dismutase. *J Biol Chem* **289**: 20139–20149.

Schneider, C. A., Rasband, W. S., and Eliceiri, K. W. (2012). NIH Image to ImageJ: 25 years of image analysis. *Nat Methods* **9**: 671-675.

Shepherd, M., Heras, B., Achard, M. E. S., King, G. J., Argente, M. P., Kurth, F., Taylor, S. L., Howard, M. J., King, N. P., Schembri, M. A., and McEwan, A. G. (2013). Structural and functional characterization of ScsC, a periplasmic thioredoxin-like protein from *Salmonella enterica* serovar *Typhimurium*. *Antioxid Redox Signal* **19**: 1494–1506.

Shevchenko, A., Wilm, M., Vorm, O., and Mann, M. (1996). Mass spectrometric sequencing of proteins from silver-stained polyacrylamide gels. *Anal Chem* **68**: 850–858.

Singh, R. J., Hogg, N., Joseph, J., and Kalyanaraman, B. (1996). Mechanism of nitric oxide release from S -Nitrosothiols. *J Biol Chem* **271**: 18596–18603.

Slauch, J. M. (2011). How does the oxidative burst of macrophages kill bacteria? Still an open question. *Mol Microbiol* **80**: 580–583.

Smirnova, G., Muzyka, N., and Oktyabrsky, O. (2012). Transmembrane glutathione cycling in growing *Escherichia coli* cells. *Microbiol Res* **167**: 166–172.

Solano, C., García, B., Valle, J., Berasain, C., Ghigo, J-M., Gamazo, C., and Lasa, I. (2002). Genetic analysis of *Salmonella enteritidis* biofilm formation: Critical role of cellulose. *Mol Microbiol* **43**: 793–808.

Spadiut, O., Capone, S., Krainer, F., Glieder, A., and Herwig, C. (2014). Microbials for the production of monoclonal antibodies and antibody fragments. *Trends Biotechnol* **32**: 54–60.

Spiliotis, B. E. (2008). Recombinant human growth hormone in the treatment of Turner syndrome. *Ther Clin Risk Manag* **4**: 1177–1183.

Srikanth, C. V., Mercado-Lubo, R., Hallstrom, K., and McCormick, B. A. (2011). *Salmonella* effector proteins and host-cell responses, *Cell Mol Life Sci* **68**: 3687–3697.

Stafford, S. L., Bokil, N. J., Achard, M. E. S., Kapetanovic, R., Schembri, M. A., McEwan, A. G., and Sweet, M. J. (2013). Metal ions in macrophage antimicrobial pathways: emerging roles for zinc and copper. *Biosci Rep* **33**: 541–554.

Totsika, M., Heras, B., Wurpel, D. J., and Schembri, M. A. (2009). Characterization of two homologous disulfide bond systems involved in virulence factor biogenesis in uropathogenic *Escherichia coli* CFT073. *J Bacteriol* **191**: 3901–3908.

Tsirigotaki, A., De Geyter, J., Šoštarić, N., Economou, A., and Karamanou, S. (2017). Protein export through the bacterial Sec pathway. *Nat Rev Microbiol* **15**: 21–36.

Vatansever, F., de Melo, W. C. M. A., Avci, P., Vecchio, D., Sadasivam, M., Gupta, A., Chandran, R., Karimi, M., Parizotto, N. A., Yin, R., Tegos, G. P., and Hamblin, M. R. (2013). Antimicrobial strategies centered around reactive oxygen species-bactericidal antibiotics, photodynamic therapy, and beyond. *FEMS Microbiol Rev* **37**: 955–989.

Vázquez-Torres, A., Jones-Carson, J., Mastroeni, P., Ischiropoulos, H., and Fang, F. C. (2000). Antimicrobial actions of the NADPH phagocyte oxidase and inducible nitric oxide synthase in experimental salmonellosis. I. effects on microbial killing by activated peritoneal macrophages *in vitro*. *J Exp Med* **192**: 237–248.

Vázquez-Torres, A. (2012). Redox active thiol sensors of oxidative and nitrosative stress. *Antioxid Redox Signal* **17**: 1201–1214.

Verbrugghe, E., Dhaenens, M., Leyman, B., Boyen, F., Shearer, N., Van Parys, A., Haesendonck, R., Bert, W., Favoreel, H., Deforce, D., Thompson, A., Haesebrouck, F., and Pasmans, F. (2016). Host stress drives *Salmonella* recrudescence. *Sci Rep* **6**: 20849.

Wang, Y., Branicky, R., Noë, A. and Hekimi, S. (2018). Superoxide dismutases: Dual roles in controlling ROS damage and regulating ROS signaling. *J Cell Biol* **217**: 1915–1928.

Wang, Yi., Lu, Q., Wu, S-L., Karger, B. L., and Hancock, W. S. (2011). Characterization and comparison of disulfide linkages and scrambling patterns in therapeutic monoclonal antibodies - Using LC-MS with electron transfer dissociation. *Anal Chem* **83**: 3133-3140.

Waterman, S. R., and Holden, D. W. (2003). Functions and effectors of the *Salmonella* pathogenicity island 2 type III secretion system. *Cell Microbiol* **5**: 501–511.

Weiss, G., and Schaible, U. E. (2015). Macrophage defense mechanisms against intracellular bacteria. *Immunol Rev* **264**: 182–203.

Wissenbach, U., Six, S., Bongaerts, J., Ternes, D., Steinwachs, S., and Unden, G. (1995). A third periplasmic transport system for l-arginine in *Escherichia coli*: molecular characterization of the artPIQMJ genes, arginine binding and transport. *Mol Microbiol* **17**: 675–686.

White, C., Lee, J., Kambe, T., Fritsche, K., and Petris, M. J. (2009). A role for the ATP7A copper-transporting ATPase in macrophage bactericidal activity. *J Biol Chem* **284**: 33949–33956.

Wilkinson-White, L. E., and Easterbrook-Smith, S. B. (2008). A dye-binding assay for measurement of the binding of Cu (II) to proteins. *J Inorg Biochem* **102**: 1831–1838.

Wilson, F. R., Coombes, M. E., Wylie, Q., Yurchenko, M., Brezden-Masley, C., Hutton, B., Skidmore, B., and Cameron, C. (2017). Herceptin (trastuzumab) in HER2-positive early breast cancer: protocol for a systematic review and cumulative network meta-analysis. *Syst Rev* **6**: 196.

Winter, J., Neubauer, P., Glockshuber, R., and Rudolph, R. (2000). Increased production of human proinsulin in the periplasmic space of *Escherichia coli* by fusion to DsbA. *J Biotechnol* **84**: 175–185.

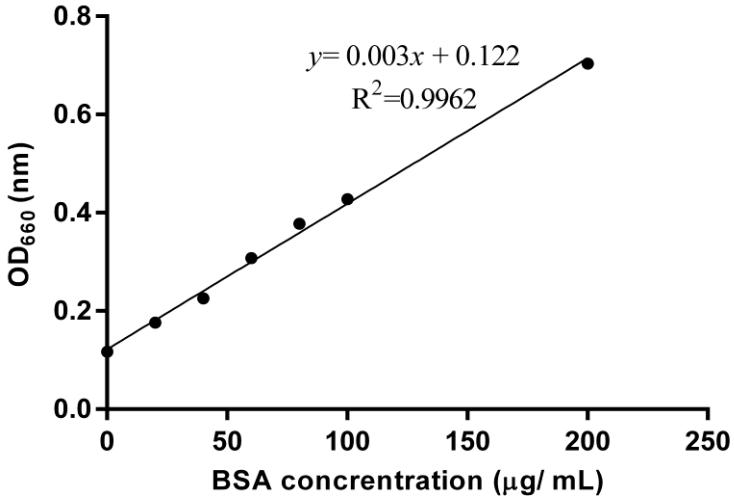
Xiao, Z., Brose, J., Schimo, S., Ackland, S. M., La Fontaine, S., and Wedd, A. G. (2011). Unification of the Copper (I) binding affinities of the metallo-chaperones Atx1 , Atox1 , and related proteins. *J Biol Chem* **286**: 11047–11055.

Yamamoto, K., and Ishihama, A. (2005). Transcriptional response of *Escherichia coli* to external copper. *Mol Microbiol* **56**: 215–227.

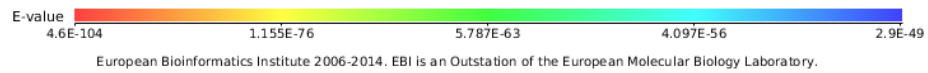
Youngman, K. M., Spencer, D. B., Brems, D. N., and DeFelippis, M. R. (1995). Kinetic analysis of the folding of Human Growth Hormone. *J Biol Chem* **270**: 19816-19822.

Appendix

Appendix 1- BSA standard curve. The absorance (at 660 nm) of known concentrations of BSA standards were measured. The protein concentrations of unknown samples were calculated by using the equation of the line and the R^2 value which is shown on the graph. (Section 2.5.3.1).

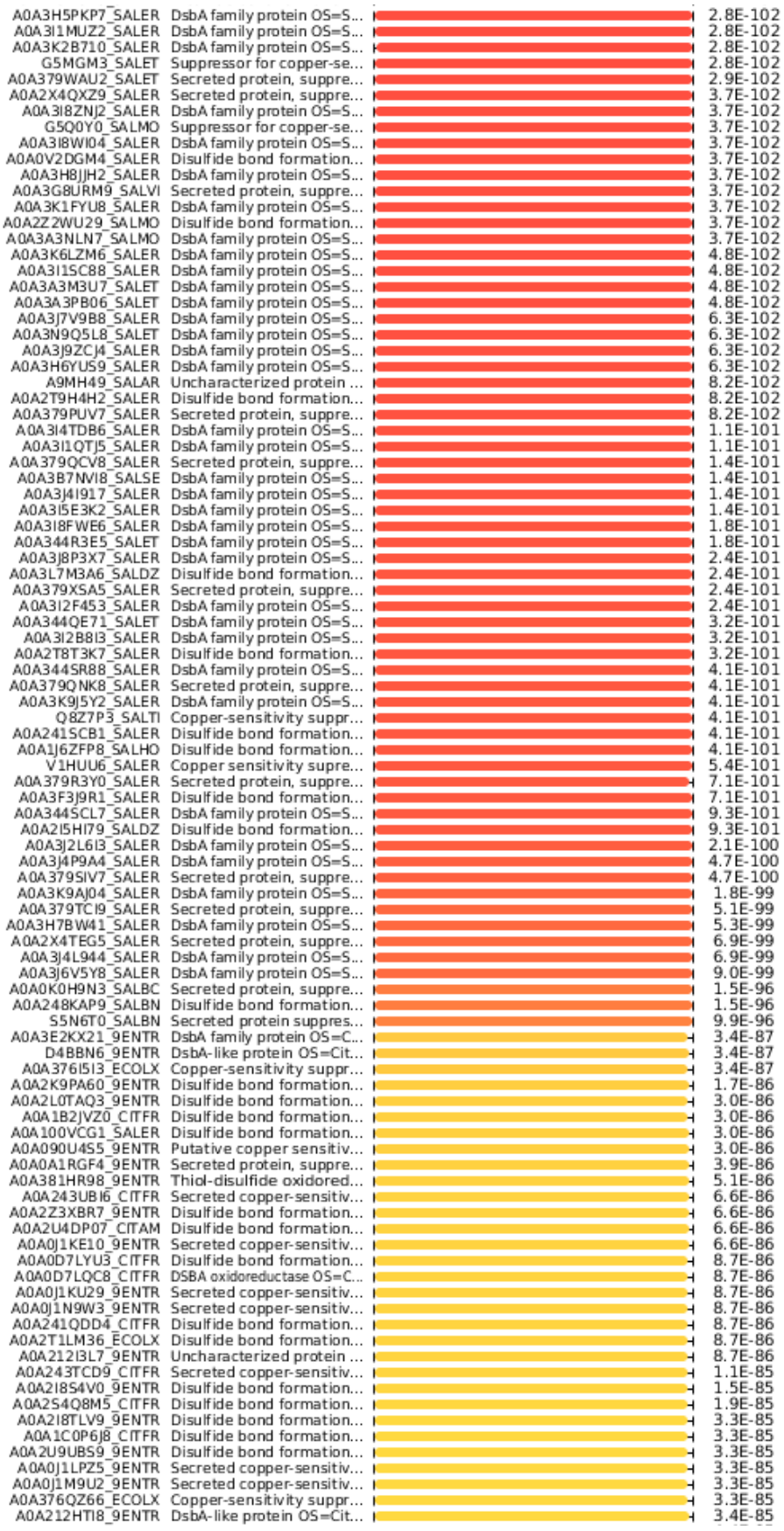


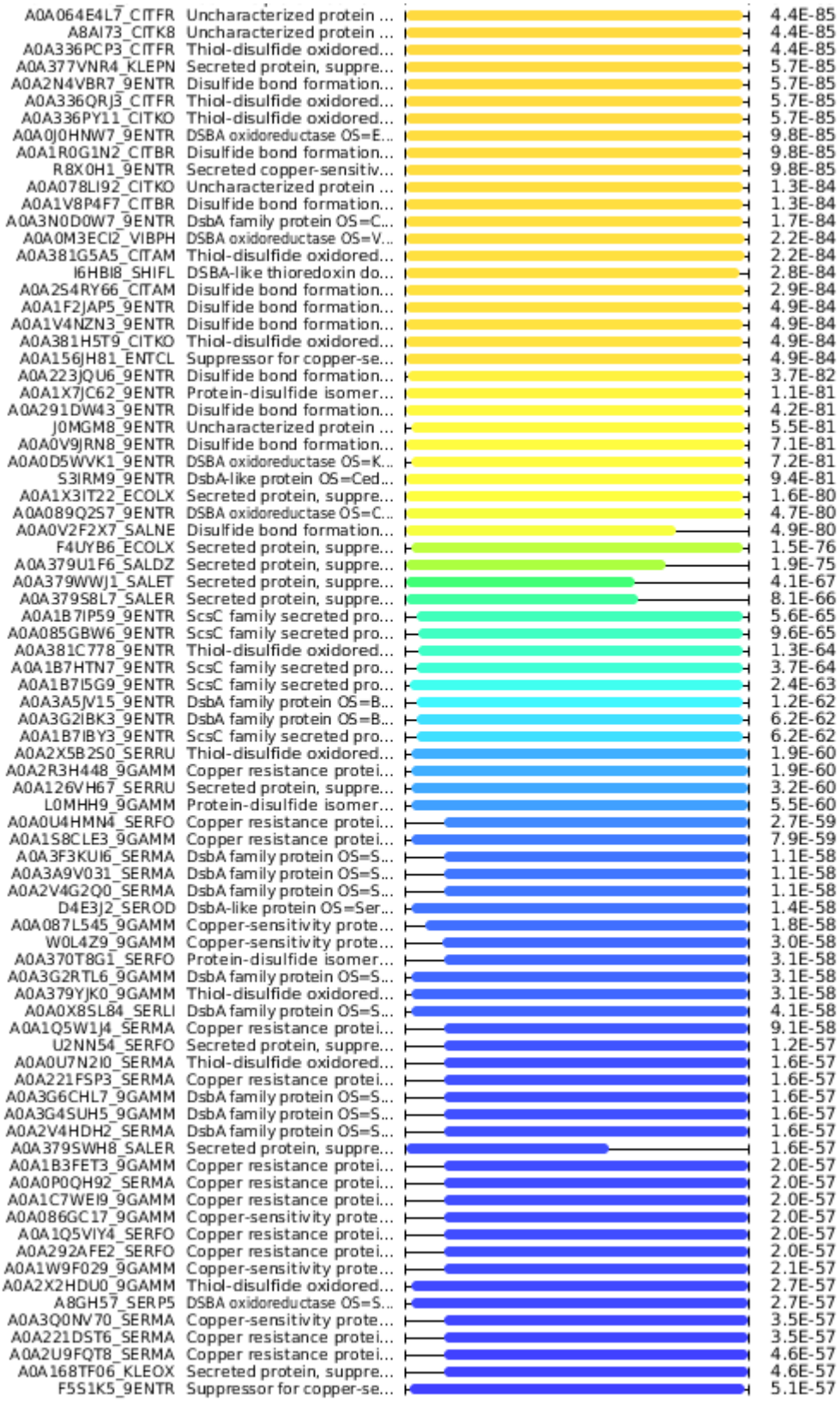
Appendix 2- E-values of orthologues protein sequences from StScsC. During the search for the orthologous ScsC proteins in different species, PSI-Search tool from EMBL-EBI was used where 250 matched sequences were selected and the E-values are shown below. (Section 3.2.1).



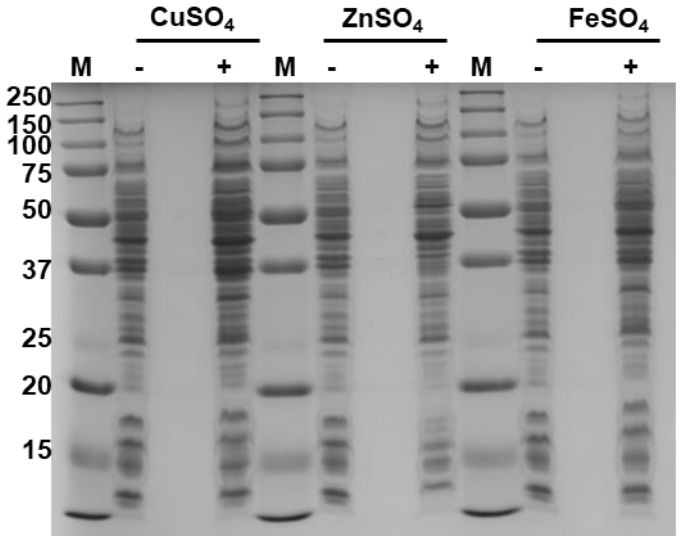
European Bioinformatics Institute 2006-2014. EBI is an Outstation of the European Molecular Biology Laboratory.

		Sequence Match (1 – 189)	E-value
A0A0U1FQS6_SALTM	Copper-sensitivity secre...		4.9E-104
E8XE72_SALT4	Suppression of copper se...		4.9E-104
A0A0F6AZT6_SALT1	Suppression of copper se...		4.9E-104
A0A0W4XST4_SALER	Disulfide bond formation...		4.9E-104
H9L4C1_SALTY	Suppression of copper se...		4.9E-104
O33919_SALTM	DsbA family protein OS=S...		4.9E-104
A0A0H3NBX5_SALTS	Secreted protein, suppre...		4.9E-104
A0A2J0RCN0_SALET	Disulfide bond formation...		4.9E-104
A0A3J2FB61_SALER	DsbA family protein OS=S...		1.9E-103
A0A0F7J869_SALET	Suppression of copper se...		3.2E-103
A0A315H0D5_SALET	Disulfide bond formation...		3.2E-103
A0A2T8QXY2_SALET	Disulfide bond formation...		3.2E-103
A0A0W4GAS2_SALER	DSBA oxidoreductase OS=S...		3.2E-103
A0A0J5HNX6_SALTM	DSBA oxidoreductase OS=S...		3.2E-103
A0A0U0WGF0_SALET	Copper-sensitivity secre...		7.3E-103
A0A3G3DB98_SALON	DsbA family protein OS=S...		7.3E-103
M7S4J0_SALDU	DsbA-like protein OS=Sal...		7.3E-103
A0A2T9EK16_SALET	Disulfide bond formation...		7.3E-103
G5QYC2_SALSE	Suppressor for copper-se...		7.3E-103
A0A1R3D9A4_SALEN	DsbA family protein OS=S...		7.3E-103
A0A3K1P0H6_SALER	DsbA family protein OS=S...		7.3E-103
A0A1J7RL25_SALER	Disulfide bond formation...		7.3E-103
G5LM71_SALET	Suppressor for copper-se...		7.3E-103
A0A2T9ESM7_SALET	Disulfide bond formation...		7.3E-103
V1XNK1_SALMU	Suppressor for copper-se...		7.3E-103
A0A1U7FPM9_SALET	Disulfide bond formation...		7.3E-103
B5R6G6_SALG2	Secreted protein, suppre...		7.3E-103
G4C0U4_SALIN	DSBA-like thioredoxin do...		7.3E-103
A0A2T8L2C5_SALET	Disulfide bond formation...		7.3E-103
A0A2C9P1D3_SALET	Disulfide bond formation...		9.5E-103
G5NBB2_SALET	Suppressor for copper-se...		9.5E-103
A0A1S0ZLF8_SALET	Disulfide bond formation...		9.5E-103
Q57QP0_SALCH	Suppression of copper se...		9.5E-103
A0A2T8XNA3_SALET	Disulfide bond formation...		9.5E-103
A0A2T9I4E3_SALET	Disulfide bond formation...		9.5E-103
A0A232SBT1_SALER	Disulfide bond formation...		9.5E-103
C0Q890_SALPC	Secreted protein, suppre...		9.5E-103
A0A3K9LMF9_SALER	DsbA family protein OS=S...		9.5E-103
A0A2V3NGE2_SALET	Secreted protein, suppre...		9.5E-103
A0A315G737_SALET	Disulfide bond formation...		9.5E-103
A0A3N9RL46_SALDE	DsbA family protein OS=S...		9.5E-103
A0A2R4DD12_SALET	Disulfide bond formation...		9.5E-103
A0A2T8Y1L8_SALIN	Disulfide bond formation...		9.5E-103
A0A2T9Q637_SALET	Disulfide bond formation...		9.5E-103
G5QHJ2_SALRU	Suppressor for copper-se...		9.5E-103
A0A3J3N524_SALER	DsbA family protein OS=S...		9.5E-103
A0A0H2WQ01_SALPA	Secreted protein, suppre...		9.5E-103
V7IK37_SALET	DsbA-like protein OS=Sal...		9.5E-103
B5F1Z8_SALA4	Suppressor for copper-se...		9.5E-103
A0A0R9N3U0_SALNE	Disulfide bond formation...		1.6E-102
A0A3J5DWV3_SALER	DsbA family protein OS=S...		1.6E-102
A0A386NLT6_SALPU	Disulfide bond formation...		1.6E-102
G5SA75_SALET	Suppressor for copper-se...		1.6E-102
A0A387CJG2_SALET	DsbA family protein OS=S...		1.6E-102
A0A0H3BRJ6_SALNS	Suppression of copper se...		1.6E-102
A0A379UP17_SALET	Secreted protein, suppre...		1.6E-102
A0A3K6NFT5_SALER	DsbA family protein OS=S...		1.6E-102
A0A265B8I4_SALET	Disulfide bond formation...		1.6E-102
G5RDX2_SALET	Secreted protein, suppre...		1.6E-102
A0A3H7ZVC2_SALER	DsbA family protein OS=S...		2.1E-102
A0A3E1J9K0_SALET	DSBA oxidoreductase OS=S...		2.1E-102
A0A1J4R6Q1_SALET	Disulfide bond formation...		2.1E-102
G5RTK9_SALET	Suppressor for copper-se...		2.1E-102
A0A1X2RU47_SALET	Disulfide bond formation...		2.1E-102
A0A3I2LG52_SALER	DsbA family protein OS=S...		2.1E-102
A0A271CLT1_SALET	DsbA family protein OS=S...		2.1E-102
A0A379VSJ1_SALET	Secreted protein, suppre...		2.1E-102
G5L7H2_SALET	Suppressor for copper-se...		2.1E-102
A0A3K1QYG5_SALER	DsbA family protein OS=S...		2.1E-102
A0A3G3DZW5_SALET	DsbA family protein OS=S...		2.1E-102
A0A0L3J9B4_SALET	Disulfide bond formation...		2.1E-102
A0A0N1R157_SALSV	Suppression of copper se...		2.1E-102
A0A1Z3Q2W2_SALET	Disulfide bond formation...		2.1E-102
A0A2T8MCB9_SALAN	Disulfide bond formation...		2.1E-102

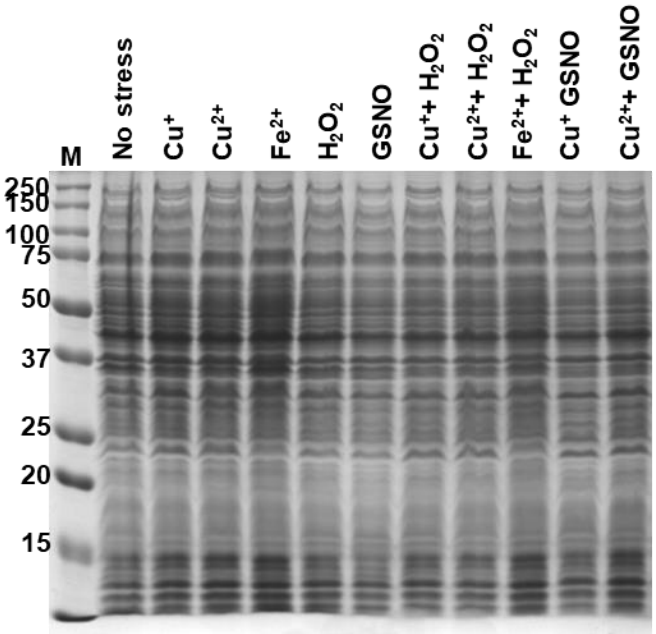

A0A3H5PKP7_SALER DsbA family protein OS=S... 2.8E-102
A0A3I1MUZ2_SALER DsbA family protein OS=S... 2.8E-102
A0A3K2B710_SALER DsbA family protein OS=S... 2.8E-102
G5MGM3_SALET Suppressor for copper-se... 2.8E-102
A0A379WAU2_SALET Secreted protein, suppre... 2.9E-102
A0A2X4QXZ9_SALER Secreted protein, suppre... 3.7E-102
A0A3I8ZNJ2_SALER DsbA family protein OS=S... 3.7E-102
G5Q0Y0_SALMO Suppressor for copper-se... 3.7E-102
A0A3I8WI04_SALER DsbA family protein OS=S... 3.7E-102
A0A0V2DGM4_SALER Disulfide bond formation... 3.7E-102
A0A3H8JJH2_SALER DsbA family protein OS=S... 3.7E-102
A0A3G8URM9_SALVI Secreted protein, suppre... 3.7E-102
A0A3K1FYU8_SALER DsbA family protein OS=S... 3.7E-102
A0A2Z2WU29_SALMO Disulfide bond formation... 3.7E-102
A0A3A3NLN7_SALMO DsbA family protein OS=S... 3.7E-102
A0A3K6LZM6_SALER DsbA family protein OS=S... 4.8E-102
A0A3I1SC88_SALER DsbA family protein OS=S... 4.8E-102
A0A3A3M3U7_SALET DsbA family protein OS=S... 4.8E-102
A0A3A3PB06_SALET DsbA family protein OS=S... 4.8E-102
A0A3J7V9B8_SALER DsbA family protein OS=S... 6.3E-102
A0A3N9Q5L8_SALET DsbA family protein OS=S... 6.3E-102
A0A3J9ZCJ4_SALER DsbA family protein OS=S... 6.3E-102
A0A3H6YUS9_SALER DsbA family protein OS=S... 6.3E-102
A9MH49_SALAR Uncharacterized protein ... 8.2E-102
A0A2T9H4H2_SALER Disulfide bond formation... 8.2E-102
A0A379PUV7_SALER Secreted protein, suppre... 8.2E-102
A0A3I4TDB6_SALER DsbA family protein OS=S... 1.1E-101
A0A3I1QTJ5_SALER DsbA family protein OS=S... 1.1E-101
A0A379QCV8_SALER Secreted protein, suppre... 1.4E-101
A0A3B7NVI8_SALSE DsbA family protein OS=S... 1.4E-101
A0A3J4I917_SALER DsbA family protein OS=S... 1.4E-101
A0A3I5E3K2_SALER DsbA family protein OS=S... 1.4E-101
A0A3I8FWE6_SALER DsbA family protein OS=S... 1.8E-101
A0A344R3E5_SALET DsbA family protein OS=S... 1.8E-101
A0A3J8P3X7_SALER DsbA family protein OS=S... 2.4E-101
A0A3L7M3A6_SALDZ Disulfide bond formation... 2.4E-101
A0A379XSA5_SALER Secreted protein, suppre... 2.4E-101
A0A3I2F453_SALER DsbA family protein OS=S... 2.4E-101
A0A344QE71_SALET DsbA family protein OS=S... 3.2E-101
A0A3I2B8I3_SALER DsbA family protein OS=S... 3.2E-101
A0A2T8T3K7_SALER Disulfide bond formation... 3.2E-101
A0A344SR88_SALER DsbA family protein OS=S... 4.1E-101
A0A379QNK8_SALER Secreted protein, suppre... 4.1E-101
A0A3K9J5Y2_SALER DsbA family protein OS=S... 4.1E-101
Q8Z7P3_SALTI Copper-sensitivity suppr... 4.1E-101
A0A241SCB1_SALER Disulfide bond formation... 4.1E-101
A0A1J6ZFP8_SALHO Disulfide bond formation... 4.1E-101
V1HUU6_SALER Copper sensitivity supre... 5.4E-101
A0A379R3Y0_SALER Secreted protein, suppre... 7.1E-101
A0A3F3J9R1_SALER Disulfide bond formation... 7.1E-101
A0A344SCL7_SALER DsbA family protein OS=S... 9.3E-101
A0A2I5HI79_SALDZ Disulfide bond formation... 9.3E-101
A0A3J2L6I3_SALER DsbA family protein OS=S... 2.1E-100
A0A3J4P9A4_SALER DsbA family protein OS=S... 4.7E-100
A0A379SIV7_SALER Secreted protein, suppre... 4.7E-100
A0A3K9AJ04_SALER DsbA family protein OS=S... 1.8E-99
A0A379TCI9_SALER Secreted protein, suppre... 5.1E-99
A0A3H7BW41_SALER DsbA family protein OS=S... 5.3E-99
A0A2X4TEG5_SALER Secreted protein, suppre... 6.9E-99
A0A3J4L944_SALER DsbA family protein OS=S... 6.9E-99
A0A3J6V5Y8_SALER DsbA family protein OS=S... 9.0E-99
A0A0K0H9N3_SALBC Secreted protein, suppre... 1.5E-96
A0A248KAP9_SALBN Disulfide bond formation... 1.5E-96
S5N6T0_SALBN Secreted protein suppres... 9.9E-96
A0A3E2KX21_9ENTR DsbA family protein OS=C... 3.4E-87
D4BBN6_9ENTR DsbA-like protein OS=Cit... 3.4E-87
A0A376I5I3_ECOLX Copper-sensitivity suppr... 3.4E-87
A0A2K9PA60_9ENTR Disulfide bond formation... 1.7E-86
A0A2L0TAQ3_9ENTR Disulfide bond formation... 3.0E-86
A0A1B2JVZ0_CITFR Disulfide bond formation... 3.0E-86
A0A100VCG1_SALER Disulfide bond formation... 3.0E-86
A0A090U4S5_9ENTR Putative copper sensitiv... 3.0E-86
A0A0A1RGF4_9ENTR Secreted protein, suppre... 3.9E-86
A0A381HR98_9ENTR Thiol-disulfide oxidored... 5.1E-86
A0A243UBI6_CITFR Secreted copper-sensitiv... 6.6E-86
A0A2Z3XBR7_9ENTR Disulfide bond formation... 6.6E-86
A0A2U4DP07_CITAM Disulfide bond formation... 6.6E-86
A0A0J1KE10_9ENTR Secreted copper-sensitiv... 6.6E-86
A0A0D7LYU3_CITFR Disulfide bond formation... 8.7E-86
A0A0D7LQC8_CITFR DSBA oxidoreductase OS=C... 8.7E-86
A0A0J1KU29_9ENTR Secreted copper-sensitiv... 8.7E-86
A0A0J1N9W3_9ENTR Secreted copper-sensitiv... 8.7E-86
A0A241QDD4_CITFR Disulfide bond formation... 8.7E-86
A0A2T1LM36_ECOLX Disulfide bond formation... 8.7E-86
A0A212I3L7_9ENTR Uncharacterized protein ... 8.7E-86
A0A243TCD9_CITFR Secreted copper-sensitiv... 1.1E-85
A0A2I8S4V0_9ENTR Disulfide bond formation... 1.5E-85
A0A2S4Q8M5_CITFR Disulfide bond formation... 1.9E-85
A0A2I8TLV9_9ENTR Disulfide bond formation... 3.3E-85
A0A1C0P6J8_CITFR Disulfide bond formation... 3.3E-85
A0A2U9UBS9_9ENTR Disulfide bond formation... 3.3E-85
A0A0J1LPZ5_9ENTR Secreted copper-sensitiv... 3.3E-85
A0A0J1M9U2_9ENTR Secreted copper-sensitiv... 3.3E-85
A0A376QZ66_ECOLX Copper-sensitivity suppr... 3.3E-85
A0A212HTI8_9ENTR DsbA-like protein OS=Cit... 3.4E-85


A0A064E4L7_CITFR Uncharacterized protein ... 4.4E-85
A8AI73_CITK8 Uncharacterized protein ... 4.4E-85
A0A336PCP3_CITFR Thiol-disulfide oxidored... 4.4E-85
A0A377VNR4_KLEPN Secreted protein, suppre... 5.7E-85
A0A2N4VBR7_9ENTR Disulfide bond formation... 5.7E-85
A0A336QRJ3_CITFR Thiol-disulfide oxidored... 5.7E-85
A0A336PY11_CITKO Thiol-disulfide oxidored... 5.7E-85
A0A0J0HNW7_9ENTR DSBA oxidoreductase OS=E... 9.8E-85
A0A1R0G1N2_CITBR Disulfide bond formation... 9.8E-85
R8X0H1_9ENTR Secreted copper-sensitiv... 9.8E-85
A0A078LI92_CITKO Uncharacterized protein ... 1.3E-84
A0A1V8P4F7_CITBR Disulfide bond formation... 1.3E-84
A0A3N0D0W7_9ENTR DsbA family protein OS=C... 1.7E-84
A0A0M3ECI2_VIBPH DSBA oxidoreductase OS=V... 2.2E-84
A0A381G5A5_CITAM Thiol-disulfide oxidored... 2.2E-84
I6HBI8_SHIFL DSBA-like thioredoxin do... 2.8E-84
A0A2S4RY66_CITAM Disulfide bond formation... 2.9E-84
A0A1F2JAP5_9ENTR Disulfide bond formation... 4.9E-84
A0A1V4NZN3_9ENTR Disulfide bond formation... 4.9E-84
A0A381H5T9_CITKO Thiol-disulfide oxidored... 4.9E-84
A0A156JH81_ENTCL Suppressor for copper-se... 4.9E-84
A0A223JQU6_9ENTR Disulfide bond formation... 3.7E-82
A0A1X7JC62_9ENTR Protein-disulfide isomer... 1.1E-81
A0A291DW43_9ENTR Disulfide bond formation... 4.2E-81
J0MGM8_9ENTR Uncharacterized protein ... 5.5E-81
A0A0V9JRN8_9ENTR Disulfide bond formation... 7.1E-81
A0A0D5WVK1_9ENTR DSBA oxidoreductase OS=K... 7.2E-81
S3IRM9_9ENTR DsbA-like protein OS=Ced... 9.4E-81
A0A1X3IT22_ECOLX Secreted protein, suppre... 1.6E-80
A0A089Q2S7_9ENTR DSBA oxidoreductase OS=C... 4.7E-80
A0A0V2F2X7_SALNE Disulfide bond formation... 4.9E-80
F4UYB6_ECOLX Secreted protein, suppre... 1.5E-76
A0A379U1F6_SALDZ Secreted protein, suppre... 1.9E-75
A0A379WWJ1_SALET Secreted protein, suppre... 4.1E-67
A0A379S8L7_SALER Secreted protein, suppre... 8.1E-66
A0A1B7IP59_9ENTR ScsC family secreted pro... 5.6E-65
A0A085GBW6_9ENTR ScsC family secreted pro... 9.6E-65
A0A381C778_9ENTR Thiol-disulfide oxidored... 1.3E-64
A0A1B7HTN7_9ENTR ScsC family secreted pro... 3.7E-64
A0A1B7I5G9_9ENTR ScsC family secreted pro... 2.4E-63
A0A3A5JV15_9ENTR DsbA family protein OS=B... 1.2E-62
A0A3G2IBK3_9ENTR DsbA family protein OS=B... 6.2E-62
A0A1B7IBY3_9ENTR ScsC family secreted pro... 6.2E-62
A0A2X5B2S0_SERRU Thiol-disulfide oxidored... 1.9E-60
A0A2R3H448_9GAMM Copper resistance protei... 1.9E-60
A0A126VH67_SERRU Secreted protein, suppre... 3.2E-60
L0MHH9_9GAMM Protein-disulfide isomer... 5.5E-60
A0A0U4HMN4_SERFO Copper resistance protei... 2.7E-59
A0A1S8CLE3_9GAMM Copper resistance protei... 7.9E-59
A0A3F3KUI6_SERMA DsbA family protein OS=S... 1.1E-58
A0A3A9V031_SERMA DsbA family protein OS=S... 1.1E-58
A0A2V4G2Q0_SERMA DsbA family protein OS=S... 1.1E-58
D4E3J2_SEROD DsbA-like protein OS=Ser... 1.4E-58
A0A087L545_9GAMM Copper-sensitivity prote... 1.8E-58
W0L4Z9_9GAMM Copper-sensitivity prote... 3.0E-58
A0A370T8G1_SERFO Protein-disulfide isomer... 3.1E-58
A0A3G2RTL6_9GAMM DsbA family protein OS=S... 3.1E-58
A0A379YJK0_9GAMM Thiol-disulfide oxidored... 3.1E-58
A0A0X8SL84_SERLI DsbA family protein OS=S... 4.1E-58
A0A1Q5W1J4_SERMA Copper resistance protei... 9.1E-58
U2NN54_SERFO Secreted protein, suppre... 1.2E-57
A0A0U7N2I0_SERMA Thiol-disulfide oxidored... 1.6E-57
A0A221FSP3_SERMA Copper resistance protei... 1.6E-57
A0A3G6CHL7_9GAMM DsbA family protein OS=S... 1.6E-57
A0A3G4SUH5_9GAMM DsbA family protein OS=S... 1.6E-57
A0A2V4HDH2_SERMA DsbA family protein OS=S... 1.6E-57
A0A379SWH8_SALER Secreted protein, suppre... 1.6E-57
A0A1B3FET3_9GAMM Copper resistance protei... 2.0E-57
A0A0P0QH92_SERMA Copper resistance protei... 2.0E-57
A0A1C7WEI9_9GAMM Copper resistance protei... 2.0E-57
A0A086GC17_9GAMM Copper-sensitivity prote... 2.0E-57
A0A1Q5VIY4_SERFO Copper resistance protei... 2.0E-57
A0A292AFE2_SERFO Copper resistance protei... 2.0E-57
A0A1W9F029_9GAMM Copper-sensitivity prote... 2.1E-57
A0A2X2HDU0_9GAMM Thiol-disulfide oxidored... 2.7E-57
A8GH57_SERP5 DSBA oxidoreductase OS=S... 2.7E-57
A0A3Q0NV70_SERMA Copper-sensitivity prote... 3.5E-57
A0A221DST6_SERMA Copper resistance protei... 3.5E-57
A0A2U9FQT8_SERMA Copper resistance protei... 4.6E-57
A0A168TF06_KLEOX Secreted protein, suppre... 4.6E-57
F5S1K5_9ENTR Suppressor for copper-se... 5.1E-57

Appendix 3- SDS-PAGE loading control. Wild-type *Salmonella* strains are grown in the presence and absence of 2 mM $ZnSO_4$, $FeSO_4$ and $CuSO_4$. The whole cell samples were loaded on an SDS-PAGE as loading control. Equal amount of protein was loaded for each whole cell samples. Dual Colour protein marker was used (Bio-Rad). (Section 3.2.2.2).



Appendix 4- SDS-PAGE loading control. Wild-type *S*. Typhimurium grown in the presence of various stresses as indicated on the gel. Periplasmic fractions were isolated, and equal amount of protein was loaded on an SDS-PAGE as a loading control. Dual Colour protein marker was used (Bio-Rad). (Section 3.2.2.3).



Appendix 5- Sequencing data for the pET23b_P*scsA_gfp* vector. First sequence shows the sequencing with the Reverse primer, middle sequence is the desired plasmid sequence and the last sequence shows the sequencing with the Forward primer. The start and end of the 400 bp insert is highlighted in blue and the *gfp* start codon is highlighted in yellow. The sequences were aligned using Bioedit sotware (Hall, 1999) using ClustalW Multiple alignment. (Section 3.2.2.4).

```
R primer          GATCTCGATCCCGCGAAATTAATACGACTCACTATAGGGAGACCACAACG
pET23b_PscsA_gfp  GATCTCGATCCCGCGAAATTAATACGACTCACTATAGGGAGACCACAACG
F primer          GATCTCGATCCCGCGAAATTAATACGACTCACTATAGGGAGACCACAACG

R primer          GTTTCCCTCTAGAGCACTTCCCATGCTTCAGCAACCTCTTTGAAACGGGC
pET23b_PscsA_gfp  GTTTCCCTCTAGAGCACTTCCCATGCTTCAGCAACCTCTTTGAAACGGGC
F primer          GTTTCCCTCTAGAGCACTTCCCATGCTTCAGCAACCTCTTTGAAACGGGC

R primer          TTCGGCATCGGGTTCTTTGCTGACATCTGGATGGTACTTGCGGGCCAGTC
pET23b_PscsA_gfp  TTCGGCATCGGGTTCTTTGCTGACATCTGGATGGTACTTGCGGGCCAGTC
F primer          TTCGGCATCGGGTTCTTTGCTGACATCTGGATGGTACTTGCGGGCCAGTC

R primer          GGCGATAGGCGGTCTTAATCGTCTTGAGATCGTCCGTCGGTTTCACGCCC
pET23b_PscsA_gfp  GGCGATAGGCGGTCTTAATCGTCTTGAGATCGTCCGTCGGTTTCACGCCC
F primer          GGCGATAGGCGGTCTTAATCGTCTTGAGATCGTCCGTCGGTTTCACGCCC

R primer          ATAATGGCGTAATAATCCTTAAGTTCCATAGCATCATCTCGCTAAATCAA
pET23b_PscsA_gfp  ATAATGGCGTAATAATCCTTAAGTTCCATAGCATCATCTCGCTAAATCAA
F primer          ATAATGGCGTAATAATCCTTAAGTTCCATAGCATCATCTCGCTAAATCAA

R primer          TACATACAGAAGGGACCCCAAAAGGTTTCTCCACTAAGTGTAGGGTAAAC
pET23b_PscsA_gfp  TACATACAGAAGGGACCCCAAAAGGTTTCTCCACTAAGTGTAGGGTAAAC
F primer          TACATACAGAAGGGACCCCAAAAGGTTTCTCCACTAAGTGTAGGGTAAAC

R primer          CTGAAAAGTGCGTATGAAAACACCAGTTATATCATTAGTAAGAATAAATT
pET23b_PscsA_gfp  CTGAAAAGTGCGTATGAAAACACCAGTTATATCATTAGTAAGAATAAATT
F primer          CTGAAAAGTGCGTATGAAAACACCAGTTATATCATTAGTAAGAATAAATT

R primer          ACGTTGTTCGACTATCAGAAGGTTGCGCAGCGCGCCGACATAACTTTACA
pET23b_PscsA_gfp  ACGTTGTTCGACTATCAGAAGGTTGCGCAGCGCGCCGACATAACTTTACA
F primer          ACGTTGTTCGACTATCAGAAGGTTGCGCAGCGCGCCGACATAACTTTACA

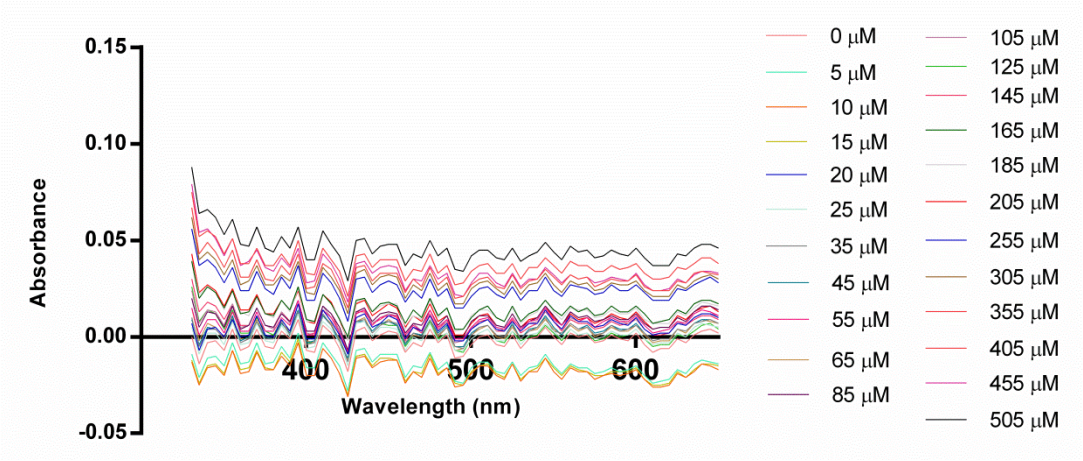
R primer          GGGGAAAGGTTGCCAAAACCGCGCCAGTGGCTAAGATAACTCGCGTTAAA
pET23b_PscsA_gfp  GGGGAAAGGTTGCCAAAACCGCGCCAGTGGCTAAGATAACTCGCGTTAAA
F primer          GGGGAAAGGTTGCCAAAACCGCGCCAGTGGCTAAGATAACTCGCGTTAAA

R primer          CAGTGAGGGCGCAGAGCTCATGAGCAAAGGAGAAGAACTTTTCACTGGAG
pET23b_PscsA_gfp  CAGTGAGGGCGCAGAGCTCATGAGCAAAGGAGAAGAACTTTTCACTGGAG
F primer          CAGTGAGGGCGCAGAGCTCATGAGCAAAGGAGAAGAACTTTTCACTGGAG

R primer          TTGTCCCAATTCTTGTTGAATTAGATGGTGATGTTAATGGGCACAAATTT
pET23b_PscsA_gfp  TTGTCCCAATTCTTGTTGAATTAGATGGTGATGTTAATGGGCACAAATTT
F primer          TTGTCCCAATTCTTGTTGAATTAGATGGTGATGTTAATGGGCACAAATTT

R primer          TCTGTCAGTGGAGAGGGTGAAGGTGATGCTACAT--------
pET23b_PscsA_gfp  TCTGTCAGTGGAGAGGGTGAAGGTGATGCTACATACGGAAAG
F primer          TCTGTCAGTGGAGAGGGTGAAGGTGATGCTACATACGGAAAG
```

Appendix 6- Absorbance spectra of Cu^{+} titration into the reaction buffer. This assay has been performed in order to test if high concentrations of Cu^{+} interferes with the absorbance signal. No definitive peak at around 483 nm was detected suggesting that copper does not interfere with the competition assay of StScsC and BCS. (Section 4.2.4).



Appendix 7- Sequencing data for the pSU2718*scsC*$_{CXXA}$ vector. First sequence shows the sequencing with the Reverse primer, middle sequence is the desired plasmid sequence and the last sequence shows the sequencing with the Forward primer. The ribosome binding site is highlighted in green. The start codon of *scsC*$_{CXXA}$ is highlighted in yellow. The his$_6$-tag is highlighted in blue and the stop codon is highlighted in pink. The CPYA catalytic motif is coloured in red and blue. The sequences were aligned using Bioedit sotware (Hall, 1999) using ClustalW Multiple alignment. (Section 4.2.5.2).

```
R primer          ------GCAAAAGCACCGCCGGACATCAGCGCCATTCGCCATTCAGGCTGCGCATTAATG
pSU2718scsCCXXA   ------GCAAAAGCACCGCCGGACATCAGCGCCATTCGCCATTCAGGCTGCGCATTAATG
F primer          ------GCAAAAGCACCGCCGGACATCAGCGCCATTCGCCATTCAGGCTGCGCATTAATG

R primer          ATGATGATGATGATGCCCGCCATTGGCAGACGCCAGTTTTTCTTTCACCACCGCTTCCAG
pSU2718scsCCXXA   ATGATGATGATGATGCCCGCCATTGGCAGACGCCAGTTTTTCTTTCACCACCGCTTCCAG
F primer          ATGATGATGATGATGCCCGCCATTGGCAGACGCCAGTTTTTCTTTCACCACCGCTTCCAG

R primer          CGTATCCCAGGGCACTGCGCCCGGAATCAGCTCGTCGCCAATGATCGTCGCTGGCGTTCC
pSU2718scsCCXXA   CGTATCCCAGGGCACTGCGCCCGGAATCAGCTCGTCGCCAATGATCGTCGCTGGCGTTCC
F primer          CGTATCCCAGGGCACTGCGCCCGGAATCAGCTCGTCGCCAATGATCGTCGCTGGCGTTCC

R primer          TTGCACGCCGACCAGCCTTGCCAACTGCAAATTAGTGCGTATCGTTTCCATGCTTTTTTC
pSU2718scsCCXXA   TTGCACGCCGACCAGCCTTGCCAACTGCAAATTAGTGCGTATCGTTTCCATGCTTTTTTC
F primer          TTGCACGCCGACCAGCCTTGCCAACTGCAAATTAGTGCGTATCGTTTCCATGCTTTTTTC

R primer          ATCCAGCGTCACTGGCGTAGCCCCTGCTTTCTGCTGGGCCTGTTTAATACTGTCATCCGT
pSU2718scsCCXXA   ATCCAGCGTCACTGGCGTAGCCCCTGCTTTCTGCTGGGCCTGTTTAATACTGTCATCCGT
F primer          ATCCAGCGTCACTGGCGTAGCCCCTGCTTTCTGCTGGGCCTGTTTAATACTGTCATCCGT

R primer          ATGGTAAACGCGCTTTTGCATGAGTTTTTCATGTAGCGCGAGGAACTGTTGCGGATGCTC
pSU2718scsCCXXA   ATGGTAAACGCGCTTTTGCATGAGTTTTTCATGTAGCGCGAGGAACTGTTGCGGATGCTC
F primer          ATGGTAAACGCGCTTTTGCATGAGTTTTTCATGTAGCGCGAGGAACTGTTGCGGATGCTC

R primer          GCGCCAGGTGGTCAGCGCAATACGCGCCGCCAGAACGGAACTCTCTCCTTTAAATGGCAG
pSU2718scsCCXXA   GCGCCAGGTGGTCAGCGCAATACGCGCCGCCAGAACGGAACTCTCTCCTTTAAATGGCAG
F primer          GCGCCAGGTGGTCAGCGCAATACGCGCCGCCAGAACGGAACTCTCTCCTTTAAATGGCAG

R primer          CGGTTTAATAATGACCGCAACGTCAGGATATTTCTGCACAATCTTTTCCAGCATCGGATC
pSU2718scsCCXXA   CGGTTTAATAATGACCGCAACGTCAGGATATTTCTGCACAATCTTTTCCAGCATCGGATC
F primer          CGGTTTAATAATGACCGCAACGTCAGGATATTTCTGCACAATCTTTTCCAGCATCGGATC

R primer          GAGCTGTTTAGCGTACGGGCAGTTGTAATCCGTAAAGTTCACCAGCGTCAGCTTAGGGTG
pSU2718scsCCXXA   GAGCTGTTTAGCGTACGGGCAGTTGTAATCCGTAAAGTTCACCAGCGTCAGCTTAGGGTG
F primer          GAGCTGTTTAGCGTACGGGCAGTTGTAATCCGTAAAGTTCACCAACGTCAGCTTAGGGTG

R primer          TTTAGCGCCTATCCGCGGGCTGGCAGGATCGTTAAACAACGCCGCATGGATCAGATTTTC
pSU2718scsCCXXA   TTTAGCGCCTATCCGCGGGCTGGCAGGATCGTTAAACAACGCCGCATGGATCAGATTTTC
F primer          TTTAGCGCCTATCCGCGGGCTGGCAGGATCGTTAAACAACGCCGCATGGATCAGATTTTC

R primer          AATCTGCTTTTCCTGATCCGGCGTAAAAGGAGCGGTTTCTTGAGCTTGCGCTACGGTAGC
pSU2718scsCCXXA   AATCTGCTTTTCCTGATCCGGCGTAAAAGGAGCGGTTTCTTGAGCTTGCGCTACGGTAGC
F primer          AATCTGCTTTTCCTGATCCGGCGTAAAAGGAGCGGTTTCTTGAGCTTGCGCTACGGTAGC

R primer          GAAACCAGCCAAGGCCACTGCAATTGCGATAGCTGTCTTTTTCATATGGTCTTCCTTTCA
pSU2718scsCCXXA   GAAACCAGCCAAGGCCACTGCAATTGCGATAGCTGTCTTTTTCATATGGTCTTCCTTTCA
F primer          GAAACCAGCCAAGGCCACTGCAATTGCGATAGCTGTCTTTTTCATATGGTCTTCCTTTCA

R primer          TGGATCCCCGGGTACCGAGCTCGAATTCGTAA
pSU2718scsCCXXA   TGGATCCCCGGGTACCGAGCTCGAATTCGTAA
F primer          TGGATCCCCGGGTACCGAGCTCGAATTCGTAA
```

Appendix 8- Sequencing data for the pTrcHis_*artI* vector. First sequence shows the sequencing with the Reverse primer, middle sequence is the desired plasmid sequence and the last sequence shows the sequencing with the Forward primer. The start codon is highlighted in red, N-terminal his_6-tag is highlighted in green, the TEV cleavage site is highlighted in yellow and the start of *artI* gene without the signal peptide is highlighted in blue and. The sequences were aligned using Bioedit sotware (Hall, 1999) using ClustalW Multiple alignment. (Section 4.2.6.1).

```
R primer      ATGTATCGATTAAATAAGGAGGAATAAACCATGGGGGGTTCTCATCATCA
pTrcHis_artI  ATGTATCGATTAAATAAGGAGGAATAAACCATGGGGGGTTCTCATCATCA
F primer      ATGTATCGATTAAATAAGGAGGAATAAACCATGGGGGGTTCTCATCATCA

R primer      TCATCATCATGGTATGGCTAGCGAGAATTTATACTTCCAAGGTTCTAACG
pTrcHis_artI  TCATCATCATGGTATGGCTAGCGAGAATTTATACTTCCAAGGTTCTAACG
F primer      TCATCATCATGGTATGGCTAGCGAGAATTTATACTTCCAAGGTTCTAACG

R primer      CCGCCCAGACCATTCGTTTTGCGACCGAAGCGTCCTATCCGCCGTTCGAA
pTrcHis_artI  CCGCCCAGACCATTCGTTTTGCGACCGAAGCGTCCTATCCGCCGTTCGAA
F primer      CCGCCCAGACCATTCGTTTTGCGACCGAAGCGTCCTATCCGCCGTTCGAA

R primer      TCGATGGATGCTAATAACAAGATTGTCGGCTTTGACGTCGACCTGGCCAA
pTrcHis_artI  TCGATGGATGCTAATAACAAGATTGTCGGCTTTGACGTCGACCTGGCCAA
F primer      TCGATGGATGCTAATAACAAGATTGTCGGCTTTGACGTCGACCTGGCCAA

R primer      CGCGCTATGTAAAGAGATCGACGCCTCCTGTACCTTTACCAATCAGGCGT
pTrcHis_artI  CGCGCTATGTAAAGAGATCGACGCCTCCTGTACCTTTACCAATCAGGCGT
F primer      CGCGCTATGTAAAGAGATCGACGCCTCCTGTACCTTTACCAATCAGGCGT

R primer      TCGACAGCCTGATCCCCAGCCTGAAATTCCGCCGCTTCGACGCTGTAATG
pTrcHis_artI  TCGACAGCCTGATCCCCAGCCTGAAATTCCGCCGCTTCGACGCTGTAATG
F primer      TCGACAGCCTGATCCCCAGCCTGAAATTCCGCCGCTTCGACGCTGTAATG

R primer      GCGGGAATGGATATCACGCCGGAACGTGAAAAGCAGGTGCTGTTTACCAC
pTrcHis_artI  GCGGGAATGGATATCACGCCGGAACGTGAAAAGCAGGTGCTGTTTACCAC
F primer      GCGGGAATGGATATCACGCCGGAACGTGAAAAGCAGGTGCTGTTTACCAC

R primer      GCCATATTACGACAACTCCGCGCTGTTCGTGGGTCAGCAGGGCAAATACA
pTrcHis_artI  GCCATATTACGACAACTCCGCGCTGTTCGTGGGTCAGCAGGGCAAATACA
F primer      GCCATATTACGACAACTCCGCGCTGTTCGTGGGTCAGCAGGGCAAATACA

R primer      CCAGCGTTGATCAACTGAAAGGCAAGAAAGTCGGCGTACAGAACGGTACG
pTrcHis_artI  CCAGCGTTGATCAACTGAAAGGCAAGAAAGTCGGCGTACAGAACGGTACG
F primer      CCAGCGTTGATCAACTGAAAGGCAAGAAAGTCGGCGTACAGAACGGTACG

R primer      ACGCACCAGAAATTCATCATGGATAAGTATCCGGAAATCACCACCGTACC
pTrcHis_artI  ACGCACCAGAAATTCATCATGGATAAGTATCCGGAAATCACCACCGTACC
F primer      ACGCACCAGAAATTCATCATGGATAAGTATCCGGAAATCACCACCGTACC

R primer      GTATGACAGCTATCAGAACGCGAAGCTGGATCTACAAAATGGCCGTATCG
pTrcHis_artI  GTATGACAGCTATCAGAACGCGAAGCTGGATCTACAAAATGGCCGTATCG
F primer      GTATGACAGCTATCAGAACGCGAAGCTGGATCTACAAAATGGCCGTATCG

R primer      ACGCTGTTTTCGGCGACACGGCGGTCGTGACCGAATGGCTGAAAGCCAAT
pTrcHis_artI  ACGCTGTTTTCGGCGACACGGCGGTCGTGACCGAATGGCTGAAAGCCAAT
F primer      ACGCTGTTTTCGGCGACACGGCGGTCGTGACCGAATGGCTGAAAGCCAAT

R primer      CCTAAGCTGGCGCCGGTCGGCGATAAAGTCACCGATAAAGATTATTTCGG
pTrcHis_artI  CCTAAGCTGGCGCCGGTCGGCGATAAAGTCACCGATAAAGATTATTTCGG
F primer      CCTAAGCTGGCGCCGGTCGGCGATAAAGTCACCGATAAAGATTATTTCGG

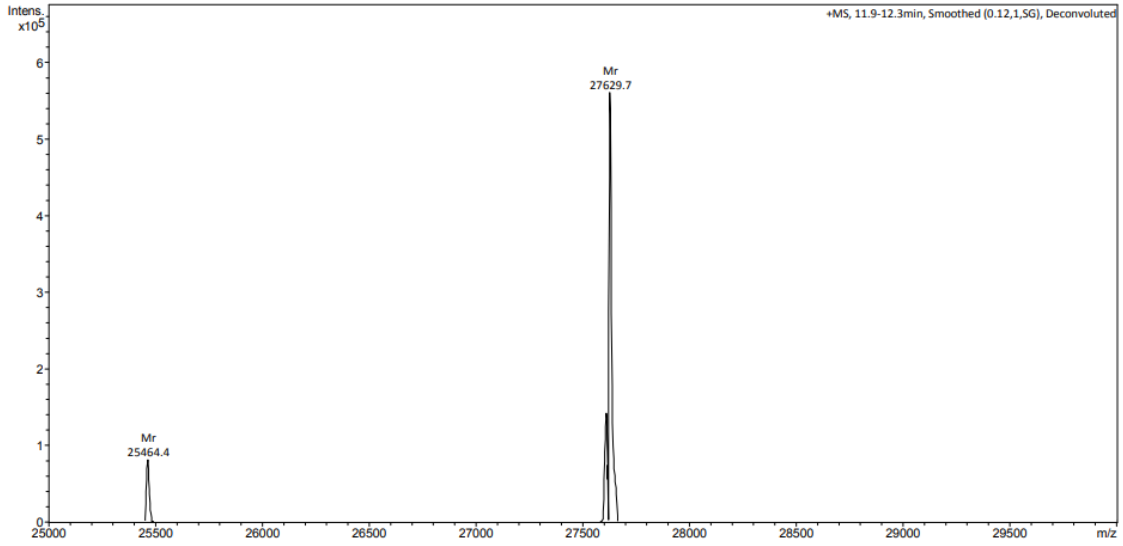
R primer      CACCGGCCTGGGTATCGCGGTACGCCAGGGCAACACCGAGCTGCAGCAGA
pTrcHis_artI  CACCGGCCTGGGTATCGCGGTACGCCAGGGCAACACCGAGCTGCAGCAGA
F primer      CACCGGCCTGGGTATCGCGGTACGCCAGGGCAACACCGAGCTGCAGCAGA

R primer      AATTCAATACTGCGCTGGAAAAAGTGAAGAAAGATGGGACTTACGAGACC
pTrcHis_artI  AATTCAATACTGCGCTGGAAAAAGTGAAGAAAGATGGGACTTACGAGACC
F primer      AATTCAATACTGCGCTGGAAAAAGTGAAGAAAGATGGGACTTACGAGACC

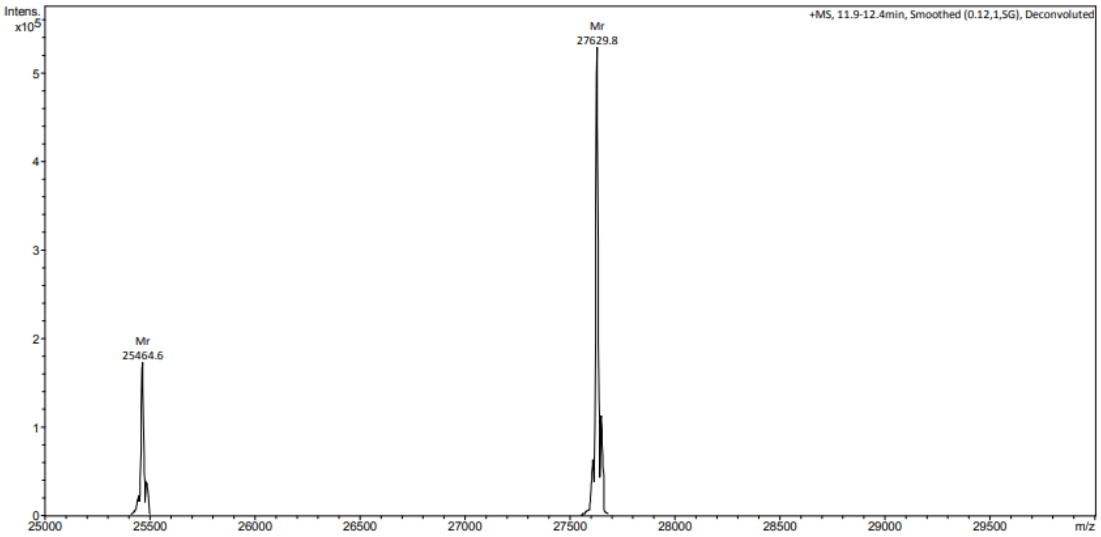
R primer      ATCTATAACAAATGGTTCCAGAAGTAAAAGCTTGGCTGTTTTGGCGGATG
pTrcHis_artI  ATCTATAACAAATGGTTCCAGAAGTAAAAGCTTGGCTGTTTTGGCGGATG
F primer      ATCTATAACAAATGGTTCCAGAAGTAAAAGCTTGGCTGTTTTGGCGGATG


R primer      AGAGAAGATTTTCAGCCTGATACAGATTAAATCAGAACGCA
pTrcHis_artI  AGAGAAGATTTTCAGCCTGATACAGATTAAATCAGAACGCA
F primer      AGAGAAGATTTTCAGCCTGATACAGATTAAATCAGAACGCA
```

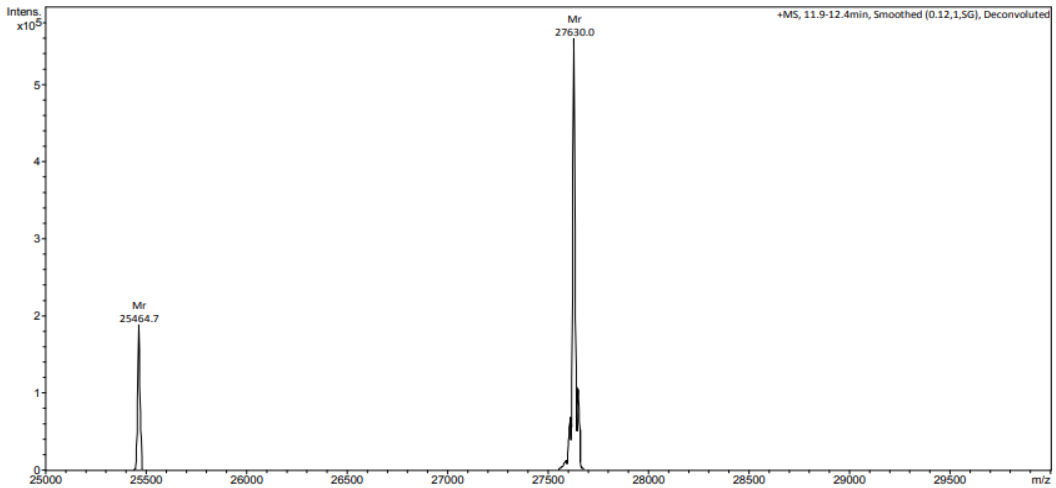
Appendix 9A- Intact mass analysis of 'as purified' ArtI. As purified ArtI cannot be reduced or oxidized with DTT and GSSG, it was hypothesized that one or both of the cysteines of the protein was modified by a post-translational modification that may affect the folding of the protein so that the cysteines are not available for reduction or oxidation or the modification itself is hard to reduce. The protein sample was then subjected to mass spectrometry for analysis of intact mass. Protein was not treated with trypsin. Theoretical predicted mass of the protein N-terminal his_6-tagged ArtI is 27768 Da and the measured intact mass of the protein was 27630 Da as shown on the large peak. One possibility is that the purified protein had lost the initiation methionine where the amino acid after the start methionine was not charged and weak so that it was cleaved off. Another possible modification that was predicted was Gluconoylation of the protein which is usually detected on histidine tagged proteins. Small 25464 Da protein peak that was detected could be B-lactamase which is usually co-purifies with the protein of interest. It has to be also noted that there was +/- 2.7 Da mass error. (Section 4.2.7.4).



Appendix 9B- Addition of alkylation reagent does not alter the mass of ArtI. No specific modification has been detected for cysteine residues as shown on Appendix 9A. To address this question, purified protein sample was incubated with iodoacetamide for thiol alkylation. Increase on the experimental mass was expected if the protein has a reduced thiol due to addition of iodoacetamide however, no change on the mass has been observed. (Section 4.2.7.4).



Appendix 9C- Cysteine residues of the ArtI are inaccessible to DTT. The reducing agent DTT was added to the protein sample prior to alkylation with chloroacetamide in order to detect a mass change on free thiols. However, no mass change was detected. This result suggested that the cysteines are not accessible. (Section 4.2.7.4).



Appendix 10- Docking models for ScsC and ArtI. The ribbon structure of StScsC is shown in white and the ribbon structure of the ArtI is shown in coral. The sulphur atoms are shown as yellow spheres. Models were generated using the ClusPro software (Kozakov *et al.*, 2017) and edited using CCP4MG software (McNicholas *et al.*, 2011). 12 models are selected to be presented out of 30 models predicted with ClusPro software. (Section 4.2.8).

